Tesis Doctoral
Ingeniería de Caminos, Canales y Puertos

Parameter estimation of dynamic systems: application to civil engineering structures

Autor: Javier Naranjo Pérez
Directores: Javier Fernando Jiménez Alonso y Andrés Sáez Pérez

Tesis Doctoral

Programa de Doctorado en Ingeniería Mecánica y de Organización
Industrial

Parameter estimation of dynamic systems: application to civil engineering structures

Estimación de parámetros de sistemas dinámicos: aplicación a estructuras
de ingeniería civil

Autor:

Javier Naranjo Pérez

Tesis para la obtención del grado de Doctor por la
Universidad de Sevilla

Director:

Javier Fernando Jiménez Alonso

Profesor Ayudante Doctor de la Universidad Politécnica de Madrid

Codirector:

Andrés Sáez Pérez

Catedrático de Universidad de la Universidad de Sevilla

Departamento de Mecánica de Medios Continuos y Teoría de Estructuras
Escuela Técnica Superior de Ingeniería
Universidad de Sevilla

2020

Tesis Doctoral: Parameter estimation of dynamic systems: application to civil engineering structures

Autor: Javier Naranjo Pérez
Director: Javier Fernando Jiménez Alonso
Codirector: Andrés Sáez Pérez

El tribunal nombrado para juzgar la Tesis arriba indicada, compuesto por los siguientes doctores:

Presidente:

Vocales:

Secretario:

acuerdan otorgarle la calificación de:

El Secretario del Tribunal

Fecha:

Prefacio

Esta Tesis Doctoral se ha realizado en el Departamento de Mecánica de Medios Continuos y Análisis Estructural de la Universidad de Sevilla. Este trabajo ha sido supervisado por los profesores Javier Fernando Jiménez Alonso y Andrés Sáez Pérez. La tesis se basa en los seis artículos científicos indicados a continuación. Partes de los artículos se emplean en el resumen ampliado de la tesis. Los artículos incluidos como apéndices han sido preparados en colaboración con los autores.

La lista de los seis artículos científicos es la siguientes:

A: Jiménez-Alonso, J. F., Naranjo-Pérez, J., Pavic, A., Sáez, A. Maximum likelihood finite-element model updating of civil engineering structures using nature-inspired computational algorithms. *Structural Engineering International*. 2020. (*Accepted*).

B: Naranjo-Pérez, J., Sáez, A., Jiménez-Alonso, J.F., Pachón, P., Compán, V. (2019). A hybrid UKF-MGA algorithm for finite element model updating of historical constructions. IABSE Symposium, Guimaraes 2019: Towards a Resilient Built Environment Risk and Asset Management – Report pp. 29-36.

C: Naranjo-Pérez, J., Jiménez-Alonso, J. F., Pavic, A., Sáez, A. Finite-element model updating of civil engineering structures using a hybrid UKF-HS algorithm. *Structure and Infraestructure Engineering*. 2020.

D: Naranjo-Pérez, J., Jiménez-Alonso, J. F., Sáez, A. Parameter identification of the dynamic Winkler soil-structure interaction model using a hybrid UKF-MHS algorithm. *Advances in Structural Engineering*. 2020.

E: Infantes M, Naranjo-Pérez J, Jiménez-Alonso JF, Sáez A (2019). Determining the Best Pareto-solution in a Multi-Objective Approach for Model Updating. IABSE Symposium, Guimaraes 2019: Towards a Resilient Built Environment Risk and Asset Management – Report pp. 523-530.

F: Naranjo-Pérez, J., Infantes, M., Jiménez-Alonso, J.F., A. Sáez. A collaborative machine learning-optimization algorithm to improve the finite element model updating of civil engineering structures. Submitted for publication.

A mi familia

Agradecimientos

La realización de una Tesis Doctoral supone un esfuerzo que resultaría insoportable si no fuese por el apoyo de numerosas personas. En primer lugar, quiero expresar mi más sincero agradecimiento a los directores de esta tesis, los profesores Javier Fernando Jiménez Alonso y Andrés Sáez Pérez, por todo lo que he podido aprender a su lado. Además, es de obligado cumplimiento, agradecer sus sabios consejos, ya que sin ellos esta tesis no hubiese visto la luz.

Es de estricta justicia agradecer también a todos aquellos colaboradores que han hecho posible los trabajos científicos que componen esta tesis. En especial, quiero acordarme del profesor Giuseppe Quaranta de la Universidad La Sapienza por su acogida durante mi estancia en Roma.

Por último, pero no menos importante, agradecer a aquellas personas que no han colaborado directamente en la elaboración de esta tesis, pero que gracias a sus ánimos y apoyo incondicional, han hecho de estos años una etapa mucho másagradable: mi familia y amigos.

Sería excesivamente prolijo citar uno a uno a todos aquellos que merecen estar en estas líneas. Por eso quiero que todos ellos se sientan aquí incluidos y reciban mi más sincero agradecimiento.

Javier Naranjo Pérez

Sevilla, 2020

Resumen

La estimación de parámetros de sistemas dinámicos se basa en inferir los parámetros del sistema a partir del conocimiento de un conjunto de entradas y salidas. En ingeniería civil, la principal aplicación es la actualización de modelos de elementos finitos, donde el objetivo es estimar sus parámetros a partir del comportamiento real de la estructura para obtener modelos fiables. Estos problemas se pueden abordar usando estimadores puntuales, enfoque Bayesiano o lógica difusa. En esta tesis se emplea el primer método, donde la estimación de parámetros se resuelve como un problema de optimización cuyo objetivo es encontrar el mínimo de una función que representa el error.

Para resolver estos problemas, los algoritmos metaheurísticos constituyen la opción más empleada, gracias a su facilidad para hallar el óptimo global de funciones no lineales y a su independencia del valor inicial de los parámetros de la función. El principal inconveniente de estos algoritmos es su alto coste computacional. Por ello, en esta tesis se proponen dos algoritmos de optimización eficientes para la estimación de parámetros. En la primera parte de esta tesis, para caracterizar el rendimiento de algoritmos existentes, se comparan los resultados dados por tres de ellos: algoritmos genéticos, algoritmo de enjambre de partículas y algoritmo *harmony search*. Los resultados avalan a éste último como el más eficiente. Además, también se comparan los dos enfoques del problema de optimización, con funciones de un único objetivo o multiobjetivo, siendo el segundo enfoque el que presenta mejor precisión y menor coste computacional.

Las dos propuestas de esta tesis están basadas en el algoritmo *harmony search* multiobjetivo. El primero consiste en un algoritmo híbrido que resulta de la combinación de éste con un algoritmo local llamado *unscented Kalman filter*. Su validación se lleva a cabo mediante la actualización del modelo de elementos finitos de una pasarela de laboratorio y también se aplica para la estimación de los parámetros del modelo dinámico de Winkler de una pasarela real. El segundo algoritmo consiste en un proceso colaborativo donde se unifica el algoritmo *harmony search* con dos técnicas: el análisis de componentes principales y las redes neuronales. Este proceso permite no solo reducir el tiempo de simulación, sino también resolver el problema de toma de decisiones de manera automática. La validación se lleva a cabo mediante la actualización del modelo de una pasarela, comparando los resultados con los que se obtendrían empleando técnicas convencionales.

Abstract

Parameter estimation of dynamic systems in civil engineering is a relevant field in constant evolution, because of its wide variety of applications. The procedure consists in inferring the parameters from the knowledge of a set of inputs and outputs of the system. The main application in civil engineering is the finite element model updating. The objective is to estimate their parameters from the real behaviour of the structure to obtain more accurate models. These problems can be addressed using point estimators, Bayesian approach or fuzzy logic. In this thesis the first method is used, where parameter estimation is solved as an optimization problem to find the minimum of an error function.

Due to both their independence on the initial value adopted for the parameters and ability to avoid local minima when searching for the global minimum, metaheuristic algorithms are mainly used. Nevertheless, their main drawback is the high computational cost. For this reason, this thesis proposes two efficient algorithms. In the first part of the thesis, three algorithms (genetic, particle swarm and harmony search) are compared when they are applied for the finite element model updating of civil engineering structures. The results report that the harmony search is the most efficient. Besides, the single-objective and multi-objective approaches of the optimization problem are compared, concluding that the later leads to more accurate solutions while elapsing less computational time. Hence, the two proposed algorithms are based on the multi-objective harmony search.

The first one is a hybrid algorithm that combines this algorithm with the unscented Kalman filter. The implementation details of the algorithm are discussed and its validation is addressed through the finite element model updating of a laboratory footbridge. A second application involving the parameter estimation of the dynamic Winkler model of a real footbridge is also addressed in order to illustrate the potential of this new algorithm. The second algorithm is built as a collaborative process, where the harmony search is combined with principal component analysis and artificial neural networks. This process allows reducing the computatinal cost and solving the decision making problem in a systematic way. It is validated by conducting the finite element model updating of a footbridge, and further comparing the results with those obtained with a conventional methodology.

Índice

Índice de Figuras

Índice de Tablas

1 Introducción

1.1 Antecedentes

Los sistemas dinámicos se encuentran presentes en la práctica totalidad de ámbitos de la vida real, desde sistemas mecánicos y eléctricos hasta los sistemas biológicos. Conocer el comportamiento de dichos sistemas es crucial y los modelos, ya sean analíticos o numéricos, representan uno de los modos más frecuentes de simularlos. No obstante, los sistemas presentan propiedades desconocidas o inciertas que deben ser asumidas cuando se diseña el modelo. Por tanto, los modelos solo quedan bien definidos cuando los parámetros que lo caracterizan son calibrados, es decir, adoptan un valor que presenta la menor incertidumbre posible.

Para definir los parámetros hay que resolver un problema de estimación de parámetros a partir del conocimiento de las entradas y salidas del sistema dinámico. Tal y como se ilustra en la Figura 1.1, la idea principal de estos problemas es minimizar el error (definido previamente) entre las salidas que el modelo ofrece, $\hat{y}$, y las medidas (salidas del sistema dinámico) registradas experimentalmente, z, mediante la modificación de los parámetros del modelo. Las fuentes de error, como el ruido en las medidas, pueden incluirse en el análisis. El constante avance que desarrolló la ingeniería informática en el último tercio del siglo pasado trajo consigo la aparición de nuevos algoritmos que permitían estimar los parámetros de modelos cada vez más complejos, siendo la mayor parte aplicados a problemas de ingeniería aeronáutica donde los parámetros de la aeronave se estiman a partir de los datos registrados durante el vuelo [61, 62].

En el ámbito de la ingeniería civil, la estimación de parámetros se ha aplicado de manera más reciente al caso particular de la actualización de modelos de elementos finitos (EF). Para modelizar las estructuras civiles se recurre a modelos numéricos, como los modelos de elementos finitos, que se definen a partir de parámetros mecánicos y geométricos que pueden presentar incertidumbre. Es en este aspecto donde el problema de estimación de parámetros permite definir los parámetros del modelo a partir del comportamiento realmente observado de la estructura. En el caso de estructuras se recurre habitualmente a los datos obtenidos en ensayos de vibración, como las propiedades modales, las funciones de respuesta en frecuencia o las historias temporales de aceleración [81, 102].
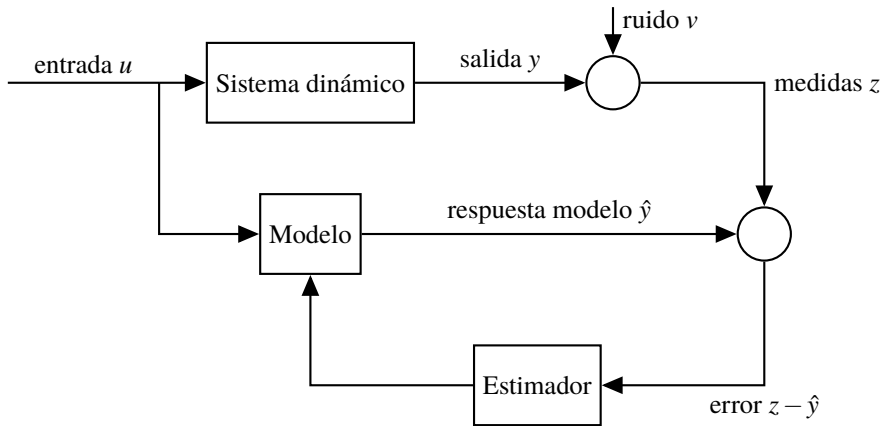
Figura 1.1 Diagrama general del proceso de estimación de parámetros.

Tener un modelo de EF que represente mejor el comportamiento real de la estructura hace de la actualización de modelos una herramienta esencial para diversas aplicaciones. Una de las aplicaciones más fundamentales es la de evaluación estructural, como por ejemplo validar el diseño u obtener predicciones más acertadas de las respuesta de la estructura. En los últimos años, la actualización de modelos de EF ha suscitado un mayor interés debido a su aplicación en la monitorización de la salud estructural (SHM *Structural Health Monitoring*). La idea principal es asociar el daño con una reducción de la rigidez, por lo que representa una solución no invasiva para evaluar la integridad de cualquier estructura [17, 10]. El plantamiento del SHM puede resumirse en cuatro etapas: detección del daño, localización del daño, cuantificación del daño y pronóstico de la vida en servicio restante de la estructura. La actualización de modelos de EF permite directamente la evaluación del daño hasta el tercer paso, lo que demuestra su gran utilidad en problemas de ingeniería civil. Además, los modelos actualizados pueden servir para simular la evolución del daño y evaluar la vida útil. Numerosos autores han realizado una evaluación del daño en estructuras aplicando la actualización de modelos [111, 104, 31, 5].

1.2 Estado del arte

La estimación de parámetros de modelos de sistemas dinámicos puede abordarse desde dos metodologías diferentes: métodos directos y métodos iterativos. Los métodos directos obtienen las matrices de masa y rigidez del modelo a partir de las ecuaciones que gobiernan el sistema. De este modo, permiten obtener los parámetros en un único paso reproduciendo directamente los resultados experimentales. No obstante, esta metodología presenta dos limitaciones principales. En primer lugar, los parámetros se estiman sin criterio físico pudiendo dar lugar a pérdida de conectividad de los nodos del modelo de EF. Segundo, las matrices del sistema pueden perder sus características intrínsecas, es decir, dejar de ser simétricas y definidas positiva. Por otro lado, los métodos iterativos calculan valores actualizados de los parámetros del modelo con el objetivo de reducir las diferencias entre

la respuesta del sistema y las salidas del modelo en cada iteración. A diferencia de lo que sucede en los métodos directos, las matrices del sistema preservan sus características. Sin embargo, el número de iteraciones puede llegar a ser muy elevado, lo que hace que sean menos eficientes en términos de tiempo de computación y, además, que puedan tener problemas de convergencia. A continuación se detallan algunas de las principales investigaciones de ambos métodos.

Las primeras aplicaciones vinieron de la mano de Baruch y Bar-Itzhack en 1978 [8] cuando actualizaron la matriz de rigidez asumiendo que la matriz de masa no presentaba incertidumbre. Más adelante Berman [12] siguió el enfoque matemático de Baruch para formular un método directo que actualizase la matriz de masa. Estas primeras técnicas se conocen con el nombre de técnicas de referencia ya que una de las tres variables (autovectores, matriz de masa y matriz de rigidez) se toma como referencia mientras las otras dos se actualizan. No fue hasta 1983 cuando Berman y Nagy [13] propusieron un método combinado para actualizar la matriz de rigidez y de masa de manera secuencial. Una aplicación de este método se puede encontrar en [7] para el diseño de una máquina perforadora. Las investigaciones más actuales se orientan al desarrollo de técnicas directas cuyo objetivo es reducir las discrepancias entre las respuestas numéricas y experimentales, pero ajustando las propiedades físicas del modelo numérico. Hu et al. [44] propusieron el método CMCM (*cross-model-cross-mode*), en el que se ajustan las propiedades físicas del modelo para actualizar las matrices de masa y rigidez simultáneamente. Otros enfoques de este tipo son el SEA (*substructure energy approach*) [26] o el método probabilístico directo de Jacquelin et al. [47].

Los métodos iterativos se originaron hacia 1974 cuando Collins et al. [20] desarrollaron una metodología conocida como IESM (*Inverse Eigensensitivity Method*). Ésta usaba los autovalores, autovectores y factores de amortiguamiento modal para definir una función de error a minimizar en cada iteración. La identificación de estas propiedades modales podía acarrear ciertos errores, que se transmitían luego a la estimación de los parámetros. Por ello, Lin y Ewins [66] propusieron un nuevo enfoque denominado RFM (*Response Function Method*) en el que el error resultaba de la comparación entre las funciones de respuesta en frecuencia experimentales y numéricas, evitando los errores asociados a la extracción de las propiedades modales. La eficiencia de estos dos enfoques se comparan en las Referencias [46] y [79]. La técnica RFM demuestra un mejor rendimiento para los casos en los que los datos experimentales son incompletos, sin embargo, la técnica IESM es más adecuada cuando las medidas contienen mayor ruido. En la década de 1990 surgió la actualización de modelos de EF de la mano de Friswell y Mottershead [81, 30]. Este nuevo planteamiento trata el problema como una actualización de los parámetros que caracterizan el modelo resolviendo un problema de optimización de una función objetivo. Los primeros métodos empleados para resolver estos problemas de optimización presentaban problemas de convergencia, quedándose, en algunas ocasiones, en mínimos locales. En ese momento se recurrió al uso de algoritmos de optimización global como *Simulated Annealing*, Algoritmos Genéticos o Algoritmo de Enjambre de Partículas. En el Capítulo 2 se describen con mayor detalle estos algoritmos y sus aplicaciones. Para el caso de ingeniería civil, Brownjohn et al. [18] realizan una revisión completa del proceso de actualización del modelo de EF de puentes.

Las tendencias más actuales en materia de estimación de parámetros de sistemas dinámicos persiguen reducir el alto coste computacional que conllevan los métodos iterativos. En este contexto, la reducción de los grados de libertad del modelo numérico a actualizar juega un papel determinante. Por ello, las técnicas conocidas como *substructuring model* y más recientemente *surrogate model* reciben especial atención. En la primera de ellas, una estructura global se divide de manera racional en subestructuras que se analizan independientemente. El análisis de estos componentes estructurales ejecutada de manera adecuada tiene ventajas sobre los métodos globales que manejan el problema completo. En primer lugar, las subestructuras se analizan de forma más eficiente. En segundo lugar, los comportamientos o parámetros locales pueden ser identificados de manera más precisa debido a su menor incertidumbre dando lugar a una convergencia más rápida. Finalmente, la paralelización de los cálculos de distintas subestructuras ayuda a reducir significativamente el tiempo de computación. En la Referencia [112] se puede encontrar una revisión sobre esta técnica aplicada a la actualización de modelos e identificación de daño de estructuras de gran escala. Sin embargo, esta técnica carece de un planteamiento sistemático que sirva de guía para realizar la subestructuración, pudiendo afectar al valor final de los parámetros estimados. Para solventar esta limitación se propuso el uso de *surrogate models* que imitan el comportamiento del sistema pero que tienen un menor coste computacional. Estos modelos se construyen utilizando un enfoque basado en datos mediante análisis de regresión para establecer una función explícita que modele la relación entre la respuesta estructural y los parámetros del modelo. Algunos de los *surrogate models* más empleados son: modelo de *kriging* [113], *response surfaces* [93] y redes neuronales [88]. Estas dos técnicas fueron combinadas por Shan et al. [98] para aplicarlo en la actualización del modelo de un puente colgante. A pesar de que los *surrogate model* pueden simplificar el proceso de actualización de modelos de EF complejos, presenta algunas limitaciones [65]. En primer lugar, debido a que los datos empleados para llevar a cabo la simplificación son limitados, la precisión del *surrogate model* solo puede garantizarse para el entorno más cercano de los datos proporcionados. En segundo lugar, para que el *surrogate model* sea apropiado, se requiere un elevado número de análisis numéricos del modelo de EF original para generar suficientes puntos de muestreo. Por último, si la simplificación no es adecuada o el modelo de EF original es muy complejo, puede no converger o converger a un óptimo local. Por estos motivos, en el caso de modelos de EF complejos la tendencia actual es obtener, a través de la actualización del modelo, un modelo preciso y de alta fidelidad. Para ello, no se realiza ninguna simplificación y la estructura se modeliza de forma completa. De esta forma se reduce la incertidumbre y el número de parámetros a actualizar y con ello, el número de iteraciones que requieren los algoritmos. Para evitar elevados tiempo de simulación, se recurre a técnicas de paralelización en el cálculo o servidores de cálculo. Lin et al. [65] realizaron la actualización del modelo de EF completo formado por más de 16000 elementos de un puente atirantado de gran vano.

Otra alternativa que persigue reducir el coste computacional consiste en implementar algoritmos de optimización híbridos, es decir, que combinen dos o más algoritmos en uno mismo. Uno de las primeras investigaciones sobre algoritmos híbridos para la actualización de modelos de EF fue llevada a cabo por Teughels et al. en 2003 [103]. Los autores propusieron un método de optimización global basado en el acoplamiento de múltiples minimizadores locales y lo aplicaron para la actualización del modelo de EF de una viga

de hormigón armado con el objetivo de identificar el daño.

Los modelos se definen mediante numerosos parámetros. Si se tomaran todos como parámetros a estimar resultaría en un problema excesivamente complejo. Además, se podría incurrir en un mal condicionamiento del problema o una convergencia en un óptimo local. Para seleccionar e identificar únicamente un conjunto reducido de parámetros influyentes se han desarrollado distintas propuestas. Ya en 1968, Fox y Kapoor [29] propusieron una manera de identificar aquellos parámetros que más relevancia tienen en la respuesta de un modelo, a través de su influencia en la energía de deformación modal. Fissette et al. [28] desarrollaron un método de balance de fuerzas para localizar el error y actualizar solo los parámetros de esas regiones con errores en la modelización. Recientemente, Kim y Park [60] desarrollaron un procedimiento automático de selección de parámetros consistente en dos fases. El proceso se basa en ir agrupando los parámetros vecinos para los que la sensibilidad de la respuesta con respecto a ellos es del mismo signo, hasta que todos los conjuntos vecinos tienen sensibilidad de signo contrario. Este método fue validado y comparado con el de Fissette et al. para una actualización de modelo de elementos finitos [60].

Una última consideración sobre los parámetros concierne a su variabilidad dentro del sistema, es decir, no tienen un único valor discreto. En la Referencia [2] se expresan los parámetros de actualización como variables aleatorias espacialmente correlacionadas. Esta naturaleza estocástica de los parámetros se considera en la Referencia [72] que fue ampliada más adelante por Mottershead et al. [82]. El enfoque estocástico de la estimación de parámetros se basa en modelos probabilísticos o en lógica difusa. En el Capítulo 2 se puede encontrar asimismo mayor información sobre estos métodos.

1.3 Motivación

La actualización de modelos de EF, teniendo en cuenta el continuo avance en SHM y la importancia de la evaluación estructural con modelos más precisos, hacen que la estimación de parámetros esté en constante desarrollo. Sin embargo, a pesar de los esfuerzos realizados en los años anteriores, uno de los mayores inconvenientes sigue siendo el elevado tiempo de computación que requieren. Realmente los métodos iterativos, ya sean con enfoques deterministas o probabilísticos, conllevan un elevado número de iteraciones y por ello se ha recurrido a la simplificación de los modelos a través de las técnicas de *surrogate models* y subestructuración.

Por estos motivos, esta tesis surge con el objetivo de desarrollar e implementar nuevas técnicas de optimización eficientes para la estimación de parámetros que a la vez que permitan reducir el tiempo de simulación también presenten otras virtudes respecto a los algoritmos convencionales, como la reducción del error. De este modo, estas propuestas no contemplan la necesidad de simplificar los modelos ya que el objetivo se focaliza en los algoritmos únicamente.

1.4   Objetivos de la tesis

Debido al elevado tiempo de simulación comentado anteriormente, el objetivo principal de esta tesis es desarrollar nuevas técnicas eficientes para resolver problemas de estimación de parámetros en ingeniería civil.

Para lograr dicho objetivo se hace necesario realizar diversos análisis sobre las técnicas de optimización. Estos análisis se basan en las dos actividades siguientes:

- Análisis comparativo de algoritmos de optimización empleados para la estimación de parámetros.
- Comparación de los dos enfoques que pueden seguirse para definir el problema de optimización cuando se realiza la estimación de parámetros de modelos de EF: consideración de una función con un único objetivo o de una función multiobjetivo.

Para alcanzar el anterior objetivo principal se pueden definir los dos siguientes objetivos específicos:

- Desarrollo de un algoritmo híbrido que permita resolver de manera eficiente el problema de estimación de parámetros teniendo en consideración los errores que pueden aparecer a lo largo del proceso.
- Desarrollo de un algoritmo colaborativo que resuelva eficientemente la identificación de parámetros y el problema de toma de decisiones en un enfoque multiobjetivo de manera sistemática.

1.5   Publicaciones relacionadas con la tesis

En este apartado se recogen las publicaciones que suponen el cuerpo de esta tesis así como aquellas publicaciones que están parcialmente relacionadas con la misma.

1.5.1   Artículos en revistas internacionales

Naranjo-Pérez J, Jiménez-Manfredi J, Jiménez-Alonso JF, Sáez A. Motion-Based Design of Passive Damping Devices to Mitigate Wind-Induced Vibrations in Stay Cables. *Vibration*. 2018; 1(2):269-289.

Naranjo-Pérez, J., Jiménez-Alonso, J. F., García-Sanchez, F., Sáez, A. Modal parameter identification of a spectator–grandstand interaction model under different rhythmic activities. *Advances in Structural Engineering*. 2019; 22(9): 2061–2075.

Naranjo-Pérez J., Jiménez-Alonso J.F., M. Díaz I., Quaranta G., Sáez A. Motion-Based Design of Passive Damping Systems to Reduce Wind-Induced Vibrations of Stay Cables under Uncertainty Conditions. *Applied Sciences*. 2020; 10(5): 1740.

Naranjo-Pérez, J., Jiménez-Alonso, J. F., Pavic, A., Sáez, A. Finite-element model updating of civil engineering structures using a hybrid UKF-HS algorithm. *Structure and Infraestructure Engineering*. 2020.

Naranjo-Pérez, J., Jiménez-Alonso, J. F., Sáez, A. Parameter identification of the dynamic Winkler soil-structure interaction model using a hybrid UKF-MHS algorithm. *Advances in Structural Engineering*. 2020.

Jiménez-Alonso, J. F., Naranjo-Pérez, J., Pavic, A., Sáez, A. Maximum likelihood finite-element model updating of civil engineering structures using nature-inspired computational algorithms. *Structural Engineering International*. 2020. (*Accepted*).

Naranjo-Pérez, J., Infantes, M., Jiménez-Alonso, J.F., A. Sáez. A collaborative machine learning-optimization algorithm to improve the finite element model updating of civil engineering structures. Submitted for publication.

1.5.2   Artículos en congresos

Infantes M, Naranjo-Pérez J, Jiménez-Alonso JF, Sáez A (2019). Determining the Best Pareto-solution in a Multi-Objective Approach for Model Updating. IABSE Symposium, Guimaraes 2019: Towards a Resilient Built Environment Risk and Asset Management – Report pp. 523-530.

Naranjo-Pérez, J., Sáez, A., Jiménez-Alonso, J.F., Pachón, P., Compán, V. (2019). A hybrid UKF-MGA algorithm for finite element model updating of historical constructions. IABSE Symposium, Guimaraes 2019: Towards a Resilient Built Environment Risk and Asset Management – Report pp. 29-36.

Naranjo-Pérez, J., Sáez, A., Jiménez-Alonso, J.F., González-Gómez, N., García-Sánchez, F. (2019). Finite element model updating of a grandstand as basis to assess its vibration serviceability limit state. IABSE Symposium, Guimaraes 2019: Towards a Resilient Built Environment Risk and Asset Management – Report pp. 745-751.

Jiménez-Alonso, J.F., Naranjo-Perez, J., Díaz, I.M., Sáez, A. (2019). Motion-based design of vibrating civil engineering structures under uncertainty conditions, Proceedings of the International fib Symposium on Conceptual Design of Structures pp. 263-270

Naranjo-Pérez, J., Jiménez-Alonso, J.F., Díaz, I.M., Sáez, A. Motion-based design of viscous dampers for cable-stayed bridges under uncertainty conditions. In Proceedings of the 5th International Conference on Mechanical Models in Structural Engineering, CMMoST 2019, Alicante.

1.6   Organización del texto

El documento de esta tesis se compone de cinco capítulos que contienen los fundamentos principales de la estimación de parámetros, las metodologías propuestas y validadas y seis apéndices donde se recogen los artículos publicados que constituyen el cuerpo de la tesis. Cada capítulo se resume de la siguiente manera.

El **Capítulo 2** presenta el problema de la estimación de parámetros así como los tipos de algoritmos que se emplean para ello. Se finaliza con una comparación entre algoritmos cuando se emplean para la actualización del modelo de elementos finitos de una pasarela de laboratorio.

En el **Capítulo 3** se introduce un nuevo algoritmo híbrido eficiente basado en dos algoritmos, uno global y otro local, donde no se ignoran los errores que hay presentes en el problema. Se incluyen dos aplicaciones del algoritmo a problemas reales.

El **Capítulo 4** propone un nuevo algoritmo colaborativo que permite reducir el tiempo de computación así como resolver el problema de toma de decisiones que se da en optimización multiobjetivo de manera sistemática.

El **Capítulo 5** cierra la tesis incluyendo las principales conclusiones y con una discusión de los trabajos futuros.

El **Apéndice A** contiene al artículo "Jiménez-Alonso, J. F., Naranjo-Pérez, J., Pavic, A., Sáez, A. (2020). Maximum likelihood finite-element model updating of civil engineering structures using nature-inspired computational algorithms".

El **Apéndice B** contiene al artículo "J. Naranjo-Pérez, J.F. Jiménez-Alonso, P. Pachón, V. Compán, A. Sáez (2019). A hybrid UKF-MGA algorithm for finite element model updating of historical constructions".

El **Apéndice C** contiene al artículo "J. Naranjo-Pérez, J.F. Jiménez-Alonso, A. Pavic, A. Sáez (2020). Finite element model updating of civil engineering structures using a hybrid UKF-HS algorithm".

El **Apéndice D** contiene al artículo "J. Naranjo-Pérez, J.F. Jiménez-Alonso, A. Sáez (2020). Parameter identification of the dynamic Winkler soil-structure interaction model using a hybrid UKF-MHS algorithm".

El **Apéndice E** contiene al artículo "M. Infantes, J. Naranjo-Pérez, J.F. Jiménez-Alonso, A. Sáez (2019). Determining the best Pareto-solution in a multi-objective approach for model updating".

El **Apéndice F** contiene al artículo "J. Naranjo-Pérez, M. Infantes, J.F. Jiménez-Alonso, A. Sáez (2020). A collaborative machine learning-optimization algorithm to improve the finite element model updating of civil engineering structures".

El **Apéndice G** contiene al artículo "J. Naranjo-Pérez, J.F. Jiménez-Alonso, I. Díaz M., G. Quaranta, A. Sáez (2020). Motion-Based Design of Passive Damping Systems to Reduce Wind-Induced Vibrations of Stay Cables under Uncertainty Conditions.

2 Estimación de parámetros a través de problema inverso

Cuando el problema de estimación de los parámetros de un modelo se lleva a cabo a partir de medidas o datos observados se le conoce como problema inverso. Este tipo de problemas puede plantearse según tres métodos: métodos basados en teoría de conjuntos difusos, el método Bayesiano (estimadores de intervalo) o usando estimadores puntuales. Los tres se resuelven de manera iterativa recurriendo a algoritmos de optimización. El presente capítulo pretende arrojar luz sobre los algoritmos que presentan mejor rendimiento para resolver problemas de ingeniería civil.

En este sentido, el capítulo se estructura de la siguiente manera. En primer lugar se describen los enfoques del problema inverso, haciendo hincapié en los dos estimadores que se usan en esta tesis, el estimador de máxima verosimilitud y el filtro de Kalman. Seguidamente, se exponen los distintos tipos de algoritmos de optimización basados en métodos metaheurísticos, describiendo con mayor detalle los tres que se emplean en los siguientes capítulos.

Finalmente se realiza un estudio comparativo de los tres algoritmos descritos y de los dos planteamientos que puede adoptar el problema, único objetivo o multiobjetivo, mediante la aplicación a un problema de actualización de modelo de EF de una pasarela de laboratorio.

Partes de este capítulo han sido publicado en el Artículo del Apéndice A.

2.1 Enfoques del problema inverso

Un problema inverso se define como aquel donde los parámetros de un modelo o sistema se derivan a partir de los datos observados o medidas. La variación de los valores de los parámetros provoca un cambio en la salida del sistema, por lo que de esta manera, el problema consiste en obtener aquellos valores de los parámetros que proporcionen valores de la salida del sistema más cercanos a los datos observados.

Existen tres principales enfoques a la hora de resolver un problema de estimación de parámetros resolviendo un problema inverso: aplicando teoría de conjuntos difusos, aplicando métodos Bayesianos o aplicando estimadores puntuales.

En el enfoque de la teoría difusa, la incertidumbre en el valor de los parámetros se trata de manera no probabilística, lo que es especialmente apropiado para modelizar incertidumbre sistemática (no aleatoria). La mayoría de los métodos no probabilísticos se basan en el análisis por intervalos, donde la incertidumbre de los parámetros se representa por un determinado rango de valores acotado. La teoría difusa fue propuesta en 1965 por Zadeh [116] con el objetivo de extender los operadores lógicos clásicos a un marco conceptual donde tratar la incertidumbre no probabilística. La idea de este planteamiento es dar un grado de pertenencia haciendo que el rango de valores de pertenencia de un elemento a un conjunto pueda variar en el intervalo [0,1] en lugar de seguir la lógica clásica, es decir, tomar el valor 0 o 1. Es un método muy adecuado para tratar la incertidumbre en situaciones donde, además de los límites de los intervalos, se dispone de valores de referencia de los parámetros a estimar.

La teoría difusa ha sido aplicada a varios problemas de ingeniería estructural como, por ejemplo, dinámica estructural [1], análisis de fiabilidad [97], actualización de modelos de EF [59] o diseño estructural [77].

Los métodos Bayesianos, que permiten conocer la función de distribución de los parámetros, están basados en el teorema de Bayes, que puede formularse para la identificación de parámetros como [76]:

$$P(\boldsymbol{\theta}|\mathscr{D}) = \frac{P(\mathscr{D}|\boldsymbol{\theta})(P(\boldsymbol{\theta})}{P(\mathscr{D})} \tag{2.1}$$

donde $\boldsymbol{\theta}$ representa el vector de parámetros a identificar y $\mathscr{D}$ es el vector que recoge los datos observados. Por tanto, cada término de la ecuación se define del siguiente modo: $P(\boldsymbol{\theta}|\mathscr{D})$ es la función de densidad de probabilidad posterior de los parámetros condicionada por el valor de los datos observados, $P(\mathscr{D}|\boldsymbol{\theta})$ es la función de verosimilitud de los datos condicionada por el valor de los parámetros, $P(\boldsymbol{\theta})$ es la función de densidad de probabilidad anterior, es decir, en ausencia de los datos observados y $P(\mathscr{D})$ es un factor de normalización. La esperanza posterior condicionada de una función $f(\boldsymbol{\theta})$ se calcula como:

$$E[f(\boldsymbol{\theta})|\mathscr{D}] = \frac{\int f(\boldsymbol{\theta})P(\mathscr{D}|\boldsymbol{\theta})P(\boldsymbol{\theta})\,\mathrm{d}\boldsymbol{\theta}}{P(\mathscr{D})}. \tag{2.2}$$

Resolver la Ecuación 2.2 analíticamente puede no ser posible para sistemas complejos ya que la integral depende de la función de densidad de probabilidad posterior. Para salvar esta limitación, existen varias alternativas que permiten obtener una aproximación de la solución de la ecuación.

La primera alternativa consiste en resolverla mediante evaluaciones numéricas, utilizando por ejemplo el método de aproximación asintótica, el cual considera una aproximación gaussiana de la función de densidad de probabilidad posterior. Sin embargo, si el tamaño de la función de densidad es grande este método no es preciso [11].

La segunda alternativa la constituyen las aproximaciones analíticas, como las aproximaciones de máxima verosimilitud, máximo a posteriori y de Laplace. El inconveniente de

estos métodos es su carácter local, por lo que la convergencia puede no ser a un mínimo global.

Finalmente, las técnicas de muestreo, como los métodos de Monte Carlo basados en cadenas de Markov, son las más empleadas ya que dan como resultado una mejor aproximación para funciones complejas [9]. A continuación se esbozarán solo brevemente las técnicas de muestreo más comunes para la identificación de parámetros en ingeniería civil.

Los métodos de Monte Carlo tratan de estimar la distribución de probabilidad mediante repeticiones aleatorias de muestreo [94]. El proceso comienza por crear de manera aleatoria muestras de los parámetros a partir de la función de distribución posterior. Esta nueva muestra es aceptada o rechazada al azar y se repite iterativamente hasta que el número de muestras ha alcanzado un valor prefijado. El valor medio de la función de distribución se calcula a partir del conjunto de muestras aceptadas.

El método de Monte Carlo basado en cadenas de Markov es una técnica en la cual la función de distribución de probabilidad se identifica mediante una cadena de Markov. En este sentido, se asume que la evolución del sistema se caracteriza a través de un proceso estocástico de variables aleatorias (cuyo dominio forman el espacio estado), $\mathbf{K}_i$, donde cada variable es un vector que contiene los parámetros a identificar. Como las variables aleatorias forman una cadena de Markov, la probabilidad de que el sistema esté en un estado $\mathbf{K}_n$ en un tiempo n depende únicamente de que el sistema estuviera en un estado $\mathbf{X}_{n-1}$ en el tiempo $n-1$. El estado actual se acepta o rechaza aplicando el algoritmo Metropolis.

Para llevar a cabo una simulación de Monte Carlo basada en cadenas de Markov existen diferentes algoritmos, como el algoritmo Metropolis-Hastings, el algoritmo *Slice Sampling* o el algoritmo Metropolis-Hastings adaptativo [76].

Los métodos Bayesianos requieren, en general, de un tiempo de computación excesivamente alto para calcular la función de distribución de los parámetros. Además, el cálculo de la media de los parámetros no es muy preciso, por lo que debe calcularse previamente usando estimadores para asegurar que la función de distribución sea adecuada al problema. Este segundo enfoque mediante estimadores puntuales es en el que se basa la presente tesis.

Uno de los aspectos fundamentales de los estimadores puntuales es el método para definir el error que se considere [92]. El primer método es el de error de ecuación (*equation error*), donde el error es la diferencia entre la medida y la salida obtenida por la ecuación del modelo con los valores de los parámetros estimados. La función de coste es lineal en los parámetros. El segundo método es el de error en la salida (*output error*), donde el error es la diferencia entre la salida del modelo y la medida del sistema real. Para la aplicación de este método, la entrada al modelo y al sistema debe ser la misma. Finalmente, el método de error de parámetros (*parameter error*) se define como la diferencia entre los valores estimados de los parámetros y sus valores reales. De este modo, el error de parámetro sólo puede ser obtenido si el valor real es conocido, lo que limita su aplicación para problemas reales.

Entre los estimadores más comunes se encuentran el estimador de mínimos cuadrados, el estimador de máxima verosimilitud y los filtros de Kalman.

El estimador de mínimos cuadrados se basa en un modelo de ecuación de la medida que toma la siguiente forma:

$$\mathbf{z} = \mathbf{y} + \mathbf{v} = \mathbf{X}\boldsymbol{\theta} + \mathbf{v} \qquad (2.3)$$

siendo $\mathbf{z}$ el vector que recoge las medidas, $\mathbf{y}$ las salidas del modelo, $\mathbf{v}$ un vector que representa el ruido/error en las medidas, que se asume como gaussiano y con media cero, $\boldsymbol{\theta}$ el vector de parámetros y $\mathbf{X}$ una matriz que contiene las variables explicativas del problema, las cuales representan el comportamiento del modelo y son perfectamente conocidas. El objetivo del estimador de mínimos cuadrados es encontrar el valor de los parámetros que minimice la función de coste, J, definida como la suma de los errores al cuadrado entre las medidas y las predicciones del modelo:

$$J \cong \sum_{j=1}^{M} v_j^2 = (\mathbf{z} - \mathbf{X}\boldsymbol{\theta})^T (\mathbf{z} - \mathbf{X}\boldsymbol{\theta}) \qquad (2.4)$$

donde M es el número de medidas. La minimización con respecto a $\boldsymbol{\theta}$ de la función J conduce a una expresión analítica de la estimación de mínimos cuadrados de $\boldsymbol{\theta}$: $\hat{\boldsymbol{\theta}} = (\mathbf{X}^T\mathbf{X})^{-1}\mathbf{X}^T\mathbf{z}$. Por consiguiente, como el vector de medidas $\mathbf{z}$ y la matriz $\mathbf{H}$ son conocidos, las estimaciones se obtienen de manera directa. El estimador de mínimos cuadrados presenta tres propiedades principales. La primera es que la estimación $\hat{\boldsymbol{\theta}}$ es una función lineal del vector de medidas $\mathbf{z}$. La segunda es que el error en el estimador, $\boldsymbol{\theta} - \hat{\boldsymbol{\theta}}$, es una función lineal de los errores en las medidas $\mathbf{v}$. La tercera es que si la esperanza matemática del error en las medidas $\mathbf{v}$ es cero, la estimación $\hat{\boldsymbol{\theta}}$ es no sesgada ya que la esperanza del error en la estimación, $E[\boldsymbol{\theta} - \hat{\boldsymbol{\theta}}]$, también es nula. Por tanto, si $\mathbf{z} = \mathbf{y}$, $\hat{\boldsymbol{\theta}}$ es una cantidad determinista igual a $\boldsymbol{\theta}$. No obstante, en presencia de ruido en la medida la estimación $\hat{\boldsymbol{\theta}}$ es sesgada y el estimador de mínimos cuadrados es empleado como punto de partida para otros métodos de estimación como el estimador de mínimos cuadrados generalizado o el método de error en la salida basado en el estimador de máxima verosimilitud. El método de mínimos cuadrados generalizado, también llamado mínimos cuadrados ponderado, consiste en incluir una matriz de peso simétrica y definida positiva en la definición de la función J que sirve para controlar la influencia de medidas específicas en las estimaciones de los parámetros. El estimador de mínimos cuadrados puede aplicarse para sistemas no lineales asumiendo que las salidas del modelo (también no lineal) adopta la forma $\mathbf{y} = h(\boldsymbol{\theta})$, donde h es una función no lineal conocida. Para este caso, la estimación $\hat{\boldsymbol{\theta}}$ se obtiene a través de un proceso iterativo.

El estimador de máxima verosimilitud es el caso general del estimador de mínimos cuadrados ya que la estimación es idéntica cuando se trata de un sistema lineal con ruido gaussiano. La idea principal es definir una función de las medidas y de los parámetros, llamada función de verosimilitud, y maximizarla con respecto a los parámetros. La función de verosimilitud representa la densidad de probabilidad de las medidas dados los parámetros. El estimador de máxima verosimilitud puede aplicarse para los métodos de error de ecuación (se considera ruido únicamente en el proceso de estimación) y de error en la salida (se considera ruido únicamente en las medidas). No obstante, para poder considerar ambos ruidos en el problema es necesario recurrir a otras técnicas.

El filtro de Kalman [53] es un método de estimación de parámetros que permite tener

en cuenta ruido en el proceso de estimación y en las medidas. En el caso de sistemas no lineales, la estimación del filtro de Kalman no es óptima y hay que recurrir a variaciones del filtro de Kalman, como el filtro de Kalman extendido (EKF de *Extended Kalman Filter*) [49]. No obstante, su aplicación para estimación de parámetros revela que los resultados son muy sensibles a los valores iniciales de las matrices de covarianza del ruido en las medidas [92].

La otra alternativa consiste en aplicar los denominados métodos de error de filtro, los cuales implementan el filtro de Kalman dentro de la estructura del método de error en la salida basado en el estimador de máxima verosimilitud, de modo que permite manejar ruidos en las medidas y en el proceso de estimación. Esta idea justifica el planteamiento del algoritmo híbrido que se propone en esta tesis. En concreto, se emplea una variante del filtro de Kalman para sistemas no lineales y el estimador de máxima verosimilitud por lo que serán explicados con mayor detalle en los siguientes apartados.

2.2 Filtro de Kalman

El filtro de Kalman es un algoritmo que permite estimar las medias y las covarianzas de los parámetros llevando a cabo un proceso iterativo en el que se reduce la covarianza del error en el proceso de estimación hasta converger en una solución en los parámetros no sesgada.

La representación matemática de un problema de identificación de parámetros se basa en el modelo de espacio de estados donde la Ecuación 2.5 representa el proceso de transición estacionario en la estimación y la Ecuación 2.6 representa la ecuación del modelo:

$$\theta_k = \theta_{k-1} + w_{k-1} \tag{2.5}$$
$$y_k = h(\theta) + v_k \tag{2.6}$$

siendo h una función de modelización, w el ruido en el proceso de estimación y v el ruido en la modelización. Ambos términos de ruido se consideran ruido blanco gaussiano con media cero y matrices de covarianza Q y R, respectivamente. La matriz R presenta dos contribuciones, el ruido en la modelización y el ruido en las medidas.

El filtro de Kalman se basa en un proceso iterativo en el que cada iteración ejecuta dos pasos: predicción y corrección. El primer paso se basa en las estimaciones del paso anterior (Ecuación 2.5) para predecir las estimaciones del paso actual. El segundo paso tiene en cuenta las medidas para corregir las estimaciones de manera que se reduzca la covarianza del error.

Para problemas no lineales se desarrolló el EKF que tiene mejores prestaciones para sistemas ligeramente no lineales. El EKF requiere la linelización de la Ecuación 2.6 (la Ecuación 2.5 ya lo es), por lo que es necesario calcular el Jacobiano de la función de modelización h. Sin embargo, cuando el sistema presenta una fuerte no linealidad, el rendimiento del EKF disminuye. En el caso de que la función h se defina mediante un modelo numérico no hay una expresión analítica para calcular el Jacobiano y hay que aproximarlo numéricamente.

Más recientemente se desarrolló el *Unscented Kalman Filter* (UKF) [52]. Se trata de un algoritmo que no requiere ninguna operación diferencial ya que no hay que linealizar ninguna función [105, 84]. La premisa del UKF es que un conjunto de puntos pueden capturar y propagar la media y covarianza de los parámetros a través de la función *h* para obtener la media y covarianza posterior, que se usan en la siguiente iteración para predecir la media y covarianza anterior. Varios estudios han demostrado que el algoritmo UKF supera al EKF. Mariani y Ghisi los compararon para la calibración de la ley constitutiva de un sistema dinámico de un grado de libertad [73]. Más recientemente, Nguyen y Nestorović compararon estos dos algoritmos para la estimación de parámetros geomecánicos en modelos del suelo para problemas de túneles [85]. Por tanto, en esta tesis se considera el algoritmo UKF para su implementación en problemas de estimación de parámetros.

2.3 Estimador de máxima verosimilitud

El estimador de máxima verosimilitud se basa en la definición de una función, llamada función de verosimilitud, que depende de las medidas experimentales del sistema y de los parámetros del modelo. El objetivo de este estimador es maximizar dicha función, es decir, buscar aquellos parámetros que hacen que de manera más probable la función conduzca a las medidas. Como se dijo anteriormente, la función de verosimilitud es la densidad de probabilidad de las medidas y se calcula para las medidas estadísticamente independientes donde el error se asume que está normalmente distribuido. La densidad de probabilidad conjunta se halla como el producto de las probabilidades de las medidas individuales.

La función de verosimilitud puede escribirse como el logaritmo de la función de densidad de probabilidad ya que esta función y su logaritmo siguen teniendo el máximo en el mismo argumento. Esta función depende del error entre las medidas y las salidas del modelo, asumido como normalmente distribuido, y está definida de manera que la minimización del error conlleve la maximización de la probabilidad, es decir, de la función de verosimilitud. Por tanto, el problema de maximización se reduce a un problema de minimización. A diferencia del estimador de mínimos cuadrados, la estimación no es directa y es necesario realizar un proceso iterativo.

El proceso comienza por realizar una primera estimación de los parámetros y calcular a partir de ellos la salida del modelo. Teniendo en cuenta las medidas y la salida del modelo se evalúa el error y la función objetivo. En la siguiente iteración, los parámetros se actualizan a partir de los parámetros del paso anterior y del valor de la función objetivo. Este proceso continua hasta que se logra la convergencia. Esta metodología puede ser aplicada a sistemas no lineales. Además, el estimador de máxima verosimilitud presenta varias ventajas matemáticas. En primer lugar, la estimación es consistente. Segundo, en diversas condiciones el estimador tiene una distribución asintótica normal. Finalmente, el estimador de máxima verosimilitud es eficiente [92].

Estos motivos justifican su elección para la resolución de problemas de estimación de parámetros. El proceso iterativo puede definirse como un problema de optimización, donde el objetivo es encontrar los valores de los parámetros que optimicen la función, expresado

matemáticamente como:

$$\min f(\boldsymbol{\theta}) \tag{2.7}$$

$$\text{sujeto a: } \boldsymbol{\theta}_l \leq \boldsymbol{\theta} \leq \boldsymbol{\theta}_u \tag{2.8}$$

donde f es la función objetivo a minimizar, $\boldsymbol{\theta}$ es el vector de parámetros a estimar y $\boldsymbol{\theta}_l$ y $\boldsymbol{\theta}_u$ son los límites inferiores y superiores de los parámetros.

Para la ejecución del proceso iterativo se recurre a algoritmos de optimización que solucionen el problema de manera automática [86]. En el siguiente apartado se describirán los principales algoritmos de optimización y su aplicación a los distintos enfoques del problema de estimación de parámetros.

2.4 Algoritmos de optimización

Cuando se elige el algoritmo de optimización hay que considerar el carácter local o global de la solución que obtiene. Un óptimo local es una solución óptima en un entorno próximo, mientras que un óptimo global es la solución óptima de todas las posibles soluciones. Por consiguiente, según sea la función objetivo (o de coste), puede resultar más apropiado elegir un tipo de algoritmo u otro.

Los algoritmos locales convergen a óptimos locales ya que se basan en el gradiente y son los más adecuados cuando la función objetivo tiene forma cóncava/convexa para las que el óptimo local es la solución óptima del problema. Por el contrario, los algoritmos globales permiten hallar óptimos globales y su aplicación es adecuada cuando la función objetivo presenta múltiples mínimos o máximos locales [86].

A la hora de definir la función objetivo que hay que optimizar hay que tener en cuenta los errores residuales entre las salidas del modelo y las medidas. La función objetivo se define a partir de uno o varios residuos según el número de criterios de optimización, asumiendo en este último caso unos factores de peso que representan la influencia de cada residuo (Figura 2.1). A este tipo de planteamiento se le conoce como optimización de un único objetivo. El objetivo de este tipo de planteamiento es sencillo ya que se trata de hallar el valor de los parámetros que encuentre el óptimo de dicha función.

En múltiples casos, no es adecuado o posible unir los residuos en una misma función objetivo. En estos casos se recurre a la optimización multiobjetivo, donde cada función objetivo está definida por un residuo. Para este planteamiento se recurre al concepto de óptimo de Pareto formulado en el siglo XIX. El objetivo de este enfoque es encontrar una solución Pareto-óptima cuando no existe otra solución que mejore un objetivo sin sacrificar al menos uno de los otros. Al conjunto de soluciones que cumplen este criterio se les denomina frente de Pareto o soluciones no dominadas. El resultado de este tipo de problemas es una curva formada por un conjunto de puntos donde cada uno de ellos es una posible solución óptima al problema. Por tanto, para finalizar el problema es necesario elegir el mejor punto mediante técnicas de toma de decisiones (Figura 2.1).

Es preciso remarcar en este punto que el carácter local o global del algoritmo no está directamente relacionado con el enfoque de un único objetivo o multiobjetivo, ya que un
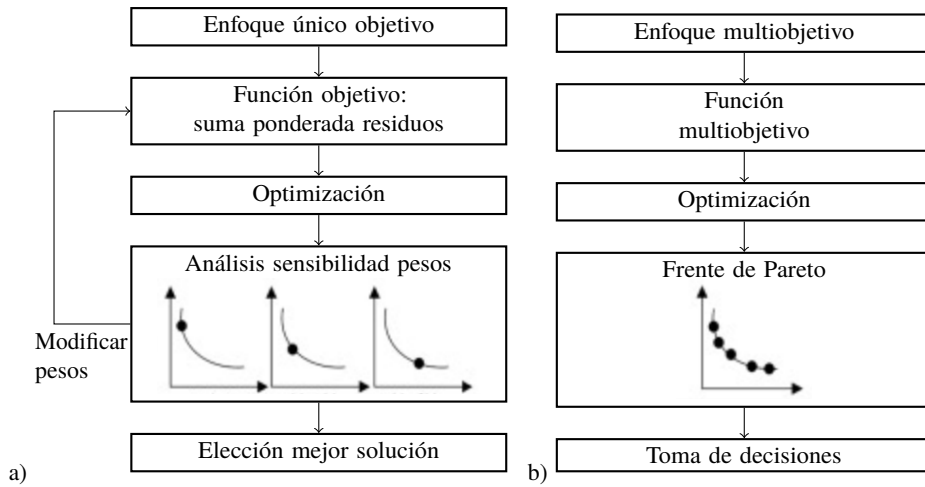
Figura 2.1 Comparación de enfoques: a) un único objetivo y b) multiobjetivo.

único objetivo puede presentar un único óptimo local (también global) o varios óptimos locales.

En el caso de que la relación entre los parámetros y la función objetivo sea no lineal o el espacio de solución sea muy amplio, las técnicas metaheurísticas representan la mejor opción para resolver el problema frente a los algoritmos deterministas convencionales [74]. Son métodos que enfocan el problema desde un punto de vista probabilístico, como el método de Monte Carlo. Los métodos metaheurísticos se basan en criterios que permiten discernir qué alternativa es la más efectiva para logar un objetivo, es decir, qué candidato a solución es el más efectivo para seguir considerándolo en la generación de nuevos candidatos.

Los algoritmos metaheurísticos se pueden clasificar según su estrategia de búsqueda por puntos singulares o basada en poblaciones. Los primeros generan una única solución en cada iteración. Los segundos mantienen un conjunto de candidatos que van evolucionando a raíz de la exploración en el espacio de búsqueda.

Las principales ventajas de este tipo de algoritmos es su independencia del valor inicial de los candidatos (que son estimados aleatoriamente dentro de un rango definido a partir del conocimiento físico del problema) y su habilidad para encontrar el óptimo global. No obstante, presentan un claro inconveniente: el alto tiempo de simulación requerido para resolver el problema de optimización.

Aunque la mayoría de los algoritmos metaheurísticos son algoritmos globales, existen también algoritmos locales como es el caso del algoritmo *Hill Climbing* (escalada simple o escalada de colinas) [39] que comienza por una solución arbitraria y busca encontrar una mejor solución variando incrementalmente un único elemento (parámetro) de la solución. El proceso continua hasta que no se encuentra ninguna solución mejor.

Hay una amplia variedad de algoritmos metaheurísticos globales que han sido usados para aplicaciones de ingeniería civil [107, 114]. Moradi et al. [80] exploraron la eficiencia del algoritmo de colonia de abejas para la resolución de un problema de actualización

del modelo de EF de un sistema de tuberías. Las redes neuronales artificiales también han demostrado su eficiencia para resolver problemas de optimización no lineales [63, 88, 42, 40, 68]. El algoritmo de colonia de hormigas ha sido igualmente usado para problemas de optimización [25]. Los algoritmos genéticos han sido ampliamente usados para aplicaciones de ingeniería, como es el caso de problemas de actualización de modelos o para detección de daño [51, 67, 50]. El algoritmo *Harmony Search*, ideado en 2001 [38], sigue un proceso muy similar a los algoritmos genéticos aunque más simplificado ya que no se basa en poblaciones. Aunque existan múltiples aplicaciones para estimación de parámetros en ingeniería estructural, su uso en problemas de actualización de modelos de EF es escaso [71]. El algoritmo de enjambre de partículas, a diferencia de los algoritmos genéticos, mantiene la misma población la cual va evolucionando durante el proceso iterativo. En [96] se aplica este algoritmo para la actualización del modelo de EF de vigas con el objetivo de identificar el daño. El algoritmo de evolución diferencial puede considerarse como una versión más desarrollada de los algoritmos genéticos donde las ecuaciones de actualización de la población son explícitas. Quaranta et al. [91] emplearon este algoritmo para el diseño óptimo (en términos económicos) de vigas de hormigón pretensadas. El algoritmo *Cuckoo search* es uno de los más recientes. Fue desarrollado por Yang y Deb en 2009 [115] y está basado en el parasitismo de algunas especies de cuco que dejan sus huevos en nidos de otras especies. Gandomi et al. [33] emplearon este algoritmo para el diseño óptimo de estructuras en celosía. El algoritmo *colliding bodies* (cuerpos en colisión) se basa en las leyes de conservación del momento y la energía de una colisión unidimensional [54]. Cada cuerpo posee una masa, posición y velocidad y la colisión con otros cuerpos actualiza la posición de acuerdo a unas leyes de colisión. El algoritmo de búsqueda gravitacional está basado en las leyes de la gravitación de Newton. Este algoritmo ha sido aplicado a una amplia variedad de problemas de optimización, como el diseño óptimo de la forma de presas de gravedad de hormigón [57] o el diseño basado en la fiabilidad de structuras de hormigón reforzado considerando interacción suelo-estructura [58].

Los resultados obtenidos por el algoritmo de enjambre de partículas y el algoritmo genético fueron comparados por Perera et al. [89] para la actualización del modelo de EF de un pórtico de una planta de hormigón armado. Igualmente, Levin y Lieven compararon los resultados entre los algoritmos genéticos y el algoritmo *simulated annealing* para la actualización de un modelo de EF considerando datos simulados [64]. Estos tres algoritmos, enjambre de partículas, genéticos y *simulated annealing*, fueron comparados en un mismo estudio por Marwala, concluyendo que el algoritmo de enjambre de partículas era superior a los otros dos [75].

Para vencer el problema del alto tiempo de simulación requerido, la tendencia actual es usar algoritmos híbridos aprovechando la sinergia del algoritmo resultante. Algunos ejemplos de esta tendencia es la combinación de algoritmo genético y *simulated annealing* propuesto por Feng et al. [27], la combinación del algoritmo *simulated annealing* con el UKF [4] o la combinación del algoritmo de enjambre de partículas con un *surrogate model* [90].

Dentro del amplio abanico de algoritmos de optimización existentes, los algoritmos genéticos constituyen la opción más empleada para resolver problemas de actualización de modelos de EF en problemas prácticos de ingeniería civil. El algoritmo de enjambre de

partículas posee un rendimiento superior a los algoritmos genéticos, de manera que su uso para resolver problemas de estimación de parámtros en casos prácticos ha aumentado en los últimos años. Finalmente, el algoritmo *Harmony Search* se presenta como una buena alternativa por su mayor simplicidad respecto a los dos algoritmos anteriores. Por estos motivos, a continuación se describirán con mayor detalle estos tres algoritmos metaheurísticos.

2.4.1   Algoritmos genéticos

Los algoritmos genéticos (GA) son algoritmos de computación inspirados en la naturaleza, que están basados en el mecanismo de la selección natural de la teoría de la evolución de Darwin. Es en la década de los sesenta cuando se comienzan a emplear como un método evolutivo para la resolución de problemas de optimización [16]. No obstante, no es hasta el final de esa década cuando se produce el mayor avance de estas técnicas de la mano de Holland y de Bagley, siendo éste último quien acuñó por primera vez el término algoritmo genético [6, 43].

Los algoritmos géneticos se basan en un planteamiento probabilístico del problema, cuya capacidad de convergencia a un óptimo global es muy alta ya que realiza la búsqueda por poblaciones. Imitando el mecanismo de la selección natural, los algoritmos genéticos crean nuevas soluciones más evolucionadas, es decir, que mejoran el valor de la función objetivo en cada iteración.

La ejecución de un algoritmo genético sigue los siguientes pasos. En primer lugar se genera una población inicial aleatoriamente, donde cada individuo de la población es un vector de parámetros a estimar y constituye una posible solución al problema. El tamaño de la población depende de la complejidad del problema debiendo garantizarse que represente adecuadamente todo el espacio de soluciones. Para cada uno de los individuos de la población inicial se evalúa la función objetivo. A continuación comienza el proceso iterativo. En cada iteración se selecciona una parte de la población anterior para generar la nueva población. Esta generación hace uso de dos mecanismos: cruce y mutación. El mecanismo de cruce es el que permite crear un nuevo individuo a partir de dos individuos seleccionados previamente. La mutación consiste en modificar algún parámetro aleatorio de algún individuo para explorar nuevas zonas del espacio de búsqueda que quedaban descubiertas por la población anterior. Hay que remarcar que la mutación se produce según una probabilidad dada y no en todas las generaciones. La reproducción prosigue hasta alcanzar un tamaño de la nueva población igual a la inicial. Con la nueva población generada completamente, se vuelve a evaluar la función objetivo para cada uno de los individuos. El bucle se repite iterativamente hasta que se alcanza el criterio de parada. En la Figura 2.2 se muestra el proceso seguido por el GA en forma de diagrama de flujo.

Algoritmo genético multiobjetivo

Fue también a finales de los años sesenta cuando se propuso la aplicación de algoritmos basados en la selección natural para problemas de optimización con más de un objetivo [95]. En esta tesis, el enfoque multiobjetivo del algoritmo genético se implementa a través del algoritmo NSGA-II (*Non-dominated Sorting Genetic Algorithm*) [24]. El algoritmo NSGA-II se basa en el empleo de la técnica de *Non-dominated Sorting* [100] para clasificar las soluciones no dominadas (las que forman el frente de Pareto) de forma eficiente y en
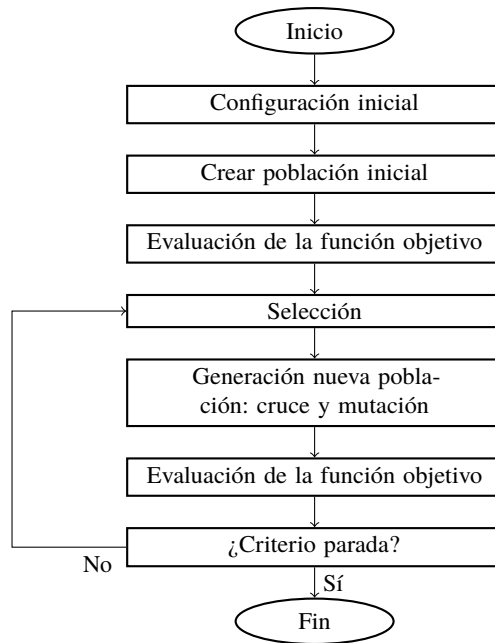
Figura 2.2 Diagrama de flujo del algoritmo GA.

la definición de un operador de selección que asegure que los individuos seleccionados pertenecen a la élite. Para llevar a cabo estos dos procesos se crea un operador para cada individuo de la de población llamado *crowded comparison operator* que depende del rango y de la distancia de hacinamiento del individuo. La distancia de hacinamiento estima la densidad de soluciones en el entorno de un individuo a partir de la media de los lados del mayor ortoedro que encierra al individuo sin incluir ningún otro que pertenezca al mismo rango.

La implementación del algoritmo NSGA-II consta de los siguientes pasos. En primer lugar se genera aleatoriamente una población inicial y se evalúa la función multiobjetivo para cada individuo. Las soluciones de la función objetivo se clasifican de acuerdo al operador *crowded comparison operator*. A continuación comienza el proceso iterativo que empieza por generar una nueva población utilizando los mecanismos de selección, cruce y mutación de manera análoga al caso anterior partiendo de una solución ya clasificada. La función multiobjetivo se vuelve a evaluar para los individuos creados. Empleando el operador *crowded comparison operator* se combina la población anterior y la nueva y se seleccionan los mejores individuos para construir una nueva población. El proceso iterativo se repite hasta que se alcanza el criterio de parada establecido. Como solución al problema se obtiene el frente de Pareto, que está formado por todos los individuos de rango 1. Cada punto de esta curva es una solución al problema y la elección de la mejor debe realizarse siguiendo algún criterio establecido.

2.4.2 Algoritmo *Harmony Search*

El algoritmo *Harmony Search* (HS) fue desarrollado por Geem [38] a principios de siglo y su patrón de búsqueda se encuentra inspirado en la improvisación que realizan los músicos para buscar armonías durante la actuación. A la hora de improvisar, el músico puede tomar tres vías distintas: tocar una melodía que tenga en la memoria, tocar una melodía que recuerde modificándola ligeramente o tocar una melodía completamente nueva. En este contexto, las armonías en memoria se representan en la matriz de memoria $\mathbf{H}$, y la ligera modificación por medio del parámetro de ajuste tonal, *par* (*pitch adjustment rate*). La técnica de búsqueda se basa en puntos singulares, de forma que es un algoritmo de rápida ejecución a diferencia de los algoritmos genéticos que basan su búsqueda en poblaciones.

Los pasos a seguir para la implementación del HS se describen a continuación (ver Figura 2.3). Primero, se inicializa la matriz $\mathbf{H}$ que se rellena con las armonías (vectores de parámetros) creadas aleatoriamente. El número de armonías debe ser suficiente para representar todo el espacio de búsqueda. Para cada una de las armonías se evalúa la función objetivo y se ordena la matriz $\mathbf{H}$ según el valor de la función objetivo. A continuación comienza el proceso iterativo. En cada iteración se genera una nueva armonía definiendo cada parámetro de la misma a partir de un valor aleatorio almacenado en $\mathbf{H}$ o a partir de un valor aleatorio de entre todas las opciones posibles. El parámetro *hmcr* (*harmony memory consideration rate*) refleja la probabilidad de que el parámetro se elija de un valor en la memoria. En el caso de que se tome de un valor almacenado se puede modificar ligeramente según el parámetro *par*, el cual refleja la probabilidad de que se produzca el ajuste, que es el resultado de sumar o restar un valor establecido previamente llamado ancho de banda, b_w. Para la nueva armonía se evalúa la función objetivo y si el resultado mejora el peor almacenado, la nueva armonía se incluye y se excluye la anterior. La matriz se vuelve a ordenar en términos del valor de la función objetivo. La nueva generación se repite hasta alcanzar un criterio de parada del algoritmo.

Harmony Search multiobjetivo

La implementación del algoritmo HS en optimización multiobjetivo (MHS) [37] se basa en las reglas principales de la técnica de *Non-dominated sorting* para la clasificación de las soluciones no dominadas. De este modo, el proceso es muy similar a la versión de un único objetivo adaptando la clasificación de soluciones. Los primeros pasos consisten en generar la matriz $\mathbf{H}$ y evaluar la función multiobjetivo para cada armonía. En el bucle principales se genera un número establecido de nuevas armonías, donde cada una de ellas se crea con las mismas reglas indicadas anteriormente, es decir, según los parámetros *hmcr* y *par*. La función multiobjetivo se vuelve a evaluar para los individuos creados y las armonías se clasifican aplicando la técnica *non-dominated sorting*. El tamaño original de la matriz se restituye eliminado las peores armonías en función del valor de la distancia de hacinamiento. El proceso se repite hasta alcanzar el criterio de parada. El resultado obtenido es el frente de Pareto del problema.

2.4.3 Algoritmo de enjambre de partículas

El algoritmo de optimización por enjambre de partículas (PS en adelante, *Particle Swarm*) fue propuesto por Kennedy y Eberhart [55] y al igual que el GA también está inspirado en la naturaleza (comportamiento de bandadas de pájaros) y su estrategia de búsqueda está

Inicio

Configuración inicial

Crear armonías iniciales (matriz **H**)

Evaluación de la función objetivo

Ordenar **H**

Generación nueva armonía según los valores de *hmcr*, *par* y b_w

Evaluación de la función objetivo

¿Mejora la matriz **H**?   No   Sí

Reordenar **H**

¿Criterio de parada?   No   Sí

Fin
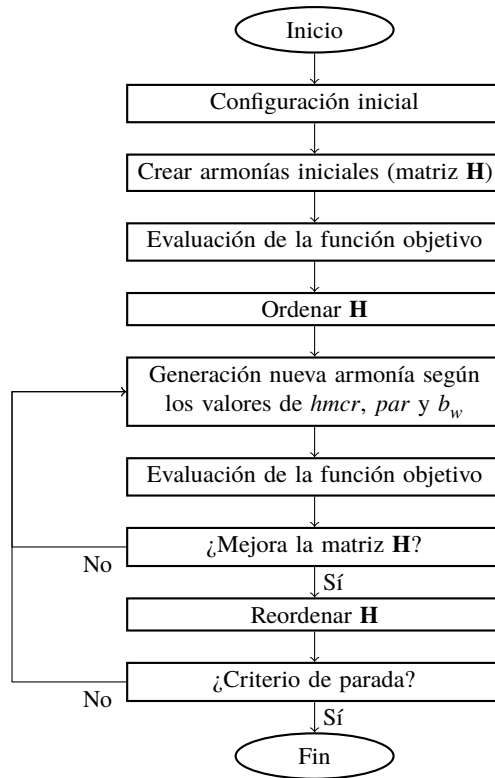
Figura 2.3 Diagrama de flujo del algoritmo HS.

basada en poblaciones. En este caso, se basa en el comportamiento social de un grupo de organismos movidos para lograr un objetivo. Grosso modo puede describirse el proceso de la siguiente forma. Las partículas se mueven a través del espacio de búsqueda siguiendo leyes sencillas referidas a su posición y velocidad. La posición representa el valor de los parámetros y se mejora mediante su propia mejor posición histórica y la mejor posición de las partículas restantes. La velocidad de la partícula depende de tres parámetros. El primero es la inercia de la partícula, que controla el impacto de la velocidad actual en la velocidad posterior. Un valor alto fomenta una exploración global del espacio de búsqueda mientras que un valor bajo centra la búsqueda en un entorno más local. El segundo es el peso de auto-ajuste que indica la influencia de la mejor posición histórica de la partícula en la velocidad posterior. Finalmente, el peso de ajuste social que indica la influencia de la mejor posición histórica de la mejor partícula en la velocidad posterior.

Los pasos del algoritmo son los siguientes. Se crea un conjunto de partículas cuya posición representa un vector de parámetros. La función objetivo se evalúa para cada partícula y se actualiza la mejor posición individual y del conjunto. En el bucle principal, siguiendo una ley establecida previamente se calcula la velocidad para cada una de las partículas y a partir de la misma, se actualiza la posición y la mejor posición individual y

del conjunto. Estos pasos se repiten hasta alcanzar el criterio de parada establecido. En la Figura 2.4 se representa el esquema del algoritmo PS.
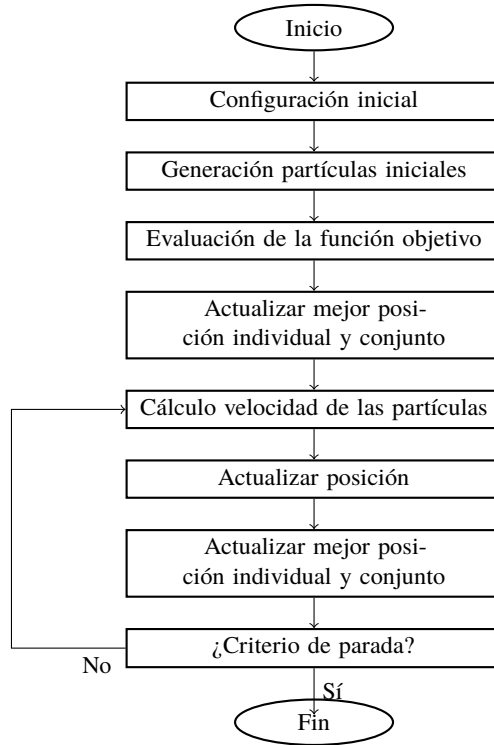
Figura 2.4 Diagrama de flujo del algoritmo PS.

Enjambre de partículas multiobjetivo

La versión para problemas de optimización multiobjetivo se basa igualmente en la clasificación de soluciones no dominadas y en la posibilidad de mutación de una posición aleatoria [19].

La implementación del algoritmo comienza por generar un conjunto de partículas cuya posición es creada aleatoriamente. La función multiobjetivo se evalúa para cada partícula y se clasifican las soluciones según sean dominadas o no. El bucle principal del algoritmo consiste en calcular la velocidad y actualizar la posición para evaluar nuevamente la función multiobjetivo. La posición de cada partícula puede modificarse ligeramente según la probabilidad de mutación indicada inicialmente. En ese caso, la función multiobjetivo se vuelve a evaluar y se clasifican las soluciones. El repositorio de partículas se actualiza quedando únicamente las soluciones no dominadas. Una vez el bucle termina se obtiene el frente de Pareto del problema.

2.5 Comparación de algoritmos metaheurísticos para estimación de parámetros

Ambos enfoques, un único objetivo y multiobjetivo, se han aplicado indistintamente para resolver problemas de ingeniería no habiendo apenas estudios que comparen el rendimiento de estos dos planteamientos. Por esta razón, uno de los objetivos de esta tesis es arrojar luz sobre la implementación de estos enfoques a problemas de ingeniería civil.

Por otro lado, dado el alto coste computacional de los algoritmos, se lleva a cabo un segundo análisis comparativo de la eficiencia de los tres algoritmos metaheurísticos explicados anteriormente, tanto en su versión de un único objetivo como multiobjetivo.

Para lograr estos dos objetivos se desarrolla un problema de estimación de parámetros basado en un caso de estudio real. En particular, el rendimiento de los tres algoritmo bajo los dos planteamientos se compara cuando se implementan para realizar la actualización del modelo de EF de una estructura de laboratorio. Todas las simulaciones numéricas se realizan en un ordenador con un procesador de 3.6 GHz y una memoria RAM de 8 Gb.

2.5.1 Actualización de modelos de EF

La actualización de un modelo de EF se centra en obtener un modelo numérico más preciso que caracterice de una manera más realista el comportamiento dinámico real de la estructura [30]. Para tal fin se estiman un conjunto de parámetros con incertidumbre basado en las medidas experimentales llevadas a cabo en la estructura. Estos parámetros minimizan las diferencias entre los valores numéricos y experimentales de las propiedades modales de la estructura (frecuencias naturales y modos de vibración).

Como cualquier otro problema de estimación de parámetros, la actualización de los modelos de EF se formulan como problemas de optimización donde el objetivo es hallar el óptimo de la función objetivo. Los dos enfoques, de un único objetivo y multiobjetivo, se formulan como se describe a continuación.

El enfoque de un único objetivo se caracteriza por una única función objetivo que se define por medio de los residuos de las frecuencias naturales y de los modos de vibración. Los residuos son ponderados por factores de peso. La formulación del problema siguiendo este planteamiento es:

$$\min f(\boldsymbol{\theta}) = \min \sum_{j}^{n} w_j^f (r_j^f)^2 + \sum_{j}^{n} w_j^m (r_j^m)^2 \tag{2.9}$$

siendo $f(\boldsymbol{\theta})$ la función objetivo, n el número de modos de vibración considerado, w_j^f y w_j^m los factores de peso de los residuos de las frecuencias naturales y de los modos de vibración, respectivamente, y r_j^f y r_j^m los residuos de las frecuencias naturales y de los modos de vibración, respectivamente. Los residuos se calculan de la siguiente manera:

$$r_j^f = \frac{f_{num,j} - f_{exp,j}}{f_{exp,j}} \tag{2.10}$$

$$(r_j^m)^2 = \frac{(1 - \sqrt{\text{MAC}_j})^2}{\text{MAC}_j} \tag{2.11}$$

donde $f_{num,j}$ y $f_{exp,j}$ son la frecuencia natural numérica y experimental j, respectivamente, y MAC_j es un parámetro para medir la correlación entre dos modos de vibración que se calcula como [3]:

$$\text{MAC}_j = \frac{(\phi_{num,j} \cdot \phi_{exp,j})^2}{(\phi_{num,j}^T \cdot \phi_{num,j}) \cdot (\phi_{exp,j}^T \cdot \phi_{exp,j})} \tag{2.12}$$

siendo $\phi_{num,j}$ y $\phi_{exp,j}$ los vectores con las coordenadas modales del modo de vibración j numérico y experimental, respectivamente.

En segundo lugar, el enfoque multiobjetivo se formula como [51]:

$$\min f(\boldsymbol{\theta}) = \min \left[f_1 = \frac{1}{2} \left[\sum_j^n (r_j^f)^2 \right]^{1/2}, f_2 = \frac{1}{2} \left[\sum_j^n (r_j^m)^2 \right]^{1/2} \right]^T \tag{2.13}$$

siendo f_1 y f_2 las dos componentes de la función multiobjetivo, estando la primera de ellas definida en términos de los residuos de las frecuencias naturales y la segunda a partir de los residuos de los modos de vibración. La solución de este planteamiento es el frente de Pareto del problema, donde cada punto representa una posible solución, es decir, un vector de parámetros del modelo de EF que permite reducir las diferencias entre las propiedades modales numéricas y experimentales.

2.5.2   Ejemplo de aplicación

La estructura de laboratorio consiste en una pasarela porticada de un solo vano de 15 m de longitud situada en el laboratorio de la sección de Vibraciones de la Universidad de Exeter [45]. Dos vigas de acero separadas 2.5 m en la dirección transversal a la pasarela la recorren longitudinalmente. Estas vigas se encuentran sujetas por diafragmas de acero colocados cada 1.25 m cuya sección transversal es una placa rectangular de 200×12 mm. Toda la pasarela se apoya en cuatro pilares de acero situados en los extremos de las dos vigas laterales que están anclados al suelo. El tablero de la pasarela está formado por un panel compuesto atornillado a las vigas laterales y a los diafragmas. En la Figura 2.5 se ilustra la pasarela en estudio.

El modelo inicial de EF de la estructura se construye en el software ANSYS [78]. Para las dos vigas laterales, los diafragmas y los paneles compuestos se consideran elementos tipo placa de cuatro nodos con seis grados de libertad por nodo (elemento Shell181). Los tornillos que unen los paneles a los elementos metálicos se modelizan mediante elementos tipo viga de dos nodos y seis grados de libertad por nodo (elemento Beam188). Finalmente, los apoyos se modelizan a través de elementos tipo muelle en la dirección longitudinal
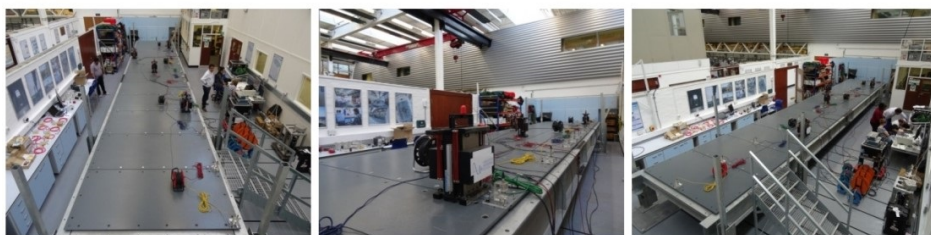
Figura 2.5 Pasarela de laboratorio de la Universidad de Exeter y configuración del ensayo de vibración forzada. [Tomada del Artículo del Apéndice A].

Tabla 2.1 Propiedades modales numéricas y experimentales de la pasarela del laboratorio de la Universidad de Exeter.

Modo	f_{num} [Hz]	f_{exp} [Hz]	Δf [%]	MAC [-]
1	3.638	3.810	-4.509	0.999
2	5.329	5.144	3.600	0.994
3	10.185	8.485	20.033	0.990
4	11.310	12.366	-8.540	0.877
5	17.364	18.605	-6.670	0.985
6	20.238	20.459	-1.080	0.993
7	21.105	22.980	-8.159	0.910

y transversal (elemento COMBIN14). El modelo de EF (ver Figura 2.6) consiste en una malla de 31903 elementos. El análisis modal numérico realizado al modelo de EF de la pasarela da como resultado las siete frecuencias numéricas y sus correspondientes modos de vibración que se muestran en la Tabla 2.1.

Las propiedades modales experimentales se obtienen a partir del análisis modal experimental de las señales de aceleración registradas durante un ensayo de vibración forzada, llevado a cabo en la pasarela cuya configuración se representa en la Figura 2.6 (consúltese el Artículo del Apéndice A para mayor información). En la Tabla 2.1 se indican los valores de las frecuencias naturales experimentales. Para analizar la correlación entre las propiedades modales numéricas y experimentales se indican en la Tabla 2.1 los valores de las diferencias relativas entre frecuencias y del parámetro MAC. A pesar de los buenos valores del MAC, las diferencias relativas de cuatro de las siete frecuencias son todavía grandes [117]. Por tanto, para mejorar el modelo de EF de manera que se ajuste mejor al comportamiento real de la pasarela es necesario actualizarlo.

Para elegir los parámetros a actualizar, que representan las variables de diseño del problema, se realiza un análisis de sensibilidad de varios parámetros para conocer la influencia de cada uno de ellos en una característica de referencia de la estructura. Siguiendo la formulación de Fox y Kapoor se adopta la energía de deformación modal como esta característica de referencia [29]. De esta manera, los parámetros seleccionados son aquellos que tienen una mayor influencia en la energía de deformación modal para cada modo de
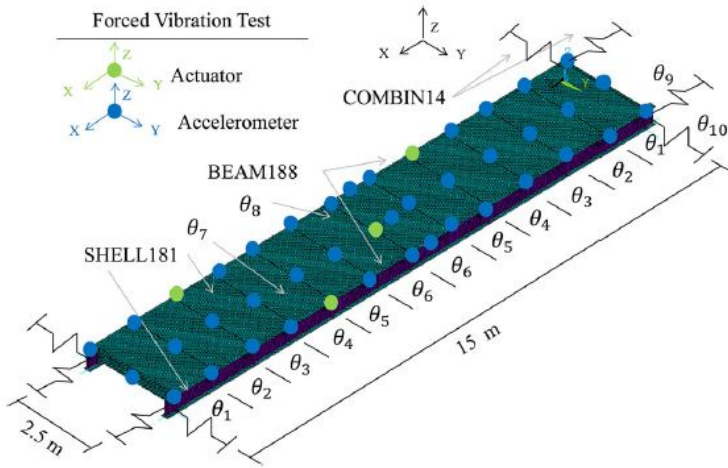
Figura 2.6 Modelo de EF de la pasarela de laboratorio de la Universidad de Exeter, configuración del ensayo de vibración forzada y parámetros de actualización. [Tomada del Artículo del Apéndice C].

vibración. En la Figura 2.7 se muestra la matriz de sensibilidad en forma de diagrama de barras. De acuerdo a dicha matriz, las parámetros físicos más relevantes son los diez siguientes: el módulo de Young del acero de las vigas longitudinales en 6 secciones $(\theta_1 - \theta_6)$, el módulo de Young del poliuretano del panel compuesto (θ_7), el módulo de Young del acero de los tornillos (θ_8), la rigidez longitudinal equivalente de los apoyos (θ_9) y la rigidez transversal equivalente de cada apoyo (θ_{10}). En la Figura 2.6 se ilustran los parámetros de actualización. En el Artículo del Apéndice A se puede encontrar los límites inferiores y superiores impuestos a cada parámetro para garantizar un significado físico adecuado de los parámetros.

2.5.3   Comparación de los tres algoritmos con un único objetivo

En primer lugar se soluciona el problema de actualización del modelo de EF siguiendo el planteamiento de un único objetivo mediante la implementación de los tres algoritmos descritos anteriormente, GA, HS y PS. Se consideran dos criterios de comparación para validar el rendimiento de los algoritmos: el coste computacional (tiempo de simulación) y la exactitud del ajuste. Para todos los algoritmos las variables siguientes se consideran comunes: tamaño de la población (100), número máximo de iteraciones (50) y tolerancia de la función objetivo (10^{-5}). Los parámetros intrínsecos de cada algoritmo se indican con detalle en el Artículo del Apéndice A.

Se consideran once casos distintos en función de los valores de los pesos asociados a las frecuencias naturales, $\sum w_j^f$, y a los modos de vibración, $\sum w_j^m$, para considerar su impacto en los residuos [104]. Además, cada caso se ejecuta diez veces para tener en cuenta la aleatoriedad con la que la población inicial se genera.

En la Tabla 2.2 se muestra la solución al problema para los once casos y los tres
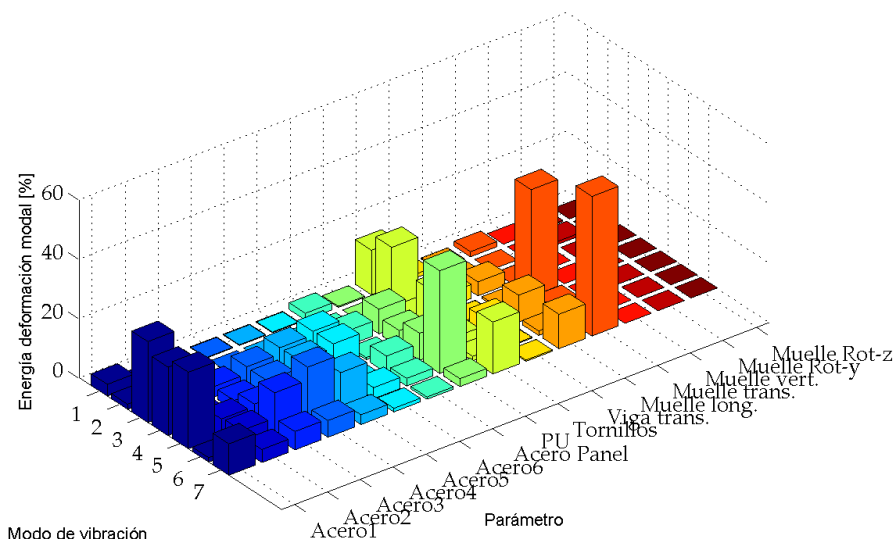
Figura 2.7 Análisis de sensibilidad de los parámetros del modelo de EF: matriz de sensibilidad representada en un diagrama de barras.

algoritmos metaheurísticos. Además, en la Figura 2.8a se muestran estas soluciones en el espacio funcional multiobjetivo. El coste computacional de cada algoritmo se calcula como la media de los tiempo de simulación de los once casos, dando como resultado los valores siguientes. Para el GA: $t = 74072$ s, para el HS, $t = 34380$ s y para el PS, $t = 43857$ s.

De acuerdo con los valores obtenidos y analizando la exactitud en la solución y el tiempo de simulación se pueden extraer dos conclusiones principales. La primera es que la precisión de los tres algoritmos es similar. La segunda es que el algoritmo HS es más eficiente, ya que permite reducir el tiempo de computación requerido para ejecutar la actualización del modelo de EF sin comprometer la precisión en el ajuste.

2.5.4 Comparación de los tres algoritmos multiobjetivo

Los dos mismos criterios se establecen para la comparación de la solución dada por los tres algoritmos cuando se aplican a la actualización del modelo de EF siguiendo el enfoque multiobjetivo. Los parámetros relativos a los tres algoritmos se asumen iguales al caso anterior. De igual manera, se ejecuta diez veces cada algoritmo para tener en cuenta la generación aleatoria de la población inicial.

En la Figura 2.8b se representa el frente de Pareto obtenido por los tres algoritmos.

Tabla 2.2 Valores medios de los residuos en términos de los factores de peso para la actualización del modelo de EF basado en un único objetivo para los tres algoritmos metaheurísticos.

Caso	$\sum w_j^f$	$\sum w_j^m$	GA ($\cdot 10^{-3}$)		PS ($\cdot 10^{-3}$)		HS ($\cdot 10^{-3}$)	
			$\sum (r_j^f)^2$	$\sum (r_j^m)^2$	$\sum (r_j^f)^2$	$\sum (r_j^m)^2$	$\sum (r_j^f)^2$	$\sum (r_j^m)^2$
1	1	0	3,63	2,69	3,56	2,68	3,55	2,69
2	0,9	0,1	3,57	2,66	3,56	2,68	3,55	2,69
3	0,8	0,2	3,59	2,62	3,58	2,51	3,58	2,66
4	0,7	0,3	3,58	2,53	3,57	2,52	3,61	2,52
5	0,6	0,4	3,57	2,56	3,57	2,5	3,62	2,5
6	0,5	0,5	3,58	2,51	3,58	2,51	3,58	2,57
7	0,4	0,6	3,58	2,52	3,58	2,49	3,62	2,51
8	0,3	0,7	3,59	2,48	3,58	2,49	3,63	2,51
9	0,2	0,8	3,58	2,51	3,58	2,49	3,62	2,49
10	0,1	0,9	3,58	2,53	3,59	2,47	3,7	2,47
11	0	1	3,59	2,5	3,59	2,49	3,64	2,46

a)   b)
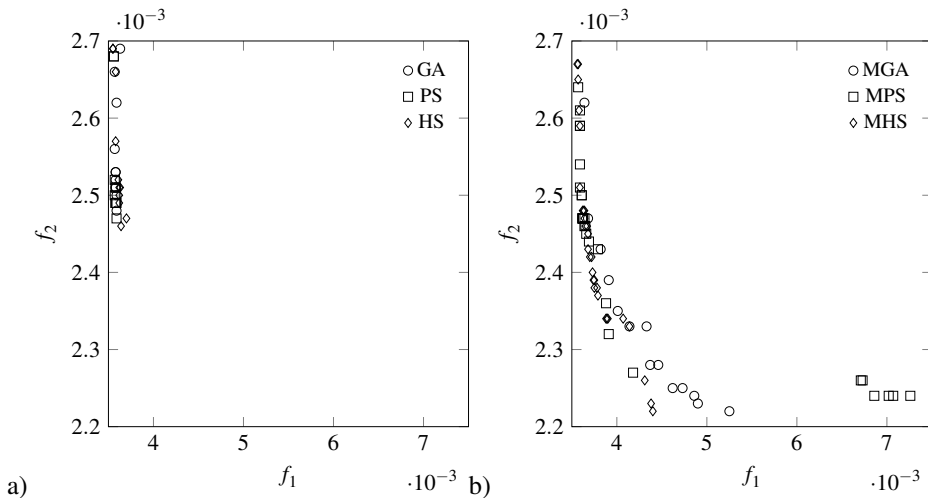
Figura 2.8 Comparación de los valores residuales en el espacio funcional multiobjetivo, siendo f_1 la componente de la función multiobjetivo asociada a los residuos de las frecuencias naturales y f_2 la componente asociada a los residuos de los modos de vibración, para los tres algoritmos comparados, a) enfoque de un único objetivo y b) enfoque multiobjetivo.

Los tiempos que ha tardado cada simulación son: $t = 307057\,\text{s}$ para el GA, $t = 121676\,\text{s}$ para el MHS y $t = 240663\,\text{s}$ para el PS.

De acuerdo a los resultados para las diez simulaciones pueden sacarse tres conclusiones. La primera es que la precisión de los algoritmos PS y MHS es mayor que la del GA ya que

el frente de Pareto de ambos permite reducir el valor total de los residuos. La segunda es que la precisión entre el PS y el MHS es similar. La última es que el tiempo de simulación del MHS es significativamente menor al de los otros dos algoritmos. Por tanto, nuevamente el MHS es el algoritmo más eficiente para resolver la actualización del modelo de EF siguiendo un planteamiento multiobjetivo.

2.5.5 Comparación de los planteamientos de único objetivo y multiobjetivo

La comparación entre ambos enfoques se efectúa en base a tres criterios: la capacidad de rastreo, el coste computacional y el ajuste de la solución.

En la Figura 2.9 se representa la solución obtenida por los tres algoritmos para los dos enfoques. Puede apreciarse que a pesar de que las soluciones obtenidas siguiendo el planteamiento de un único objetivo pertenecen al frente de Pareto, se centran en una sola rama de la curva. De este modo, la capacidad de rastreo del enfoque de un único objetivo es menor.

Por otro lado, el conjunto de soluciones del enfoque multiobjetivo presentan un mejor ajuste ya que la distancia al origen de coordenadas es menor que la de los puntos del enfoque de un objetivo, que se encuentran más lejos del punto de la curva que mejor equilibra ambos residuos (llamado *knee point*) [23].

Finalmente, para comparar los tiempos de simulación es preciso remarcar que bajo el enfoque de un único objetivo se considera la suma de los once casos ya que el estudio de sensibilidad de los pesos es fundamental y necesario para cada problema. De este modo, se obtiene que el tiempo de simulación del algoritmo MHS es menor que el del algoritmo HS (121676 s frente a 378180 s).

Por todos estos motivos se puede justificar que el enfoque multiobjetivo del algoritmo HS (MHS) representa la mejor opción para llevar a cabo la actualización del modelo de EF de estructuras civiles.

2.6 Conclusiones

En este capítulo se han descrito los dos enfoques más generales que pueden seguirse para estimar parámetros resolviendo un problema inverso. El estimador de máxima verosimilitud es el empleado en esta tesis debido a su buena relación coste computacional/precisión en la solución. La estimación de los parámetros se realiza siguiendo un proceso iterativo que puede plantearse de dos maneras: considerando una única función objetivo o una función multiobjetivo.

Existen diversos algoritmos de optimización para resolver el proceso iterativo, siendo los métodos metaheurísticos los más adecuados, ya que no tienen dependencia del valor inicial y logran encontrar el óptimo global.

En este capítulo se ha llevado a cabo un análisis comparativo para estimar qué algoritmo es el que mejor rendimiento ofrece. Además, también se han analizado y comparado los dos enfoques del problema, el de un único objetivo y el de multiobjetivo.

Como resultado de esta comparación se han obtenido dos conclusiones: la primera es que el algoritmo HS es el más eficiente en los dos enfoques y la segunda es que el enfoque multiobjetivo permite obtener una mejor solución al problema.
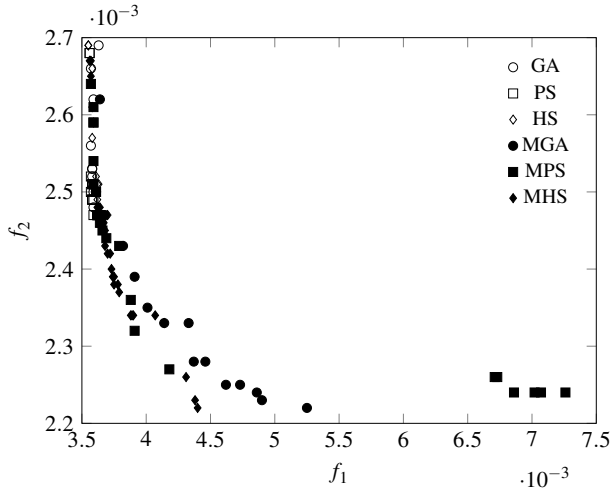
Figura 2.9 Comparación de los valores residuales en el espacio funcional multiobjetivo, siendo f_1 la componente de la función multiobjetivo asociada a los residuos de las frecuencias naturales y f_2 la componente asociada a los residuos de los modos de vibración, para los tres algoritmos comparados siguiendo ambos enfoques.

Estas dos conclusiones son la base para el desarrollo teórico de los algoritmos que se proponen en esta tesis en los Capítulos 3 y 4.

3   Algoritmo híbrido UKF-HS para estimación de parámetros

En este capítulo se aborda la consideración de los errores en el proceso de estimación y en las medidas que aparecen en el problema de actualización de parámetros de modelos. En primer lugar se esbozan las distintas fuentes de error que aparecen al construir un modelo numérico y estimar sus parámetros. A continuación se explica la teoría que encierra el filtro de Kalman empleado y su formulación, así como una primera aplicación. En este ejemplo se implementa un algoritmo híbrido que combina el algoritmo GA y el filtro de Kalman explicado anteriormente.

Seguidamente y atendiendo a las conclusiones del Capítulo 2, se describe la implementación de un algoritmo híbrido basado en el MHS que resuelva el problema de optimización. Para tal fin, el algoritmo MHS se combina con el filtro de Kalman explicado. La ventaja de la implementación de este algoritmo híbrido es doble. En primer lugar el tiempo de computación es reducido y, en segundo lugar, el error en la medida y en el proceso de estimación no se ignoran en la resolución del problema. La validación del algoritmo se realiza resolviendo un problema de actualización del modelo de EF de una pasarela de laboratorio. Los resultados se comparan con los obtenidos por dos algoritmos convencionales.

Finalmente, se describe una aplicación adicional del algoritmo híbrido propuesto basado en el MHS y en el filtro de Kalman, para la estimación de los parámetros del modelo dinámico de Winkler en un problema de interacción suelo-estructura de una pasarela.

Partes de este capítulo se han publicado en los Artículos B, C y D.

3.1   Fuentes de error

Cuando se construye el modelo numérico/matemático de un sistema entran en juego numerosos tipos de error, algunos de los cuales se corrigen mediante la resolución del problema de estimación de parámetros (incertidumbre de los parámetros). En cambio, hay otros a los que hay que prestar atención. Dentro de este segundo grupo se encuentran las dos fuentes de error que se indican a continuación [82]. En primer lugar, los errores debido

a las hipótesis asumidas para caracterizar al sistema. Estos errores generalmente surgen de simplificaciones en la modelización (por ejemplo, una placa modelizada como una viga) o asumir comportamiento lineal cuando realmente es no lineal. En segundo lugar, los errores generados por la distretización de la que hacen uso los métodos numéricos, aunque suelen ignorarse al ser de un orden muy inferior a los errores en la modelización [99].

Sin embargo, cuando se formula un problema de estimación de parámetros no solo aparecen los errores citados arriba asociados al modelo numérico sino que también existe incertidumbre en los datos experimentales. Estos errores pueden ser aleatorios o sistemáticos debido a imperfecciones en los equipos de medida o en el procesamiento de las señales.

Finalmente, cuando se realiza la actualización de parámetros del modelo aparece un error, denominado error en el proceso de estimación. Este error se utiliza para establecer las estimaciones de una iteración basadas en la bondad de las estimaciones del paso anterior.

Para tener en cuenta las fuentes de error, tanto del modelo como de las medidas y proceso de estimación, el algoritmo híbrido que se propone en este capítulo hace uso de las ventajas que presenta el algoritmo UKF. En el siguiente apartado se explica la formulación que sigue este algoritmo.

3.2   Unscented Kalman Filter

Debido a las ventajas sobre el EKF (*Extended Kalman Filter*), el algoritmo de minimización local usado para acelerar al algoritmo *harmony search* multiobjetivo (MHS) es el UKF (*Unscented Kalman Filter*). Se trata de un algoritmo que no precisa de realizar ninguna operación diferencial ya que no es necesario calcular el Jacobiano ni el Hessiano. El UKF se desarrolló para resolver problemas de estimación de parámetros de la mano de Wan y van der Merwe [109, 108], asumiendo que puede ser formulado como:

$$\boldsymbol{\theta}_k = \boldsymbol{\theta}_{k-1} + \mathbf{w}_{k-1} \tag{3.1}$$

$$\mathbf{z}_k = h(\boldsymbol{\theta}_k) + \mathbf{v}_k \tag{3.2}$$

con $\boldsymbol{\theta}$ siendo el vector de parámetros a estimar, h la función de modelización no lineal, $\boldsymbol{z}$ el vector que agrupa las salidas del sistema dinámico y $\boldsymbol{w}$ y $\boldsymbol{v}$ los ruidos estadísticos del proceso de estimación y de las observaciones, respectivamente. Para la definición de estos dos últimos términos se asume que no están correlacionados y que se trata de ruido blanco con media cero y matrices de covarianza $\mathbf{Q}$ y $\mathbf{R}$, respectivamente. La matriz $\mathbf{R}$ se calcula como la suma de dos componentes, el ruido en la medida y el ruido en la modelización [101].

La estimación se realiza por medio de $2n_d + 1$, siendo n_d el número de parámetros a estimar, puntos de muestreo deterministas o puntos *sigma* que toman la anterior media y covarianza real de las cantidades a estimar. La propagación de estos puntos a través de la función no lineal **h** permite derivar la media y la covarianza posterior. Los puntos *sigma* se calculan mediante la factorización raíz cuadrática de la matriz de covarianza posterior, **P**. Por ello, esta matriz debe ser semidefinida positiva en cada paso, lo que supone el principal esfuerzo computacional del algoritmo. La factorización de Cholesky

puede emplearse de manera eficiente para realizar este proceso. No obstante, la matriz **P** ha de actualizarse en cada paso y la aparición de errores numéricos puede dar lugar a una matriz no semidefinida positiva. El algoritmo *square-root* UKF propuesto por van der Merwe y Wan [106] supera esta limitación ya que se evita factorizar en cada paso. En su lugar, la factorización de Cholesky ($\mathbf{A} = \sqrt{\mathbf{P}} = \text{chol}(\mathbf{P})$, siendo $\mathbf{P} = \mathbf{A}\mathbf{A}^T$) se propaga directamente asegurándose que la matriz de covarianza es semidefinida positiva.

El algoritmo consiste en los dos siguientes pasos. El paso de predicción se lleva a cabo considerando los resultados anteriores para calcular los puntos *sigma*, predecir las estimaciones de la matriz de covarianza del error en la estimación, $\mathbf{A}^{\boldsymbol{\theta}}$, y calcular las salidas del modelo $z_{k|k-1}$.

El paso de corrección o actualización estima la media y covarianza del error en la estimación posterior en términos de la matriz de ganancia de Kalman, **K**, las medidas, $\mathbf{z}^{obs}$, y las salidas del modelo ponderadas, $\hat{\mathbf{z}}$.

La formulación del algoritmo UKF es la siguiente (en el Artículo del Apéndice C se encuentran más detalles de los fundamentos matemáticos de la formulación):

$$\hat{\boldsymbol{\theta}} = \boldsymbol{\theta}_{prior} \tag{3.3}$$

$$\mathbf{A}_0^{\theta} = \text{chol}(\mathbf{P}_0^{\theta}) \tag{3.4}$$

Bucle principal: $para\, k = 1 : N_{UKF}$ (número de iteraciones)

Predicción

Calcula los $2n_d + 1$ puntos *sigma* : $(\chi_{k-1})_i$ $\tag{3.5}$

$$(\chi_{k|k-1})_i = (\chi_{k-1})_i \tag{3.6}$$

$$\boldsymbol{\theta}_{k|k-1} = \sum_0^{2n_d} W_i \cdot (\chi_{k|k-1})_i \tag{3.7}$$

$$\mathbf{A}_{k|k-1}^{\theta} = \gamma^{-0.5}\mathbf{A}_{k-1|k-1}^{\theta} \tag{3.8}$$

$$(z_{k|k-1})_i = h((\chi_{k-1})_i) \tag{3.9}$$

$$\hat{z}_{k|k-1} = \sum_0^{2n_d} W_i \cdot (z_{k|k-1})_i \tag{3.10}$$

Corrección

$$\mathbf{S}_{k|k-1}^z = \text{qr}([\sqrt{W_{1:2n_d}} \cdot [(\mathbf{z}_{k|k-1})_{1:2n_d} - \hat{\mathbf{z}}_{k|k-1}]\sqrt{\mathbf{R}}]) \tag{3.11}$$

$$\mathbf{S}_{k|k-1}^z = \text{cholupdate}(\mathbf{S}_{k|k-1}^z, (\mathbf{z}_{k|k-1})_0 - \hat{\mathbf{z}}_{k|k-1}, \text{sgn}(W_0)) \tag{3.12}$$

$$\mathbf{P}_{k|k-1}^{\theta z} = \sum_{0}^{2n_d} (W_i[(\chi_{k|k-1})_i - \hat{\theta}_{k|k-1}] \cdot [(\mathbf{z}_{k|k-1})_i - \hat{\mathbf{z}}_{k|k-1}]^T) \tag{3.13}$$

$$\mathbf{K}_k = \frac{\mathbf{P}_{k|k-1}^{\theta z}/(\mathbf{S}_{k|k-1}^z)^T}{\mathbf{S}_{k|k-1}^z} \tag{3.14}$$

$$\hat{\theta}_{k|k} = \hat{\theta}_{k|k-1} + \mathbf{K}_k \cdot (\mathbf{z}^{obs} - \hat{\mathbf{z}}_{k|k-1}) \tag{3.15}$$

$$\mathbf{U} = \mathbf{K}_k \cdot \mathbf{S}_{k|k-1}^z \tag{3.16}$$

$$\mathbf{A}_{k|k} = \text{cholupdate}(\mathbf{A}_{k|k-1}, \mathbf{U}, -1) \tag{3.17}$$

$$fin$$

3.2.1   Actualización del modelo de EF de una cúpula de fábrica

Con el objetivo de obtener una primera aproximación de los beneficios de definir un algoritmo híbrido usando el algoritmo UKF, se lleva a cabo, empleando un algoritmo híbrido GA-UKF, la actualización del modelo de EF de una estructura de fábrica. Concretamente, se trata de la cúpula de la capilla que se encuentra integrada en la Residencia Würzburg (Alemania) (ver Figura 3.1a). La estructura de la cúpula está formada por una única capa de ladrillos de 30 cm de ancho que aumenta hasta los 45 cm de ancho en la base a modo de refuerzo (Figura 3.1b).

El modelo de EF, diseñado en el software ANSYS [78], consiste en elementos tridimensionales tipo placa con cuatro nodos por elemento y seis grados de libertad por nodo (elemento SHELL63 para modelizar los ladrillos, tal y como se muestra en la Figura 3.1c. El efecto de los muros laterales de la capilla sobre la cúpula se considera a través de dos elementos unidimensionales tipo muelle (elemento COMBIN14) por nodo situados en las dos direcciones transversales. El modelo de EF resultante consiste en una malla de 4905 nodos y 5660 elementos. El análisis modal numérico da como resultados las tres frecuencias naturales que se recogen en la Tabla 3.1. En la Figura 3.2 se ilustran los tres modos de vibración de la cúpula.

Para la obtención de las propiedades modales experimentales de la cúpula se lleva a cabo el análisis modal operacional de las mediciones registradas mediante un ensayo de vibración ambiental. Las aceleraciones se miden durante 10 minutos mediante ocho acelerómetros uniaxiales colocados en 51 puntos de instrumentación [87]. Las señales se procesan utilizando el algoritmo SSI (*Stochastic Subspace Identification*) [69]. En el Artículo del Apéndice B se incluye una descripción detallada de la configuración del ensayo de vibración ambiental. En la Tabla 3.1 se muestran asimismo las frecuencia naturales experimentales de la cúpula. Además, para comparar los resultados numéricos y experimentales se calcula la diferencia relativa entre frecuencias naturales y el valor del parámetro MAC. A partir de estos valores puede concluirse que el modelo no está ajustado y que para simular el comportamiento real de la estructura es necesario actualizar el modelo.

La elección de los parámetros a actualizar se basa en los resultados de un análisis de sensibilidad donde se mide la influencia en la energía de deformación modal. En el Artículo
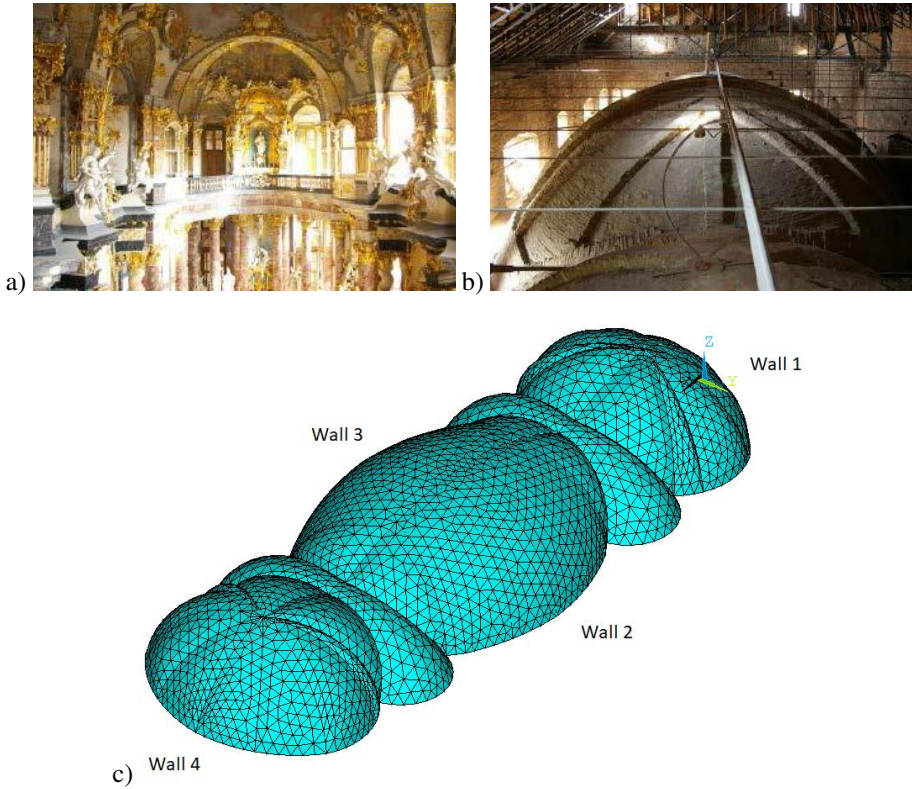
Figura 3.1 a) Vista interior de la capilla de la Residencia Würzburg, b) estructura de la cúpula y c) modelo de EF de la estructura. [Tomada del Artículo del Apéndice B].

Tabla 3.1 Propiedades modales numéricas y experimentales de la cúpula de la capilla de la Residencia Würzburg antes de la actualización. f_{num} y f_{exp} son las frecuencias naturales numéricas y experimentales, respectivamente.

Modo	f_{num} [Hz]	f_{exp} [Hz]	Δf [%]	MAC [-]
1: lateral	3.362	2.764	21.635	0.809
2: longitudinal	3.431	3.231	6.190	0.877
3: lateral	3.988	4.015	-0.672	0.648

del Apéndice B se puede consultar más detalles de los parámetros seleccionados para la actualización así como de los detalles acerca de los parámetros del algoritmo.

Las propiedades modales después de la actualización se muestran en la Tabla 3.2. La implementación del algoritmo híbrido conduce a un buen ajuste entre las propiedades numéricas y experimentales, ya que las diferencias relativas entre frecuencias naturales se
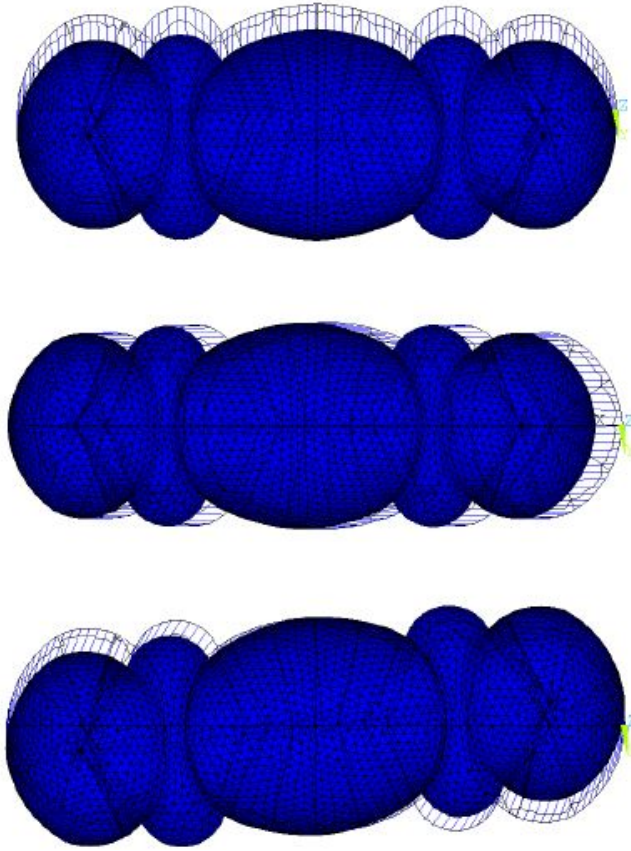
Figura 3.2 Ilustración de los tres modos de vibración de la cúpula.

Tabla 3.2 Propiedades modales numéricas y experimentales de la cúpula de la capilla de la Residencia Würzburg después de la actualización usando el algoritmo híbrido. $f_{num,act.}$ son las frecuencias naturales numéricas actualizadas.

Modo	$f_{num,act.}$ [Hz]	f_{exp} [Hz]	Δf [%]	MAC [-]
1: lateral	2.741	2.764	-0.832	0.859
2: longitudinal	3.207	3.231	-0.743	0.928
3: lateral	4.423	4.015	10.161	0.695

han reducido, excepto para el tercer modo y el valor del parámetro MAC ha aumentado.

Estos resultados se comparan con los proporcionados por el GA para comprobar el rendimiento del mismo. En la Tabla 3.3 se muestran los valores de las frecuencias naturales numéricas actualizadas, así como las diferencias relativas entre frecuencias naturales y el valor del MAC, tras la actualización del modelo usando el algoritmo GA. Puede apreciarse

Tabla 3.3 Propiedades modales numéricas y experimentales de la cúpula de la capilla de la Residencia Würzburg después de la actualización usando el GA.

Modo	$f_{num,act.}$ [Hz]	f_{exp} [Hz]	Δf [%]	MAC [-]
1: lateral	2.725	2.764	-1.411	0.860
2: longitudinal	3.237	3.231	-0.186	0.921
3: lateral	4.188	4.015	4.299	0.728

que los valores son muy similares a los obtenidos por el algoritmo híbrido. Por ello, la comparación se realiza en términos del tiempo de simulación. Ambos casos se han implementado en un ordenador con un procesador de 3.6 GHz y una memoria RAM de 8 Gb. El algoritmo híbrido requiere un tiempo total de 16068 s frente al algoritmo GA, que requiere 47710 s. Por estas razones, la formulación del algoritmo híbrido basado en el UKF se presenta como una herramienta eficiente para resolver problemas de estimación de parámetros.

3.3 Implementación del algoritmo híbrido UKF-MHS

El algoritmo que se propone en este capítulo combina dos algoritmos de optimización para resolver el problema de estimación de parámetros, el algoritmo MHS descrito en el Capítulo 2 y el algoritmo UKF. De este modo, el algoritmo propuesto tiene un carácter global/local, que se beneficia tanto del carácter de búsqueda global del algoritmo MHS como del esquema de aceleración que proporciona el algoritmo UKF.

A pesar de las ventajas indicadas en el Capítulo 2 que la implementación de un problema de optimización multiobjetivo presenta en relación al enfoque considerando un único objetivo, el proceso de minimización local seguido por el algoritmo *square root* UKF se implementa tanto en el HS como en el MHS para comprobar que el algoritmo híbrido presenta un buen rendimiento en términos de la reducción del tiempo de simulación siguiendo ambas estrategias. El algoritmo híbrido presenta las dos principales ventajas siguientes: la primera es que la solución al problema de estimación de parámetros se realiza de manera más eficiente y la segunda es que los errores, ya sean en el proceso de estimación, en las medidas o en la modelización, son considerados en la definición del algoritmo.

El esquema general del algoritmo híbrido propuesto sigue el esquema general del algoritmo HS (y MHS). Asumiendo que el proceso seguido por el HS es similar y más sencillo que el del MHS, en la Figura 3.3 se muestra el diagrama de flujo del algoritmo híbrido UKF-MHS propuesto, del que puede deducirse fácilmente el esquema del algoritmo híbrido UKF-HS. De acuerdo a la Figura 3.3, los pasos a seguir para resolver un problema empleando el algoritmo híbrido propuesto son los siguientes. En primer lugar, el algoritmo MHS crea un conjunto de soluciones iniciales aleatorias contenidas en una matriz H que agrupa los vectores con las soluciones $\boldsymbol{\theta}$. A continuación, el algoritmo *square root* UKF calcula la media posterior, $\boldsymbol{\theta}_{k|k}$, de cada vector de soluciones y se evalúa la función objetivo para cada vector. Mediante la técnica de *non-dominating sorting* se clasifican las

soluciones en dominadas y no dominadas y se eliminan las primeras. Estos pasos se repiten iterativamente hasta alcanzar algún criterio de convergencia. Como resultado, se obtiene el frente de Pareto del problema. Una descripción más detallada de la implementación de ambos algoritmos puede consultarse en el Artículo del Apéndice C.

3.3.1   Validación del algoritmo propuesto

Para analizar el rendimiento del algoritmo híbrido propuesto a la hora de resolver problemas de estimación de parámetros se resuelve la actualización del modelo de EF de una pasarela de laboratorio. Con ese fin, la actualización se realiza resolviendo el problema siguiendo dos estrategias distintas, considerando un único objetivo y, por otro lado, considerando una función multiobjetivo. Los resultados obtenidos por ambos métodos se comparan con los resultados obtenidos por dos algoritmos convencionales, el algoritmo genético (GA) y el algoritmo HS. La estructura en estudio es la misma pasarela de laboratorio descrita en el capítulo 2 y las características del ordenador empleado para las simulaciones son las mismas. De igual modo, el análisis de sensibilidad fue descrito en el capítulo 2. Los detalles sobre la identificación experimental se encuentran en el Artículo del Apéndice C.

Actualización utilizando el algoritmo UKF-HS

La solución al problema de optimización con un único objetivo se halla utilizando el algoritmo UKF-HS, donde se consideran los siguientes valores de los parámetros para su implementación. Respecto a los parámetros intrínsecos al HS se adopta un valor de $hmcr = 0.9$, $par = 0.3$ y b_w igual al 1 % del rango de búsqueda de cada parámetro [110]. Los pesos asociados a los residuos de las frecuencias y modos de vibración se hallan a partir de un estudio de sensibilidad. Para ello los valores de los pesos varían entre 0 y 1 (once casos en total) y aquella combinación con un menor valor de la función objetivo es la seleccionada. Como resultado, se obtienen los valores siguientes: peso asociado a los de las frecuencias: 0.7 y peso asociado a los residuos de los modos de vibración: 0.3.

Por otro lado, los valores de los parámetros propios del UKF que se asumen son:

- factor para el cálculo de los puntos *sigma* es $\lambda = 0.0001$ [4]

- factor de escala para la actualización la matriz de covarianza del error en la estimación es $\gamma = 0.99$ [106]

- el vector de medidas se construye en términos de las 7 frecuencias experimentales y otro vector de 7 componentes con valores unitarios debido a que el objetivo es hacer el valor del MAC lo más próximo a la unidad

A continuación se realiza un estudio de sensibilidad de los parámetros intrínsecos del algoritmo UKF. Los parámetros seleccionados son: el número de iteraciones del UKF, N_{UKF}, la matriz de covarianza del ruido en la medición, $\mathbf{R}$, y la matriz de covarianza del error en la estimación inicial, $\mathbf{P}_0^\theta$. Hay que remarcar que la contribución en la matriz $\mathbf{R}$ del ruido en la modelización se ignora ya que se considera el mismo modelo de EF para todo el proceso y que $\mathbf{R}$ es una matriz diagonal [4]. El número de iteraciones, Iter = 2, y el tamaño de la población, Pob = 5, se mantienen constante.

En la Tabla 3.4 se reflejan los resultados de este estudio de sensibilidad de los parámetros. En base a los tiempos de simulación y al valor de la función objetivo, f, se adoptan los
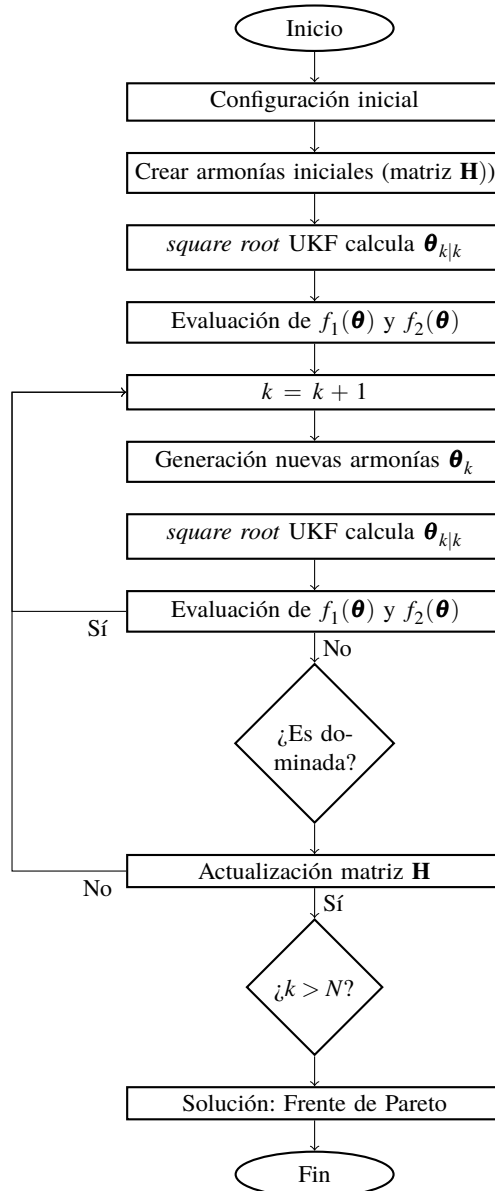
Figura 3.3 Diagrama de flujo del algoritmo híbrido UKF-MHS propuesto en este capítulo para resolver problemas de estimación de parámetros.

Tabla 3.4 Comparación de los tres algoritmos para la actualización del modelo de EF de la pasarela de laboratorio siguiendo el enfoque de un único objetivo. *Iter* es el número de iteraciones, *Pob* es el tamaño de la población, *Eval* es el número de evaluaciones de la función objetivo y *f* el valor de la función objetivo.

	Iter	*Pob*	N_{UKF}	$\mathbf{P}_0^\theta$	$\mathbf{R}_{jj}$	*Eval*	Tiempo [s]	*f*
GA	50	20	-	-	-	1020	9790	0.0036
HS	500	20	-	-	-	520	6640	0.0033
	2	5	1	$\text{diag}((\frac{\boldsymbol{\theta}_u - \boldsymbol{\theta}_l}{2000})^2)$	0.001	147	2100	0.0037
	2	5	3	$\text{diag}((\frac{\boldsymbol{\theta}_u - \boldsymbol{\theta}_l}{500})^2)$	0.001	441	5680	0.0034
UKF-HS	2	5	3	$\text{diag}((\frac{\boldsymbol{\theta}_u - \boldsymbol{\theta}_l}{2000})^2)$	0.001	441	5710	0.0033
	2	5	3	$\text{diag}((\frac{\boldsymbol{\theta}_u - \boldsymbol{\theta}_l}{4000})^2)$	0.001	441	5690	0.0036
	2	5	3	$\text{diag}((\frac{\boldsymbol{\theta}_u - \boldsymbol{\theta}_l}{2000})^2)$	0.1	441	5680	0.0060
	2	5	3	$\text{diag}((\frac{\boldsymbol{\theta}_u - \boldsymbol{\theta}_l}{2000})^2)$	0.0001	441	5640	0.0040
	2	5	5	$\text{diag}((\frac{\boldsymbol{\theta}_u - \boldsymbol{\theta}_l}{2000})^2)$	0.001	735	9440	0.0033

siguientes valores: $N_{UKF} = 3$, $\mathbf{R}_{jj} = 0.001$ y $\mathbf{P}_0^\theta = \text{diag}((\frac{\boldsymbol{\theta}_u - \boldsymbol{\theta}_l}{2000})^2)$, ya que mejoran la precisión sin sacrificar el tiempo de computación.

Los resultados se comparan con los proporcionados por dos algoritmos diferentes, el HS y el GA. Para el primero se adoptan los mismos valores de los parámetros *hmcr*, *par* y b_w. En el segundo caso, se asume que la relación de cruce es de 0.8 y la de mutación 0.4 [74]. Esta comparación se establece en base a dos criterios, la velocidad de convergencia, analizada a través del tiempo de simulación y el número de evaluaciones de la función objetivo, y la precisión del ajuste, analizada a través del valor de la función objetivo. Los resultados obtenidos mediante estos dos algoritmos se incluyen en la Tabla 3.4.

A la vista de los resultados, el algoritmo híbrido UKF-HS demuestra ser el más eficiente ya que presenta la misma precisión en el resultado que el HS pero siendo el tiempo de simulación y el número de evaluaciones de la función objetivo menor. Además, es preciso incidir en que el GA es el menos eficiente de los tres comparados para resolver este problema de actualización.

Actualización utilizando el algoritmo UKF-MHS

La actualización del modelo de EF de la pasarela se lleva a cabo también aplicando el algoritmo híbrido basado en un enfoque multiobjetivo del problema de optimización. Los parámetros del algoritmo híbrido son los mismos que los adoptados para la resolución del problema de un único objetivo. La selección del punto óptimo de entre todos aquellos que forman el frente de Pareto se hace aplicando el método de intersección normal al

contorno [23]. Con el fin de comparar los resultados con otros algoritmos, la actualización del modelo de EF se realiza también aplicando los algoritmos MHS y el GA multiobjetivo (MGA), adoptando los mismos valores de los parámetros de los dos algoritmos que en el caso anterior.

En primer lugar, se realiza un análisis de sensibilidad de los parámetros del algoritmo híbrido. Para ello, se consideran los tres mismos parámetros, N_{UKF}, $\mathbf{R}_{jj}$ y $\mathbf{P}_0^\theta$. Los resultados de este análisis se muestran en la Tabla 3.5. En relación al parámetro N_{UKF} se obtiene una relación directa entre el valor de este parámetro y la precisión del ajuste y una relación inversa entre este parámetro y el tiempo de simulación. Respecto al parámetro $\mathbf{R}_{jj}$, un valor intermedio, $\mathbf{R}_{jj} = 0.001$, mejora la precisión del ajuste sin comprometer el tiempo de simulación. Finalmente, el parámetro $\mathbf{P}_0^\theta$ dota de una mayor precisión en el ajuste cuando su valor disminuye aunque su influencia no es significativa. Los valores que se adoptan para los tres parámetros son los siguientes: $N_{UKF} = 3$, $\mathbf{R}_{jj} = 0.001$ y $\mathbf{P}_0^\theta = \mathrm{diag}((\frac{\boldsymbol{\theta}_u - \boldsymbol{\theta}_l}{2000})^2)$.

Finalmente, el rendimiento del algoritmo híbrido aplicado a la actualización del modelo de EF se compara con el de los dos algoritmos convencionales mencionados anteriormente, el MHS y el GA. Como criterios de comparación se tienen en consideración el número de evaluaciones de la función objetivo y el tiempo de simulación para analizar la velocidad de convergencia y, por otro lado, la precisión en el ajuste evaluada en términos de la distancia entre el punto seleccionado del frente de Pareto y el origen y de la suma de los dos términos de la función objetivo. En la Tabla 3.5 se detallan los resultados obtenidos para la actualización del modelo de EF implementando los tres algoritmos. Atendiendo a los resultados puede comprobarse que el algoritmo UKF-MHS es más eficiente, ya que tiene un tiempo de simulación menor alcanzando la misma precisión en el ajuste. Por otro lado, es nuevamente destacable que el algoritmo MGA es el que proporciona un peor ajuste, además, con un tiempo de simulación mayor.

Mediante estos dos problemas de optimización se ha validado el algoritmo híbrido propuesto tanto en la versión para un único objetivo como la de multiobjetivo.

3.4 Aplicación para estimar los parámetros del modelo dinámico de Winkler

Además de estimar los parámetros del modelo de EF de una estructura, el algoritmo híbrido propuesto en este capítulo puede implementarse para resolver cualquier problema donde haya que estimar parámetros de un sistema donde hay involucradas mediciones. En este apartado, el algoritmo se aplica para estimar los parámetros del modelo dinámico de Winkler para la interacción suelo-estructura de una pasarela integral de estructura mixta de acero y hormigón situada en la provincia de Sevilla (ver Figura 3.4).

El modelo de Winkler es un modelo simplificado para simular la interacción suelo-estructura. Su formulación depende del tipo de cimentación que tenga la estructura, que grosso modo, pueden clasificarse en cimentaciones directas y cimentaciones profundas.

El primer caso se caracteriza por que las cimentaciones son, generalmente, estructuras masivas rígidas que se modelizan a través de elementos muelle-amortiguador equivalentes

Tabla 3.5 Comparación de los tres algoritmos para la actualización del modelo de EF de la pasarela de laboratorio siguiendo el enfoque multiobjetivo. *Iter* es el número de iteraciones, *Pob* es el tamaño de la población, *N.Pob* es el tamaño de la población que se crea en cada iteración, *Eval* es el número de evaluaciones de la función objetivo, *Dist* es la distancia euclídea al origen y *Sum* es la suma de f_1 y f_2.

	Iter	*Pob*	*N.Pob*	N_{UKF}	$\mathbf{P}_0^\theta$	$\mathbf{R}_{jj}$	*Eval*	Tiempo [s] $(\cdot 10^{-5})$	*Dist* $(\cdot 10^{-4})$	*Sum* $(\cdot 10^{-4})$
MGA	25	50	-	-	-	-	1450	0.18	50.7	68.6
	45	50	-	-	-	-	2570	0.33	50.2	66.9
	150	10	-	-	-	-	16600	2.12	52.0	68.0
MHS	50	50	25	-	-	-	1300	0.17	45.4	62.1
	100	100	25	-	-	-	2600	0.33	45.1	61.8
	300	200	50	-	-	-	15200	1.98	43.7	60.6
UKF-MHS	3	10	3	3	$\mathrm{diag}((\frac{\boldsymbol{\theta}_u - \boldsymbol{\theta}_l}{2000})^2)$	0.001	1197	0.16	45.2	62.1
	3	10	3	3	$\mathrm{diag}((\frac{\boldsymbol{\theta}_u - \boldsymbol{\theta}_l}{500})^2)$	0.001	1197	0.15	43.0	63.5
	3	10	3	3	$\mathrm{diag}((\frac{\boldsymbol{\theta}_u - \boldsymbol{\theta}_l}{4000})^2)$	0.001	1197	0.15	44.6	61.4
	3	10	3	3	$\mathrm{diag}((\frac{\boldsymbol{\theta}_u - \boldsymbol{\theta}_l}{2000})^2)$	0.1	1197	0.15	52.6	71.3
	3	10	3	3	$\mathrm{diag}((\frac{\boldsymbol{\theta}_u - \boldsymbol{\theta}_l}{2000})^2)$	0.0001	1197	0.15	145.0	177.6
	8	15	3	3	$\mathrm{diag}((\frac{\boldsymbol{\theta}_u - \boldsymbol{\theta}_l}{2000})^2)$	0.001	2457	0.32	44.3	61.1
	20	40	10	3	$\mathrm{diag}((\frac{\boldsymbol{\theta}_u - \boldsymbol{\theta}_l}{2000})^2)$	0.001	15120	1.96	43.7	60.4
	3	8	3	1	$\mathrm{diag}((\frac{\boldsymbol{\theta}_u - \boldsymbol{\theta}_l}{2000})^2)$	0.001	357	0.05	50.6	68.2
	3	8	3	3	$\mathrm{diag}((\frac{\boldsymbol{\theta}_u - \boldsymbol{\theta}_l}{2000})^2)$	0.001	1071	0.14	49.1	66.5
	3	8	3	5	$\mathrm{diag}((\frac{\boldsymbol{\theta}_u - \boldsymbol{\theta}_l}{2000})^2)$	0.001	1785	0.23	45.2	62.0

[35] (Figura 3.5). No obstante, para niveles bajos de vibración de la cimentación la componente de amortiguamiento puede ser excluida sin perjuicio de la validez en la simulación. La rigidez equivalente en los seis grados de libertad, tres de traslación y tres de giro, se calculan a partir de los datos geométricos de la cimentación y de los parámetros mecánicos del suelo ya sean cimentaciones embebidas en el suelo o superficiales según la formulación propuesta por Gazetas [35]. En el Artículo del Apéndice D se pueden consultar las fórmulas que permiten obtener las rigideces del modelo de interacción suelo-estructura.

Por otro lado, las cimentaciones profundas se caracterizan por ser estructuras flexibles y esbeltas cuyo comportamiento estructural depende principalmente de su longitud. En este caso es preciso tener en cuenta la componente de amortiguamiento para simular adecuadamente la interacción suelo-estructura ya que los efectos dinámicos tienen una mayor influencia (Figura 3.5). El modelo dinámico de Winkler es el modelo más simple debido a la buena relación entre complejidad y precisión en los resultados que otorga. La rigidez se calcula en función de las propiedades del suelo y de la cimentación. El amortiguamiento se calcula como la suma de dos mecanismos de disipación de energía, a saber, amortiguamiento histerético (debido al material) y amortiguamiento por radiación [36]. Se asume que la contribución del amortiguamiento histerético no se tiene en cuenta
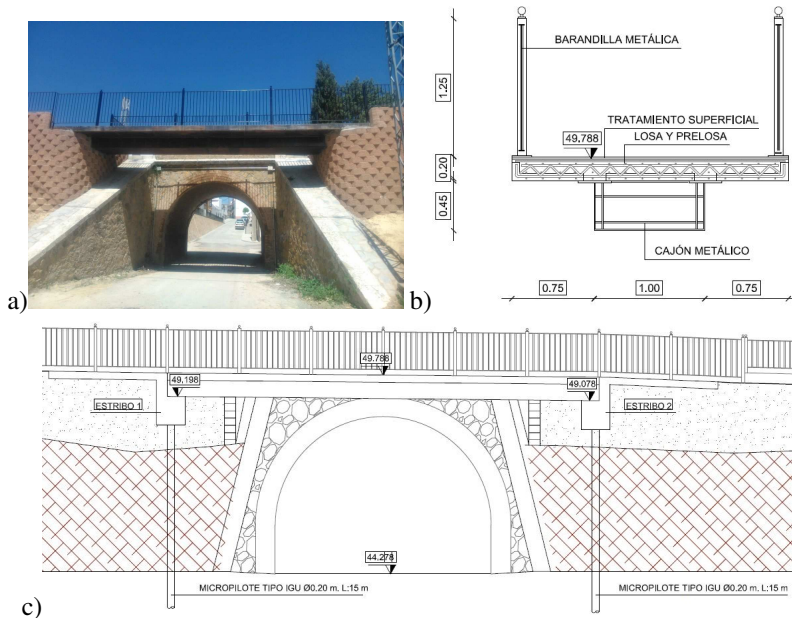
Figura 3.4 Pasarela para la estimación de los parámetros del modelo dinámico de Winkler: a) vista frontal, b) plano de la sección y c) plano de alzado.

en la formulación del problema ya que presenta dos órdenes de magnitud inferior al amortiguamiento de radiación en el rango de frecuencias de interés. En el Artículo del Apéndice D se encuentran las ecuaciones empleadas para calcular la componente de rigidez y de amortiguamiento del modelo dinámico de Winkler.

La pasarela integral tiene un único vano de 12 m de longitud y 2.5 m de ancho. La sección transversal es mixta con un cajón de acero de 0.4 m de alto y un tablero de hormigón de 0.2 m de alto y 2.5 m de ancho. Los estribos de los extremos se apoyan sobre 4 micropilotes de 0.2 m de diámetro y 15 m de longitud. El modelo de EF se implementa en el software ANSYS [78]. El tablero de hormigón, la sección cajón de acero, la barandilla y los micropilotes se modelizan mediante elementos tipo viga de dos nodos y seis grados de libertad por nodo (Beam188). La interacción suelo-estructura se simula mediante elementos tipo muelle-amortiguador unidimensionales (COMBIN14) colocados en cada nodo de los micropilotes y los estribos (Figura 3.5). El modelo de EF presenta un total de 2008 elementos.

Para la caracterización de los elementos muelle-amortiguador se parte de los datos del terreno, que consiste en una primera capa de material de relleno de 5 m de espesor y una segunda capa de arcilla de espesor indefinido y de los que se dispone el valor de la densidad, módulo de Young, coeficiente de Poisson y coeficiente de balasto. El análisis modal da como resultados las tres frecuencias naturales numéricas y sus amortiguamientos numéricos asociados, ξ_{num}, que se muestran en la Tabla 3.6. Las propiedades modales experimentales se obtienen mediante el análisis modal operacional de las señales de
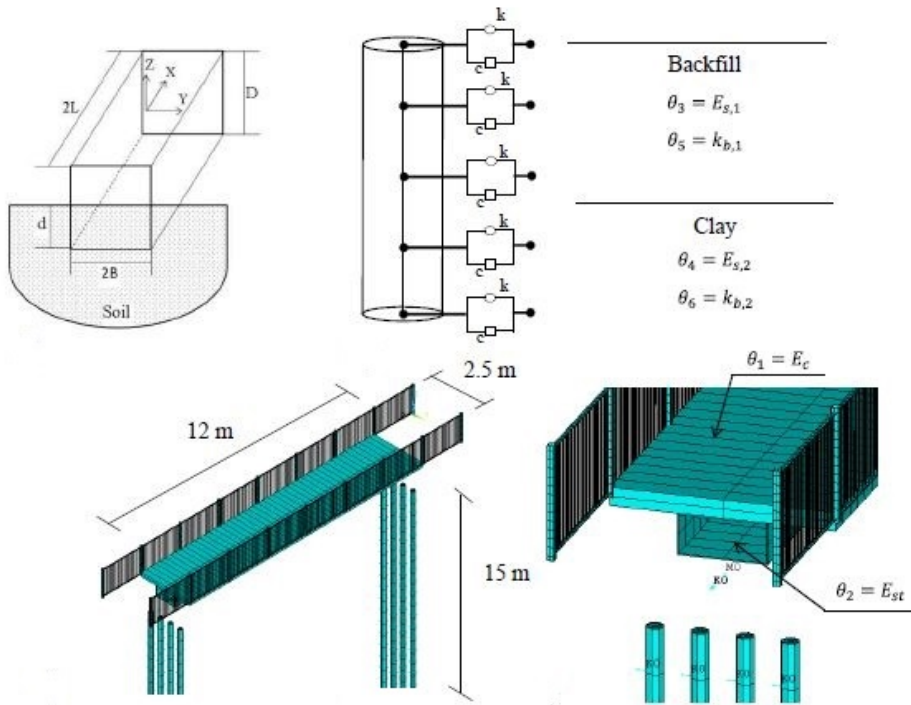
Figura 3.5 Modelo de interacción suelo-estructura de cimentaciones superficiales y profundas y modelo de EF de la pasarela. [Tomada del Artículo del Apéndice D].

Tabla 3.6 Propiedades modales numéricas y experimentales de la pasarela integral antes de la actualización.

Modo	f_{num} [Hz]	f_{exp} [Hz]	ξ_{num} [%]	ξ_{exp} [%]	Δf [%]	$\Delta \xi$ [%]	MAC [-]
1	15.322	15.602	3.103	4.650	1.795	33.268	0.975
2	32.179	35.971	1.121	1.049	10.542	6.863	0.692
3	38.614	40.017	0.700	4.846	3.506	85.555	0.907

aceleraciones medidas durante un ensayo de vibración ambiental. En el Artículo del Apéndice D se encuentran más detalles sobre la configuración del ensayo y el tratamiento de las señales. Las tres frecuencias naturales experimentales obtenidas se recogen en la Tabla 3.6. Además, también se han calculado los amortiguamientos modales experimentales, ξ_{exp}, [70]. Puede observarse que el modelo no simula el comportamiento real de la estructura ya que existen diferencias altas entre los valores numéricos y experimentales, por lo que se procede a actualizar el modelo [117].

El conjunto de parámetros seleccionado resulta de la combinación de aquellos que tienen una mayor influencia en la energía de deformación modal y los parámetros que

Tabla 3.7 Propiedades modales numéricas y experimentales de pasarela integral después de la actualización.

Modo	f_{num} [Hz]	f_{exp} [Hz]	ξ_{num} [%]	ξ_{exp} [%]	Δf [%]	$\Delta \xi$ [%]	MAC [-]
1	16.380	15.602	4.588	4.650	4.987	1.333	0.975
2	35.377	35.971	1.058	1.049	1.651	0.858	0.907
3	40.599	40.017	4.701	4.846	1.454	2.992	0.964

caracterizan el fenómenos de interacción suelo-estructura. Dentro de éstos últimos se hallan: el módulo de Young del relleno y de la arcilla y el coeficiente de balasto también de ambos materiales.

Para la implementación del algoritmo híbrido se adoptan los siguientes valores. El número de armonías generadas aleatoriamente por el algoritmo MHS al inicio de la simulación es de 40, en cada iteración del MHS se crean 20 armonías nuevas y el número de iteraciones del MHS es de 20. Respecto a la implementación del algoritmo UKF se consideran 5 iteraciones, el vector de observaciones se construye a partir de las tres frecuencias naturales experimentales, los tres amortiguamientos experimentales y tres componentes unitarias relativas al residuo de los modos. Se adoptan los siguientes valores para los factores de escala: $\lambda = 0.0001$ [4] y para $\gamma = 0.99$ [106].

A diferencia de las otras aplicaciones, en este problema se consideran tres funciones objetivos que se definen a partir de los residuos de las frecuencias naturales, modos de vibración y amortiguamientos modales, respectivamente. La actualización del modelo de EF tiene de este modo dos ventajas. La primera es obtener un modelo de EF más preciso y la segunda es definir el modelo dinámico de Winkler a partir de los valores de los parámetros del terreno actualizados.

Los parámetros del terreno obtenidos son: módulo de Young del relleno: $7.77 \cdot 10^8$ N/m^2; módulo de Young de la arcilla: $3.5 \cdot 10^7$ N/m^2; coeficiente de balasto del relleno: $4.16 \cdot 10^7$ N/m^3 y coeficiente de balasto de la arcilla: $1.27 \cdot 10^8$ N/m^3. A partir de estos valores se estiman los parámetros del modelo dinámico de Winkler dando como resultado: rigidez en la capa del relleno: $4.16 \cdot 10^6$ N/m; amortiguamiento en la capa del relleno: $7.93 \cdot 10^5$ sN/m; rigidez en la capa de arcilla: $1.27 \cdot 10^7$ N/m y amortiguamiento en la capa de arcilla: $1.68 \cdot 10^5$ sN/m. La validación de estos resultados se realiza en base a la diferencias entre las propiedades modales experimentales y actualizadas. Como puede observarse en la Tabla 3.7, las diferencias relativas entre frecuencias naturales y amortiguamientos han disminuido y el valor del MAC ha aumentado. Además, al haber definido un rango de búsqueda para los parámetros, se garantiza que los valores encontrados mantienen un significado físico adecuado.

3.5 Conclusiones

Los algoritmos de optimización usados para la estimación de parámetros de estructuras de ingeniería civil, generalmente, no tienen en consideración el error en el proceso de estimación ni en las medidas. En el presente capítulo se ha propuesto, desarrollado e

implementado un algoritmo híbrido que permita resolver de manera eficiente el problema de estimación de parámetros bajo la hipótesis de errores asumidos como ruido blanco gaussiano en las medidas y en el proceso de estimación.

Este algoritmo resulta de la combinación de dos técnicas, un algoritmo de búsqueda global, el algoritmo HS, y otro algoritmo de búsqueda local, el algoritmo UKF. Bajo este esquema, el carácter local del algoritmo UKF acelera la búsqueda de una solución global por parte del algoritmo HS. Para garantizar el buen funcionamiento del algoritmo en múltiples problemas, se ha desarrollado para dos casos distintos: el enfoque de optimización de un solo objetivo y el enfoque de optimización multiobjetivo.

Esta propuesta se ha validado a través de la solución de un problema de actualización del modelo de EF de una pasarela donde se estiman los parámetros físicos del modelo de manera que las propiedades modales numéricas y experimentales de la pasarela sean lo más parecidas posible. El problema se ha resuelto asumiendo los dos enfoques citados anteriormente y los resultados se han comparado con los obtenidos por dos algoritmos metaheurísticos convencionales. La comparación ha demostrado que el algoritmo propuesto es más eficiente ya que logra resultados más precisos en un tiempo de simulación menor.

Finalmente, se ha descrito una aplicación adicional del algoritmo para resolver un problema de estimación de parámetros. Este problema consiste en la estimación de los parámetros del modelo dinámico de Winkler para el modelo de una pasarela integral donde el fenómeno de interacción suelo-estructura tiene gran influencia. De esta forma se prueba que el algoritmo híbrido puede extenderse con éxito a otros tipos de problemas de ingeniería civil.

4 Algoritmo colaborativo de inteligencia artificial para estimación de parámetros

El presente capítulo aborda la implementación de un nuevo algoritmo colaborativo que, además de reducir el tiempo de computación, permite elegir la mejor solución entre todo el conjunto de posibles soluciones óptimas que forman el frente de Pareto de una manera robusta. Partes del presente capítulo se pueden encontrar en los Artículos de los Apéndices E y F.

La organización del capítulo es la siguiente. En primer lugar se expone el problema que presenta el uso de algoritmos de optimización multiobjetivo. Bajo este enfoque no se obtiene una solución única, sino un conjunto de soluciones y, por tanto, para finalizar el problema, hay que elegir el punto óptimo de entre todos ellos. Se describen los métodos más comunes encontrados en la literatura para resolver este problema.

Seguidamente se describe el algoritmo que se propone en esta tesis para resolver problemas de estimación de parámetros empleando algoritmos multiobjetivo, reduciendo el coste computacional e implementando un método para resolver la toma de decisiones de manera robusta. Asimismo, se detallan las técnicas de inteligencia artificial y numéricas que se consideran en el algoritmo.

Finalmente se expone una aplicación del algoritmo para su validación, aplicándolo a un problema de actualización del modelo de EF de una pasarela.

4.1 El problema de la toma de decisiones en optimización multiobjetivo

La resolución de un problema de optimización multiobjetivo da como resultado el frente de Pareto, que está formado por la frontera de puntos para los que no existe otra solución tal que mejore un objetivo sin sacrificar el otro. Cada punto que forma esta curva es una posible solución al problema y la elección de la solución más adecuada generalmente no

es inmediata ya que no existe un punto que minimice ambos objetivos simultáneamente (ver Figura 4.1). Para ayudar en la tarea de elegir la mejor solución se realiza un análisis teniendo en cuenta múltiples criterios que permite obtener la solución óptima de una manera sistemática. No obstante, como puede apreciarse en la Figura 4.1, la solución óptima es sensible a la discretización del frente de Pareto, ya que a menor número de puntos la probabilidad de que la solución óptima esté mal representada es mayor.
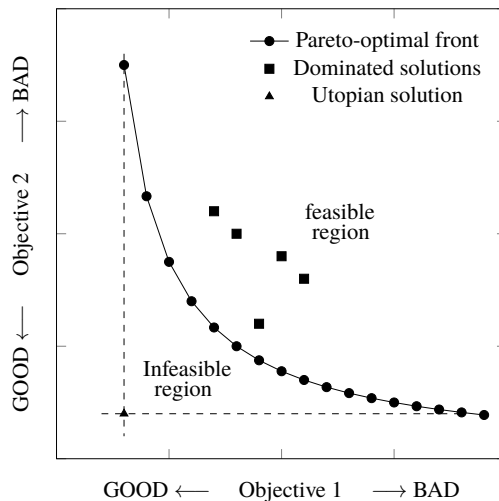
Figura 4.1 Representación de compromiso en una optimización de dos objetivos. Tomada del Artículo E.

A este tipo de análisis se les denomina problema o estrategia de toma de decisiones y pueden clasificarse según el momento en el que se aplica en [14]:

- Métodos *a priori*: antes de realizar el proceso de optimización es necesario aportar suficiente información sobre la preferencia de los objetivos.

- Métodos interactivos: consiste en expresar las preferencias en cada iteración del algoritmo de optimización.

- Métodos *a posteriori*: Las preferencias acerca de los objetivos se introducen una vez realizado el proceso de optimización.

Los métodos *a posteriori* constituyen la opción más empleada debido a dos razones. La primera de ellas es que la toma de decisión se realiza considerando toda la información de compromiso entre los objetivos. La segunda razón es que los algoritmos son más simples en comparación con aquellos empleados en los otros dos métodos ya que no es necesario modificarlos para incluir las preferencias. Las preferencias se formulan de manera que haya un compromiso entre los valores de los objetivos. En este sentido, la solución del frente de Pareto que para una pequeña mejora en un objetivo conlleve un gran deterioro en al menos otro objetivo es las más adecuada. Este punto se conoce como *knee point* [22].

Por tanto, la definición del *knee point* es fundamental a la hora de resolver el problema de toma de decisiones. Existen en la literatura diversas definiciones del *knee point*, de las cuales se describirán a continuación las más empleadas. En el Artículo del Apéndice E se puede encontrar una definición más detallada de cada uno de los siguientes métodos.

- Método de intersección normal al contorno [22].

  La idea de este método es unir mediante una línea recta los dos puntos extremos del frente de Pareto normalizado para construir el contorno. El punto que se encuentre a una mayor distancia en la dirección normal al contorno es el *knee point*.

- Método del ángulo de reflexión [15].

  Este método define el *knee point* como aquel que tenga el máximo ángulo de reflexión con el punto inmediatamente próximo a la izquierda y a la derecha.

- Método del ángulo de flexión [23].

  Análogo al anterior, el *knee point* que proporciona este método es aquel que tiene el máximo ángulo de flexión positivo.

- Método basado en la utilidad [15].

  Este método requiere definir una función de utilidad lineal que es función del valor de los dos objetivos y de un parámetro, λ:

$$U(\mathbf{f},\lambda) = \lambda f_1 + (1-\lambda)f_2 \tag{4.1}$$

  siendo f_1 y f_2 el valor de los dos objetivos de un punto del frente de Pareto. La aplicación del método consiste en los siguientes pasos: i) para cada solución del frente de Pareto se define un contador c que toma el valor nulo inicialmente, ii) se toma un vector con valores de $\lambda \in [0,1]$ dividiendo el rango en un número dado, iii) para cada valor de λ se calcula el valor de $U(\mathbf{f},\lambda)$ para todos los puntos del frente de Pareto, iv) para cada valor de λ a aquella solución del frente de Pareto que tenga el valor mínimo de U se le incrementa su contador en una unidad, v) se repiten los pasos ii)-iv) iterativamente. Para garantizar la precisión de este método es fundamental que el número de divisiones del rango realizado en el paso ii) no sea el mismo en cada iteración. La solución del frente de Pareto con mayor valor de c es el *knee point*.

- Método de compromiso [23].

  Finalmente, este método dota al usuario de un mayor control en la toma de decisiones ya que se especifican dos parámetros, α y β, para proporcionar la información sobre la preferencia en el balance de objetivos.

En el Artículo del Apéndice E se realiza un análisis comparativo de los métodos anteriores para la obtención de la mejor solución de entre el conjunto de posibles soluciones que forman el frente de Pareto. Para tal fin, el modelo de EF de una pasarela real se actualiza en base a las propiedades modales experimentales empleando un algoritmo de optimización con dos funciones objetivos. En la Figura 4.2 se muestra el frente de Pareto resultante y la solución óptima según los cuatro primeros métodos anteriores, siendo NBI el método de

intersección normal al contorno por sus siglas del inglés (*Normal Boundary Intersection method*). La decisión de cuál aporta una solución más acertada se realiza en función de la mejora relativa entre el valor inicial y el valor actualizado de los dos objetivos. En base a este criterio se concluye que el método de intersección normal al contorno es el que mejora ambos objetivos de una manera más equilibrada.
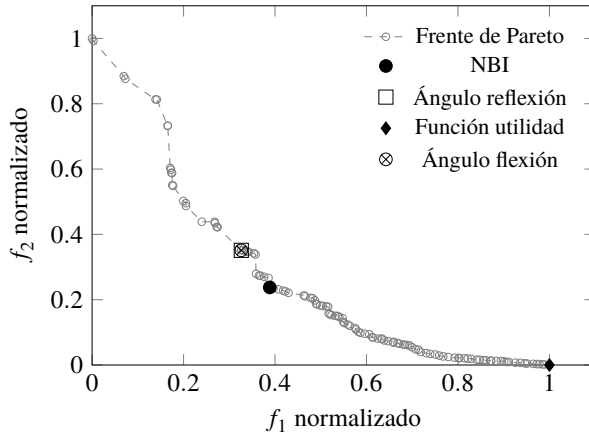
Figura 4.2 Comparación gráfica de los *knee points* obtenidos por los diferentes métodos.

El objetivo de indicar cuál de los métodos anteriores da una mejor solución en términos de mejoras relativas es el de tener un método con el que hacer la comparación entre la solución propuesta por dicho método y la solución obtenida mediante la implementación del algoritmo colaborativo que se presenta en este capítulo.

4.2   Descripción del algoritmo colaborativo

El algoritmo colaborativo que se propone en este capítulo hace uso de técnicas de inteligencia artificial, estadísticas y de optimización para resolver el problema de estimación de parámetros a partir de una optimización multiobjetivo. El término *colaborativo* hace referencia al hecho de que las técnicas se usan de manera secuencial dentro del proceso completo.

El proceso comienza con el uso de un algoritmo de optimización multiobjetivo cuyo resultado es el frente Pareto. Para este fin, el algoritmo de optimización utilizado es el MHS descrito en el Capítulo 2. Al frente de Pareto se le realiza un análisis de componentes principales para obtener la representación del frente de Pareto en componentes principales. Esta transformación presenta dos ventajas principales: i) permite mejorar la precisión de cualquier modelo predictivo ajustado a los datos procesados y ii) el frente de Pareto en el espacio de componente principales posee forma convexa, simplificando la resolución del problema de toma de decisiones para hallar el *knee point*. Esta representación del frente de Pareto en el espacio de componentes principales es simulada por una red neuronal, que relaciona los parámetros del modelo de EF con la función multiobjetivo, y que permite

obtener un frente continuo y convexo. Para obtener el *knee point* se emplea un algoritmo de minimización local debido al carácter continuo y convexo que presenta el frente de Pareto aproximado por la red neuronal.

En los siguientes subapartados se explican en qué consisten las técnicas empleadas y la descripción del proceso completo realizado por el algoritmo colaborativo.

4.2.1 Análisis de componentes principales

Al disponer de una muestra de datos, es común considerar el mayor número de variables que sea posible. En ocasiones, esta tendencia trae consigo que el número de coeficientes de correlación sea tan elevado que dificulte extraer relaciones entre variables. Además, se presenta la posibilidad de que algunas variables estén muy relacionadas y considerar solo una de ellas aporte la misma información que contemplarlas todas.

En este contexto, el análisis de componentes principales (ACP) permite reducir el número de variables identificando y extrayendo patrones a partir de la muestra de datos de variables correlacionadas para transformarlo en otro conjunto de nuevas variables no correlacionadas entre sí que se denomina conjunto de componentes principales.

El análisis de componentes principales se realiza aplicando uno de los dos siguientes métodos [48]. El primero se basa en la matriz de covarianza de los datos y el segundo en la matriz de correlaciones. En el Artículo del Apéndice F se ha optado por seguir el primer método debido a que los datos son dimensionalmente homogéneos. Para llevar a cabo el análisis empleando la matriz de covarianza, el primer paso es normalizar los datos; es decir, transformarlos de manera que tengan media 0 y varianza 1. Seguidamente, se calcula la matriz de covarianza de estas variables estandarizadas y se obtienen sus autovalores y autovectores. Los autovalores se ordenan de manera decreciente y los correspondiente autovectores son las componetes principales.

Explicado de manera más precisa, suponiendo un conjunto inicial de datos de p variables correlacionadas, la matriz de covarianzas será de orden p y sus p autovalores, $\lambda_1, \ldots, \lambda_p$, serán distintos si es definida positiva. Ordenando de mayor a menor los autovalores, sus autovectores asociados, $a_1, \ldots, a_p$, son las componentes principales. Como las variables deben ser no correlacionadas $Cov(a_i, a_j) = 0$ para $i \neq j$. Si se desea reducir el número de variables, se toman $q < p$ variables atendiendo a la relación entre cada autovalor y la suma total de los autovalores $\dfrac{\lambda_i}{\sum_1^p \lambda_j}$. Multiplicando el conjunto de datos originales por los autovectores se obtienen las proyecciones de los datos en el espacio de componentes principales.

Una de las principales ventajas de este análisis es que los datos originales se pueden transformar a ese nuevo espacio (generalmente de tres o menos dimensiones para facilitar la representación gráfica) donde se evidencian mejor las relaciones entre las nuevas variables.

4.2.2 Redes neuronales artificiales

Una red neuronal artificial (ANN del inglés *Artificial Neural Network*) es una técnica de inteligencia artificial que permite crear relaciones no lineales y acopladas entre un conjunto de parámetros de entrada y un conjunto de parámetros de salida de la propia red, es decir, expresar una función de $\Re^n \to \Re^2$, siendo n el número de parámetros a estimar.

La principal ventaja que poseen las redes neuronales es su buena habilidad para aprender adaptándose a las condiciones. No es casual, por tanto, que su empleo haya tenido un gran auge recientemente en múltiples aplicaciones de ingeniería [92].

La tipología de red más usada es la del perceptrón multicapa (MLP en adelante por sus siglas en inglés *Multilayer Perceptron*) que puede observarse en la Figura 4.3. El diseño de este tipo de red consiste en una primera capa de entrada, un conjunto de capas ocultas y finalmente una capa de salida. Las neuronas de las múltiples capas están conectadas de forma secuencial (*feed forward*) donde la información fluye unidireccionalmente ya que cada neurona envía información a todas las neuronas de la siguiente capa pero no recibe ninguna información de ellas.
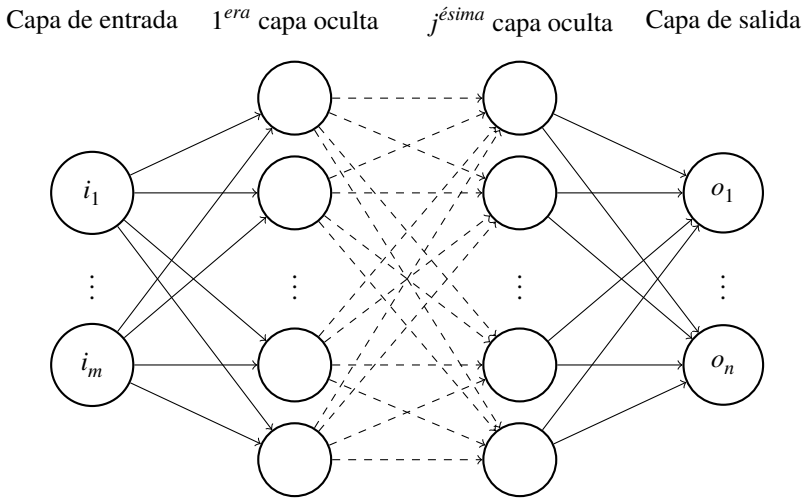
Figura 4.3 Arquitectura del MLP con una capa de entrada, j capas ocultas y la capa de salida. La capa de entrada tiene m neuronas (parámetros de entrada) y la capa de salida tiene n neuronas (parámetros de salida).

El proceso por el que una neurona produce una salida se realiza mediante una transformación no lineal de la suma ponderada de las entradas que recibe. Para llevar a cabo dicha ponderación se utilizan pesos. El cálculo de los pesos se realiza con el llamado entrenamiento de la red, el cual constituye la fase más importante para la construcción de la red neuronal. El entrenamiento de la red consiste en ajustar los pesos de la conexión entre dos neuronas realizando una propagación hacia atrás, es decir, los pesos se ajustan iterativamente minimizando el error entre la salida estimada y la salida deseada. Por tanto, el entrenamiento de la red neuronal se formula como un problema no lineal de minimización que se resuelve empleando algoritmos basados en el gradiente cuyo resultado es el conjunto de pesos que definen las conexiones de la red.

El número de capas ocultas y de neuronas en cada capa oculta es un asunto clave a la hora de diseñar la red para garantizar su precisión. El número de neuronas se calcula siguiendo dos posibles vías: la primera es mediante un proceso de prueba y error que

minimice el mínimo error cuadrático [68] y la segunda es aplicando relaciones empíricas [56, 34]. En el Artículo del Apéndice F se considera una única capa oculta ya que ha sido demostrado que es suficiente para aproximar uniformemente cualquier función continua [21, 32].

4.2.3   Algoritmo colaborativo para estimación de parámetros y toma de decisiones

El algoritmo propuesto en este capítulo consiste en la aplicación de manera secuencial de las técnicas explicadas para conseguir una reducción del tiempo de ejecución a la hora de resolver un problema de estimación de parámetros y, además, resolver el problema de la toma de decisiones de manera robusta.

Para entender la reducción de tiempo es necesario remarcar que la consecución de una buena solución óptima en un problema de optimización multiobjetivo pasa por disponer de un frente de Pareto con muchos puntos. Este proceso requiere un gran número de iteraciones y poblaciones en el algoritmo y, por tanto, un elevado tiempo de simulación. Es en ese proceso donde el algoritmo colaborativo que se propone permite reducir el coste computacional, ya que un frente de Pareto con menos puntos precisa de menos tiempo de ejecución.

En la Figura 4.4 se puede observar el esquema general que sigue el algoritmo propuesto. En los siguientes párrafos se irán desgranando cada uno de los pasos.

En primer lugar se parte de un conjunto de soluciones iniciales generadas aleatoriamente que no tienen por qué necesariamente ser soluciones no dominadas (las que forman el frente de Pareto). El algoritmo de optimización MHS resuelve el problema de optimización. Al existir una relación proporcional entre el número de puntos que forman el frente de Pareto y el tiempo de simulación, la idea principal del algoritmo colaborativo es que el MHS calcula un frente de Pareto poco poblado. No obstante, un frente de Pareto poco poblado trae consigo la problemática de que su *knee point* no sea una solución óptima al problema.

Para solventar este posible problema se emplean las dos técnicas descritas anteriormente: un análisis de componentes principales y la implementación de una red neuronal artificial. Primero, se realiza el análisis de componentes principales al frente de Pareto. Como resultado, el frente de Pareto se proyecta en el espacio de componentes principales, donde los datos quedan representados en un espacio que maximiza su variabilidad. A este frente de Pareto se le denomina procesado. Una característica del frente de Pareto procesado es que exhibe una forma convexa por lo que el problema de toma de decisiones se puede formular de una manera más simple. En primer lugar, porque la definición de *knee point* es la de aquél punto que represente el mínimo de la curva en el espacio de componentes principales. En segundo lugar, porque el mínimo local en una función convexa es el mínimo global. De este modo, el problema de optimización para obtener el *knee point* puede resolverse empleando un algoritmo de optimización local.

Sin embargo, el frente de Pareto procesado también es poco poblado y podría no contener el *knee point* óptimo del problema. Para tratar este asunto se diseña, entrena y valida una red neuronal que aproxima el frente de Pareto procesado. Esta red neuronal establece las relaciones entre los parámetros de entrada y los valores de las funciones objetivo. El frente

de Pareto aproximado por la red neuronal es una función convexa y continua en el rango donde está definida.

El problema de la toma de decisiones se resuelve sistemáticamente minimizando el valor de la segunda componente principal aplicando un algoritmo de minimización local. Estos algoritmos resultan más efectivos que algoritmos más complejos cuando el problema a resolver es minimizar una función convexa. En esta propuesta se hace uso del algoritmo *Active Set* (A-S), del que puede ampliar su información consultando el artículo del Apéndice F. Como resultado, se obtiene el mínimo de la función que representa el *knee point* y el valor de los parámetros de entrada asociados. Merece la pena remarcar que el *knee point* obtenido no tiene por qué pertenecer al frente de Pareto procesado sino simplemente a la curva aproximada mediante el empleo de la red neuronal, justificándose así que el frente de Pareto original no precisa ser muy poblado.

Finalmente, la solución obtenida por el algoritmo de minización local (solución óptima del problema) se puede proyectar en el frente de Pareto original para su visualización.

4.3   Ejemplo de aplicación

La propuesta de un nuevo algoritmo requiere de una validación. Con tal objetivo, el algoritmo colaborativo desarrollado se emplea para resolver un problema de estimación de parámetros y se comparan los resultados con los obtenidos por un algoritmo convencional.

El problema a resolver es la actualización de un modelo de EF de una pasarela real situada en la provincia de Sevilla. Como algoritmo convencional se considera el MHS.

La estructura de la pasarela (Figura 4.5a) consiste en una celosía Warren de acero con una longitud total de 96 m dividida en cuatro vanos continuos. El tablero tiene un ancho de 3.5 m y se apoya en tres pilas de acero que se encuentran cimentadas al terreno por un pilote de 1 m de diámetro y 11 m de longitud. En los estribos, la pasarela está simplemente apoyada mediante dos apoyos de neopreno. El modelo de EF de la pasarela se construye usando el software ANSYS [78] (Figura 4.5b). Todos los elementos estructurales se modelizan mediante elementos tipo viga de dos nodos con seis grados de libertad por nodo (elemento Beam188), excepto el tablero y el techo que se modelizan mediante elementos tipo placa de cuatro nodos y seis grados de libertad por nodo (elemento Shell181). La interacción suelo-estructura de la pasarela se modeliza considerando un modelo estático de Winkler. En este modelo, los estribos se modelizan como elementos masivos con rigideces en los 6 grados de libertad y el suelo adyacente a los pilotes como muelles colocados a lo largo de la longitud del pilote en las dos direcciones transversales al mismo. En ambos se emplean elementos tipo muelle unidimensionales (elemento Combin14). El modelo de EF consta de 7503 elementos y 9419 nodos. Realizando el análisis modal al modelo de EF se obtienen las frecuencias naturales y los modos de vibración que se muestran en la Tabla 4.1.

Las propiedades experimentales de la pasarela se obtienen mediante el análisis modal operacional de las mediciones realizadas en un ensayo de vibración ambiental (Figura 4.5c). Para realizar dichas mediciones, se emplearon tres acelerómetros triaxiales colocados en una malla de 34 puntos de medición (2 filas longitudinales de 17 puntos cada una). Más detalles de la configuración del ensayo y el tratamiento de las señales se pueden encontrar
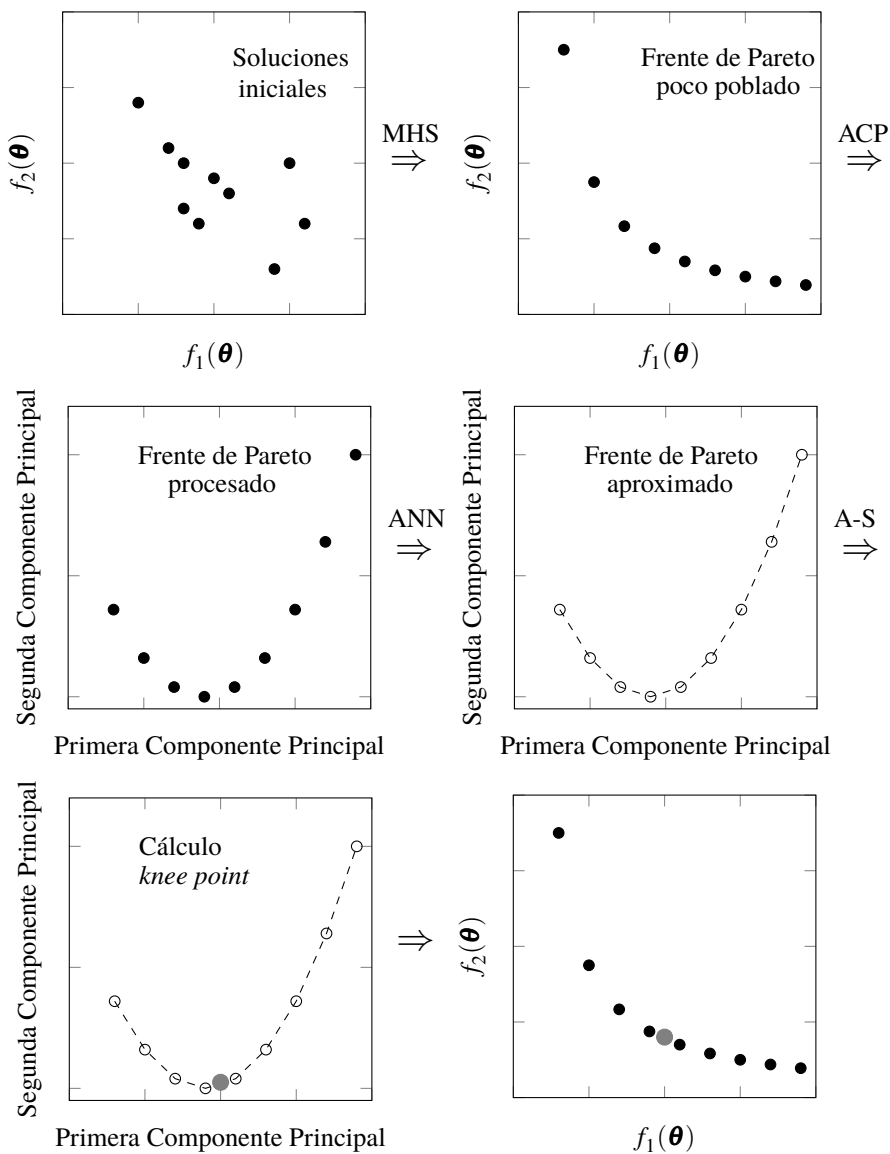
Figura 4.4 Esquema del algoritmo colaborativo de inteligencia artificial y optimización multiobjetivo.

en el Artículo del Apéndice F. En la Tabla 4.1 se indican asimismo los valores de las propiedades modales experimentales así como la diferencia relativa entre las frecuencias numéricas y experimentales y el MAC.
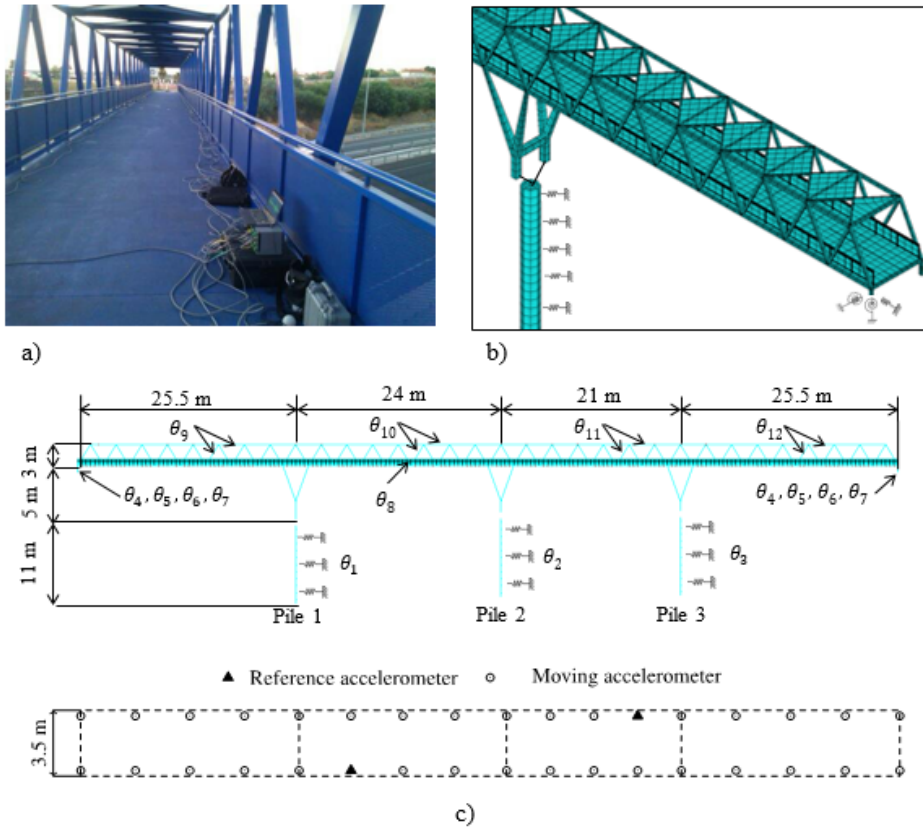
Figura 4.5 Pasarela en estudio: a) ilustración de la pasarela, b) modelo de EF y c) configuración del ensayo de vibración ambiental.

4.3.1   Actualización del modelo de EF aplicando el algoritmo colaborativo

Para resolver el problema de actualización del modelo de EF de la pasarela se eligen como variables de diseño los parámetros físicos del modelo que presentan mayor incertidumbre. La elección de estos parámetros a actualizar se hace de manera sistemática realizando un análisis de sensibilidad que permite conocer aquellos que tengan mayor influencia en alguna característica de referencia de la estructura. La energía de deformación modal, siguiendo la formulación de Fox y Kapoor [29], es el parámetro empleado para dilucidar cuáles son los parámetros físicos que más influyen en el comportamiento dinámico de la pasarela. En la Figura 4.6 se representa la matriz de sensibilidad, donde puede apreciarse aquellos parámetros que tienen una mayor influencia en la energía de deformación modal. En vista a los resultados, se toman los siguientes doce parámetros de actualización: rigidez de la interacción suelo-pilote de cada pilote (tres), rigideces en los estribos (longitudinal, transversal, giro sobre eje vertical y giro sobre eje transversal), módulo de Young del tablero y módulos de Young del acero de cada vano (cuatro). En el Artículo del Apéndice F

Tabla 4.1 Propiedades modales numéricas y experimentales de la pasarela.

Modo	f_{num} [Hz]	f_{exp} [Hz]	Δf [%]	MAC [-]
1. Lateral	1.704	1.872	-8.974	0.997
2. Lateral	3.560	3.506	1.540	0.969
3. Lateral	6.424	5.851	9.793	0.922
4. Longitudinal	6.610	6.914	-4.397	0.966
5. Lateral	8.868	8.217	7.923	0.958
6. Lateral	9.486	8.515	11.403	0.929
7. Vertical	9.483	9.189	3.199	0.947
8. Vertical	9.720	9.483	2.499	0.914
9. Vertical	11.788	11.240	4.875	0.875
10. Lateral	13.854	11.828	17.129	0.765
11. Vertical	14.068	12.812	9.803	0.816

se puede encontrar una descripción más detallada del análisis de sensibilidad llevado a cabo.
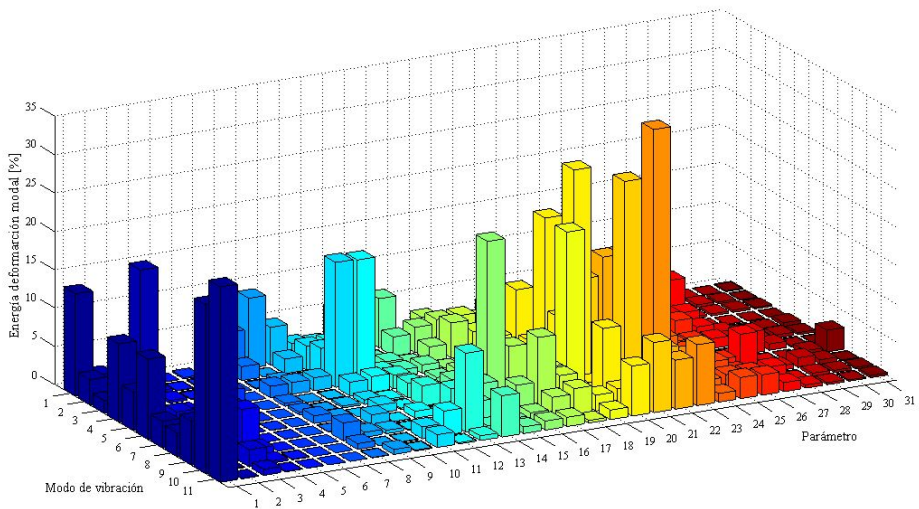
Figura 4.6 Representación gráfica de la matriz de sensibilidad para la elección de los parámetros a actualizar.

La estimación de parámetros empleando el algoritmo colaborativo comienza con la generación de un conjunto de posibles soluciones aleatorias. Para ello, 100 armonías iniciales se crean aleatoriamente usando el algoritmo MHS donde cada armonía es un vector de 12 componentes (los 12 parámetros físicos a actualizar). Para obtener el frente de Pareto poco poblado se adoptan los siguientes valores para los parámetros del algoritmo MHS: número máximo de iteraciones, 100; nuevas armonías en cada iteración, 25; *hmcr* = 0.8 y

par = 0.4 [110]. La ejecución de este proceso iterativo tiene una duración de $t_1 = 11700$ s, empleado un ordenador con un procesador de 3.6 GHz y una memoria RAM de 8 Gb. En la Figura 4.7a se muestra el frente de Pareto poco poblado obtenido mediante el algoritmo MHS.

A continuación, se realiza el análisis de componentes principales del frente de Pareto. La matriz de covarianza de los datos se descompone aplicando el método de descomposición en valores singulares. En la Figura 4.7b se puede observar la representación en el espacio de componentes principales del frente de Pareto procesado. Como se indicó anteriormente, esta representación toma la forma de una curva convexa cuya principal ventaja es la simplicidad que toma la definición de *knee point*. La ejecución de este paso es inmediata asumiendo que el orden de magnitud del proceso completo será del orden de t_1. Por ello, el tiempo de ejecución de este paso se redondea a $t_2 = 1$ s.

Al ser el frente de Pareto procesado una curva formada por pocos puntos, cabe la posibilidad de que no tenga representada la solución óptima del problema. La red neuronal artificial permite tener una función continua que aproxima al frente de Pareto procesado. La configuración de esta red neuronal consiste en una capa de entrada con 12 neuronas (parámetros a estimar), una capa de salida con 2 neuronas (número de funciones objetivo) y una capa oculta como se justificó anteriormente. El número de neuronas de esta capa oculta se calcula empleando la regla de Kermanshahi [56]

$$neuronas = \frac{m+n}{2} + \delta \tag{4.2}$$

siendo $m = 12$, $n = 2$ y δ un factor de normalización que puede tomar el valor de 1 o 2. Asumiendo $\delta = 1$ se obtiene que el número de neuronas de la capa oculta de 8. El entrenamiento de la red para calcular los pesos de las conexiones entre neuronas se realiza usando el algoritmo de Levenberg-Marquardt, formulando la función de error mediante el error cuadrático medio [41]. La convergencia del algoritmo de entrenamiento se alcanza en la iteración 8 teniendo un tiempo de ejecución del orden de $t_3 = 1$ s. En la Figura 4.7b se representa el frente de Pareto aproximado por la red neuronal donde puede contemplarse la exactitud con la que la red aproxima los puntos.

Finalmente, aprovechando las virtudes que el frente de Pareto aproximado presenta por sus propiedades convexas, la elección del *knee point* se realiza resolviendo un problema de minimización con restricciones usando el algoritmo de minimización local active-set. Las restricciones implementadas en el algoritmo representan los límites donde el frente de Pareto aproximado queda definido. El tiempo de simulación de este paso es de aproximadamente $t_4 = 2$ s. En el Artículo del Apéndice F se pueden consultar más detalles sobre la resolución del problema de actualización del modelo de EF empleando el algoritmo colaborativo propuesto.

La solución obtenida es la solución óptima al problema de estimación de parámetros y los parámetros físicos asociados son aquellos que aseguran el mejor ajuste entre las propiedades modales numéricas y experimentales de la pasarela.
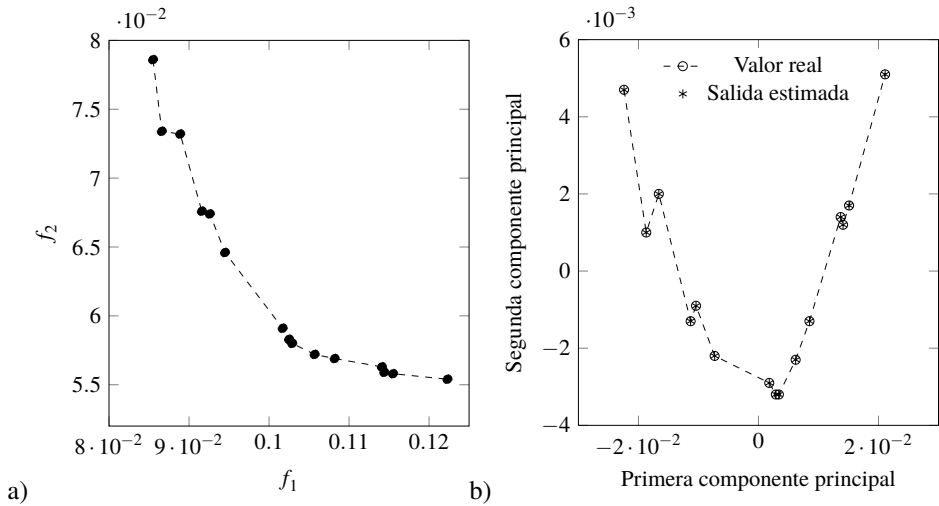
Figura 4.7 Frente de Pareto del problema de estimación de parámetros de la pasarela: a) Original poco poblado, b) frente de Pareto procesado en el espacio de componentes principales y aproximado por la red neuronal artificial.

4.3.2 Comparación de resultados y tiempos de ejecución con un algoritmo convencional

Para evaluar el rendimiento del algoritmo colaborativo propuesto, se comparan los resultados y el tiempo de simulación con los de la actualización del modelo de EF considerando el algoritmo MHS de manera clásica, es decir, generando como resultado un frente de Pareto con muchos puntos y procesándolo con alguno de los métodos de toma de decisiones.

Se asume, por tanto, que para garantizar que el frente de Pareto está bien definido la población inicial del algoritmo MHS es de 200 armonías generadas aleatoriamente. Los valores de *hmcr* y *par* son los mismos indicados anteriormente. El problema de la toma de decisiones para obtener la solución óptima se resuelve empleando el método de intersección normal al contorno descrito en el apartado 4.1 [22]. Para enriquecer la comparación entre ambos métodos se lleva a cabo un estudio de sensibilidad para analizar la variación de la mejor solución en términos del número de iteraciones considerado. Con este propósito, la actualización del modelo de EF se resuelve para cuatro valores diferentes del número de iteraciones: 150, 200, 250 y 300.

En las Figuras 4.8a-d se representa una comparación gráfica de la solución obtenida empleando el algoritmo colaborativo y las soluciones considerando el algoritmo MHS convencional. Además, en la Tabla 4.2 se muestra numéricamente la comparación entre las soluciones en términos de distancia entre los puntos obtenidos por el algoritmo colaborativo y el convencional y en términos del tiempo de simulación. El tiempo que tarda el algoritmo colaborativo se obtiene como la suma de t_1, t_2, t_3 y t_4.

Queda ilustrado el buen rendimiento del algoritmo colaborativo para abordar problemas de estimación de parámetros basados en optimización multiobjetivo debido a la clara convergencia que exhibe la solución con la solución obtenida mediante la aplicación del método convencional cuando el número de iteraciones aumenta. En particular, el algoritmo
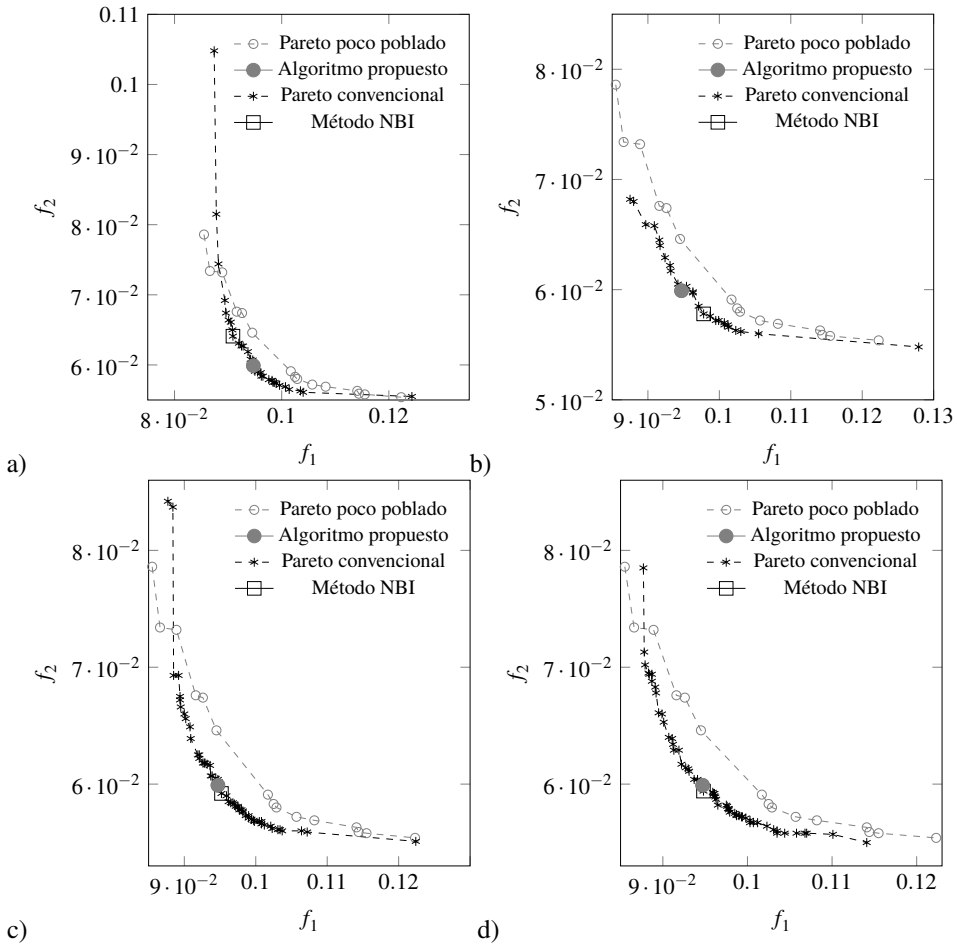
Figura 4.8 Comparación entre las soluciones del algoritmo propuesto y el convencional para a) 150 iteraciones, b) 200 iteraciones, c) 250 iteraciones y d) 300 iteraciones.

propuesto permite reducir el tiempo de simulación en más de un 50 %. De este modo, se ha validado el algoritmo propuesto. Además, se postula como una herramienta eficiente para resolver problemas de estimación de parámetros, reduciendo el tiempo de computación sin perder precisión en los resultados y abordando el problema de la toma de decisiones de manera robusta.

4.4 Conclusiones

Los problemas de optimización multiobjetivo presentan dos principales inconvenientes: el primero es el alto coste computacional que requieren y el segundo es la necesidad de

Tabla 4.2 Valores de la función multiobjetivo para el modelo mejor actualizado, distancia entre las mejores soluciones obtenidas por ambos algoritmos y tiempo total de simulación.

Algoritmo	Iteraciones	$f_1(\boldsymbol{\theta})$	$f_2(\boldsymbol{\theta})$	distancia $[-]$	$t\,[\text{s}]$
Colaborativo	100	$9.47 \cdot 10^{-2}$	$5.99 \cdot 10^{-2}$	-	11704
MHS	150	$9.09 \cdot 10^{-2}$	$6.41 \cdot 10^{-2}$	$5.66 \cdot 10^{-3}$	16336
MHS	200	$9.78 \cdot 10^{-2}$	$5.78 \cdot 10^{-2}$	$3.74 \cdot 10^{-3}$	23640
MHS	250	$9.52 \cdot 10^{-2}$	$5.92 \cdot 10^{-2}$	$8.60 \cdot 10^{-4}$	25194
MHS	300	$9.48 \cdot 10^{-2}$	$5.94 \cdot 10^{-2}$	$5.10 \cdot 10^{-4}$	29582

resolver un problema de toma de decisiones para elegir el mejor punto del frente de Pareto cuya precisión depende de la definición de un Pareto suficientemente poblado.

A pesar de la existencia de varios métodos para resolver este problema de toma de decisiones, el objetivo de este capítulo es desarrollar e implementar un algoritmo colaborativo que afronta los dos inconvenientes anteriores de manera simultánea. Para ello se emplean técnicas de inteligencia artificial, estadísticas y de optimización. En concreto, el algoritmo propuesto se describe como una sucesión de pasos empleando el algoritmo MHS, el análisis de componentes principales, una red neuronal y finalmente un algoritmo de minimización local para obtener el punto óptimo.

El rendimiento del algoritmo se ha validado mediante la aplicación del mismo para resolver un problema de actualización del modelo de EF de una pasarela y comparando los resultados con los obtenidos por un algoritmo convencional. Esta comparación reporta unas reducciones de tiempo de computación de más del 50 % sin comprometer la precisión de la solución.

5 Conclusiones y trabajos futuros

5.1 Conclusiones

En esta tesis se han propuesto, implementado y validado dos algoritmos de optimización para la estimación de parámetros, que de un modo u otro, presentan una mayor eficiencia que los algoritmos convencionales cuando se emplean para problemas de ingeniería civil.

Para llevar a cabo estas propuestas se ha realizado, en primer lugar, un análisis comparativo para conocer el algoritmo de optimización que mejor rendimiento ofrece, así como cual de los dos enfoques posibles, la optimización de un único objetivo y la optimización multiobjetivo, presenta mejores resultados. Para la comparación entre algoritmos de optimización se ha optado por tres algoritmos metaheurísticos, dos de ellos ampliamente aplicados para la actualización de modelos de EF, el GA y el PS. El tercero es el algoritmo HS, del que existen muy pocos casos prácticos donde se aplique a la actualización de modelos de EF.

Para realizar la comparación se ha resuelto un problema de actualización del modelo de EF de una pasarela de laboratorio. Los resultados de este análisis comparativo han reportado una mayor eficiencia del algoritmo HS, tanto en un único objetivo como en multiobjetivo, ya que obtiene una solución con la misma precisión que el PS pero con coste computacional menor. Es destacable también que el GA es el que presenta una peor eficiencia de los tres. Comparando los dos enfoques entre sí, se concluye que el enfoque multiobjetivo ofrece soluciones más precisas en términos de los valores de los residuos ya que los puntos de la optimización de un único objetivo se encuentran más lejos del *knee point* del frente de Pareto. Además, el tiempo de simulación es mayor para el caso de un único objetivo ya que es necesario llevar a cabo un análisis de sensibilidad de los pesos de los residuos. Estos dos motivos justifican la elección del algoritmo HS en optimización multiobjetivo (MHS) para la formulación de los dos algoritmos que se han propuesto en esta tesis.

El primer algoritmo que se ha propuesto es un algoritmo híbrido UKF-MHS que aprovecha las virtudes que un algoritmo global (el MHS) y uno local (el UKF) presentan de manera independiente. El algoritmo UKF, al pertenecer a la familia de los filtros de Kalman, permite considerar el error tanto en las medidas (observaciones) como en el

proceso de estimación para converger a un valor esperado de los parámetros. Además, el carácter global del MHS asegura que el algoritmo no convergerá a un mínimo local de la función objetivo. De este modo, la ventajas de este algoritmo es doble: primero, el modelo actualizado es más preciso ya que al considerar los errores, las discrepancias entre el modelo numérico actualizado y la estructura real se reducen y, segundo, se aprovecha el carácter local-global para acelerar la búsqueda de soluciones sin caer en un mínimo local.

La validación del algoritmo se ha realizado a través de la actualización del modelo de EF de una pasarela de laboratorio, comparando los resultados con los reportados por los algoritmos GA y HS. Como principal conclusión cabe indicar que el algoritmo propuesto presenta una mayor eficiencia ya que la solución elegida del frente de Pareto se encuentra a menor distancia del origen de coordenadas. El GA es el que presenta un peor rendimiento de los tres en términos de precisión y tiempo de simulación. Se ha presentado también una segunda aplicación del algoritmo para estimar los parámetros del modelo dinámico de Winkler en el estudio del fenómeno de interacción suelo-estructura de una pasarela integral. Los parámetros se han definido a partir de los valores de las propiedades mecánicas del terreno calibrados en base a las propiedades modales de la estructura.

El enfoque multiobjetivo de la optimización da como resultado un conjunto de soluciones óptimas representado en el frente de Pareto. Elegir la adecuada exige resolver un problema de toma de decisiones donde la precisión de la solución depende del número de puntos que formen el Pareto. Para abordar esta cuestión, el segundo algoritmo propuesto en esta tesis se define como un algoritmo colaborativo, ya que las técnicas no se combinan sino que se aplican de manera sucesiva, eficiente y que resuelve el problema de toma de decisiones de manera sistemática sin necesidad de disponer de un elevado número de puntos en el Pareto.

Este algoritmo colaborativo comienza por la aplicación del algoritmo MHS para obtener el frente de Pareto poco poblado. En segundo lugar, utiliza el análisis de componentes principales para representar el frente de Pareto en el espacio de componentes principales. Posteriormente, se emplea una red neuronal para simular el comportamiento de este nuevo frente de Pareto que presenta la característica de ser convexo. Esta red neuronal permite establecer una relación no lineal entre los parámetros a estimar y los valores de los residuos. La toma de decisiones se resuelve a través de un algoritmo de minimización local que encuentre el mínimo de la función convexa definida por la red neuronal. Este proceso otorga al algoritmo colaborativo dos ventajas principales. La primera es que el tiempo de computación se reduce significativamente ya que son precisas menos iteraciones para obtener el frente de Pareto poco poblado. La segunda hace referencia a la robustez del método para resolver el problema de toma de decisiones y hallar el *knee point* del problema.

El rendimiento de este algoritmo se ha validado a través de la actualización del modelo de EF de una pasarela comparando los resultados con aquellos obtenidos por el algoritmo MHS convencional y resolviendo el problema de toma de decisiones mediante el método de intersección normal al contorno. Sin comprometer la precisión en la solución, el algoritmo colaborativo reduce el tiempo de simulación en un 50 %.

5.2   Líneas de investigación futuras

El alcance de esta tesis puede extenderse a través de nuevos trabajos de investigación. El punto más inmediato concierne al desarrollo e implementación de un algortimo que combine los dos algoritmos propuestos en esta tesis. En este contexto, este nuevo algoritmo se caracterizaría por calcular un frente de Pareto poco poblado utilizado el algoritmo híbrido UKF-MHS y a partir de él continuar con el proceso del algoritmo colaborativo para acabar teniendo la solución óptima del problema.

Otra posible futura aplicación de los algoritmos propuestos es la actualización de modelos de EF de alta fidelidad de estructuras de ingeniería civil. Estos modelos de EF se caracterizan por representar con un alto nivel de detalle la estructura en consideración. De este modo, la incertidumbre es menor y el proceso de actualización del modelo tiene menor coste computacional.

Las aplicaciones de los algoritmos propuestos pueden ir más allá de la actualización de modelos de EF, como por ejemplo, estimar los parámetros de los dispositivos de control pasivo de vibraciones aplicando el método de diseño basado en el movimiento (*motion-based design*). Este trabajo, incluido en el Apéndice G, ha sido abordado por los autores considerando como algoritmo de optimización el GA para calcular los parámetros de los amortiguadores pasivos que mitigan las vibraciones de los cables de puentes atirantados [83]. Como continuación a esta investigación se propone realizar el diseño de amortiguadores aplicando el algoritmo colaborativo ya que los análisis transitorios involucrados aumentan significativamente el tiempo de cálculo.

Bibliografía

[1] S. Adhikari, R. Chowdhury, and M.I. Friswell, *High dimensional model representation method for fuzzy structural dynamics*, Journal of Sound and Vibration **330** (2011), no. 7, 1516–1529.

[2] S. Adhikari and M.I. Friswell, *Distributed parameter model updating using the karhunen–loève expansion*, Mechanical Systems and Signal Processing **24** (2010), no. 2, 326–339.

[3] R. J. Allemang and D. L. Brown, *A correlation coefficient for modal vector analysis*, Proceedings of the 1st international modal analysis conference, vol. 1, Orlando: Union College Press, 1982, pp. 110–116.

[4] R. Astroza, L.T. Nguyen, and T. Nestorović, *Finite element model updating using simulated annealing hybridized with unscented kalman filter*, Computers & Structures **177** (2016), 176–191.

[5] F.J. Baeza, S. Ivorra, D. Bru, and F.B. Varona, *Structural health monitoring systems for smart heritage and infrastructures in spain*, pp. 271–294, Springer International Publishing, 2018.

[6] J.D. Bagley, *The behavior of adaptive systems which employ genetic and correlation algorithms*, Ph.D. thesis, University of Michigan, 1967.

[7] R.S. Bais, A.K. Gupta, B.C. Nakra, and T.K. Kundra, *Studies in dynamic design of drilling machine using updated finite element models*, Mechanism and Machine Theory **39** (2004), no. 12, 1307–1320.

[8] M. Baruch and I.Y. Bar-Itzhack, *Optimal weighted orttiogonalization of measured modes*, AIAA journal **16** (1978), no. 4, 346–351.

[9] J.L. Beck and S.K. Au, *Bayesian updating of structural models and reliability using markov chain monte carlo simulation*, Journal of engineering mechanics **128** (2002), no. 4, 380–391.

[10] J.L. Beck, S.K. Au, and M.W. Vanik, *Monitoring structural health using a probabilistic measure*, Computer-Aided Civil and Infrastructure Engineering **16** (2001), no. 1, 1–11.

[11] J.L. Beck and L.S. Katafygiotis, *Updating models and their uncertainties. i: Bayesian statistical framework*, Journal of Engineering Mechanics **124** (1998), no. 4, 455–461.

[12] A. Berman, *Mass matrix correction using an incomplete set of measured modes*, AIAA journal **17** (1979), no. 10, 1147–1148.

[13] A. Berman and E.J. Nagy, *Improvement of a large analytical model using test data*, AIAA journal **21** (1983), no. 8, 1168–1173.

[14] X. Blasco, J.M. Herrero, J. Sanchis, and M. Martínez, *A new graphical visualization of n-dimensional pareto front for decision-making in multiobjective optimization*, Information Sciences **178** (2008), no. 20, 3908–3924.

[15] J. Branke, K. Deb, H. Dierolf, and M. Osswald, *Finding knees in multi-objective optimization*, International conference on parallel problem solving from nature, Springer, 2004, pp. 722–731.

[16] H.J. Bremermann, *Optimization through evolution and recombination*, Self-organizing systems **93** (1962), 106.

[17] J.M.W. Brownjohn, *Structural health monitoring of civil infrastructure*, Philosophical Transactions of the Royal Society A: Mathematical, Physical and Engineering Sciences **365** (2007), no. 1851, 589–622.

[18] J.M.W. Brownjohn, P.Q. Xia, H. Hao, and Y. Xia, *Civil structure condition assessment by fe model updating:: methodology and case studies*, Finite elements in analysis and design **37** (2001), no. 10, 761–775.

[19] C.A. Coello and M.S. Lechuga, *MOPSO: A proposal for multiple objective particle swarm optimization*, Proceedings of the 2002 Congress on Evolutionary Computation. CEC'02 (Cat. No. 02TH8600), vol. 2, IEEE, 2002, pp. 1051–1056.

[20] J.D. Collins, G.C. Hart, T.K. Hasselman, and B. Kennedy, *Statistical identification of structures*, AIAA journal **12** (1974), no. 2, 185–190.

[21] G. Cybenko, *Approximation by superpositions of a sigmoidal function*, Mathematics of control, signals and systems **2** (1989), no. 4, 303–314.

[22] I. Das, *On characterizing the "knee" of the pareto curve based on normal-boundary intersection*, Structural optimization **18** (1999), no. 2-3, 107–115.

[23] K. Deb and S. Gupta, *Understanding knee points in bicriteria problems and their implications as preferred solution principles*, Engineering optimization **43** (2011), no. 11, 1175–1204.

[24] K. Deb, A. Pratap, S. Agarwal, and T. Meyarivan, *A fast and elitist multiobjective genetic algorithm: NSGA-II*, IEEE transactions on evolutionary computation **6** (2002), no. 2, 182–197.

[25] M. Dorigo, *Optimization, learning and natural algorithms*, Ph.D. thesis, Politecnico di Milano, Italy, 1992.

[26] H. Fang, T.J. Wang, and X. Chen, *Model updating of lattice structures: a substructure energy approach*, Mechanical systems and signal processing **25** (2011), no. 5, 1469–1484.

[27] F.Z. Feng, Y.H. Kim, and B.S. Yang, *Applications of hybrid optimization techniques for model updating of rotor shafts*, Structural and Multidisciplinary Optimization **32** (2006), no. 1, 65–75.

[28] E. Fissette, C. Stavrinidis, and S. Ibrahim, *Error location and updating of analytical dynamic models using a force balance method*, Proc of the 6th IMAC, 1988, pp. 1063–1070.

[29] R.L. Fox and M.P. Kapoor, *Rates of change of eigenvalues and eigenvectors*, AIAA journal **6** (1968), no. 12, 2426–2429.

[30] M. Friswell and J.E. Mottershead, *Finite element model updating in structural dynamics*, vol. 38, Springer Science & Business Media, 1995.

[31] C-P Fritzen, D Jennewein, and Th Kiefer, *Damage detection based on model updating methods*, Mechanical systems and signal processing **12** (1998), no. 1, 163–186.

[32] K.I. Funahashi, *On the approximate realization of continuous mappings by neural networks*, Neural networks **2** (1989), no. 3, 183–192.

[33] A.H. Gandomi, S. Talatahari, X.S. Yang, and S. Deb, *Design optimization of truss structures using cuckoo search algorithm*, The Structural Design of Tall and Special Buildings **22** (2013), no. 17, 1330–1349.

[34] D.Q. Gao, *On structures of supervised linear basis function feedforward three-layered neural networks*, Chinese Journal of Computers- Chinese Edition- **21** (1998), 80–86.

[35] G. Gazetas, *Formulas and charts for impedances of surface and embedded foundations*, Journal of geotechnical engineering **117** (1991), no. 9, 1363–1381.

[36] G. Gazetas and R. Dobry, *Horizontal response of piles in layered soils*, Journal of Geotechnical engineering **110** (1984), no. 1, 20–40.

[37] Z.W. Geem, *Multiobjective optimization of time-cost trade-off using harmony search*, Journal of Construction Engineering and Management **136** (2009), no. 6, 711–716.

[38] Z.W. Geem, J.H. Kim, and G.V. Loganathan, *A new heuristic optimization algorithm: harmony search*, Simulation **76** (2001), no. 2, 60–68.

[39] R. Greiner, *Palo: A probabilistic hill-climbing algorithm*, Artificial Intelligence **84** (1996), no. 1-2, 177–208.

[40] J. Guo, X. Zhao, J. Guo, X. Yuan, S. Dong, and Z. Xiong, *Model updating of suspended-dome using artificial neural networks*, Advances in Structural Engineering **20** (2017), no. 11, 1727–1743.

[41] M.T. Hagan and M.B. Menhaj, *Training feedforward networks with the Marquardt algorithm*, IEEE transactions on Neural Networks **5** (1994), no. 6, 989–993.

[42] O. Hasançebi and T. Dumlupınar, *Linear and nonlinear model updating of reinforced concrete T-beam bridges using artificial neural networks*, Computers and Structures **119** (2013), 1 – 11.

[43] J.H. Holland, *Adaptation in natural and artificial systems: an introductory analysis with applications to biology, control, and artificial intelligence*, Ann Arbor: The University of Michigan Press, 1975.

[44] S.L.J Hu, H. Li, and S. Wang, *Cross-model cross-mode method for model updating*, Mechanical Systems and Signal Processing **21** (2007), no. 4, 1690–1703.

[45] E.J. Hudson and P. Reynolds, *Design and construction of a reconfigurable pedestrian structure*, Experimental Techniques **41** (2017), no. 2, 203–214.

[46] M. Imregun, D.J. Ewins, I. Hagiwara, and T. Ichikawa, *A comparison of sensitivity and response function based updating techniques*, Proceedings of the 12th International Modal Analysis, vol. 2251, 1994, p. 1390.

[47] E. Jacquelin, S. Adhikari, and M.I. Friswell, *A second-moment approach for direct probabilistic model updating in structural dynamics*, Mechanical systems and signal processing **29** (2012), 262–283.

[48] G. James, D. Witten, T. Hastie, and R. Tibshirani, *An introduction to statistical learning*, vol. 112, Springer, 2013.

[49] A.H. Jazwinski, *Stochastic processes and filtering theory*, New York: Academic Press, 1970.

[50] J.F. Jiménez-Alonso and A. Sáez, *Model updating for the selection of an ancient bridge retrofitting method in almeria, spain*, Structural Engineering International **26** (2016), no. 1, 17–26.

[51] S.S. Jin, S. Cho, H.J. Jung, J.J. Lee, and C.B. Yun, *A new multi-objective approach to finite element model updating*, Journal of Sound and Vibration **333** (2014), no. 11, 2323–2338.

[52] S.J. Julier and J.K. Uhlmann, *A new extension of the kalman filter to nonlinear systems*, Signal processing, sensor fusion, and target recognition VI, vol. 3068, International Society for Optics and Photonics, 1997, pp. 182–193.

[53] R.E. Kalman, *A new approach to linear filtering and prediction problems*, Journal of Basic Engineering (1960), 35–45.

[54] A. Kaveh and V.R. Mahdavi, *Colliding bodies optimization: a novel meta-heuristic method*, Computers & Structures **139** (2014), 18–27.

[55] J. Kennedy and R. Eberhart, *Particle swarm optimization*, International Conference on Neural Networks. Perth, Australia, IEEE, 1995.

[56] B. Kermanshahi, *Design and application of neural networks*, Shokodo Co.,Ltd., Tokyo, 1999.

[57] M. Khatibinia and S.H. Khosravi, *A hybrid approach based on an improved gravitational search algorithm and orthogonal crossover for optimal shape design of concrete gravity dams*, Applied Soft Computing **16** (2014), 223–233.

[58] M. Khatibinia, E. Salajegheh, J. Salajegheh, and M.J. Fadaee, *Reliability-based design optimization of reinforced concrete structures including soil–structure interaction using a discrete gravitational search algorithm and a proposed metamodel*, Engineering Optimization **45** (2013), no. 10, 1147–1165.

[59] H.H. Khodaparast, Y. Govers, I. Dayyani, S. Adhikari, M. Link, M.I. Friswell, J.E. Mottershead, and J. Sienz, *Fuzzy finite element model updating of the dlr airmod test structure*, Applied Mathematical Modelling **52** (2017), 512–526.

[60] G.H. Kim and Y.S. Park, *An automated parameter selection procedure for finite-element model updating and its applications*, Journal of Sound and Vibration **309** (2008), no. 3-5, 778–793.

[61] V. Klein, *Aircraft parameter estimation in frequency domain*, 4th Atmospheric Flight Mechanics Conference, 1978, p. 1344.

[62] V. Klein and J.R. Schiess, *Compatibility check of measured aircraft responses using kinematic equations and extended kalman filter*, (1977).

[63] R.I. Levin and N.A.J. Lieven, *Dynamic finite element model updating using neural networks*, Journal of Sound and Vibration **210** (1998), no. 5, 593–607.

[64] R.I. Levin and N.A.J. Lieven, *Dynamic finite element model updating using simulated annealing and genetic algorithms*, Mechanical Systems and Signal Processing **12** (1998), no. 1, 91–120.

[65] K. Lin, Y.L. Xu, X. Lu, Z. Guan, and J. Li, *Cluster computing-aided model updating for a high-fidelity finite element model of a long-span cable-stayed bridge*, Earthquake Engineering & Structural Dynamics **49** (2020), no. 9, 904–923.

[66] R.M. Lin and D.J. Ewins, *Model updating using frf data*, Proceeding of the 15th International Seminar on Modal Analysis, 1990, pp. 141–162.

[67] T. Liu, Q. Zhang, T. Zordan, and B. Briseghella, *Finite element model updating of canonica bridge using experimental modal data and genetic algorithm*, Structural Engineering International **26** (2016), no. 1, 27–36.

[68] Y. Lu and Z. Tu, *A two-level neural network approach for dynamic FE model updating including damping*, Journal of Sound and Vibration **275** (2004), no. 3-5, 931–952.

[69] F. Magalhães and Á. Cunha, *Explaining operational modal analysis with data from an arch bridge*, Mechanical systems and signal processing **25** (2011), no. 5, 1431–1450.

[70] F. Magalhães, A. Cunha, E. Caetano, and R. Brincker, *Damping estimation using free decays and ambient vibration tests*, Mechanical Systems and Signal Processing **24** (2010), no. 5, 1274–1290.

[71] D. Manjarres, I. Landa-Torres, S. Gil-Lopez, J. Del Ser, M.N. Bilbao, S. Salcedo-Sanz, and Z.W. Geem, *A survey on applications of the harmony search algorithm*, Engineering Applications of Artificial Intelligence **26** (2013), no. 8, 1818–1831.

[72] C. Mares, J.E. Mottershead, and M.I. Friswell, *Stochastic model updating: part 1—theory and simulated example*, Mechanical systems and signal processing **20** (2006), no. 7, 1674–1695.

[73] S. Mariani and A. Ghisi, *Unscented kalman filtering for nonlinear structural dynamics*, Nonlinear Dynamics **49** (2007), no. 1-2, 131–150.

[74] T. Marwala, *Finite element model updating using computational intelligence techniques: applications to structural dynamics*, Springer, London, 2010.

[75] T. Marwala, *Finite-element-model updating using compuional intelligence techniques*, ch. Finite-element-model Updating Using Particle-swarm Optimization, pp. 67–84, Springer, London, 2010.

[76] T. Marwala, I. Boulkaibet, and S. Adhikari, *Probabilistic finite element model updating using bayesian statistics: applications to aeronautical and mechanical engineering*, John Wiley & Sons, 2016.

[77] F. Massa, T. Tison, and B. Lallemand, *A fuzzy procedure for the static design of imprecise structures*, Computer methods in applied mechanics and engineering **195** (2006), no. 9-12, 925–941.

[78] Ansys Mechanical 19.0, *Ansys inc. 2019*, Available online: *http://www.ansys.com/*.

[79] S.V. Modak, T.K. Kundra, and B.C. Nakra, *Comparative study of model updating methods using simulated experimental data*, Computers & structures **80** (2002), no. 5-6, 437–447.

[80] S. Moradi, L. Fatahi, and P. Razi, *Finite element model updating using bees algorithm*, Struct Multidisc Optim **42** (2010), no. 2, 283–291.

[81] J.E. Mottershead and M.I. Friswell, *Model updating in structural dynamics: a survey*, Journal of sound and vibration **167** (1993), no. 2, 347–375.

[82] J.E. Mottershead, M. Link, and M.I. Friswell, *The sensitivity method in finite element model updating: a tutorial*, Mechanical systems and signal processing **25** (2011), no. 7, 2275–2296.

[83] J. Naranjo-Pérez, J.F. Jiménez-Alonso, I.M. Díaz, G. Quaranta, and A. Sáez, *Motion-based design of passive damping systems to reduce wind-induced vibrations of stay cables under uncertainty conditions*, Applied Sciences **10** (2020), no. 5, 1740.

[84] L.T. Nguyen and T. Nestorović, *The extended kalman filter and the unscented kalman filter for material parameter identification with application in tunneling*, PAMM **13** (2013), no. 1, 393–394.

[85] L.T. Nguyen and T. Nestorović, *Nonlinear kalman filters for model calibration of soil parameters for geomechanical modeling in mechanized tunneling*, Journal of Computing in Civil Engineering **30** (2016), no. 2, 04015025.

[86] J. Nocedal and S. Wright, *Numerical optimization*, Springer Science & Business Media, 2006.

[87] P. Pachón, V. Compán, and J.F. Jiménez-Alonso, *Ambient vibration testing, dynamic identification and model updating of a historical building. chapel of the würzburg residence (germany)*, International Operational Modal Analysis Conference (IOMAC) (Gijón, Spain), 2015.

[88] Y.S. Park, S. Kim, N. Kim, and J.J. Lee, *Finite element model updating considering boundary conditions using neural networks*, Engineering Structures **150** (2017), 511–519.

[89] R. Perera, S.E. Fang, and A. Ruiz, *Application of particle swarm optimization and genetic algorithms to multiobjective damage identification inverse problems with modelling errors*, Meccanica **45** (2010), no. 5, 723–734.

[90] S. Qin, Y. Zhang, Y.L. Zhou, and J. Kang, *Dynamic model updating for bridge structures using the kriging model and pso algorithm ensemble with higher vibration modes*, Sensors **18** (2018), no. 6, 1879.

[91] G. Quaranta, A. Fiore, and G.C. Marano, *Optimum design of prestressed concrete beams using constrained differential evolution algorithm*, Structural and Multidisciplinary Optimization **49** (2014), no. 3, 441–453.

[92] J.R. Raol, G. Girija, and J. Singh, *Modelling and parameter estimation of dynamic systems*, vol. 65, Iet, 2004.

[93] W.X. Ren and H.B. Chen, *Finite element model updating in structural dynamics by using the response surface method*, Engineering structures **32** (2010), no. 8, 2455–2465.

[94] C.P. Robert and G. Casella, *Monte carlo statistical methods*, London: Springer, 2004.

[95] R.S. Rosenberg, *Simulation of genetic populations with biochemical properties*, Ph.D. thesis, University of Michigan, 1967.

[96] M.M. Saada, M.H. Arafa, and A.O. Nassef, *Finite element model updating approach to damage identification in beams using particle swarm optimization*, Engineering optimization **45** (2013), no. 6, 677–696.

[97] M. Savoia, *Structural reliability analysis through fuzzy number approach, with application to stability*, Computers & Structures **80** (2002), no. 12, 1087–1102.

[98] D. Shan, Q. Li, I. Khan, and X. Zhou, *A novel finite element model updating method based on substructure and response surface model*, Engineering Structures **103** (2015), 147–156.

[99] E. Simoen, G. De Roeck, and G. Lombaert, *Dealing with uncertainty in model updating for damage assessment: A review*, Mechanical Systems and Signal Processing **56** (2015), 123–149.

[100] N. Srinivas and K. Deb, *Multi-objective function optimisation using non-dominated sorting genetic algorithm*, Evolutionary Comp **2** (1994), no. 3, 221–248.

[101] A. Tarantola, *Inverse problem theory and methods for model parameter estimation*, vol. 89, SIAM, 2005.

[102] A. Teughels and G. De Roeck, *Damage detection and parameter identification by finite element model updating*, Archives of Computational Methods in Engineering **12** (2005), no. 2, 123–164.

[103] A. Teughels, G. De Roeck, and J.A.K. Suykens, *Global optimization by coupled local minimizers and its application to fe model updating*, Computers & structures **81** (2003), no. 24-25, 2337–2351.

[104] A. Teughels, J. Maeck, and G. De Roeck, *Damage assessment by fe model updating using damage functions*, Computers & structures **80** (2002), no. 25, 1869–1879.

[105] R. Van Der Merwe, *Sigma-point kalman filters for probabilistic inference in dynamic state-space models*, Ph.D. thesis, OGI School of Science & Engineering at OHSU, 2004.

[106] R. Van Der Merwe and E.A. Wan, *The square-root unscented kalman filter for state and parameter-estimation*, 2001 IEEE international conference on acoustics, speech, and signal processing. Proceedings (Cat. No. 01CH37221), vol. 6, IEEE, 2001, pp. 3461–3464.

[107] A. Vasuki, *Nature-inspired optimization algorithms*, CRC Press, 2020.

[108] E.A. Wan and R. Van Der Merwe, *The unscented kalman filter for nonlinear estimation*, Proceedings of the IEEE 2000 Adaptive Systems for Signal Processing, Communications, and Control Symposium (Cat. No. 00EX373), IEEE, 2000, pp. 153–158.

[109] E.A. Wan, R. Van Der Merwe, and A.T. Nelson, *Dual estimation and the unscented transformation*, Advances in neural information processing systems, 2000, pp. 666–672.

[110] X. Wang, X.Z. Gao, and K. Zenger, *An introduction to harmony search optimization method*, Springer, 2015.

[111] Y.Q. Wang, L. Zong, Y.J. Shi, and N. Yao, *Damage detection and rehabilitation on a curvilinear steel box girder bridge by multistage model updating*, Structure and Infrastructure Engineering **11** (2015), no. 11, 1420–1431.

[112] S. Weng, H. Zhu, Y. Xia, J. Li, and W. Tian, *A review on dynamic substructuring methods for model updating and damage detection of large-scale structures*, Advances in Structural Engineering **23** (2020), no. 3, 584–600.

[113] J. Wu, Q. Yan, S. Huang, C. Zou, J. Zhong, and W. Wang, *Finite element model updating in bridge structures using kriging model and latin hypercube sampling method*, Advances in Civil Engineering **2018** (2018).

[114] X.S. Yang, *Nature-inspired optimization algorithms*, Elsevier, 2014.

[115] X.S. Yang and S. Deb, *Engineering optimisation by cuckoo search*, Int. J. Mathematical Modelling and Numerical Optimisation **1** (2010), no. 4, 330–343.

[116] L.A. Zadeh, *Fuzzy sets*, Information and control **8** (1965), no. 3, 338–353.

[117] S. Živanović, A. Pavic, and P. Reynolds, *Finite element modelling and updating of a lively footbridge: The complete process*, Journal of Sound and Vibration **301** (2007), no. 1-2, 126–145.

Apéndice A
Artículo A

Jiménez-Alonso, J.F, Naranjo-Pérez, J., Paviv, A., Sáez, A. Maximum likelihood finite-element model updating of civil engineering structures using nature-inspired computational algorithms. *Structural Engineering International*. 2020. (*Accepted*).

Maximum Likelihood Finite-Element Model Updating of Civil Engineering Structures Using Nature-Inspired Computational Algorithms

Javier Fernando Jiménez-Alonso[a*], Javier Naranjo-Perez[b], Aleksandar Pavic[c] and Andrés Sáez[d]

[a*]*Assistant professor. Department of Continuum Mechanics and Structures, E.T.S. Ingenieros de Caminos, Canales y Puertos. Universidad Politécnica de Madrid, Madrid (Spain).*

[b]*PhD Candidate. Department of Continuum Mechanics and Structural Analysis, Universidad de Sevilla, Seville (Spain).*

[c]*Full professor. Vibration Engineering, College of Engineering, Mathematics and Physical Sciences, University of Exeter, Exeter (U.K.).*

[d]*Full professor. Department of Continuum Mechanics and Structural Analysis, Universidad de Sevilla, Seville (Spain).*

[*]*Corresponding author:* Assistant Professor: Javier Fernando Jiménez-Alonso. Department of Continuum Mechanics and Structures. E.T.S. Ingenieros de Caminos, Canales y Puertos. Universidad Politécnica de Madrid, Calle del Profesor Aranguren, 3, 28040 Madrid (Spain) Ph:+34 91 0674154. e-mail: *jf.jimenez@upm.es*.

Maximum Likelihood Finite-Element Model Updating of Civil Engineering Structures Using Nature-Inspired Computational Algorithms

In finite-element model updating of civil engineering structures, the numerical finite-element model is calibrated in order to fit the experimentally measured dynamic properties (say mode shapes and natural frequencies) of the structure. Such updating process is usually performed under the maximum likelihood method in practical engineering applications. According to this approach, the updating problem is transformed into an optimization problem, where the values of the most relevant physical parameters of the structure are obtained via the minimization of an objective function. This function is usually defined in terms of the relative differences between the numerical and the experimental modal properties of the structure. To this aim, either (i) a single-objective or (ii) a multi-objective approach may be adopted. In the majority of applications, and due to the complexity of the problem, global optimizers are considered. Among these algorithms, nature-inspired computational algorithms have been widely employed with satisfactory results. Nevertheless, such model updating approach presents two main limitations: (i) a clear dependence between the updated model and the objective function considered for the updating problem; and (ii) a high simulation cost in terms of computation time. In order to overcome these drawbacks, a detailed study has been performed herein both to assist in the selection of an efficient computational algorithm among several well-known nature-inspired algorithms and to further establish the most adequate (single- or multi-) objective function to tackle the updating problem. For this purpose, a laboratory footbridge has been considered as benchmark to conduct the updating process under different scenarios.

Keywords: finite-element model updating, maximum likelihood method, single-objective optimization, multi-objective optimization, nature-inspired computational algorithms, harmony search, civil engineering structures.

Introduction

Finite-element (FE) models are extensively used to simulate numerically the behaviour of civil engineering structures. However, these numerical models may not always reflect adequately the actual behaviour of the structure. To solve this issue, such models can be tuned based on the experimental results obtained from either field tests or continuous monitoring [1]. For practical engineering applications, the tuning of the

numerical models is usually achieved via the modification of the most relevant physical parameters of the structure, in order to reduce the differences between its numerical and experimental behaviours. After the calibrating process, the resulting updated model can be used either to assess more accurately the behaviour of civil engineering structures [2, 3, 4] or to establish strategies for their maintenance or damage detection [5, 6].

Thus, given that one of the main objectives of FE model updating is to indirectly estimate the values of some relevant physical parameters of the structure, the updating process may be formulated as a parameter identification problem [7], where appropriate estimators need to be employed [8]. Generally speaking, estimators may be classified into two categories [9, 10]: (i) Point estimators, which return the expected value of each considered design parameter; and (ii) Interval estimators, which determine either an interval in which the value of each parameter lies or a probability density function for each parameter. Among the interval estimators, the Bayesian method [11] has prevailed, since the determination of the probabilistic density function of the design parameters is relevant when performing subsequent structural reliability analyses [12]. Meanwhile, among the point estimators, the maximum likelihood method (MLM) has been widely implemented due to its proved efficiency and accuracy when tackling model updating [8].

In this paper, we will focus on analysing the performance of FE model updating under the MLM, based on the advantages this approach exhibits for practical civil engineering applications, when compared to Bayesian methods, in particular in terms of: (i) ease of implementation, (ii) lower simulation times required; and (iii) straightforward use of the updated models for deterministic applications [2, 13]. In this manner, the parameter identification problem under the MLM, assuming a normal distribution of the adjustment errors, is equivalent to an ordinary least squares problem [14]. Therefore, the FE model updating aims at solving an optimization problem, whose objective is to determine the values of the design parameters that minimize the difference between the numerical (FE) modal properties of the structure and its experimental counterparts. The experimental data follow from the signal processing (applying either experimental or operational modal analysis) of a forced or an ambient vibration test [15].

At this stage, the formulation of the optimization problem requires to adopt two key decisions: (i) the definition of an adequate objective function; and (ii) the selection of an efficient computational optimization algorithm.

On the one hand, the objective function is usually defined in terms of the residuals between the numerical and experimental modal properties of the structure. Since two types of modal properties are normally considered (natural frequencies and associated vibration modes), two types of residuals come into play. As both sets of modal properties have different nature, a new problem arises, namely, how to weigh the influence of each residual. Two approaches may be adopted, depending on whether a single-objective function (SOF) or a multi-objective function (MOF) [16] is considered. Whilst in the SOF approach a single objective is optimized with different weighting factors assigned to balance the influence of each residual, in the MOF approach the different terms of a multi-objective function are optimized (without the need to define weighting factors). Although both approaches have been used interchangeably for practical engineering applications [17, 18], the number of studies in which their performance has been compared is scarce.

On the other hand, the selection of an appropriate optimization algorithm is a key ingredient for the success of the FE model updating. Due to the nonlinear relationship between the modal properties of the structure and the considered physical parameters, computational intelligence algorithms are usually considered to ensure the finding of the

global optimum [8]. Among these algorithms, nature-inspired computational (NIC) algorithms have been widely employed to this end [8]. Nevertheless, special attention must be paid to the simulation time required to perform the updating process, in order to select an efficient NIC algorithm.

At this point, two are the main objectives of our study: (1) to establish which is the most adequate approach, either SOF or MOF, to formulate the updating problem under the MLM; and (2) to assist in the election of an efficient NIC algorithm to address the FE model updating of civil engineering structures. To this aim, the performance of three NIC algorithms, using SOF or MOF approaches, is next compared when applied to the updating of a benchmark civil structure.

The three NIC algorithms considered herein are:

(i)   Genetic Algorithms (GA), since they have been the most commonly implemented computational algorithms to tackle the updating problem [19];

(ii)   Particle Swarm (PS) algorithm, which has proved more efficient to address the FE model updating problem of mechanical structures [20]; and

(iii)   Harmony Search (HS) algorithm, a more recent global optimization algorithm [21] that, although has been successfully applied for different structural engineering applications [22], it has been rarely implemented for the FE model updating of civil engineering structures.

Although there are many alternative robust metaheuristic optimization algorithms in the literature, such as Colliding Bodies Optimization (CBO) [23] or Gravitational Search Algorithm (GSA) [24] to mention a couple of them, we have restricted ourselves to compare the performance of just three algorithms (GA, PS and HS) when applied to civil engineering structures for the sake of conciseness. A broader comparison with other NIC algorithms is out of the scope of this paper.

As benchmark structure, a laboratory steel footbridge located at the Vibration Engineering Section of the University of Exeter (U.K.) has been considered [25]. A FE model of the structure has been built to compute the numerical modal properties of the structure. The experimental modal properties have been identified from the records obtained in a forced vibration test. Subsequently, the FE model updating of the structure has been performed using the different approaches indicated above and the obtained results have been critically compared in terms of the following criteria: sweep capacity, computational cost and accuracy of the adjustment.

The paper is organized as follows: Some basics of FE model updating under the MLM are summarized in the second section. In the third section, the three NIC algorithms considered herein are briefly described. In the fourth section, the FE model updating of the benchmark laboratory footbridge is performed under the two mentioned approaches (SOF and MOF) and the three considered NIC algorithms (GA, PS and HS). Following the discussion of the obtained results, some concluding remarks are drawn to close the paper in the last section.

Basics of FE Model Updating under the Maximum Likelihood Method (MLM)

As sketched above, the FE model updating under the MLM transforms the updating problem into an optimization problem, where the objective is to determine the values of several design parameters that minimize the relative differences (residuals)

between the numerical and experimental modal properties of the structure. As design parameters, one should select those physical parameters that have the greatest influence on the dynamic behaviour of the structure [8]. Of course, the parameters search space must be constrained (search domain) in order to guarantee the physical meaning of the obtained solution. The values determined for such design parameters after the updating process, allow reducing the uncertainty level of the numerical model (due to geometrical tolerances, damage, …) and improve the adjustment between the experimental and numerical behaviours of the structure.

Two types of residuals are usually considered to define the objective function in the updating problem: those associated with the natural frequencies and those residuals associated with the corresponding vibration modes. As previously indicated, the influence of these two types of residuals on the objective function can be evaluated via two different approaches: (i) the single-objective function (SOF) approach; and (ii) the multi-objective function (MOF) approach.

Under the SOF approach, the objective function is defined in terms of the weighted residuals between the numerical and experimental modal properties of the structure. These weights are established to consider the relative contribution of each residual. Their value can be determined either by a statistical criterion [1] or by a trial-and-error criterion [5]. According to the statistical criterion, the weights are defined in terms of the uncertainty associated with the estimates of the experimental modal properties of the structure. According to the trial-and-error criterion, the weights are defined by an iterative process aimed at ensuring the best agreement between the numerical and experimental modal properties of the structure. Here, this second criterion has been adopted.

Under the MOF approach, the objective function is defined in terms of several functional components. For practical engineering applications, this objective function is defined by two functional components [16]: (i) the first component is defined in terms of the residuals associated with the natural frequencies, $r_j^f(\boldsymbol{\theta})$; and (ii) the second component is defined in terms of the residuals associated with the vibration modes, $r_j^m(\boldsymbol{\theta})$ (being j the considered vibration mode). Although, this approach presents the advantage that it is not necessary to define the weights of the residuals, it has a clear drawback: a subsequent decision-making problem must be addressed in order to select the best solution among the set of possible solutions (the so-called Pareto front) provided by the optimization algorithm. In order to solve this decision-making problem, the normal boundary intersection (NBI) method has been considered herein [26], among the different criteria provide in literature [27].

Thus, the general formulation of the FE model updating problem under the SOF approach may be stated as follows [16]:

$$\min f(\boldsymbol{\theta}) = min \sum_{j=1}^{m} w_j r_j(\boldsymbol{\theta})^2 = min \sum_{j=1}^{m_f} w_j^f r_j^f(\boldsymbol{\theta})^2 + \sum_{j=1}^{m_m} w_j^m r_j^m(\boldsymbol{\theta})^2 \qquad (1)$$

$$\boldsymbol{\theta}^l \leq \boldsymbol{\theta} \leq \boldsymbol{\theta}^u \quad \sum w_j = \sum w_j^f + w_j^m = 1 \quad w_j \geq 0$$

where $f(\boldsymbol{\theta})$ is the objective function for the single-objective function approach (SOF); m_f is the size of the residuals vector related to the natural frequencies, $\mathbf{r^f}(\boldsymbol{\theta})$; m_m is the size of the residuals vector related to the vibration modes, $\mathbf{r^m}(\boldsymbol{\theta})$; m is the size of the

residuals vector, $\mathbf{r}(\boldsymbol{\theta})$; w_j is the weighting factor of the element j of the residuals vector, $r_j(\boldsymbol{\theta})$; w_j^f is the weighting factor of the element j of the residuals vector associated with the natural frequencies, $r_j^f(\boldsymbol{\theta})$; w_j^m is the weighting factor of the element j of the residuals vector associated with the vibration modes, $r_j^m(\boldsymbol{\theta})$; $\boldsymbol{\theta} = [\theta_1, \ldots, \theta_i, \ldots, \theta_{n_v}]$ is the physical parameters vector/design parameters vector (with n_v being the number of terms of this vector); $\boldsymbol{\theta}^l = [\theta_1^l, \ldots, \theta_i^l, \ldots, \theta_{n_v}^l]$ is the lower bound vector of the search domain for the parameters vector; and $\boldsymbol{\theta}^u = [\theta_1^u, \ldots, \theta_i^u, \ldots, \theta_{n_v}^u]$ stands for the upper bound vector for the search domain of the parameters vector.

On the other hand, the general formulation of the FE model updating problem under the MOF approach may be stated as follows [16]:

$$\min \mathbf{f}(\boldsymbol{\theta}) = (f_1(\boldsymbol{\theta}) \quad f_2(\boldsymbol{\theta})) = min\left(\sum_{j=1}^{m_f} r_j^f(\boldsymbol{\theta})^2 \quad \sum_{j=1}^{m_m} r_j^m(\boldsymbol{\theta})^2\right) \tag{2}$$
$$\boldsymbol{\theta}^l \leq \boldsymbol{\theta} \leq \boldsymbol{\theta}^u$$

where $f_1(\boldsymbol{\theta})$ and $f_2(\boldsymbol{\theta})$ are respectively the first and the second sub-objective functions for the multi-objective function approach.

In order to guarantee that the two types of residuals are well-balanced, the residuals may be normalized as follows [16]:

$$r_j^f(\boldsymbol{\theta}) = \frac{f_{num,j}(\boldsymbol{\theta}) - f_{exp,j}}{f_{exp,j}} j = 1,2,\ldots,m_f \tag{3}$$

$$r_j^m(\boldsymbol{\theta}) = \sqrt{\left(\frac{\left(1-\sqrt{MAC_j(\boldsymbol{\theta})}\right)^2}{MAC_j(\boldsymbol{\theta})}\right)} j = 1,2,\ldots,m_m \tag{4}$$

Therefore, the FE model updating process consists of the following steps [8]: (i) the modal properties of the structure are identified experimentally via the signal processing of the records obtained during a vibration test; (ii) the numerical modal properties of the structure are obtained via a FE modal analysis; (iii) the objective function is evaluated; (iv) the design parameters are modified; and (v) the steps (ii) to (iv) are repeated iteratively until some convergence criterion is met.

As result of this process, either a vector of updated design parameters (SOF approach) or the Pareto front (MOF approach) is obtained. Additionally, a subsequent decision-making problem must be implemented to select the vector of updated parameters under the MOF approach. Fig. 1 shows the flowchart of the FE model updating problem under the MLM.
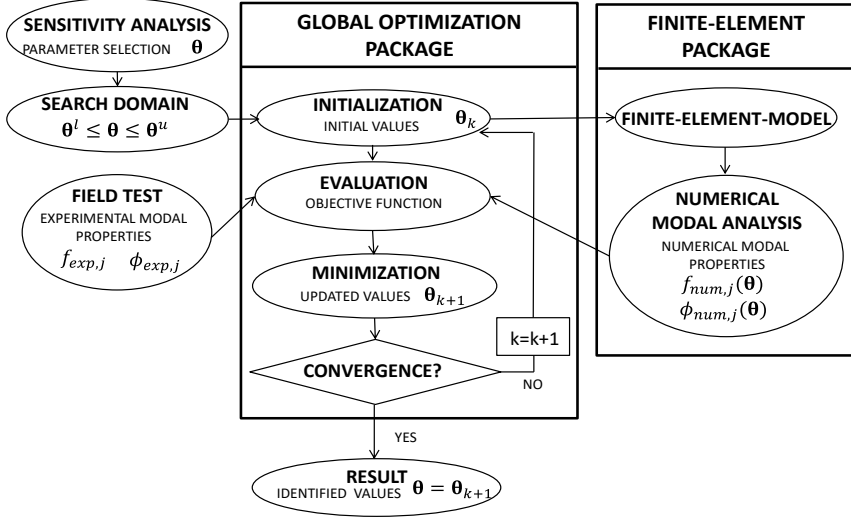
Fig. 1. Flowchart of the FE model updating problem under the MLM [28].

In order to assess the performance of the updating process, the correlation between the numerical and experimental modal properties must be determined. For this purpose, several ratios have been proposed [15]. Among the different proposals, the relative difference between the numerical and experimental natural frequencies, $\Delta f_{exp,j}^{num,j}(\boldsymbol{\theta})$, and the modal assurance criterion, $MAC_{exp,j}^{num,j}(\boldsymbol{\theta})$, are widely used [1]. Both ratios are defined as:

$$\Delta f_{exp,j}^{num,j}(\boldsymbol{\theta}) = \frac{f_{num,j}(\boldsymbol{\theta}) - f_{exp,j}}{f_{exp,j}} 100 \, [\%] \tag{5}$$

$$MAC_{exp,j}^{num,j}(\boldsymbol{\theta}) = \frac{\left(\phi_{num,j}^{T}(\boldsymbol{\theta}) \cdot \phi_{exp,j}\right)^{2}}{\left(\phi_{num,j}^{T}(\boldsymbol{\theta}) \cdot \phi_{num,j}(\boldsymbol{\theta})\right)\left(\phi_{exp,j}^{T} \cdot \phi_{exp,j}\right)} \tag{6}$$

where $f_{num,j}(\boldsymbol{\theta})$ and $f_{exp,j}$ are respectively the numerical and experimental j natural frequencies of the structure; $\phi_{num,j}(\boldsymbol{\theta})$ and $\phi_{exp,j}$ are the numerical and experimental j vibration modes; and ^{T} denotes transpose.

A good correlation between the numerical and experimental modal properties of the structure is achieved if both the relative differences, $\Delta f_{exp,j}^{num,j}(\boldsymbol{\theta})$, are lower than 5.00 % and their corresponding $MAC_{exp,j}^{num,j}(\boldsymbol{\theta})$ ratios are greater than 0.90 [29].

Nature-Inspired Computational Algorithms for Numerical Optimization

Nature-inspired computational (NIC) algorithms have been widely used to address the FE model updating problem under the MLM. The main advantages of these computational algorithms are: (i) their independence in relation to the initial values of the design parameters; and (ii) their ability to find the global optimum of the objective function. However, they present the high simulation time required to solve the updating problem as main drawback. For this reason, it becomes necessary to assess the

performance of each NIC algorithm when it is implemented in a particular optimization problem (the updating of civil engineering structures in our case).

To this end, the performance of three NIC algorithms, under both the SOF approach and the MOF approaches, is compared herein. Namely: (i) Genetic Algorithms (GA); (ii) Particle Swarm (PS) algorithm; and (iii) Harmony Search (HS) algorithm. These NIC algorithms are described briefly in this section.

Genetic Algorithms (GA)

Genetic algorithms (GA) are NIC algorithms based on Darwin's natural selection theory [19]. According to this theory, each possible value of the design parameters is identified as a chromosome. Then, each set of design parameters is grouped into an individual (parameter vector). Subsequently, the value of this parameter vector is improved via an iterative process where the value of the objective function is optimized. The GA can be summarized in the following steps: (i) an initial random population of parameter vectors is created; (ii) the objective function is evaluated for all the individuals; (iii) a new population is created using three mechanisms (selection, crossover and mutation); (iv) the objective function is evaluated for the individuals of the new population; (v) the steps (iii) and (iv) are repeated until some convergence criterion is met. Fig. 2a shows the corresponding flowchart.

Three mechanisms are used by this algorithm to find the optimum value of the objective function: (i) the selection, where a part of the initial population is maintained when a new population is generated; (ii) the crossover, where a new parameter vector is derived from two previous ones; and (iii) the mutation, where a new parameter vector is generated from a previous one by modifying randomly the value of one element of the vector. The combination of these two last mechanisms allows sweeping the search domain of the optimization problem. Three design variables are defined to characterize these three mechanisms: (i) the selection ratio, $selr$, which establishes the number of individuals that constitute the elite of the population (they are maintained in the next generation and they are used as parents for the generation of new individuals using the crossover and mutation mechanism); (ii) the crossover ratio, $crosr$, which determines the percentage of the remaining population that is modified by crossover mechanism; and (iii) the mutation ratio, $mutr$, which establishes the percentage of the remaining population that is modified by the mutation mechanism.

Particle Swarm (PS) Algorithm

The particle swarm (PS) algorithm was proposed by Kennedy and Eberhart [20]. It is a NIC algorithm based on social behaviour of biological organisms when they move in a single group to achieve a desired overall objective.

According to this, the particles move through the search space following simple laws related to their position (value of the physical parameters) and velocity. The position of each particle is improved in terms of both its own best position and the best position of the remaining particles. Thus, as the position of each particle is updated in terms of its velocity, the performance of the algorithm depends mainly on this design variable.

Hence, the particle's velocity depends on three main parameters: (i) the particle's inertia, $ipar$, which controls the impact of the current velocity on the subsequent velocity; (ii) a self-adjustment weight, $selw$, which weighs the influence of the best position achieved by this particle on the subsequent velocity; and (iii) a social-adjustment weight, $socw$, which weighs the influence of the best position achieved by the best particle in the swarm on the subsequent velocity. The particle's inertia, $ipar$, controls the exploratory

properties of the simulation. Thus, a high value of the inertia encourages a global exploration, while a low value of the inertia encourages local exploration. The self-adjustment weight, $selw$, indicates the confidence that the current particle has on itself and the social-adjustment weight, $socw$, indicates the confidence the current particle has on the success of the population [8].

The PS algorithm consists of the following steps: (i) a population of particles' position and velocities are generated randomly (the particles' position must be distributed in the search domain); (ii) the velocity of each particle is evaluated; (iii) the position of each particle is updated; (iv) steps (ii) and (iii) are repeated until some convergence criterion is met. Fig. 2b sketches the flowchart of the PS algorithm.

Harmony Search (HS) Algorithm

The HS algorithm was originally formulated by Geem *et al.* [21]. It is based on the improvisation carried out by the musicians when they are searching for the harmony, by following aesthetic requirements. The HS algorithm consists of the following steps: (i) an initial random population of possible solutions, which is stored in the harmony memory matrix, **HM**, is created; (ii) the objective function is evaluated for each of the candidate solutions; (iii) a new harmony is created at each iteration; (iv) the objective function is evaluated for each new harmony, (v) the harmony memory matrix, **HM**, is updated comparing the original and new harmonies; and (vi) the steps (iii) to (v) are repeated until some convergence criterion is met. Fig. 2c illustrates the flowchart of the HS algorithm.

For the generation of a new harmony, three mechanisms are considered: (i) harmonies in memory; (ii) pitch adjustment; and (iii) randomization. Each parameter from a new vector may be defined either from a previous value stored in the harmony memory matrix, **HM,** or from a new random value. These two possibilities are controlled by the harmony memory consideration rate, $HMCR$ which establishes the probability of selecting a previous element of the harmony memory matrix, **HM**. Additionally, if the value is adopted from a previous one, it can be mutated according to the pitch adjustment rate, PAR, and considering a predefined bandwidth, bw, of possible values.

MOF Approach for the Three Considered NIC Algorithms

The MOF approach of the GA is implemented via the NSGA-II (Non-dominated Sorting Genetic Algorithm) [30]. This algorithm makes use of the non-dominated sorting technique [31] to distinguish between dominated and non-dominated (those that improve the value of one objective function without sacrificing the others) solutions. For this purpose, each individual (possible solution) is characterized by an operator, the so-called crowded comparison operator. This operator takes into account two attributes of the solution: (i) the rank; and (ii) the crowding distance.

The steps of the GA under the MOF approach are: (i) an initial population is randomly created; (ii) the multi-objective function is evaluated for each individual; (iii) subsequently, the non-dominated sorting technique is employed to sort the solutions based on the rank and the crowding distance; (iv) then an iterative process is initialized where a new population is generated using both the crossover and mutation mechanisms; (v) the multi-objective function is evaluated for the new population and the non-dominated sorting technique is used again; (vi) the initial size of the population is restored via its truncation based on the worst crowding distance solutions; and (vii) the steps (iv) to (vi) are repeated until some convergence criterion is met. As result of this process, the

so-called Pareto front defining a set of possible solutions of the updating problem, is obtained.
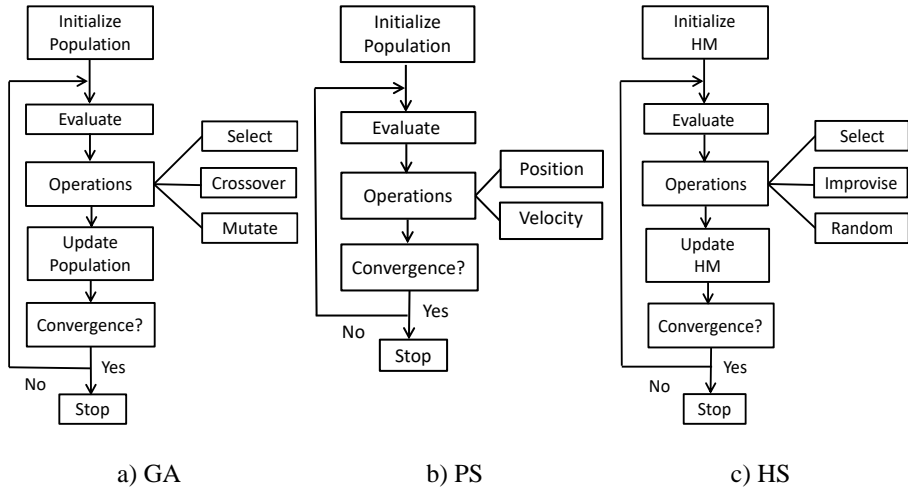
Fig. 2. Flowchart of the three considered NIC algorithms: a) genetic algorithms (GA); b) particle swarm (PS); and c) harmony search (HS).

Similarly, the MOF approach of the PS algorithm is also based on the classification of the non-dominated particles [32]. Hence, once the initial particles' population is created and the multi-objective function is evaluated, the non-dominated solutions are obtained and stored in the particles' repository. A similar process, to define the Pareto front, is obtained after the mutation of the position. Thus, if the mutated particle dominates the non-mutated, the latter is updated. This step is applied iteratively to both the updated particle's position and the best particle's position. Then, the non-dominated solutions are added to the repository and finally, the domination is evaluated for the overall repository to dismiss the dominated particles. These steps are repeated iteratively until some convergence criterion is met. As results of this process, the Pareto font is obtained.

Finally, the MOF approach of the HS algorithm has also been implemented [33] considering the main rules of the NSGA-II algorithm. In this manner, the HS algorithm under a MOF approach consists of the following steps: (i) an initial set of harmonies is generated (harmony memory matrix, **HM**); (ii) the multi-objective function is evaluated for all of harmonies; (iii) the attributes of each individual are calculated using the crowded comparison operator; (iv) the harmonies are sorted based on the crowding distance; (v) a new set of harmonies is created based on the three mentioned design variables ($HMCR$, PAR and bw); (vi) the multi-objective function is evaluated for the new harmonies; (vii) the harmony memory matrix, **HM**, is truncated using both the non-dominated sorting technique and the crowding distance; and (viii) the steps (v) to (vii) are repeated until some convergence criterion is met. Finally, as result of this process, the Pareto front is obtained.

Preliminary discussion on the Performance of the Three Considered Nature-Inspired Algorithms

As Fig. 2 illustrates, the three considered NIC algorithms under the SOF approach share three common characteristics: (i) the random initialization of a population; (ii) the implementation of several mathematical operations to modify this population; and (iii) the iterative application of this re-generation process until some convergence criteria is met. Similarly, they also share the use of the non-dominated sorting rules for their implementation under a MOF approach.

However, some particular differences among these NIC algorithms make interesting comparing their performance when they are implemented for the FE model updating of civil engineering structures.

Between the GA and the HS algorithm, the main difference lies in the different complexity of the operations that control the updating of the population: the operations associated with the HS algorithm (selection, improvement and randomization) are computationally easier than the operations associated with the GA (selection, crossover and mutation). Thus, it is expected that the computational time required to solve an optimization problem using the HS algorithm is lower than the one required employing GA. However, the simplicity of the operations can have a negative influence on both the accuracy of the solution and the sweeping capacity of the algorithm, reducing the performance of the HS algorithm when it is implemented for a practical engineering application.

Additionally, among these two algorithms (GA and HS) and the PS algorithm, the main difference is related to the re-generation of the population. While the two mentioned algorithms (GA and HS) generate iteratively different populations (new populations) during the updating process; the PS algorithm maintains the initial population and it only updates iteratively its attributes. In this manner, the PS algorithm may reduce the simulation time required to solve an optimization problem. However, as on the one hand, the sweeping capacity of the algorithm is lower than the GA; and on the other hand, the computational operations needed to compute the position and the velocity of each particle are more complex than the re-generating operations of the HS algorithm, it is not possible to establish a priori whether the PS algorithm is the most efficient computational algorithm among the three considered NIC ones.

For all these reason, it is not possible to preliminary conclude which will be the most efficient algorithm to solve a particular optimization problem, being necessary to perform a comparative study to analyse their performance. This will be done in the next section.

Application Example: FE Model Updating of a Laboratory Footbridge

A real case-study is next analysed to shed some light onto the two objectives of this paper: (i) establishing the most adequate approach (SOF or MOF) to formulate the updating problem under the MLM; and (ii) determining the most efficient NIC algorithm among the three selected above (GA, PS and HS). A comparison of the performance of the different approaches when applied to the FE model updating of a benchmark laboratory footbridge is conducted in this section.

Preliminary FE Model and Numerical Modal Analysis of the Laboratory Footbridge

The laboratory footbridge adopted for this study is a frame structure with a single span of 15 m. The structure is configured by two lateral steel beams separated
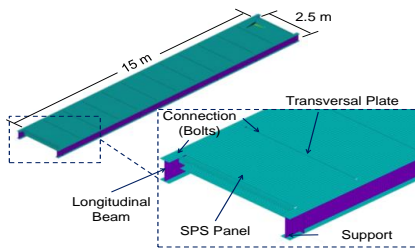
transversally 2.5 m. These beams are braced by diaphragms separated longitudinally 1.25 m. The diaphragms consist of rectangular plates of 200x12 mm. The lateral beams are connected at both sides to steel columns. These columns are directly pinned to the ground. The deck of the structure is formed by composite SPS panels [34]. These composite SPS panels are bolted to both the longitudinal and transversal elements. An overall view of the structure and its main constitutive components is illustrated in Fig. 3. A more detailed description of this benchmark structure may be found in Ref [25].

The structure was modelled with three types of elements in the commercial FE package Ansys [35]. All the numerical simulations were performed using a laptop computer with a processor of 3.6 GHz and a RAM memory of 8 GB. The mesh consisted of 31903 elements (Fig. 5). The FE model has been realized according to the following scheme: (i) the two main lateral beams and the transversal plates have been modelled with a four node shell elements with six degrees of freedom at each node (SHELL181); (ii) the SPS panels have been modelled with the same type of element (SHELL181), considering its sandwich-type behaviour through the first-order shear-deformation theory; (iii) the bolts that configure the connection between the SPS panel and the steel structure have been modelled by 3-D beam elements (BEAM188); and (iv) the supports were modelled by means of longitudinal and lateral spring elements (COMBIN14) and assuming that the vertical displacement was constrained.

The initial value for these spring parameters has been estimated from a simplified FE model of just the column that configure the support, resulting an equivalent stiffness of $k_{lon} = 5.5 \cdot 10^7$ N/m in the longitudinal direction and $k_{lat} = 1.9 \cdot 10^7$ N/m in the lateral direction.

The mechanical properties of the constitutive materials adopt the following values: (i) for the steel [36], a density $\gamma_s = 7850$ kg/m^3, a Young's modulus $E_s = 2.1 \cdot 10^5$ MPa and a Poisson's ratio $\nu_s = 0.3$; and (ii) for the polyurethane [37], a density $\gamma_p = 1100$ kg/m^3, a Young's modulus $E_p = 750$ MPa and a Poisson's ratio $\nu_p = 0.5$.

This FE model has been used to perform a numerical modal analysis: The obtained first seven natural frequencies, $f_{num,j}(\boldsymbol{\theta})$, are given in Table 1; whilst the associated numerical vibration modes, $\boldsymbol{\phi}_{num,j}(\boldsymbol{\theta})$, are depicted in Fig. 3 (j being the considered vibration mode).

Laboratory Footbridge

$f_{num,1}(\boldsymbol{\theta}) = 3.638$ Hz

$f_{num,2}(\boldsymbol{\theta}) = 5.329$ Hz $\qquad\qquad$ $f_{num,3}(\boldsymbol{\theta}) = 10.185$ Hz

$f_{num,4}(\boldsymbol{\theta}) = 11.310$ Hz $\qquad\qquad$ $f_{num,5}(\boldsymbol{\theta}) = 17.364$ Hz
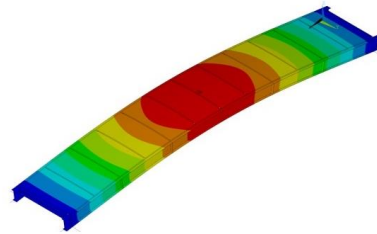
$f_{num,6}(\boldsymbol{\theta}) = 20.238$ Hz $\qquad\qquad$ $f_{num,7}(\boldsymbol{\theta}) = 21.105$ Hz
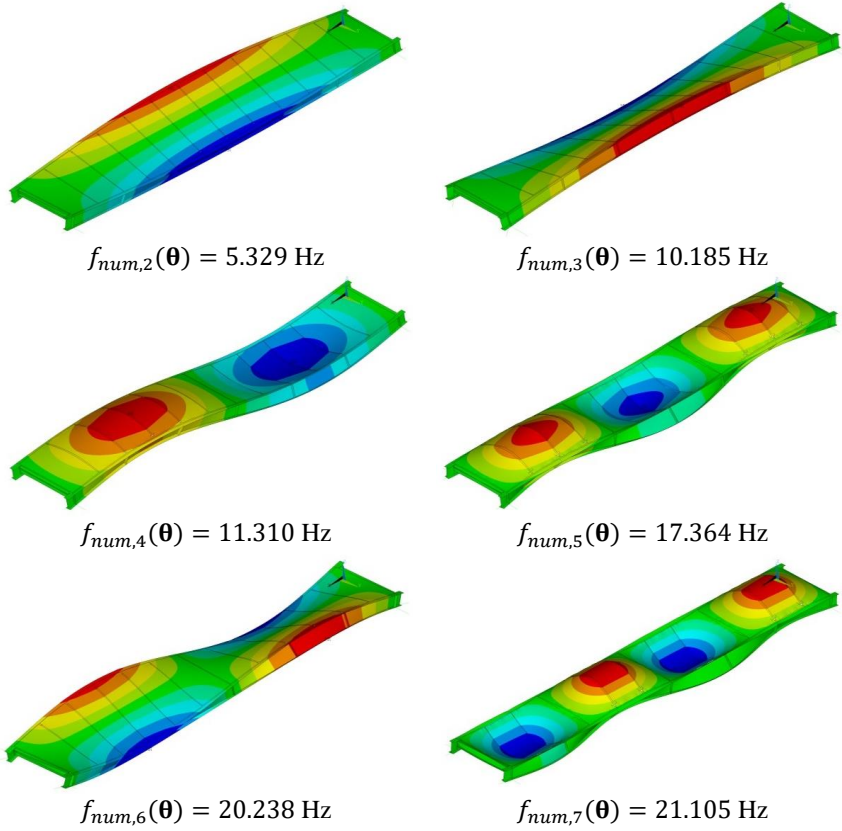
Fig. 3. Description of the structure and initial first seven numerical vibration modes, $\boldsymbol{\phi}_{num,j}(\boldsymbol{\theta})$, being j the considered vibration mode.

Experimental Identification of the Modal Properties of the Laboratory Footbridge

Subsequently, a forced vibration test was conducted to identify experimentally the modal properties of the footbridge. A set of proof-mass actuators and rowing accelerometers were used for this purpose (Fig. 4). The actuators were simultaneously driven by uncorrelated random signals considering a Multi-input Multi-output (MIMO) configuration [15, 25]. At all the considered reference points (instrumented points), the Frequency Response Functions (FRFs) were determined considering an overlap of 50%. Later, probable mode locations were identified in the FRFs fitted curves via a complex mode indicator function. Finally, a global polynomial curve fitting method was used to identify experimentally the first seven natural frequencies and associated vibration modes based on the mentioned probable mode locations [15]. Both the forced vibration test and the corresponding experimental modal analysis are described with more detail in Ref [25].
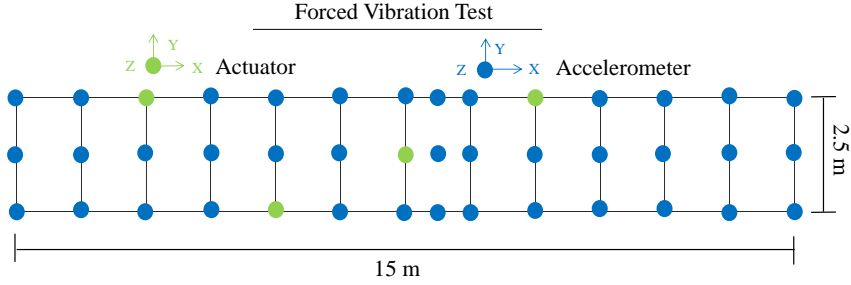
Fig. 4. Forced vibration test of the laboratory footbridge [25].

The first seven experimental natural frequencies (Table 1), $f_{exp,j}$, and associated experimental vibration modes (Fig. 5), $\boldsymbol{\phi}_{exp,j}$, were obtained as result of this experimental modal analysis (being j the considered vibration mode).

Correlation between the Preliminary Numerical and Experimental Modal Properties of the Laboratory Footbridge

In order to analyse the correlation between the numerical and experimental modal properties of the laboratory footbridge, the relative differences, $\Delta f_{exp,j}^{num,j}(\boldsymbol{\theta})$, and the $MAC(\boldsymbol{\theta})_{exp,j}^{num,j}$ ratios were determined. Table 1 shows the correlation between the numerical and experimental modal properties of the laboratory footbridge. Additionally, Fig. 5 illustrates a comparison between the numerical, $\boldsymbol{\phi}_{num,j}(\boldsymbol{\theta})$, and experimental, $\boldsymbol{\phi}_{exp,j}$, vibration modes.

Table 1. Correlation between the initial numerical (FE) and experimental modal properties of the laboratory footbridge (being $f_{num,j}(\boldsymbol{\theta})$ the numerical natural frequencies; $f_{exp,j}$ the experimental natural frequencies; $\Delta f_{exp,j}^{num,j}(\boldsymbol{\theta})$, the relative differences between the numerical and experimental natural frequencies; and the $MAC(\boldsymbol{\theta})_{exp,j}^{num,j}$ ratio of the j considered vibration mode).

Vibration Mode	$f_{num,j}(\boldsymbol{\theta})$ [Hz]	$f_{exp,j}$ [Hz]	$\Delta f_{exp,j}^{num,j}(\boldsymbol{\theta})$ [%]	$MAC(\boldsymbol{\theta})_{exp,j}^{num,j}$ [-]
1 (1st Bending)	3.638	3.810	-4.509	0.999
2 (1st Torsional)	5.329	5.144	3.600	0.994
3 (2nd Torsional)	10.185	8.485	20.033	0.990
4 (2nd Bending)	11.310	12.366	-8.540	0.877
5 (3rd Bending)	17.364	18.605	-6.670	0.985
6 (3rd Torsional)	20.238	20.459	-1.080	0.993
7 (4th Bending)	21.105	22.980	-8.159	0.910

Table 1 shows that, although the shapes of six of the seven identified vibration modes were in good agreement (with $MAC(\boldsymbol{\theta})_{exp,j}^{num,j}$ ratios greater than 0.90), the relative differences, $\Delta f_{exp,j}^{num,j}(\boldsymbol{\theta})$, between the numerical and experimental natural frequencies of four of the seven vibration modes were too large to be acceptable. Therefore, it becom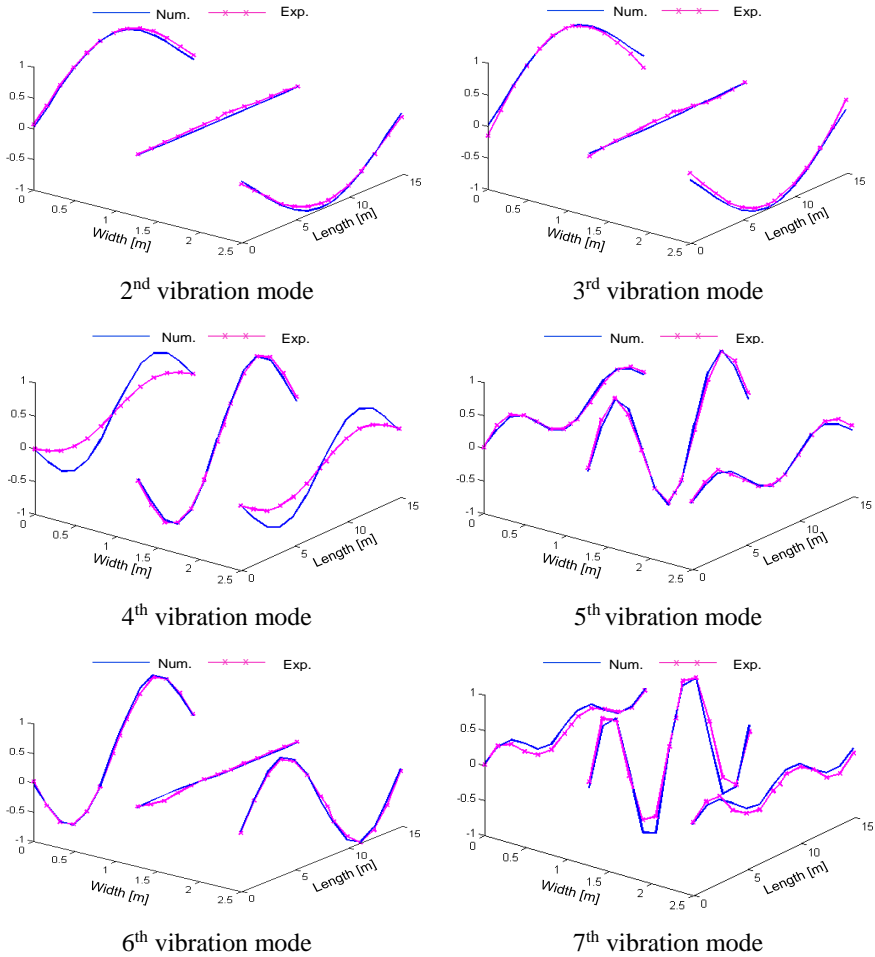es necessary to improve the FE model of this structure in order to ensure a better correlation between its numerical and experimental modal properties and, consequently, to obtain a valid FE model that reflects the actual dynamic behaviour of this structure [5].

FE Model Updating of the Laboratory Footbridge

In order to formulate the FE model updating problem of this laboratory footbridge under the MLM, the following elements must be defined: (i) the objective function; (ii) the design parameters; (iii) the search domain; and (iv) the optimization algorithm. Whilst the two approaches for the objective function (SOF/MOF) and the considered optimization algorithms (GA/PS/HS) were described previously, both the design parameters and their corresponding search domains will be established here.

Hence, a set with the most relevant physical parameters of the model needs to be selected, $\boldsymbol{\theta}$. To this end, the ratio between modal strain energy associated with each physical parameter and the overall modal strain energy of the structure was considered as selection criterion [38]. Following the sensitivity analysis carried out for this purpose, ten physical parameters of the structure were selected as design parameters (Fig. 7), $\boldsymbol{\theta} = [\theta_1, \theta_2, \theta_3, \theta_4, \theta_5, \theta_6, \theta_7, \theta_8, \theta_9, \theta_{10}]$: (i) the Young's modulus of the steel of the longitudinal beams in different sections, $\theta_1 - \theta_6$ [MPa]; (ii) the Young's modulus of the polyurethane, θ_7 [MPa]; (iii) the Young's modulus of the steel of the bolts, θ_8 [MPa]; (iv) the equivalent longitudinal stiffness of each support, θ_9 [N/m]; and (v) the equivalent lateral stiffness of each support, θ_{10} [N/m]. Additionally, a search domain has been included to constrain this optimization problem and thus, to guarantee the physical meaning of the updated model. Thus, the lower, $\boldsymbol{\theta}^l$, and the upper, $\boldsymbol{\theta}^u$, bounds of this search domain were defined as follows, $\boldsymbol{\theta}^l = [1.89 \cdot 10^5, 1.89 \cdot 10^5, 1.89 \cdot 10^5, 1.89 \cdot 10^5, 1.89 \cdot 10^5, 1.89 \cdot 10^5, 0.75 \cdot 10^3, 2.1 \cdot 10^5, 1.38 \cdot 10^7, 4.75 \cdot 10^6]$ and $\boldsymbol{\theta}^u = [2.31 \cdot 10^5, 2.31 \cdot 10^5, 2.31 \cdot 10^5, 2.31 \cdot 10^5, 2.31 \cdot 10^5, 2.31 \cdot 10^5, 1.5 \cdot 10^3, 2.1 \cdot 10^6, 1.1 \cdot 10^8, 3.8 \cdot 10^7]$.

FEM   1st vibration mode

2nd vibration mode

3rd vibration mode

4th vibration mode

5th vibration mode

6th vibration mode
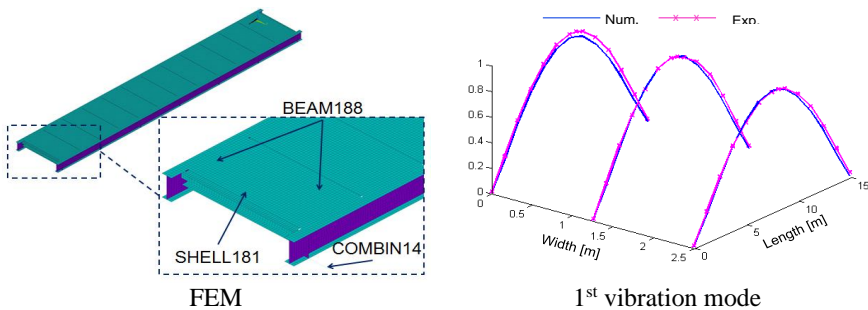
7th vibration mode

Fig. 5. FE model and comparison between the numerical, $\boldsymbol{\phi}_{num,j}(\boldsymbol{\theta})$, and experimental, $\boldsymbol{\phi}_{exp,j}$, vibration modes of the laboratory footbridge (being j the considered vibration mode).

Subsequently, the FE model updating was conducted considering the two approaches and the three considered NIC algorithms.

Comparison among GA, PS and HS for FE Model Updating under the SOF Approach

First, the initial FE model of the footbridge was updated using the SOF approach and considering the three mentioned NIC algorithms (GA, PS and HS). The solution of each updating problem was performed via its implementation using both the FE analysis package Ansys [35] and the mathematical package Matlab [39]. Two comparison criteria were considered to assess the performance of the three NIC algorithms: (i) the computational cost; and (ii) the accuracy of the adjustment.

For the three NIC algorithms, the following common design variables were adopted: (i) population size, $Pop = 100$; (ii) maximum number of iterations, $Iter = 50$;

and (iii) objective function tolerance, $TolF = 10^{-5}$ (so that the algorithm stops if the average relative change of the best value of the objective function is less than or equal to $TolF$).

Additionally, for each NIC algorithm, the following particular design variables were considered: (i) for the GA, as selection ratio, $selr = 0.1$, as crossover ratio, $crosr = 0.9$, and as mutation ratio, $mutr = 0.1$; (ii) for the PS algorithm, as particle's inertia, $ipar = 0.95$, as self-adjustment weight, $selw = 0.05$, and as social-adjustment weight, $socw = 0.02$; and (iii) for the HS algorithm, as new population size, $New\_Pop = 40$, as harmony memory consideration rate, $HMCR = 0.9$, as pitch adjustment rate, $PAR = 0.3$, and as bandwidth, $bw = \frac{1}{100}(\boldsymbol{\theta^u} - \boldsymbol{\theta^l})$.

In order to assess the impact of the residual weights on the updated value of the single-objective function, $f(\boldsymbol{\theta})$, a trial-and-error criterion [5] was adopted. Table 2 shows the eleven cases established in terms of the different values considered for the residuals associated with the natural frequencies, $\sum w_j^f$, and vibration modes., $\sum w_j^m$, respectively. Additionally, each case was run ten times to take into account the random generation of the initial population.

As result of the updating process, Table 2 shows the average values of the residuals for the three considered algorithms in terms of the different value of the weighting factors. Additionally, Fig. 6a illustrates the representation in a multi-objective functional space of the residuals associated with each case and computational algorithm. The average values of the updated parameters obtained using the three considered NIC algorithms under the SOF approach are shown in Table 3.

Table 2. Average values of the residuals in terms of the weighting factors under the SOF approach for the three considered NIC algorithms (GA, PS and HS).

Case	$\sum w_j^f$	$\sum w_j^m$	GA [$x10^{-3}$]		PS [$x10^{-3}$]		HS [$x10^{-3}$]	
			$\sum r_j^f(\boldsymbol{\theta})^2$	$\sum r_j^m(\boldsymbol{\theta})^2$	$\sum r_j^f(\boldsymbol{\theta})^2$	$\sum r_j^m(\boldsymbol{\theta})^2$	$\sum r_j^f(\boldsymbol{\theta})^2$	$\sum r_j^m(\boldsymbol{\theta})^2$
01	1.0	0.0	3.63	2.69	3.56	2.68	3.55	2.69
02	0.9	0.1	3.57	2.66	3.56	2.68	3.55	2.69
03	0.8	0.2	3.59	2.62	3.58	2.51	3.58	2.66
04	0.7	0.3	3.58	2.53	3.57	2.52	3.61	2.52
05	0.6	0.4	3.57	2.56	3.57	2.50	3.62	2.50
06	0.5	0.5	3.58	2.51	3.58	2.51	3.58	2.57
07	0.4	0.6	3.58	2.52	3.58	2.49	3.62	2.51
08	0.3	0.7	3.59	2.48	3.58	2.49	3.63	2.51
09	0.2	0.8	3.58	2.51	3.58	2.49	3.62	2.49
10	0.1	0.9	3.58	2.53	3.59	2.47	3.70	2.47
11	0.0	1.0	3.59	2.50	3.59	2.49	3.64	2.46

Finally, the average simulation time required to solve the updating problem for each case was: (i) 74072 s for the GA; (ii) 43857 s for the PS; and (iii) 34380 s for the HS.

According to these results, two main conclusions may be drawn: (i) the accuracy of the three mentioned NIC algorithm is similar; and (ii) the HS algorithm allows reducing the simulation time required to perform the updating process. In this manner, the HS algorithm allows performing the FE model updating of this structure more efficiently than

the other algorithms, since it reduces the computational cost without compromising the accuracy of the adjustment.

Comparison among GA, PS and HS for the FE Model Updating under the MOF Approach

Subsequently, the initial FE model of the laboratory footbridge was also updated under the MOF approach and considering the three mentioned NIC algorithms. Once more, the updating process was performed via its implementation using both Ansys [35] and Matlab [39] software packages and considering the same comparison criteria as above.

For the three NIC algorithms under the MOF approach, the same design variables (common and particular) as those employed for the SOF case were adopted. Additionally, the number of elements of the Pareto front was established in 25. The updating problem was solved ten times for each NIC algorithms to take into account the random generation of the initial population.

As result of the updating process, Fig. 6b illustrates the average Pareto front obtained for each considered NIC algorithm. Additionally, the average value of the updated parameters for the three considered NIC algorithms under the MOF approach is given in Table 3 (the NBI method [24] has been adopted for this purpose).

a)

b)
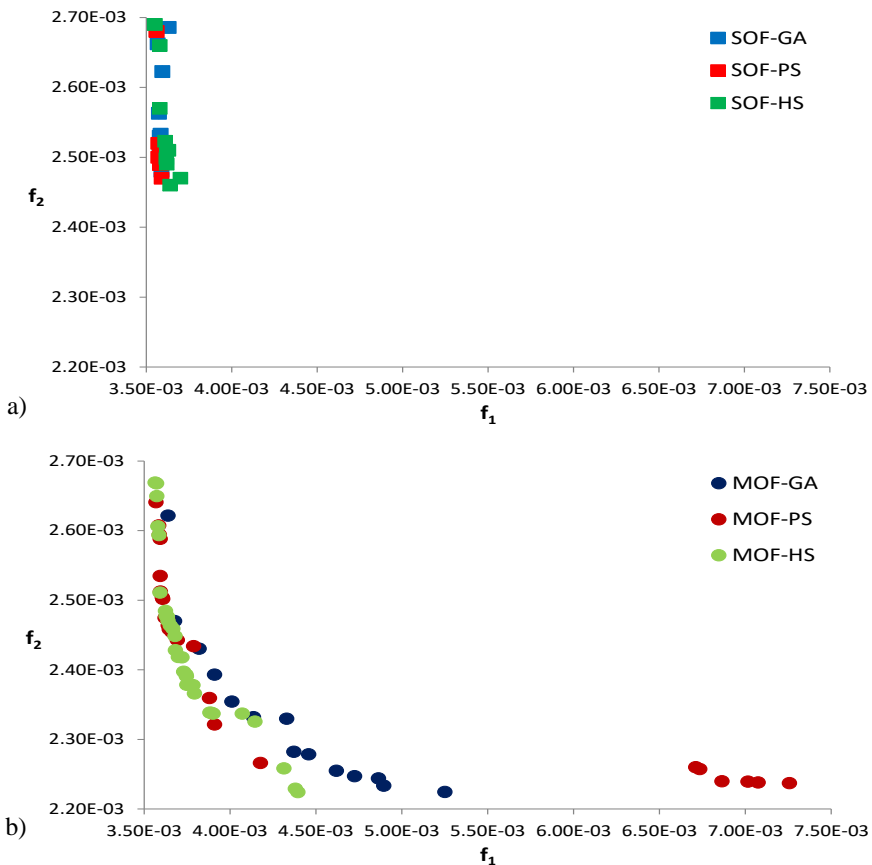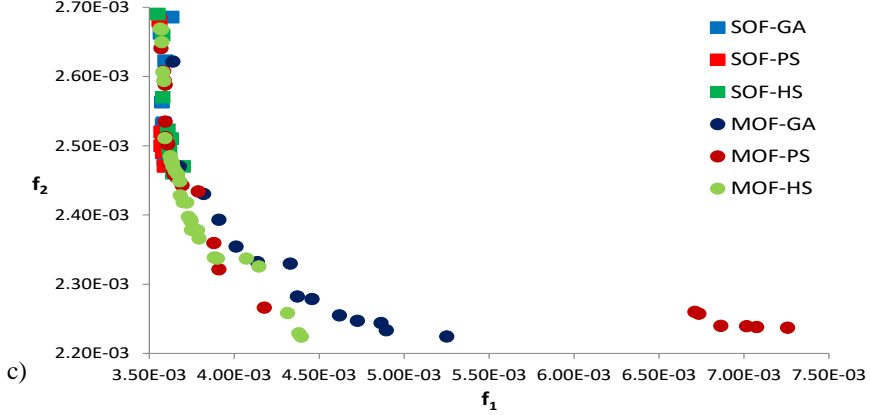
Fig. 6. Comparison among the different residuals in the functional space considering the three NIC algorithms (GA, PS and HS): a) the SOF approach; b) the MOF approach; and c) both the SOF and MOF approaches.

Additionally, the average simulation time required to obtain the Pareto front corresponding to each mentioned NIC algorithm has been recorded: (i) 307057 s for the GA; (ii) 240663 s for the PS; and (iii) 121676 s for the HS.

Table 3. Average updated value of the physical parameters of model, $\boldsymbol{\theta}$, after the updating process, considering the two approaches and the three mentioned computational algorithms.

$\boldsymbol{\theta}$	SOF			MOF		
	GA	PS	HS	GA	PS	HS
θ_1	$2.22 \cdot 10^5$	$2.23 \cdot 10^5$	$2.23 \cdot 10^5$	$2.28 \cdot 10^5$	$2.29 \cdot 10^5$	$2.29 \cdot 10^5$
θ_2	$2.11 \cdot 10^5$	$2.16 \cdot 10^5$	$2.09 \cdot 10^5$	$2.12 \cdot 10^5$	$2.25 \cdot 10^5$	$2.22 \cdot 10^5$
θ_3	$2.09 \cdot 10^5$	$2.10 \cdot 10^5$	$2.09 \cdot 10^5$	$2.02 \cdot 10^5$	$2.19 \cdot 10^5$	$2.13 \cdot 10^5$
θ_4	$2.07 \cdot 10^5$	$2.09 \cdot 10^5$	$2.05 \cdot 10^5$	$2.18 \cdot 10^5$	$2.19 \cdot 10^5$	$2.19 \cdot 10^5$
θ_5	$2.10 \cdot 10^5$	$2.04 \cdot 10^5$	$2.12 \cdot 10^5$	$2.15 \cdot 10^5$	$2.15 \cdot 10^5$	$2.17 \cdot 10^5$
θ_6	$2.14 \cdot 10^5$	$2.09 \cdot 10^5$	$2.12 \cdot 10^5$	$2.17 \cdot 10^5$	$2.12 \cdot 10^5$	$2.15 \cdot 10^5$
θ_7	$1.43 \cdot 10^3$	$1.43 \cdot 10^3$	$1.42 \cdot 10^3$	$1.02 \cdot 10^3$	$1.09 \cdot 10^3$	$1.03 \cdot 10^3$
θ_8	$4.40 \cdot 10^5$	$4.33 \cdot 10^5$	$4.29 \cdot 10^5$	$2.90 \cdot 10^5$	$2.96 \cdot 10^5$	$2.83 \cdot 10^5$
θ_9	$4.26 \cdot 10^7$	$4.24 \cdot 10^7$	$4.24 \cdot 10^7$	$4.29 \cdot 10^7$	$4.12 \cdot 10^7$	$4.13 \cdot 10^7$
θ_{10}	$1.50 \cdot 10^7$	$1.49 \cdot 10^7$	$1.49 \cdot 10^7$	$1.45 \cdot 10^7$	$1.42 \cdot 10^7$	$1.43 \cdot 10^7$

According to these results, three main conclusions can be drawn: (i) the accuracy of both the PS and HS algorithm is greater than the one provided by the GA since the Pareto front obtained by these two algorithms allows reducing the overall value of the residuals between the numerical and experimental modal properties of the structure; (ii) the accuracy between the PS and HS algorithms is similar; and (iii) the HS algorithm allows reducing again the simulation time required to perform the updating process. In this manner, the HS algorithm is again the most efficient NIC algorithm to solve the updating problem under the MOF approach.

Comparison between the SOF Approach and the MOF Approach for the FE Model Updating of the Laboratory Footbridge
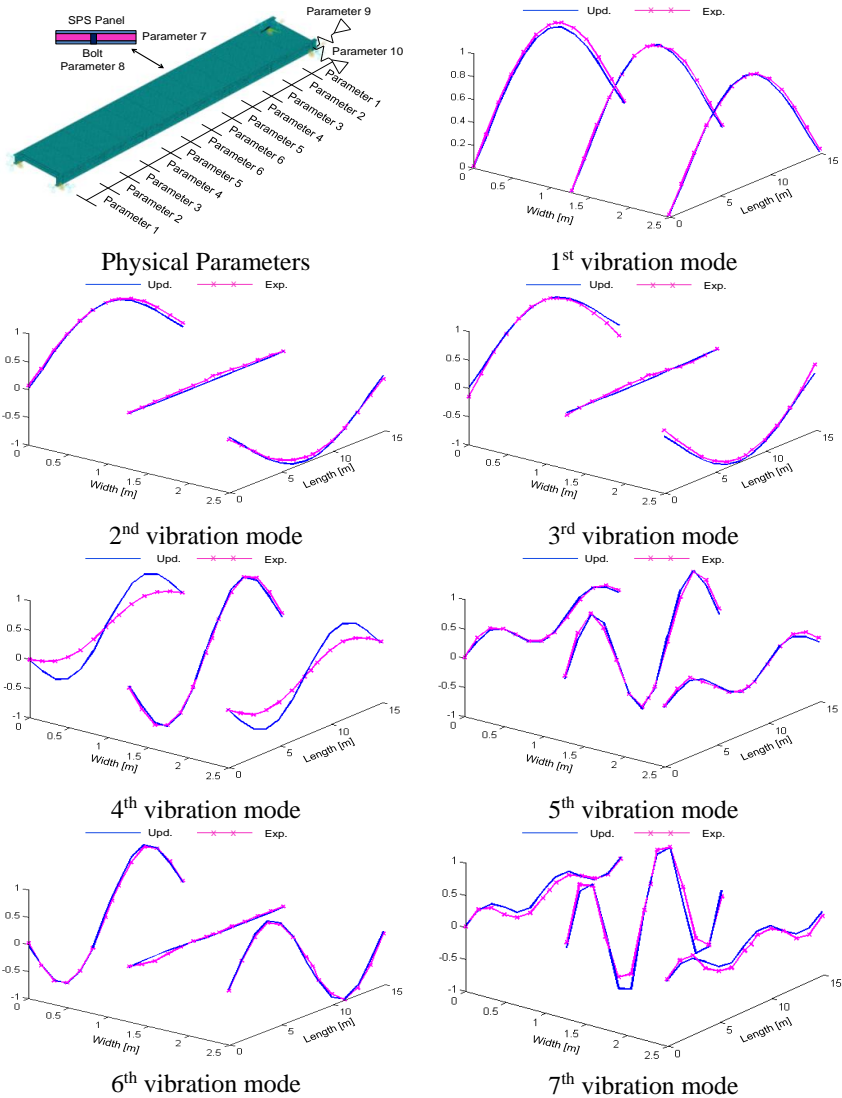
In order to assess the performance of the two approaches, three comparison criteria were taken into account: (i) the sweep capacity; (ii) the computational cost; and (iii) the goodness of the solution.

Fig. 6c illustrates a comparison among the solutions obtained considering the two approaches (SOF and MOF) and the three mentioned NIC algorithms (GA, PS and HS). The pair of residuals of each solution has been represented in a multi-objective functional space.

As Fig. 6c shows, although all the solutions obtained under the SOF approach belong to the Pareto front of the updating problem, they concentrate in just one of the branches of the curve. Thus, the sweep capacity of the SOF approach is lower than the one obtained using the MOF approach. Additionally, the set of solutions obtained under the SOF approach present a worse adjustment than the set of solutions obtained under the MOF approach. All the solutions obtained under the SOF approach both are located at greater distances from the coordinate origin (overall adjustment error) and they are farther from the so-called knee-point (point corresponding to solutions which better balance the value of the two types of residuals [26]). Furthermore, the simulation time required to perform the updating process under the MOF approach is lower than the one required under the SOF approach under equivalent computational conditions. In this regard, the most efficient algorithm, the HS algorithms, takes about 378180 s to determine the best updated model under the SOF while it only takes 121677 s under the MOF approach (121676 s to determine the Pareto front plus 1 s to solve the decision-making problem).

For all these reasons, it can be concluded that the MOF approach using the HS algorithm is the best option to perform the FE model updating of the considered civil engineering structure under the MLM.

Finally, for the sake of completeness, the modal properties of the footbridge, after the updating process, are shown in Table 4 and Fig. 7. The best solution of the Pareto front provided by the HS algorithm under the MOF approach has been considered for this purpose. This best solution has been obtained via the implementation of the NBI method [26] on the Pareto front. Table 4 shows the first seven updated natural frequencies, $f_{upd,j}(\boldsymbol{\theta})$, of the structure and Fig. 7 illustrates the first seven vibration modes, $\boldsymbol{\phi}_{upd,j}(\boldsymbol{\theta})$. As Table 4 shows, the correlation between the updated and experimental modal properties of the footbridge, after the updating process, has clearly improved and can be accepted as good. All the relative differences, $\Delta f_{exp,j}^{upd,j}(\boldsymbol{\theta})$, are lower than 5%, and all the $MAC(\boldsymbol{\theta})_{exp,j}^{upd,j}$ ratios are greater than 0.9.

Physical Parameters

1st vibration mode

2nd vibration mode

3rd vibration mode

4th vibration mode

5th vibration mode

6th vibration mode

7th vibration mode

Fig. 7. Comparison between the updated, $\boldsymbol{\phi}_{upd,j}(\boldsymbol{\theta})$, and experimental, $\boldsymbol{\phi}_{exp,j}$, vibration modes of the laboratory footbridge (being j the considered vibration mode).

Table 4. Correlation between the updated and experimental modal properties of the laboratory footbridge (being $f_{upd,j}(\boldsymbol{\theta})$ the updated natural frequencies; $f_{exp,j}$ the experimental natural frequencies; $\Delta f_{exp,j}^{upd,j}(\boldsymbol{\theta})$, the relative differences between the updated and experimental natural frequencies; and the $MAC(\boldsymbol{\theta})_{exp,j}^{upd,j}$ ratio of the j considered vibration mode).

Vibration Mode	$f_{upd,j}(\boldsymbol{\theta})$ [Hz]	$f_{exp,j}$ [Hz]	$\Delta f_{exp,j}^{upd,j}(\boldsymbol{\theta})$ [%]	$MAC(\boldsymbol{\theta})_{exp,j}^{upd,j}$ [-]
1 (1st Bending)	3.854	3.810	1.155	0.999
2 (1st Torsional)	5.489	5.144	4.907	0.994
3 (2nd Torsional)	8.365	8.485	-1.414	0.988
4 (2nd Bending)	11.896	12.366	-3.800	0.905
5 (3rd Bending)	18.662	18.605	0.306	0.987
6 (3rd Torsional)	20.016	20.459	-2.163	0.993
7 (4th Bending)	22.506	22.980	-2.063	0.957

Conclusions

This study tries to shed some light onto two key questions that must be addressed when conducting the Finite Element (FE) model updating of civil engineering structures under the Maximum Likelihood Method (MLM), namely:

(i) Establishing the most adequate approach to formulate the problem, by either employing a Single Objective Function (SOF) or a Multiple Objective Function (MOF) approach; and

(ii) Selecting a computationally efficient algorithm to solve the associated optimization problem.

To this end, the FE model updating of a real civil engineering structures, a laboratory steel footbridge located at the University of Exeter (U.K.), has been performed using two approaches (SOF and MOF) and considering three different Nature-Inspired Computational (NIC) algorithms: Genetic Algorithms (GA), Particle Swarm (PS) and Harmony Search (HS).

As the result of this study, two main conclusions may be drawn:

[1] The MOF approach is the most adequate option to perform the FE model updating of civil engineering structures under the MLM (when compared to the SOF approach), since it allows: (i) sweeping more widely the search space; (ii) reducing the overall simulation time; and (iii) further obtaining an updated model which better balances the influence of the two sets of considered residuals (those based on the natural frequencies and those based on the vibration modes); and

[2] The HS algorithm is the most efficient NIC algorithm among the three considered herein (GA/PS/HS) in order to solve the updating problem, since it allows a clear reduction of the computational cost without compromising the accuracy of the adjustment.

In this manner, the conclusions obtained in this paper could be directly extrapolated to improve the FE model updating of complex civil engineering structures in practical engineering applications. Nevertheless, additional studies are recommended to validate the performance of the HS algorithm when implemented for the FE model updating under the MOF approach for different types of civil engineering structures, as well as to conduct further comparative studies on the performance of the HS algorithm

against other more recent alternative metaheuristic optimization algorithms available in the literature.

Funding

References

[1] Friswell MI, Mottershead JE. Finite Element Model Updating in Structural Dynamics. Kluwer Academic Publishers, 1995.

[2] Brownjohn JMW, Xia P-Q, Hao H, Sia Y. (2001). Civil structure condition assessment by FE model updating: methodology and case studies. *Finite Elem. Anal. Des*. 2001; 37: 761-775. doi: https://doi.org/10.1016/S0168-874X(00)00071-8.

[3] Bucher C, Pham HA. On model updating of existing structures utilizing measured dynamic responses. *Struct. Infrastruct Eng*. 2005; 1(2): 135-143, doi: http://dx.doi.org/10.1080/15732470412331289297.

[4] Liu T, Zhang Q, Zordan T, Briseghella B. Finite Element Model Updating of Canonica Bridge Using Experimental Modal Data and Genetic Algorithm. *Struct. Eng. Int.* 2016; 26(1): 27-36. doi: https://doi.org/10.2749/101686616X14480232444405.

[5] Teughels A, Maeck J, De Roeck G. Damage assessment by FE model updating using damage functions. *Comput. Struct*. 2002; 80(25): 1869-1879. doi: https://doi.org/10.1016/S0045-7949(02)00217-1.

[6] Mordini A, Savov K, Wenzel H. The Finite Element Model Updating: A Powerful Tool for Structural Health Monitoring. *Struct. Eng. Int.* 2007; 17(4): 352-358. doi: https://doi.org/10.2749/101686607782359010.

[7] Chen B, Zhu Y, Hu J, Principe JC. System Parameter Identification. Information Criteria and Algorithms. Tsinghua University Press Ltd. Published by Elsevier Inc 2013. doi: https://doi.org/10.1016/B978-0-12-404574-3.00008-7.

[8] Marwala T. Finite-Element-Model Updating Using Computational Intelligence Techniques. Applications to Structural Dynamics. Springer, London, 2010.

[9] Chen Z. Bayesian filtering: From Kalman filters to particle filters, and beyond. *Stat*. 2003; 182: 1–69. doi: https://doi.org/10.1080/02331880309257.

[10] Rao CR, Toutenburg H, Fieger A. Linear Models and Generalizations: Least Squares and Alternatives. 2nd ed. Springer; 2007.

[11] Marwala T; Boulkaibet I; Adhikari S. Probabilistic Finite Element Model Updating Using Bayesian Statistics: Applications to Aeronautical and Mechanical Engineering. John Wiley & Sons, London, 2016.

[12] Val DV, Stewart MG. Assessment of Ageing Reinforced Concrete Structures— Current Situation and Future Challenges. *Struct. Eng. Int*. 2009; 19(2): 211-219, doi: https://doi.org/10.2749/101686609788220114.

[13] Jiménez-Alonso JF, Sáez A. Model Updating for the Selection of an Ancient Bridge Retrofitting Method. *Struct. Eng. Int*. 2016; 26(1): 17-26, doi: https://doi.org/10.2749/101686615X14355644771333.

[14] Mottershead JE, Link M, Friswell MI. The sensitivity method in finite element model updating: a tutorial. *Mech. Syst. Signal Pr.* 2011; 25(7): 2275-2296, doi: https://doi.org/10.1016/j.ymssp.2010.10.012.

[15] Maia NMM, Silva JMM. Theoretical and Experimental Modal Analysis. Research studies Press Ltd., Somerset, England, 1997.

[16] Jin S, Cho S, Jung H, Lee J, Yun C A new multi-objective approach to finite element model updating. *J. Sound Vib.* 2014; 333(11): 2323–2338. doi: https://doi.org/10.1016/j.jsv.2014.01.015.

[17] Park W, Kim H-K, Jongchil P. Finite Element Model Updating for a Cable-Stayed Bridge Using Manual Tuning and Sensitivity-Based Optimization. *Struct. Eng. Int*. 2012; 22(1): 14-19, doi: https://doi.org/10.2749/101686612X13216060212870.

[18] Kim G-H, Park Y-S. An improved updating parameter selection method and finite element model update using multi-objective optimisation technique. *Mech. Syst. Signal Pr.* 2004; 18(1): 59-78, doi: https://doi.org/10.1016/S0888-3270(03)00042-6.

[19] Ghee CK, Perry MC. Structural Identification and Damage Detection using Genetic Algorithms p. 140. CRC Press, Taylor and Francis Group, London, 2010.

[20] Kennedy J, Eberhart R. Particle swarm optimization, in Proceedings of ICNN'95 - International Conference on Neural Networks. 1995; 4, 1942–1948. doi: http://dx.doi.org/10.1109/ICNN.1995.488968.

[21] Geem ZW, Kim JH, Loganathan GV. A new heuristic optimization algorithm: harmony search. *Simul*. 2001; 76(2): 60–68. doi: https://doi.org/10.1177/003754970107600201.

[22] Saka MP, Aydogdu I, Hasancebi O, Geem ZW. Harmony Search Algorithms in Structural Engineering. In: Yang XS, Koziel S (eds) Computational Optimization and Applications in Engineering and Industry. Studies in Computational Intelligence, vol 359. Springer, Berlin, Heidelberg, 2011. doi: https://doi.org/10.1007/978-3-642-20986-4_6.

[23] Kaveh A, Mahdavi VR (2014). Colliding bodies optimization: A novel meta-heuristic method. *Comput*. *Struct.*, 2014; 139: 18-27. doi: https://doi.org/10.1016/j.compstruc.2014.04.005.

[24] Rashedi E, Nezamabadi-Pour H, Saryazdi S. GSA: A Gravitational Search Algorithm. *Inform. Sciences*, 2009 179 (13): 2232-2248. doi: https://doi.org/10.1016/j.ins.2009.03.004.

[25] Hudson E, Reynolds P. Design and Construction of a Reconfigurable Pedestrian Structure. *Exp. Techniques*. 2017; 41(2): 203-214. doi: https://doi.org/10.1007/s4079.

[26] Deb, K, Gupta, S. Understanding knee points in bicriteria problems and their implications as preferred solution principles. *Eng. Optimiz.* 2011; 43(11): 1175-1204. doi: https://doi.org/10.1080/0305215X.2010.548863.

[27] Infantes M, Naranjo-Pérez J, Sáez A, Jiménez-Alonso JF. Determining the best Pareto-solution in a multi-objective approach for model updating. IABSE Symposium, Guimaraes 2019: Towards a Resilient Built Environment Risk and Asset Management – Report, pp. 523-530, 2019.

[28] Costa C, Ribeiro D, Jorge P, Silva R, Arêde A, Calçada R. Calibration of the numerical model of a stone masonry railway bridge. *Eng. Struct*. 2016; 123: 345-371. doi: https://doi.org/10.1016/j.engstruct.2016.05.044.

[29] Zivanovic S, Pavic A, Reynolds P. Finite element modelling and updating of a lively footbridge: The complete process. *Eng. Struct* 2007; 301(1-2): 126-145. doi: http://dx.doi.org/10.1016/j.jsv.2006.09.024.

[30] Deb K, Pratap A, Agarwal S, Meyarivan T. A fast and elitist multi-objective genetic algorithm: NSGA-II. *IEEE Trans. Evol. Comput*. 2002; 6(2): 182–197. doi: http://dx.doi.org/10.1109/4235.996017.

[31] Srinivas N, Deb K. Multi-objective optimization using nondominated sorting in genetic algorithms. *IEEE Trans. Evol. Comput*. 1994; 2(3): 221–248. doi: http://dx.doi.org/10.1162/evco.1994.2.3.221.

[32] Coello CAC and Lechuga MS (2002). A proposal for multiple objective particle swarm optimization, in Proceedings of the 2002 Congress on Evolutionary Computation. CEC'02 doi: http://dx.doi.org/10.1109/CEC.2002.1004388.

[33] Geem ZW. Multi-objective optimization of time-cost trade-off using harmony search. *J. Constr. Eng. M.* 2009*;* 136(6): 711–716. doi: https://doi.org/10.1061/(ASCE)CO.1943-7862.0000167.

[34] SPS (2019). Sandwich Plate System heavy engineering composite from Intelligent Engineering n.d. http://www.ie-sps.com. (accessed May 2019).

[35] Ansys Mechanical Release 19.0. (2019). n.d. www.ansys.com. (accessed May 2019).

[36] Eurocode 3. Design of Steel Structures. CEN, 2005.

[37] Clark JL. Structural Design of Polymer Composites-EUROCOMP Design Code and Handbook, E&FN Spon, 1996.

[38] Fox R, Kapoor M. Rates of change of eigenvalues and eigenvectors. *AIAA J.* 1968; 6: 2426-2429. doi: https://doi.org/10.2514/3.5008.

[39] Matlab R2019a (2019), n.d. http://www.mathworks.com. (accessed May 2019).

Apéndice B
Articulo B

Naranjo-Pérez, J., Sáez, A., Jiménez-Alonso, J.F., Pachón, P., Compán, V. (2019). A hybrid UKF-MGA algorithm for finite element model updating of historical constructions. IABSE Symposium, Guimaraes 2019: Towards a Resilient Built Environment Risk and Asset Management – Report pp. 29-36.

A Hybrid UKF-MGA Algorithm for Finite Element Model Updating of Historical Constructions

Javier Naranjo-Pérez, Andrés Sáez

Department of Continuum Mechanics and Structural Analysis, Universidad de Sevilla, Seville, Spain

Javier F Jiménez-Alonso, Pablo Pachón, Víctor Compán

Department of Building Structures and Geotechnical Engineering, Universidad de Sevilla, Seville, Spain

Contacting author: compan@us.es

Abstract

The finite element model (FE) updating is a calibration method that allows minimizing the discrepancies between the numerical and experimental modal parameters. As result, a more accurate FE model is obtained and the structural analysis can represent the real behaviour of the structure. However, it is a high computational cost process. To overcome this issue, alternative techniques have been developed. This study focuses on the use of the unscented Kalman filter (UKF), which is a local optimization algorithm based on statistical estimation of parameters taken into account the measurements. The dome of a real chapel is considered as benchmark structure. A FE model is updated applying two different algorithms: (i) the multi-objective genetic algorithm and (ii) a hybrid unscented Kalman filter-multi-objective genetic algorithm (UKF-MGA). Finally, a discussion of the results will be presented to compare the performance of both algorithms.

Keywords: model updating; historical constructions; unscented Kalman filter; multi-objective genetic algorithm.

1. Introduction

The structural assessment of historical constructions is an increasingly relevant issue. The most usual approach for the assessment of their structural behaviour is to design a mathematical model (e.g. finite element model). To build the Finite Element (FE) model, the material and geometrical properties are assumed and the boundary conditions implemented may not be the proper. These facts may involve large discrepancies between the numerical results obtained from these mathematical models and the experimental results obtained from field vibration tests. The model updating may be formulated as an optimization procedure where these discrepancies are minimized. Friswell *et al.* [1] introduced in 1995 the main techniques which may be employed for FE model updating. The procedure consists in selecting one or several physical parameters of the numerical model and changing theirs values iteratively. For each iteration, the differences between numerical and experimental results (usually modal parameters) are evaluated. In this manner, viewed from the optimization perspective, the parameter identification solved as an inverse problem can be considered as a general minimization problem.

The objective is to find the physical parameters that minimizes the mean square error (objective function) between actual and simulated modal parameters.

Due to the high nonlinearity intrinsic to structural models, the objective functions could present many local minima. To prevent the algorithm to converge to a local minimum, the use of global optimization algorithms must be considered. Genetic algorithm (GA) has been widely used to solve a parameter identification inverse problem. The high computational cost has led to the emergence of hybrid techniques that reduce the convergence time of global optimization algorithms. In this study, a hybrid unscented Kalman filter-multi-objective genetic algorithm (UKF-MGA) is considered. The unscented Kalman filter (UKF) [6] is an algorithm used to estimate the parameters of a nonlinear system subjected to white noise. The parameters updating is based on the estimation of the Gaussian means and covariances of the quantities being estimated, minimizing the variance of the estimation error. The Kalman filter finds the local minimum around the current estimate.

This study focuses on the comparison of the results obtained using both the maximum likelihood approach and a hybrid UKF-MGA algorithm. As benchmark structure, the chapel of the Würzburg Residence (Germany) is considered. This building, whose construction dates from the early eighteenth century, was declared a World Heritage Site by UNESCO in 1981. The updating procedure is based on the actual modal parameters of the structure, obtained through the accelerations recorded during an ambient vibration test. Finally, the number of iterations, the computation time and the differences between the updated and experimental modal parameters are compared for both algorithms.

2. FE Model Updating based on the maximum likelihood method

2.1 Basics of FE Model Updating

The FE model updating tool aims to design a numerical model which is more adequate to the real behaviour of the structure [1]. It is an iterative process in which the values of certain pre-selected physical parameters are changed until the optimal solution is reached. The updated FE model, under the maximum likelihood method, is obtained by minimizing the objective functions defined in terms of the relative differences between experimental and numerical modal parameters.

Within the framework of multi-objective optimization, the problem to be solved consists in minimizing the objectives functions defined with regard to the residual of the natural frequencies and the residual of the vibration modes. The expressions to calculate both residuals are:

$$r_{f,j} = \frac{f_{num,j} - f_{exp,j}}{f_{exp,j}}, \qquad j = 1, \dots, m_f \qquad (1)$$

$$r_{s,j}^2 = \frac{\left(1 - \sqrt{MAC_j}\right)^2}{MAC_j}, \qquad j = 1, \dots, m_f \qquad (2)$$

where $f_{exp,j}$ is the experimental natural frequency j, $f_{num,j}$ is the numerical natural frequency j and MAC_j is the Modal Assurance Criterion. The MAC is a parameter used to assess the correlation between the numerical and experimental natural frequency j and is calculated by the following expression:

$$MAC_j = \frac{\left(\phi_{num,j}^T \cdot \phi_{exp,j}\right)^2}{\left(\phi_{num,j}^T \cdot \phi_{num,j}\right) \cdot \left(\phi_{exp,j}^T \cdot \phi_{exp,j}\right)} \qquad (3)$$

being ϕ_{num} and ϕ_{exp} the numerical and experimental vibration modes, respectively. Both residuals are used to define the objective functions. Therefore, the minimization problem may be defined as follows:

$$\min f_1(\theta) = \min \frac{1}{2} \left[\sum_{j=1}^{m_f} r_{f,j}^2(\theta)\right]^{\frac{1}{2}} \qquad (4)$$

$$\min f_2(\theta) = \min \frac{1}{2} \left[\sum_{j=1}^{m_f} r_{s,j}^2(\theta)\right]^{\frac{1}{2}} \qquad (5)$$

where $f_1(\theta)$ and $f_2(\theta)$ are the objective functions related to the natural frequencies and vibration modes, respectively, θ is the possible solution vector containing the updated physical parameters of the model and m_f is the number of vibration modes considered.

2.2 Multi-objective Genetic Algorithm (MGA)

The multi-objective global optimization algorithm (MGA) employed in this study is the nature-inspired NSGA-II (Non-Dominated Sorting Genetic Algorithm) algorithm [3]. This algorithm consists of the followings steps. First, the initialization consists in creating an initial random population (solutions) and the assessment of the objective functions. The value of the objective functions are then classified to distinguish between dominated and non-dominated (Pareto front) solutions. Second, the stochastic selection function selects several classified solutions and generate a new population by using the crossover and the mutation functions. The former allows creating a new solution from two previous ones and the latter is used to randomly modify the value of one parameter of the new solution in order to search on new areas of the domain. Finally, the objective functions are evaluated for the new generation and the non-dominated solutions are obtained. The two last steps are repeated until a stop criterion is reached. As result, the Pareto's optimal front is build where each point represents a possible solution.

3. FE Model Updating considering the hybrid UKF-MGA algorithm

The Kalman filter [2] is an estimator that consists in estimating the unknown variables by considering the measurements which contain statistical white noise. The mathematical representation of a general parameter identification problem solved by using the Kalman filter is based on the state-space model:

$$\boldsymbol{\theta}_k = \boldsymbol{\theta}_{k-1} + \boldsymbol{w}_{k-1} \qquad (6)$$

$$\boldsymbol{z}_k = \boldsymbol{h}(\boldsymbol{\theta}_k, \boldsymbol{x}_k) + \boldsymbol{v}_k \qquad (7)$$

where $\boldsymbol{\theta}$ is the vector containing the model parameters and $\boldsymbol{z}$ extracts the modelling outputs of the modelling function $\boldsymbol{h}(\ )$. The estimation process noise and the modelling uncertainty are taken into account in the vectors $\boldsymbol{w}$ and $\boldsymbol{v}$, respectively. Both terms are assumed to be white Gaussian noise with zero-mean and covariance matrices $\boldsymbol{Q}$ and $\boldsymbol{R}$, respectively. The matrix $\boldsymbol{R}$ is the sum of measurements noise and modelling noise: $\boldsymbol{R} = \boldsymbol{R}^{meas} + \boldsymbol{R}^{model}$ [4]. Nevertheless, the modelling uncertainty is neglected in this study as the same model is considered for each iteration of the simulation.

An extension of the Kalman filter to nonlinear systems, the so-called extended Kalman filter (EKF) was developed [5]. The EKF requires linearization (Taylor series expansion) of Equation (7). In case $\boldsymbol{h}$ is a numerical model, there is no analytical solution of the Jacobian of the function. Instead, a numerical method such as the finite difference algorithm must be used to approximate the Jacobian.

To overcome this issue, the unscented Kalman filter (UKF) was proposed by Julier *et al*. [6]. The UKF is an estimator for nonlinear systems where no linearization of the modelling function $\boldsymbol{h}$ is needed. This algorithm uses the unscented transform technique to select a group of sample points (sigma points) which are propagated through the nonlinear functions to calculate the mean and the covariance of the estimated parameters [7]. It implies that the second order Gaussian approximation of the estimates is preserved. In this study, the genetic algorithm hybridized with UKF is considered due to the advantages of this algorithm over the EKF. A detailed description of the algorithm for parameter estimation problems is given below.

As a Kalman filter, the UKF consists of two steps: (i), the prediction and; (ii) the correction (or update). The former consists in assessing the sigma points and the prior estimation error, modelling error and the cross covariance. The latter involves computing Kalman's Gain matrix ($\boldsymbol{K}$) and correcting the prior estimates of the parameters and the covariance, based on the measurements $\boldsymbol{z}^{obs}$.

The sigma points are $2n + 1$ distributed points in the vicinity of the current estimate. They are defined from the prior estimation error covariance [8]:

$$S = \eta\sqrt{P_{k-1}} \qquad (8)$$

$$(\chi_{k-1})_0 = \widehat{\theta}_{k-1} \qquad (9)$$

$$(\chi_{k-1})_i = \widehat{\theta}_{k-1} + S_i, \qquad i = 1, 2, \dots, n \qquad (10)$$

$$(\chi_{k-1})_{i+n} = \widehat{\theta}_{k-1} - S_i, \quad i = 1, 2, \dots, n \qquad (11)$$

being n the number of parameters, η is the scaling parameter computed as $\eta = \sqrt{n + \lambda}$, P is the estimation error covariance and χ are the $2n + 1$ sigma points. The sigma points are multiplied by a weight, defined as:

$$W_0 = \frac{\lambda}{n + \lambda} \qquad (12)$$

$$W_i = W_{i+n} = \frac{1}{2(n + \lambda)}, \quad i = 1, 2, \dots, n \qquad (13)$$

This algorithm is integrated into the MGA. Specifically, the UKF searches around the candidate values of the parameters proposed by the genetic algorithm. Once the value of the parameters $\widehat{\theta}_{k|k}$ are obtained, the objective functions are assessed by minimising the mean square error between numerical and experimental modal parameters. The genetic algorithm uses these values of the objective functions to propose a new possible solution (vector of parameters). The algorithm is shown below.

Initial Step:

$$\widehat{\theta}_0 = \theta_{prior}$$

$$P_0^m = P_{prior}$$

Main loop: $for\ k = 1 : N_{UKF}$ (number of iterations of the UKF)

Prediction step:

$$(\chi_{k-1})_i$$

$$(\chi_{k|k-1})_i = (\chi_{k-1})_i$$

$$\widehat{\theta}_{k|k-1} = \sum_0^{2n} W_i \cdot (\chi_{k|k-1})_i$$

$$P_{k|k-1}^{\theta} = \sum_0^{2n} \left(W_i \left[(\chi_{k|k-1})_i - \widehat{\theta}_{k|k-1} \right] \cdot \left[(\chi_{k|k-1})_i - \widehat{\theta}_{k|k-1} \right]^T \right) + Q$$

$$(z_{k|k-1})_i = h \left((\chi_{k|k-1})_i \right)$$

$$\widehat{z}_{k|k-1} = \sum_0^{2n} W_i \cdot (z_{k|k-1})_i$$

$$P_{k|k-1}^{z} = \sum_0^{2n} \left(W_i \left[(z_{k|k-1})_i - \widehat{z}_{k|k-1} \right] \cdot \left[(z_{k|k-1})_i - \widehat{z}_{k|k-1} \right]^T \right) + R$$

$$P_{k|k-1}^{\theta z} = \sum_0^{2n} \left(W_i \left[(\chi_{k|k-1})_i - \widehat{\theta}_{k|k-1} \right] \cdot \left[(z_{k|k-1})_i - \widehat{z}_{k|k-1} \right]^T \right)$$

Correction (update) step:

$$K_k = P_{k|k-1}^{\theta z}\left(P_{k|k-1}^z\right)^{-1}$$

$$\hat{\theta}_k = \hat{\theta}_{k|k-1} + K_k(z^{obs} - \hat{z}_{k|k-1})$$

$$P_k^m = P_{k|k-1}^m - K_k P_{k|k-1}^z K_k^T$$

$$end$$

4. Model updating of a real historical construction

As benchmark structure, the domes of the chapel integrated in the Würzburg Residence (Germany) is considered. The domes are masonry surfaces of bricks grown in a single lawyer. The bricks are 30 cm thick, and at the base of the dome, they are reinforced by increasing the thickness until 45 cm. The reinforcement is also presented in the radial ribs reaching a section of 45x45 cm. In the construction process of the domes, the nerves are built alongside the rest of the sheet.
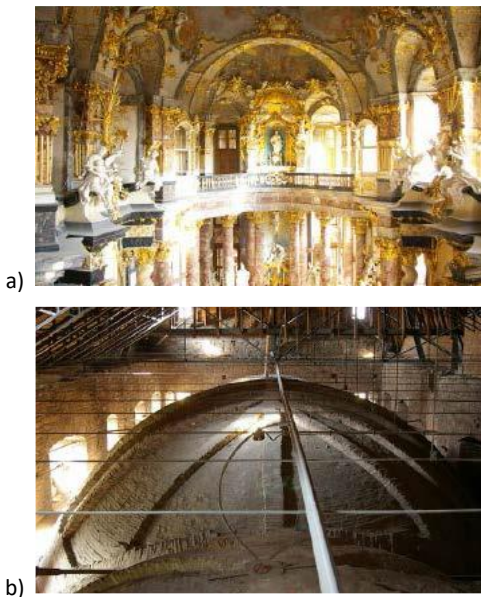

a)

b)

Figure 1. a) Interior of the chapel and b) exterior of the dome of the chapel of the Würzburg Residence

4.1 Preliminary Numerical Model

The preliminary FE model was built using the Ansys software [9]. The structural model of the dome was defined by considering 3D shell elements (SHELL63) which have 4 nodes per element. The effect of the lateral walls of the chapel on the dome was established, in a simplified manner, by means of two 1D spring elements (COMBIN14) whose stiffness represents the bending rigidity of the wall in the direction under consideration. The following mechanical properties of the material have been considered: Young's modulus, E (GPa) = 2; Poisson's ratio, ν = 0.2; density, ρ (kg/m^3) = 1700 and horizontal stiffness of the walls, k_h = 1000 kN/m. The latter was determined by considering that these elements were made with the same material than the rest and assimilating their behaviour to a cantilever. To adequately model the behaviour of the walls, four different zones were assumed (a wall for each lateral dome and two walls for the main dome) (see Figure 2). The numerical modal analysis led to the three natural frequencies shown in Table 1.
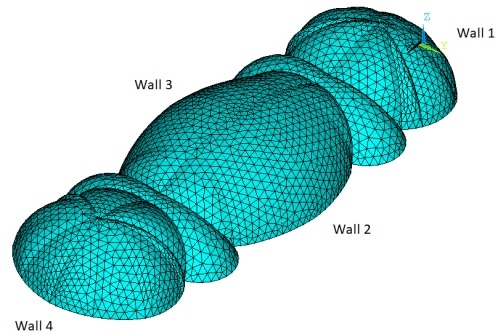

Figure 2. FE model of the dome of the chapel

4.2 Ambient Vibration Test and Operational Modal Analysis

An ambient vibration test was performed in order to experimentally identify the modal parameters of the structure. To this effect, the accelerations

were recorded during 10 minutes by eight uniaxial accelerometers at 51 instrumented points. The signals were processed using the time domain SSI algorithm [10], implemented in the software ARTeMIS Modal [11]. This whole procedure has been detailed in [12]. The three identified natural frequencies are shown in Table 1. Besides, the relative difference between the numerical and experimental natural frequencies and the MAC are calculated for each vibration mode.

Table 1. Numerical and experimental natural frequencies

Vibration Mode	f_{num} [Hz]	f_{exp} [Hz]	Δf [%]	MAC
1 (lateral)	3.362	2.764	21.635	0.809
2 (longitudinal)	3.431	3.231	6.190	0.877
3 (lateral)	3.988	4.015	-0.672	0.648

From the results in Table 1, it can be noticed that despite the use of a very detailed FE model, the natural and experimental mode shapes are not in good agreement as the errors between them are high. A FE model updating process must be conducted to guarantee that the numerical model represents more accurately the actual behaviour of the dome.

4.3   Finite Element Model Updating

This process was implemented in the software programme MATLAB [13]. As global optimization algorithm, the MGA was used. This study focuses on the comparison of the two previous described techniques to find the global minimum of the objective functions: (i), the maximum likelihood method (MLM) based on MGA and; (ii), the hybrid UKF-MGA algorithm.

The parameters selected for the model updating process are the same for both problems. A sensitivity study was performed to select the physical parameters that influence more the dynamic behaviour. This influence was taken into account on the basis of the modal strain energy. The seven parameters chosen were the followings: the Young's modulus of the dome, the Young's modulus of the ribs, the Young's modulus

of the starting wall, the longitudinal stiffness of the walls 1 and 4, the lateral stiffness of the walls 2 and 3, the lateral stiffness of the walls 1 and 4 and the longitudinal stiffness of the walls 2 and 3. The search range of the parameters were: (i) for the Young's moduli, [1–4] GPa and; (ii) for the stiffness, [200-2200] kN/m.

The objective functions were defined as expressed in Equations (4) and (5).

4.3.1   MLM-MGA method

The value of the updated parameters is shown in Table 2.

Table 2. Updated physical parameters (MLM-MGA)

Parameter	Updated value
E dome [Pa]	1.164E+9
E ribs[Pa]	1.468E+9
E starting wall [Pa]	1.319E+9
k_x walls 1 and 4 [N/m]	7.531E+5
k_y walls 2 and 3 [N/m]	3.941E+5
k_y walls 1 and 4 [N/m]	1.729E+6
k_x walls 2 and 3 [N/m]	9.793E+5

The modal analysis of the updated FE model led to the three natural frequencies given in Table 3. The improvement of the relative differences between natural frequencies (except the third vibration mode) and the increase of MAC ratios exhibit the good performance of the updating procedure.

Table 3. Natural frequencies of the updated FE model (MLM-MGA)

Vibration Mode	$f_{num,up}$ [Hz]	f_{exp} [Hz]	Δf [%]	MAC
1	2.725	2.764	-1.411	0.861
2	3.237	3.231	-0.186	0.921
3	4.188	4.015	4.299	0.728

4.3.2   Hybrid UKF-MGA algorithm

In the implementation of the UKF-MGA the following parameters were chosen [14]: initial estimation error covariance, $P_0^m = diag\left(\left(\frac{u_b - l_b}{100}\right)^2\right)$; covariance matrix of process noise, $Q = 0.005P_0$; the covariance matrix of measurements noise is taken from the OMA, $R = 0.001 \cdot \mathbf{I}(r, r)$, with $\mathbf{I}(r, r)$ the identity matrix having dimensions equal to the size of the measurements data, r and $\lambda = 0.0001$. The measurements vector, z^{obs}, was defined taking into account both the experimental natural frequencies and the mode shapes. The latter was implemented in terms of the MAC, considering the unit for the three vibration modes. In this manner, the difference $z^{obs} - \hat{z}$ represent the error between observed and numerical modal parameters. The updating process gave as a result the model parameters presented in Table 4.

Table 4. Updated physical parameters (UKF-MGA)

Parameter	Updated value
E dome [Pa]	2.848E+9
E ribs[Pa]	3.424E+9
E starting wall [Pa]	2.778E+9
k_x walls 1 and 4 [N/m]	6.418E+5
k_y walls 2 and 3 [N/m]	2.371E+5
k_y walls 1 and 4 [N/m]	1.862E+6
k_x walls 2 and 3 [N/m]	9.728E+5

The natural frequencies obtained after this optimization are shown in Table 5. This algorithm also conducts to a good adjustment of the numerical and experimental modal parameters.

Table 5. Natural frequencies of the updated FE model (UKF-MGA)

Vibration Mode	$f_{num,up}$ [Hz]	f_{exp} [Hz]	Δf [%]	MAC
1	2.741	2.764	-0.832	0.859
2	3.207	3.231	-0.743	0.928
3	4.423	4.015	10.161	0.695

4.4   Discussion of the results

A discussion of the performance of both algorithms, GA and GA-UKF, is presented. The comparison is developed in terms of two key criteria: regarding the relative differences between numerical and experimental natural frequencies and MAC ratios and with respect to the number of iterations and computation time.

First, from Table 3 and Table 5, it can be observed that the relative differences, Δf, are smaller for the MLM-GA (except the first vibration mode). In addition, the MAC ratios are larger for this algorithm (except for the second vibration mode).

Second, the number of iterations and the computational cost is compared (see Table 6). The algorithms were run in a 3.60 GHz processor with a 29.3 RAM. For the MLM-GA, the number of iterations of the multi-objective genetic algorithm was established in 100 and a population of 200 solutions (vector of possible parameters) was considered. The time to complete the procedure was around 47000 seconds. However, for the UKF-MGA, the number of iterations of the multi-objective genetic algorithm was set to 20, the initial population was made up of 10 vectors and 5 iterations of the unscented Kalman filter were considered. The reduced number of iterations and population of the genetic algorithm is due to the multiple $(2n + 1$, being n the number of parameters) evaluations of the objective functions for each iteration of the UKF. The duration of the UKF-MGA is around 16000 seconds. This is 34% less than the time of the GA.

Based on the two criteria, the UKF-MGA represents a useful tool to perform a model updating process, as the computational cost is considerably reduced and the results, although worst, are similar to those obtained with the MLM-MGA.

Table 6. Comparison of the MLM-MGA and UKF-MGA algorithms

	N (MGA)	Pop.	N (UKF)	Time [s]
MLM-MGA	100	200	-	47710
UKF-MGA	20	10	5	16068

5. Conclusions

The usual way of conducting a FE model updating is to carry out an optimization process. To this effect, optimization algorithms are used, being the evolutive algorithms, such as the GA, the most common. The high computational cost of the GA has guided to authors to employ alternative techniques. A multi-objective GA hybridized with UKF algorithm is proposed in this study. In order to analyse the performance of both algorithms, a comparative study has been carried out. It has been elaborated via the FE model updating of a real chapel, placed in Würzburg (Germany). The results of the comparison have shown that UKF-MGA is able to obtain similar results to those of the MLM-MGA. Moreover, the UKF-MGA lasted around 16000 seconds while the MLM-MGA completed the process in around 47000 seconds. The hybridized tool used in this study can be considered as an efficient technique to conduct a FE model updating to obtain a more accurate numerical model of the real structure.

Acknowledgements

References

[1] Friswell M, Mottershead JE. *Finite element model updating in structural dynamics*. Springer Science & Business Media, 1995.

[2] Kalman R. A new approach to linear filtering and prediction problems. *J Basic Eng* 1960; 82: 35–45.

[3] Srinivas N, Deb K. Muiltiobjective optimization using nondominated sorting in genetic algorithms. *Evol Comput* 1994; 2: 221–248.

[4] Tarantola A. *Inverse problem theory and methods for model parameter estimation*. siam, 2005.

[5] Julier SJ, Uhlmann JK. Unscented filtering and nonlinear estimation. *Proc IEEE* 2004; 92: 401–422.

[6] Julier SJ, Uhlmann JK. New extension of the Kalman filter to nonlinear systems. In: *Signal processing, sensor fusion, and target recognition VI*. International Society for Optics and Photonics, 1997, pp. 182–194.

[7] Nguyen LT, Nestorović T. Nonlinear Kalman filters for model calibration of soil parameters for geomechanical modeling in mechanized tunneling. *J Comput Civ Eng* 2015; 30: 04015025.

[8] Olivier A, Smyth AW. A marginalized unscented Kalman filter for efficient parameter estimation with applications to finite element models. *Comput Methods Appl Mech Eng* 2018; 339: 615–643.

[9] Ansys Mechanical 19.0. *Ansys Inc*.

[10] Magalhães F, Cunha A. Explaining operational modal analysis with data from an arch bridge. *Mech Syst Signal Process* 2011; 25: 1431–1450.

[11] *ARTeMIS Modal 2016*. Structural Vibration Solutions A/S.

[12] Pachón P, Compán V, Jiménez-Alonso J. Ambient vibration testing, dynamic identification and model updating of a historical building. Chapel of the Würzburg Residence (Germany). Gijón (Spain): International Operational Modal Analysis Conference (IOMAC), 2015.

[13] Matlab R2018b, http://www.mathworks.com/.

[14] Astroza R, Nguyen LT, Nestorović T. Finite element model updating using simulated annealing hybridized with unscented Kalman filter. *Comput Struct* 2016; 177: 176–191.

Apéndice C
Articulo C

Naranjo-Pérez, J., Jiménez-Alonso, J. F., Pavic, A., Sáez, A. Finite-element model up-dating of civil engineering structures using a hybrid UKF-HS algorithm. *Structure and Infraestructure Engineering*. 2020.

Finite-element-model updating of civil engineering structures using a hybrid UKF-HS algorithm

Javier Naranjo-Pérez[1], Javier F. Jiménez-Alonso[2*], Aleksandar Pavic[3] and Andrés Sáez[1]

[1]*Department of Continuum Mechanics and Structural Analysis, Universidad de Sevilla, Seville, Spain*

[2] *Department of Continuum Mechanics and Structures, E.T.S. Ingenieros de Caminos, Canales y Puertos. Universidad Politécnica de Madrid, Madrid, Spain*

[3] *College of Engineering, Mathematics and Physical Sciences, University of Exeter, Exeter, UK*

[*]Corresponding author: Assistant Professor: Javier Fernando Jiménez-Alonso. Department of Continuum Mechanics and Structures. E.T.S. Ingenieros de Caminos, Canales y Puertos. Universidad Politécnica de Madrid, Calle del Profesor Aranguren, 3, 28040 Madrid (Spain) Ph:+34 91 0674154. e-mail: jf.jimenez@upm.es.

Finite-element- model updating of civil engineering structures using a hybrid UKF-HS algorithm

Finite-element-model updating allows reducing the discrepancies between the numerical and the experimental dynamic behaviour of civil engineering structures. Among the different methods to tackle the updating problem, the maximum likelihood method has been widely used for practical engineering applications. In this method, the updating problem is transformed into an optimization problem where the relative differences between the numerical and experimental modal properties of the structure are reduced via the modification of the most relevant physical parameters of the model. However, this method often presents the drawback of requiring high simulation times in order to perform the updating process when dealing with complex structures. To overcome this limitation, in this paper a novel hybrid Unscented Kalman Filter – Harmony Search (UKF-HS) algorithm is proposed and its implementation details are discussed. In order to validate such hybrid algorithm and further illustrate its performance, the finite-element-model updating of a benchmark footbridge is performed using two different approaches (single-objective and multi-objective) and three different computational algorithms, namely: (i) genetic algorithms; (ii) harmony search; and (iii) the novel UKF-HS hybrid algorithm. The obtained results reveal that the proposed hybrid algorithm may be considered as an adequate alternative tool to efficiently perform the finite-element-model updating of civil engineering structures in practical engineering applications.

Keywords: finite-element-model updating; unscented Kalman filter, harmony search; genetic algorithm; hybrid algorithms; maximum likelihood method.

1. Introduction

Finite-element-model updating allows reducing the discrepancies between the predictions provided by numerical models and the real behaviour of civil engineering structures (Friswell and Mottershead, 1995). In this manner, the resulting finite-element-models will closely reproduce the actual behaviour of the structure. For this reason, finite-element-model updating has been widely used in engineering practice to conduct structural assessment analyses (Fritzen *et al.*, 1998; Fan and Qiao, 2011), in damage detection applications (Teughels *et al.*, 2002; Wang *et al.*, 2014) or for structural health monitoring of existing structures (Beck, *et al.*, 2001).

Finite-element-model updating basically focuses on obtaining the values of the most relevant physical parameters of the structure which minimize the difference between the numerical and experimental behaviour of the structure (Mottershead et al.,

2011). For this purpose, the modal properties of the structure are usually considered to characterize its behaviour. In this manner, the finite-element-model updating problem can be transformed into a parameter identification problem (Friswell and Mottershead, 1995). In order to address this identification problem, estimators are normally considered (Marwala, 2010). Among the different estimators, two have been widely used in practical engineering applications: (i) Bayesian inference; and (i) maximum likelihood method.

Bayesian inference (Marwala *et al.*, 2016) allows finding the posterior probability density function of the considered parameters via a statistical method based on Bayes' theorem. According to this theorem, the a priori information on the probability density function of the parameters can be updated based on information provided by the observations (experimental data). The expectation of the posterior probability density function may be evaluated through multi-dimensional integrals. As these integrals do not usually have analytical solutions, numerical approximations (Beck and Katafygiotis, 1998) and stochastic simulation methods (Papadimitriou *et al.*, 2018) have been widely employed to this end. Between these two methods, stochastic simulations have been extensively used due to its ease of implementation and higher accuracy (Cheung and Beck, 2009). Stochastic simulations are based on the generation of samples (sampling techniques). Among these sampling methods, the so-called Markov Chain Monte Carlo (MCMC) methods have been normally used to solve the finite-element-model updating problem (Beck and Au, 2002). Different algorithms have been developed to perform a MCMC simulation. Among these algorithms, some outstanding examples for Bayesian finite-element-model updating applications are (according to the best of the authors' knowledge): (i) the Metropolis-Hastings algorithm (Robert and Casella, 1999); the Gibbs sampling algorithm (Ching *et al.*, 2006); the transitional MCMC algorithm (Ching and Chen, 2007); and the Hamiltonian Markov Chain algorithm (Cheung and Beck, 2009). All these Bayesian methods present as main advantage that they provide the overall probabilistic distribution of the considered physical parameters rather than a point estimation of their expected value. Nevertheless, they present the drawback of the high simulation time required to perform the finite-element-model updating when tackling complex civil engineering structures (Jiménez-Alonso *et al.*, 2019). In particular for the case when the number of unknown physical parameters to be updated is large (Astroza *et al.*, 2019; Bartilson *et al.*, 2019; Vakilzadeh *et al.*, 2014), or when it is not possible to implement a parallelizable Bayesian computational approach (Astroza *et al.*, 2019; Cheung and Beck, 2009; Papadimitriou *et al.*, 2018).

On the other hand, the maximum likelihood method focuses on estimating the expected value of the considered physical parameters via the maximization of the likelihood between the numerical and experimental modal properties of the structure. Under the assumption of a normal distribution of the errors, this method is equivalent to the ordinary least squares estimator. Thus, the maximum likelihood method allows formulating the finite-element-model updating problem as an optimization problem (Wang et al., 2011). Hence, the objective function is defined in terms of the sum of the squares of the relative differences between the numerical and experimental modal properties of the structure. A limitation of this method is that, in contrast to Bayesian inference, only the expected values of the physical parameters can be obtained. Although this fact makes Bayesian inference a more robust estimator for updating problems, the high simulation time required to perform the updating process of complex civil engineering structure has motivated a more intensive use of the maximum likelihood method for practical engineering applications. Although computational times

involved in Bayesian updating may significantly be reduced by parallelization, the ease of implementation of the maximum likelihood method for such practical applications has prompted us to tackle the updating problem using these later algorithms.

In order to solve the resulting optimization problem, either local or global optimization algorithms can be employed (Nocedal and Wright, 1999). As the relationship between the considered physical parameters and the modal properties of the structure is clearly nonlinear, multiple optimums are normally expected in the objective function of this problem. Provided that local optimization algorithms may have difficulties to find the global optimum under such scenario, global optimization algorithms are usually employed to solve the updating problem. To this end, computational intelligence algorithms, like genetic algorithms (GA) and artificial neural networks (ANN) have been widely used for practical engineering applications (Marwala, 2010). Both algorithms have shown their efficiency when solving nonlinear optimization problems (Koh and Perry, 2009; Levin and Lieven, 1998a). For instance, GA have been successfully employed to assess the structural behaviour of existing bridge structures (Jiménez-Alonso and Sáez, 2016) or to detect damage in civil engineering structures (Hao and Xia, 2002). ANN have as well been implemented to conduct the finite-element-model updating of a wide variety of structural systems (Lu and Tu, 2004; Hasançebi and Dumlupınar, 2013; Guo et al., 2017). Many other success stories are scattered in the scientific literature for finite element updating.

The main limitation of these computational algorithms is the high simulation time required to perform the finite-element-model updating when the complexity of the structure increases. Two trends have been considered to overcome this drawback (if we keep parallelization aside in this review): (i) the implementation and validation of more recent global optimization algorithms and (ii) the hybridization between local and global optimization algorithms.

As representative examples of the first trend, Levin and Lieven (1998b) performed a comparison between the performance of the GA and the simulated annealing (SA) to solve the finite-element-model updating problem of a flat plate wing; Perera et al. (2010) compared the results obtained between GA and the particle swarm optimization (PSO) for the finite-element-model updating of a one-story reinforced concrete frame.

On the other hand, two outstanding examples of the second trend can be remarked: (i) the work reported by Shabbir and Omenzetter (2015), who proposed a hybrid sequential niche-PSO algorithm to perform the finite-element-model updating of a footbridge, and (ii) the study provided by Astroza et al. (2016), who implemented a hybrid unscented Kalman filter-SA algorithm to perform the finite-element-model updating of a steel frame structure.

In this paper, a novel computational algorithm devised to improve the efficiency of finite-element-model updating of civil engineering structures is proposed, implemented and further validated. The design of this new algorithm employs the maximum likelihood approach and stems from the two trends mentioned above.

On the one hand, as basis of this new algorithm, the Harmony Search (HS) global optimization algorithm is adopted. The harmony search algorithm is based on the improvisation process in which musicians seek harmony (Geem et al., 2001). This algorithm has been applied efficiently in multiple practical engineering applications (Yang and Koziel, 2011). However, according to the best of the authors' knowledge, it

has been rarely applied for the finite-element-model updating of civil engineering structures (Fadel et al., 2012; Kaveh et al., 2014).

On the other hand, the performance of the original HS algorithm is improved via its hybridization with a local optimization algorithm: the so-called Unscented Kalman Filter (UKF) is considered herein. This algorithm belongs to the Kalman filter family (Kalman, 1960) which originally focused on estimating the means and the covariance of the constitutive parameters of a linear system through a recursive process with two steps: (i) the prediction; and (ii) the correction steps. Subsequently, the original Kalman filter was adapted to nonlinear systems (Jazwinski, 1970) through the so-called Extended Kalman Filter (EKF). The basic idea of this algorithm is to linearize locally the nonlinear function, which represents the behaviour of the system, before applying the Kalman filter. Thus, one of the main drawbacks of this algorithm is that it only allows computing a first order approximation of the nonlinear function. In order to overcome this limitation, the Unscented Kalman Filter (UKF) was subsequently proposed by Julier and Uhlmann (1997). This algorithm defines a set of sampling points which allow estimating the mean and covariance of the constitutive parameters after their propagation through the nonlinear system. The direct estimation of these statistical properties allows computing a second order approximation (or even a third order approximation in case of a Gaussian random vector is propagated) of the nonlinear function (Van Der Merwe, 2004; Nguyen and Nestorović, 2015).

The resulting hybrid UKF-HS algorithm is then formulated to tackle two types of optimization problems: (i) single-objective and (ii) multi-objective approaches. The implementation details are next thoroughly presented and discussed. The performance of the new algorithm is validated and further compared with the results of other two global computational intelligence algorithms (GA and HS). To this end, the finite element model updating of a benchmark reconfigurable steel footbridge (Hudson and Reynolds, 2017) located at the laboratory of the Vibration Engineering Section of the University of Exeter (U.K.) is considered. The experimental modal properties of the structure were obtained via the signal processing of the records obtained during a forced vibration test (Maia and Silva, 1997).

The paper is organized as follows. First, some basics about finite-element-model updating under the maximum likelihood method are presented. Subsequently, the three considered computational intelligence algorithms (GA, HS, UKF-HS) are described in detail, with special emphasis on the newly proposed UKF-HS algorithm. Subsequently, the performance of the three mentioned algorithms is compared when they are implemented for the finite-element-model updating of a laboratory footbridge. Finally, some concluding remarks are drawn to close the paper in the fifth section.

2. Basics of Finite-element-model Updating under the Maximum Likelihood Method

As indicated above, the finite-element-model updating problem may be considered as a parameter identification problem in which the values of the most relevant physical parameters of the structure are to be estimated through the minimization of the differences between the numerical and experimental modal properties of the structure (Mottershead *et al.*, 2011). Different estimators are normally used to solve this parameter identification problem. Among them, the maximum likelihood method has been widely used to perform the finite-element-model updating of civil engineering structures (Marwala, 2010) and it will be the approach considered

herein.

In this manner, the finite-element-model updating problem is transformed into an optimization problem, where the updated model follows from iterative modifications of the most relevant physical parameters, until an optimal solution is obtained. The objective function of such optimization problem may be defined in terms of the square relative differences (residuals) between the numerical and the experimental modal properties of the structure (natural frequencies and vibration modes). As design parameters of this problem, the most relevant physical parameters of the model are considered. Provided that the relationship between the residuals and the design parameters is nonlinear, global optimization algorithms are needed to perform the optimization process (Nocedal and Wright, 1999). Additionally, a search domain is usually established to guarantee that the solution obtained retains its physical meaning. Two approaches can be considered to define the objective function: (i) the single-objective approach; and (ii) the multi-objective approach.

Under the single-objective approach, the optimization problem consists in minimizing a single-objective function defined in terms of the weighted residuals between the numerical and experimental modal properties of the structure. These weights take into account the relative contribution of each residual. The value of these weights can be established either by a statistical criterion (Friswell and Mottershead, 1995) or by a correlation criterion (Teughels *et al.*, 2002). According to the first criterion, the weights are determined in terms of the uncertainty associated with the estimates of the experimental modal properties of the structure. According to the second criterion, the weights are defined by an iterative process (trial and error) which ensures the best agreement between the numerical and experimental modal properties of the structure. The second criterion will be considered herein.

Under the multi-objective approach, the optimization problem consists in minimizing a multi-objective function defined by several functional components. The overall objective function is normally defined by two functional components for practical engineering applications (Jin *et al.*, 2014). One component may be defined in terms of the residuals associated with the natural frequencies, $r_{f,j}(\boldsymbol{\theta})$, whilst the other component may be defined in terms of the residuals associated with the vibration modes, $r_{m,j}(\boldsymbol{\theta})$ (j being the considered vibration mode). In this case, no weights are needed to define the objective function. However, a set of possible solutions (the so-called Pareto front) is obtained as result of the optimization process. Hence, a subsequent decision making problem must be addressed in order to select the best solution among the different elements of the Pareto front. Among the different criteria provided in literature (Infantes *et al.*, 2019), the normal boundary intersection (NBI) method has been considered herein (Deb and Gupta, 2011).

Residuals $r_{f,j}(\boldsymbol{\theta})$ and $r_{m,j}(\boldsymbol{\theta})$ can be defined as follows:

$$r_{f,j}(\boldsymbol{\theta}) = \frac{f_{\mathrm{num},j}(\boldsymbol{\theta}) - f_{exp,j}}{f_{\mathrm{exp},j}} \qquad j = 1, 2, 3, \ldots n_f \qquad (1)$$

$$r_{m,j}(\boldsymbol{\theta})^2 = \frac{\left(1 - \sqrt{MAC_j(\boldsymbol{\theta})}\right)^2}{MAC_j(\boldsymbol{\theta})} \qquad j = 1, 2, 3, \ldots n_f \qquad (2)$$

where $\boldsymbol{\theta}$ is a vector containing the most relevant physical parameters of the model; n_f is the total number of vibration modes considered to conduct the updating; $f_{num,j}$

and $f_{exp,j}$ [Hz] are the numerical and experimental natural frequencies (j being the number of the considered vibration mode), respectively; and MAC_j denotes the Modal Assurance Criterion (Allemang and Brown, 1982) which assesses the correlation between the numerical and experimental vibration modes. The MAC_j ratio can be expressed as follows:

$$MAC_j(\boldsymbol{\theta}) = \frac{\left(\phi_{\text{num},j}(\boldsymbol{\theta}) \cdot \phi_{\text{exp},j}\right)^2}{\left(\phi_{\text{num},j}^T(\boldsymbol{\theta}) \cdot \phi_{\text{num},j}(\boldsymbol{\theta})\right) \cdot \left(\phi_{\text{exp},j}^T \cdot \phi_{\text{exp},j}\right)} \qquad (3)$$

with $\phi_{num,j}$ and $\phi_{exp,j}$ being the numerical and experimental vibration modes, respectively.

On the one hand, the formulation of the finite-element-model updating problem using the single-objective approach can be formulated as follows:

$$\min f(\boldsymbol{\theta}) = \frac{1}{2}\left[\sum_j^{n_f} w_{f,j} \cdot r_{f,j}(\boldsymbol{\theta})^2\right]^{1/2} + \frac{1}{2}\left[\sum_j^{n_f} w_{m,j} \cdot r_{m,j}(\boldsymbol{\theta})^2\right]^{1/2}$$

$$\text{subject to} \left\{ \boldsymbol{\theta_l} \leq \boldsymbol{\theta} \leq \boldsymbol{\theta_u}; \sum_j^{n_f} w_{f,j} + w_{m,j} = 1 \right\} \qquad (4)$$

w_f and w_m being the weights associated with the residuals of the natural frequencies and vibrations modes; and $\boldsymbol{\theta_l}$ and $\boldsymbol{\theta_u}$ being the lower and upper bounds of the search domain of the considered physical parameters, respectively.

On the other hand, the formulation of the finite-element-model updating problem using the multi-objective approach can be formulated as follows:

$$\min f(\boldsymbol{\theta}) = \min(f_1(\boldsymbol{\theta}) \quad f_2(\boldsymbol{\theta})) \text{ where } \begin{cases} f_1(\boldsymbol{\theta}) = \frac{1}{2}\left[\sum_j^{n_f} r_{f,j}(\boldsymbol{\theta})^2\right]^{1/2} \\ f_2(\boldsymbol{\theta}) = \frac{1}{2}\left[\sum_j^{n_f} r_{m,j}(\boldsymbol{\theta})^2\right]^{1/2} \end{cases} \qquad (5)$$

$$\text{subject to: } \boldsymbol{\theta_l} \leq \boldsymbol{\theta} \leq \boldsymbol{\theta_u}$$

In summary, a typical finite-element-model updating consists of the following steps (Marwala, 2010): (i) the experimental modal properties of the structure are identified via the signal processing (either experimental or operational modal analysis may be employed to this end) of the records obtained during a vibration test (either forced vibration test or ambient vibration test); (ii) the numerical modal properties of the structure are obtained via a modal analysis based on a finite-element model; (iii) the most relevant physical parameters of the model are modified iteratively (using a global optimization algorithm); (iv) the objective function is evaluated; and (v) this iterative process is repeated until some convergence criterion is met. As result of this process, either a vector of updated parameters (single-objective approach) or a Pareto front (multi-objective approach) is obtained. In the latter case, a subsequent decision making problem must be addressed in order to select the vector of updated parameters.

3. Computational Intelligence Algorithms for the Finite-element model Updating of Civil Engineering Structures.

The finite-element-model updating problem using the maximum likelihood method is usually tackled in practical engineering applications by employing computational intelligence algorithms (Marwala, 2010). These algorithms present as main advantage that the solution obtained is a global optimum of the objective function. However, they have the drawback of the high simulation time required to perform the updating process, especially when the complexity of the model increases. In order to overcome this limitation, several strategies have been adopted, as summarized in the introduction: from parallelizing the algorithms to the development of alternative global optimizers or the devising of hybrid local-global algorithms. In this paper, a novel hybrid Unscented Kalman Filter-Harmony Search (UKF-HS) algorithm is proposed and validated. This hybrid algorithm takes advantage of both the acceleration scheme provided by the unscented Kalman filter algorithm and the global search characteristics of the harmony search algorithm.

The performance of this hybrid algorithm is assessed by comparing the results of the finite-element-model updating of a laboratory footbridge conducted using three different computational intelligence algorithms: (i) the classic genetic algorithms (GA); (ii) the harmony search algorithm (HS); and (iii) the novel hybrid UKF-HS algorithm. Further comparison of the performance of the new algorithm with the quite numerous optimizers available in the literature is out of the scope of this paper. However, it is relevant to point out here that previous studies (Marwala, 2010) reveal that Particle Swarm Optimizers (PSO) outperform other algorithms like Nelder-Mead (NM) or Simulated Annealing (SA). More recent studies (Jiménez-Alonso *et al.*, 2017) show that the HS optimizer outperforms both GA and PSO when addressing the finite element model updating of civil structures. For this reason, our proposal selects HS as global optimizer and hybridizes it with the local UKF algorithm, in order to speed up the updating process.

In order to make this paper as self-contained as possible, the three mentioned computational algorithms considering both single-objective and multi-objective approaches are next described. First, a general overview of GA is included. Next, the HS algorithm is summarized. Subsequently, the theoretical formulation of the UKF algorithm is presented. Finally, the newly proposed hybrid UKF-HS algorithm is described in detail.
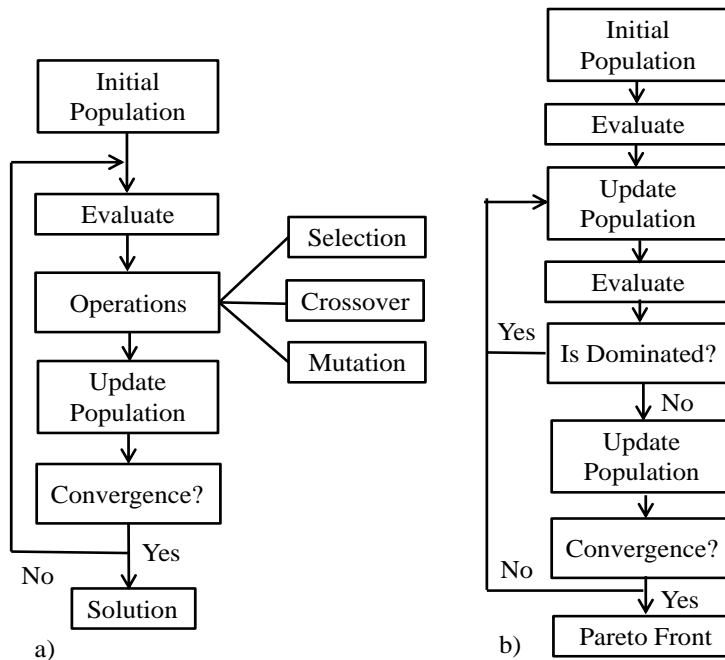
3.1. Genetic Algorithms (GA)

Genetic algorithms (GA) are nature-inspired computational algorithms based on the natural selection theory. Thus, the assessment of each chromosome (physical parameter vector) is based on the value of the objective function for each candidate.

The GA, under the single-objective approach, can be summarized in the following steps (Koh and Perry, 2009): (i) an initial population of parameter vectors is randomly created; (ii) the objective function is evaluated for all the candidates; (iii) an iterative process is developed where parameter vectors are selected in order to create a new population; (iv) a new population is created using both mechanisms, the crossover, which allows obtaining a new vector from to previous ones, and the mutation, which consists in modifying the value of one component of the parameter vector to explore new areas of the search domain; (v) the objective function is evaluated for the new population at each iteration and the candidates with higher fitness are selected; (iv) the

steps (iii) to (v) are repeated iteratively until a convergence criterion is met. The flowchart of the GA is shown in Figure 1a.

On the other hand, the genetic algorithms, under the multi-objective approach (MGA), are addressed by the non-dominated sorting genetic algorithms (the so-called NSGA-II algorithm) proposed by Deb *et al.* (2002). According to this algorithm, the non-dominated solutions are classified using the non-dominated sorting method. In this manner, a new population is generated considering only the non-dominated solutions. Both mechanisms are controlled by an operator denominated crowded comparison operator. This operator is based on two attributes of each solution: (i) the rank; and (ii) the crowding distance. As result, a set of solutions, which constitutes the Pareto front, is obtained. The flowchart of the MGA algorithm is shown in Figure 1b.

Figure 1. Flowchart of the genetic algorithms: a) GA and b) MGA.

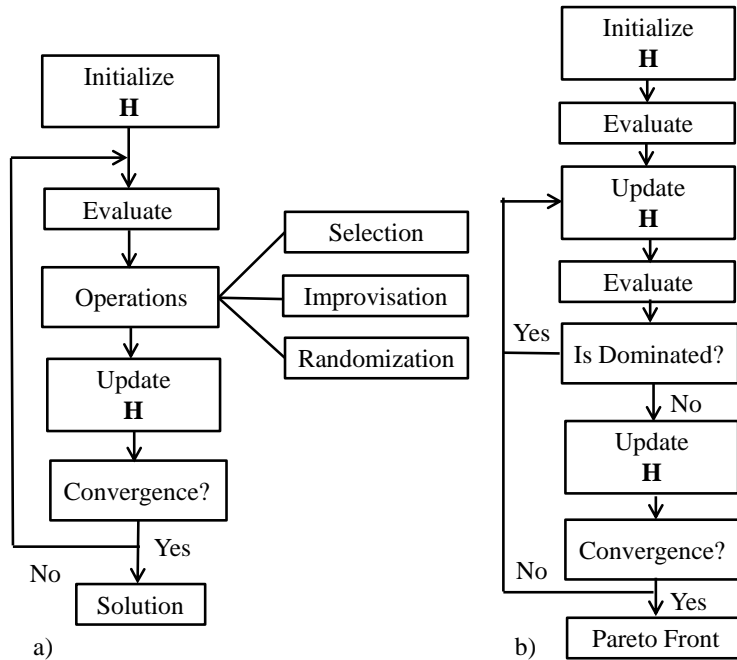### 3.2. Harmony Search Algorithm (HS)

The HS algorithm was proposed by Geem *et al*. (2001). The algorithm is inspired in the musical improvisation where harmony is searched according to aesthetic requirements. As the GA, the HS finds the global minimum of the objective function by modifying iteratively the value of the considered physical parameters of the model. Although this algorithm has been implemented successfully for several practical engineering applications (Manjarres *et al.*, 2013); however it has not been yet implemented for the finite-element-model updating of civil engineering structures according to the best of the authors' knowledge.

The HS algorithm, under the single-objective approach, can be summarized in the following steps: (i) the harmony matrix, **H**, is created (which contains the initial candidate solutions, parameter vector, created randomly); (ii) the objective function is evaluated for each solution; (iii) a new harmony is generated using three different mechanisms (memory consideration, pitch adjustments and randomization); (iv) the

objective function is evaluated for each new harmony, (v) the harmony matrix, **H**, is updated with the best generated harmonies; and (vi) the steps (iii) to (v) are repeated until a convergence criterion is met.

When a new harmony is generated, each element of a new candidate vector can be defined in terms of either a previous value stored in the harmony matrix, **H**, or adopting a new random value. This fact is controlled by the harmony memory consideration rate, $HMCR$. This ratio establishes the probability of selecting a previous component of the harmony matrix, **H**. Additionally, when some elements adopts the value of a previous one, it can be mutated according to the pitch adjustment rate, PAR. This ratio establishes the probability of mutating an element of the candidate vector. The adjustment is based on an additional parameter, the so-called bandwidth, bw, which is added or subtracted to mutate the considered candidate vector. The flowchart of the HS algorithm is shown in Figure 2a.

The HS algorithm, under the multi-objective approach (MHS), is an extension of the above mentioned algorithm which allows minimizing multi-objective functions. At each iteration, a set of new possible candidate solutions is created according to both the $HMCR$ and PAR ratios. The classification of the non-dominated solutions is performed using both the non-dominated sorting method (Deb *et al.*, 2002) and the crowding distance. In order to restore the initial size of the harmony matrix, **H**, the worst solutions in terms of crowding distance are deleted. These steps are repeated iteratively until a convergence criterion is met. As result of this process, a set of possible solutions is obtained, the so-called Pareto front. The flowchart of the MHS algorithm is shown in Figure 2b.

Figure 2. Flowchart of the harmony search algorithm: a) HS and b) MHS.

3.3. Unscented Kalman Filter (UKF)

A local minimization algorithm has been combined with the HS algorithm to reduce the simulation time needed to perform the updating process. The unscented Kalman filter (UKF) has been selected for this purpose (Julier and Uhlmann, 1997). This algorithm is a derivative free estimator, which involves that neither Jacobians nor Hessians must be computed, widely used for the state-estimation of nonlinear dynamic systems. Among the different transformations, the scaled unscented transformation proposed by Wan and Van Der Merwe (2000) has been adopted herein to define the UKF algorithm.

The formulation for a parameter identification problem may be represented as follows (Wan *et al.*, 2000):

$$\boldsymbol{\theta}_k = \boldsymbol{\theta}_{k-1} + \mathbf{w}_{k-1} \tag{6}$$

$$\mathbf{z}_k = h(\boldsymbol{\theta}_k) + \mathbf{v}_k \tag{7}$$

where $\boldsymbol{\theta}$ is the parameter vector; h is the nonlinear modelling function, $\mathbf{z}$ extracts the outputs of the dynamic system; $\mathbf{w}$ is the statistical noise of the identification process; and $\mathbf{v}$ is the statistical noise of observation process. Both type of noise are assumed to be uncorrelated and white Gaussian noise with zero-mean and covariance matrices $\mathbf{Q}$ and $\mathbf{R}$ respectively. It is necessary to remark that the matrix $\mathbf{R}$ may be computed by means of two terms (Tarantola, 2005): (i) the measurement noise; and (ii) the modelling noise. As the same models have been employed during the simulation and estimation phases, the effects of modelling noise has not been considered herein (Astroza *et al.*, 2016).

The UKF is a straightforward extension of the unscented transformation (Julier and Uhlmann, 2004). The estimation is addressed by considering $2n_d + 1$ (being n_d the number of parameters) deterministic sampling points (sigma points) which can be used to evaluate the true mean and the covariance. The propagation of these sigma points through the nonlinear function h leads to compute the true posterior mean and covariance of the estimated parameters up to the second order of the Taylor series expansion of the nonlinear function (third order of the Taylor series expansion for a Gaussian inputs). The determination of the sigma points is based on the square-root decomposition of the posterior covariance matrix, $\mathbf{P}$. For this reason, the matrix $\mathbf{P}$ must be positive semidefinite at each step. Even though the square-root decomposition can be efficiently derived using the Cholesky factorization ($\mathbf{A} = \sqrt{\mathbf{P}} = \mathrm{chol}(\mathbf{P})$ being $\mathbf{P} = \mathbf{A}\mathbf{A}^{\mathrm{T}}$), the matrix $\mathbf{P}$ is still updated at each iteration and numerical errors can give a non-positive semidefinite matrix $\mathbf{P}$. The square-root UKF algorithm, proposed by Van Der Merwe and Wan (2001), overcomes this issue since it avoids factorising at each step. This algorithm propagates directly the matrix $\mathbf{A}$ and guarantees that the covariance matrix is positive semi-definite.

The square-root UKF algorithm has two steps: (i) the prediction step; and (ii) the correction (update) step.

The prediction step is carried out considering the prior model to evaluate the sigma points and predict the estimates of the estimation error covariance, $\mathbf{A}^\theta$, and calculate the model outputs, $\mathbf{z}_{k|k-1}$. The $2n_d + 1$ sigma points are computed as:

$$(\boldsymbol{\chi}_{k-1})_0 = \widehat{\boldsymbol{\theta}}_{k-1|k-1} \tag{8}$$

$$(\boldsymbol{\chi}_{k-1})_i = \widehat{\boldsymbol{\theta}}_{k-1|k-1} + \sqrt{(n_d + \lambda)}\left(\mathbf{A}^\theta_{k-1|k-1}\right)_i \quad i = 1, 2, \dots, n_d \tag{9}$$

$$(\boldsymbol{\chi}_{k-1})_{i+n} = \widehat{\boldsymbol{\theta}}_{k-1|k-1} - \sqrt{(n_d + \lambda)}\left(\mathbf{A}^{\theta}_{k-1|k-1}\right)_i \quad i = 1, 2, \dots, n_d \quad (10)$$

where $\widehat{\boldsymbol{\theta}}_{k-1|k-1}$ are the posterior parameters estimated at the previous step and λ is a scaling parameter. The sigma points are weighted under the assumption that the sum of all the weights must be equal to the unit. The weights are defined as:

$$W_0 = \frac{\lambda}{n_d + \lambda} \quad (11)$$

$$W_i = W_{i+n} = \frac{1}{2(n_d + \lambda)} \quad i = 1, 2, \dots, n_d \quad (12)$$

For parameter identification problems, the estimation error covariance can be calculated by applying an exponential weighting on past data, $\mathbf{A}^{\theta}_k = \gamma^{-1/2}\mathbf{A}^{\theta}_{k-1}$, being γ a scalar factor slightly less than the unit (Van Der Merwe and Wan, 2001).

The correction (update) step consists in estimating the posterior mean and estimation error covariance in terms of the Kalman's gain matrix, $\mathbf{K}$; the measurements, $\mathbf{z}^{obs}$; and the model outputs.

The Kalman's gain matrix is derived from the model outputs error covariance, $\mathbf{S}^z$, and the cross covariance between the estimation error and the model outputs error covariances, $\mathbf{P}^{\theta z}$. In order to calculate the model outputs error covariance, $\mathbf{S}^z$, the following expression (considering that $W_i > 0$ for all $i \geq 1$) can be used (Terejanu, 2011):

$$\mathbf{S}^z_k = \sum_0^{2n_d} W_i \left[\left(\mathbf{z}^{i}_{k|k-1} - \widehat{\mathbf{z}}_{k|k-1}\right) \cdot \left(\mathbf{z}^{i}_{k|k-1} - \widehat{\mathbf{z}}_{k|k-1}\right)^T\right] + \mathbf{R} =$$
$$\left[\sqrt{W_i}\left(\mathbf{z}^{i}_{k|k-1} - \widehat{\mathbf{z}}_{k|k-1}\right), \ \sqrt{\mathbf{R}}\right] \cdot \left[\sqrt{W_i}\left(\mathbf{z}^{i}_{k|k-1} - \widehat{\mathbf{z}}_{k|k-1}\right)^T, \ \sqrt{\mathbf{R}}^T\right]^T +$$
$$W_0 \left[\left(\mathbf{z}^{0}_{k|k-1} - \widehat{\mathbf{z}}_{k|k-1}\right) \cdot \left(\mathbf{z}^{0}_{k|k-1} - \widehat{\mathbf{z}}_{k|k-1}\right)^T\right] \qquad for \ i = 1:2n_d \quad (13)$$

The first term can be expressed by means of a qr factorization[1] as the product of an orthogonal matrix $\mathbf{G}_k \in \mathbb{R}^{2n_d + r \times r}$ and an upper triangular matrix $\mathbf{S}^z_k \in \mathbb{R}^{r \times r}$, being r the number of measurements. The last term, can be taken into account performing a rank 1 update to Cholesky factorization[2]. Therefore, the matrix $\boldsymbol{S}^z_k$ can be calculated as (Terejanu, 2011):

$$\mathbf{S}^z_k = qr\left(\left[\sqrt{W_{1:2n_d}} \cdot \left[\left(\mathbf{z}_{k|k-1}\right)_{1:2n_d} - \widehat{\mathbf{z}}_{k|k-1}\right], \ \sqrt{\mathbf{R}}\right]\right) \quad (14)$$

$$\mathbf{S}^z_k = cholupdate\left(\mathbf{S}^z_k, \ \left(\mathbf{z}_{k|k-1}\right)_0 - \widehat{\mathbf{z}}_{k|k-1}, \ \text{sgn}(W_0)W_0\right) \quad (15)$$

Once the posterior mean of the parameter estimates, $\widehat{\boldsymbol{\theta}}_{k|k}$ and the posterior estimation error covariance, $\mathbf{A}^{\theta}_{k|k}$, are obtained, the algorithm follows a iterative process until the maximum number of iterations is reached.

The considered algorithm may be formulated as follows.

---

[1] The qr factorization of a matrix $\mathbf{M}$ allows expressing the matrix as $\mathbf{M} = \mathbf{QR}$. Here, $\mathbf{M}$ is an m-by-n matrix, $\mathbf{R}$ is an m-by-n upper triangular matrix and $\mathbf{Q}$ is an m-by-m unitary matrix.

[2] If $\mathbf{R} = chol(\mathbf{A})$, the Cholesky factor of the rank 1 update $\mathbf{A} + \mathbf{v}\mathbf{v}^T$ is written as $\mathbf{S} = cholupdate(\mathbf{R}, \mathbf{v})$.

Initial Step:

$$\widehat{\boldsymbol{\theta}}_0 = \boldsymbol{\theta}_{prior} \tag{16}$$

$$\mathbf{A}_0^\theta = chol(\mathbf{P}_0^\theta) \tag{17}$$

Main loop: $for\ k = 1{:}N_{UKF}$ (number of iterations of the UKF)

Prediction step:

$$\text{Calculate the } 2n_d + 1 \text{ Sigma Points: } (\boldsymbol{\chi}_{k-1})_i \tag{18}$$

$$\left(\boldsymbol{\chi}_{k|k-1}\right)_i = (\boldsymbol{\chi}_{k-1})_i \tag{19}$$

$$\boldsymbol{\theta}_{k|k-1} = \sum_0^{2n_d} W_i \cdot \left(\boldsymbol{\chi}_{k|k-1}\right)_i \tag{20}$$

$$\mathbf{A}_{k|k-1}^\theta = \gamma^{-\frac{1}{2}} \mathbf{A}_{k-1}^\theta \tag{21}$$

$$\left(\boldsymbol{z}_{k|k-1}\right)_i = \boldsymbol{h}\left(\left(\boldsymbol{\chi}_{k|k-1}\right)_i\right) \tag{22}$$

$$\widehat{\boldsymbol{z}}_{k|k-1} = \sum_0^{2n_d} W_i \cdot \left(\boldsymbol{z}_{k|k-1}\right)_i \tag{23}$$

Correction (update) step:

$$\mathbf{S}_{k|k-1}^z = qr\left(\left[\sqrt{W_{1:2n_d}} \cdot \left[\left(\boldsymbol{z}_{k|k-1}\right)_{1:2n_d} - \widehat{\boldsymbol{z}}_{k|k-1}\right] \quad \sqrt{\mathbf{R}}\right]\right) \tag{24}$$

$$\mathbf{S}_{k|k-1}^z = cholupdate\left(\mathbf{S}_{k|k-1}^z, \left(\boldsymbol{z}_{k|k-1}\right)_0 - \widehat{\boldsymbol{z}}_{k|k-1}, sgn(W_0)\right) \tag{25}$$

$$\mathbf{P}_{k|k-1}^{\theta z} = \sum_0^{2n_d} \left(W_i \left[\left(\boldsymbol{\chi}_{k|k-1}\right)_i - \widehat{\boldsymbol{\theta}}_{k|k-1}\right] \cdot \left[\left(\boldsymbol{z}_{k|k-1}\right)_i - \widehat{\boldsymbol{z}}_{k|k-1}\right]^T\right) \tag{26}$$

$$\mathbf{K}_k = \left(\mathbf{P}_{k|k-1}^{\theta z}/\mathbf{S}_{k|k-1}^z{}^T\right)/\mathbf{S}_{k|k-1}^z \tag{27}$$

$$\widehat{\boldsymbol{\theta}}_{k|k} = \widehat{\boldsymbol{\theta}}_{k|k-1} + \mathbf{K}_k(\boldsymbol{z}^{obs} - \widehat{\boldsymbol{z}}_{k|k-1}) \tag{28}$$

$$\mathbf{U} = \mathbf{K}_k \mathbf{S}_{k|k-1}^z \tag{29}$$

$$\mathbf{A}_{k|k}^\theta = cholupdate\left(\mathbf{A}_{k|k-1}^\theta, \mathbf{U}, -1\right) \tag{30}$$

end

3.4. Hybrid UKF-HS algorithm

The local minimization procedure followed by the square root UKF is implemented in both the HS and the MHS algorithms to reduce the simulation time required to solve the finite-element-model updating problem. The proposed hybrid algorithm is a local-global optimization algorithm which combines the main virtues of the two component algorithms. In this sense, it should be emphasized that this proposed algorithm is derivative free; not being required the computation of the Jacobian. Besides it guarantees the positive semi-definiteness of the covariance matrix as the intrinsic properties of the square root UKF algorithm are preserved.

The general layout of this new hybrid algorithm follows the general scheme of the above mentioned HS algorithm. Thus, the different steps that configure both the single-objective approach (UKF-HS) and the multi-objective approach (UKF-MHS algorithm) have been included herein. First, the new hybrid UKF-HS algorithm consists of the following steps: (i) the HS algorithm creates the initial candidate solution (parameter vector); (ii) the square-root UKF algorithm computes the mean of the

parameters vector, $\boldsymbol{\theta}_{k|k}$; (iii) the matrix **H** is updated; (iv) the steps (ii) to (ii) are repeated until some convergence criterion is met; and (v) finally, the solution is obtained.. Thus, the flowchart of the proposed hybrid UFK-HS algorithm is shown in Figure 3a.

Similarly, the new hybrid UKF-MHS algorithm consists of the following steps; (i) the MHS algorithm creates the initial candidate solutions (parameter vectors); (ii) the square-root UKF algorithm gives the mean of the parameter vector, $\boldsymbol{\theta}_{k|k}$; (iii) the objective function is evaluated for each vector $\boldsymbol{\theta}_{k|k}$; (iv) the non-dominating sorting method classifies the solutions in order to delete the dominated solutions; (v) the initial size of the matrix **H** is preserved at each iteration by means of the crowding distance; (vi) the steps (ii) to (v) are repeated until some convergence criterion is met; and (vii) finally, the Pareto front is obtained. Finally, the flowchart of the proposed hybrid UFK-MHS algorithm is shown in Figure 3b.
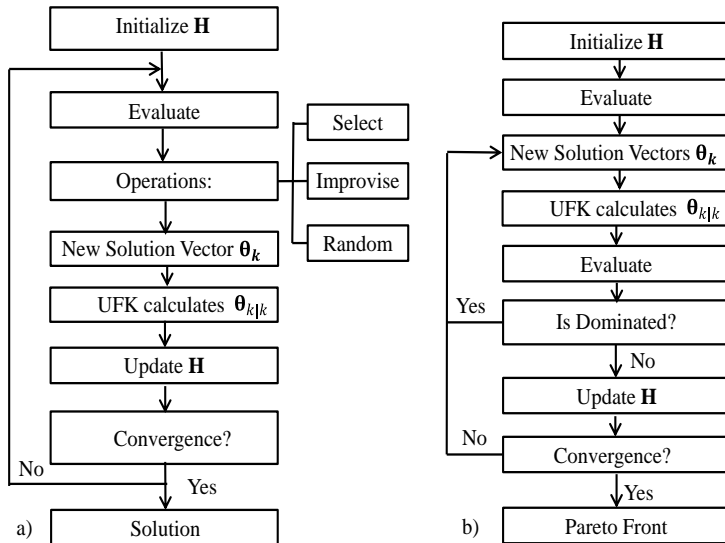
Figure 3. Flowchart of the new proposed hybrid algorithm: a) UKF-HS and b) UKF-MHS.

4. Application Example: Finite-element-model Updating of a Laboratory Footbridge.

In order to analyse the performance this new hybrid algorithm, when it is employed for the finite-element-model updating of civil engineering structures, a real case-study was studied. The finite-element-model updating of a real structure was performed for this purpose. As benchmark, a reconfigurable steel footbridge located at the laboratory of the Vibration Engineering Section of the University of Exeter (U.K.) was considered herein (Hudson and Reynolds, 2017). The updating problem was solved considering two approaches (single-objective and multi-objective) and three different computational algorithms (the conventional GA, HS and the new hybrid UKF-HS). Subsequently, the results obtained after the updating process are compared in order to assess the performance of each considered algorithm. Both the updating and comparison process are presented in detail in this section.

4.1. Description of the Structure and Preliminary Finite-element-model

The laboratory footbridge is a steel frame structure which consists of: (i) two lateral steel beams of 15 m of length; (ii) rectangular plates of 200x12 mm separated longitudinally 1.25 m; (iii) composite SPS panel (SPS, 2019) connected (bolts) to the lateral and transversal elements and (iv) four steel columns. The two lateral beams, separated transversally 2.5 m, are connected to steel columns which are pinned to the ground. An overall view of the structure is illustrated in Figure 4. A more detailed description of this structure can be found in literature (Hudson and Reynolds, 2017).

Figure 4. The reconfigurable steel footbridge located at the laboratory of the Vibration Engineering Section of the University of Exeter.

A preliminary finite-element-model of the structure was built in the software package Ansys (Ansys, 2019). A laptop computer with a 3.6 GHz processor and a RAM memory of 8 GB was used for all the numerical simulations. Three different types of elements were considered for this purpose. The two lateral steel beams, the transversal steel beams and the SPS panel where modelled using 3D shell elements (SHELL181). This element has four nodes and six degrees of freedom per node. For the SPS panel, the sandwich behaviour is considered via the first-order shear-deformation theory. The bolts that connect the SPS panel and the steel structure are modelled with 3D beam elements (BEAM188). These beam elements are characterised by two nodes and six degrees of freedom per node. Finally, each support was modelled by an equivalent spring element (COMBIN14) in the longitudinal and lateral direction. An equivalent stiffness of $5.5 \cdot 10^7$ N/m was considered for the longitudinal springs and an equivalent stiffness of $1.0 \cdot 10^7$ N/m. was taken into account for the lateral springs. Additionally, the vertical displacement of each support was constrained. The mechanical properties of the constitutive materials considered in this study were: (i) for the steel (Eurocode 3, 2005), the density, $\gamma_s = 7850$ kg/m³, the Young's modulus, $E_s = 2.1 \cdot 10^{11}$ N/m² and the Poisson's ratio, $\nu_s = 0.3$; and (ii) for the polyurethane (Clarke, 1996), the density, $\gamma_p = 1100$ kg/m³, the Young's modulus, $E_p = 7.5 \cdot 10^8$ N/m², and the Poisson's ratio, $\nu_p = 0.5$. The finite-element-model of the laboratory footbridge is shown in Figure 5.
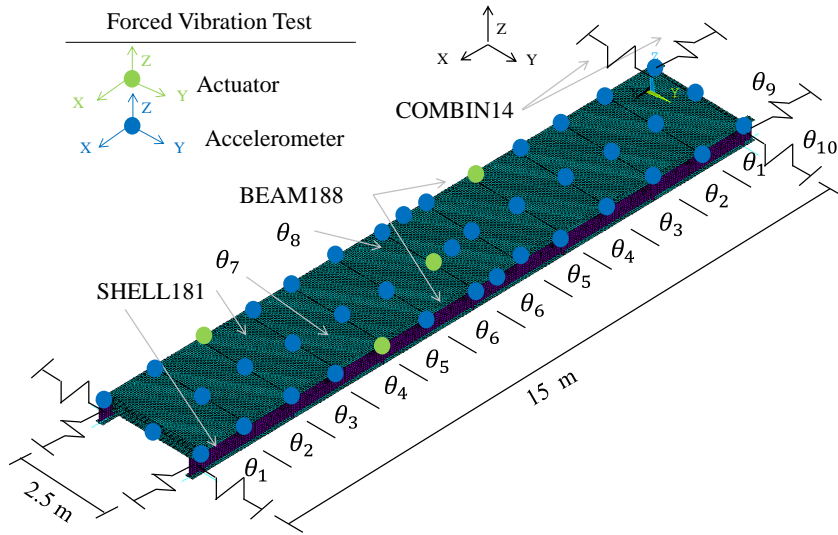
Figure 5. Finite-element-model, forced vibration test arrangement and considered physical parameters of the laboratory footbridge (Hudson and Reynolds, 2017).

A numerical modal analysis was performed to obtain the numerical natural frequencies and vibration modes. As result of this analysis, Table 1 shows the first seven numerical natural frequencies, $f_{num,j}$ (being j the considered vibration mode), of the laboratory footbridge. Additionally, Figure 6 illustrates the first seven numerical vibration modes, $\phi_{num,j}$, of this structure.

4.2. Forced Vibration Test and Experimental Modal Analysis
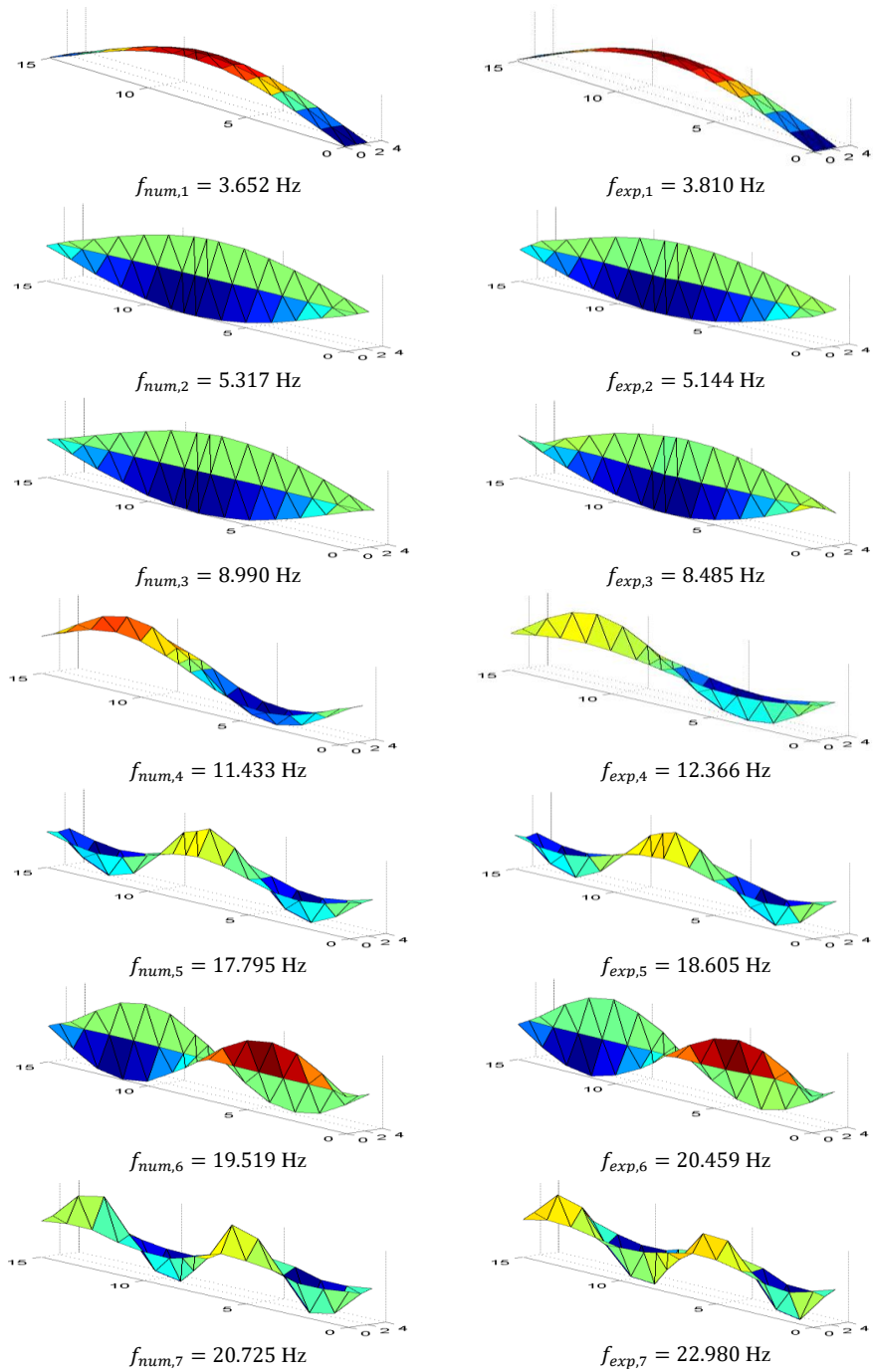
In order to identify experimentally the modal properties of the footbridge, a forced vibration test was conducted. For this purpose, a set of proof-mass actuators and rowing accelerometers were employed (Figure 5). A Multiple Input-Multiple-Output (MIMO) configuration (Maia and Silva, 1997) was considered to simultaneously drive the actuators with uncorrelated random signals. The Frequency Response Functions (FRFs) for the instrumented points are derived with a 50% overlap. Subsequently, a complex mode indicator function was used to identify probable mode locations in the FRFs fitted curves. Finally, a global polynomial curve fitting method identifies the experimental natural frequencies and their vibration modes from the previous probable locations (Maia and Silva, 1997). A more detailed description of the forced vibration test and the experimental modal analysis may be found in literature (Hudson and Reynolds, 2017).

As result of this experimental modal analysis, the first seven experimental natural frequencies, $f_{exp,j}$ (being j the considered vibration mode), are shown in Table 1. The first seven experimental vibration modes, $\phi_{exp,j}$, are also illustrates in Figure 6. Additionally, the agreement between the numerical and experimental modal properties of the footbridge has been checked. Thus, Table 1 shows the relative difference, $\Delta f_{exp,j}^{num,j}$, and the $MAC_{exp,j}^{num,j}$ ratio for each considered vibration mode j.

Table 1. Numerical, $f_{num,j}$, and experimental, $f_{exp,j}$, natural frequency, relative difference, $\Delta f_{exp,j}^{num,j}$, and the $MAC_{exp,j}^{num.j}$ ratio of the considered vibration mode j.

Mode (j)	$f_{num,j}$ [Hz]	$f_{exp,j}$ [Hz]	$\Delta f_{exp,j}^{num,j}$ [%]	$MAC_{exp,j}^{num.j}$ [-]
1	3.652	3.810	-4.147	0.998
2	5.317	5.144	3.363	0.994
3	8.990	8.485	5.952	0.988
4	11.433	12.366	-7.545	0.877
5	17.795	18.605	-4.354	0.986
6	19.519	20.459	-4.595	0.993
7	20.725	22.980	-9.813	0.634

As Table 1 shows there are some vibration modes in which the relative differences, $\Delta f_{exp,j}^{num,j}$, are greater than 5% and the $MAC_{exp,j}^{num.j}$ ratios are lower than 0.90 (Živanović *et al.*, 2007). Thus, this preliminary finite-element-model can be improved to better reflect the real behaviour of this laboratory footbridge. A finite-element-model updating was performed for this purpose. The updating process was implemented considering two approaches (single-objective and multi-objective) and the three mentioned computational intelligence algorithms (GA, HS and hybrid UKF-HS). This updating process is described in detail in next sub-sections.

$f_{num,1} = 3.652$ Hz　　　　　　　　$f_{exp,1} = 3.810$ Hz

$f_{num,2} = 5.317$ Hz　　　　　　　　$f_{exp,2} = 5.144$ Hz

$f_{num,3} = 8.990$ Hz　　　　　　　　$f_{exp,3} = 8.485$ Hz

$f_{num,4} = 11.433$ Hz　　　　　　　　$f_{exp,4} = 12.366$ Hz

$f_{num,5} = 17.795$ Hz　　　　　　　　$f_{exp,5} = 18.605$ Hz

$f_{num,6} = 19.519$ Hz　　　　　　　　$f_{exp,6} = 20.459$ Hz

$f_{num,7} = 20.725$ Hz　　　　　　　　$f_{exp,7} = 22.980$ Hz

Figure 6. First seven numerical, $\phi_{num,j}$, and experimental, $\phi_{exp,j}$, vibration modes of the laboratory footbridge (being j the considered vibration mode).

4.3. Parameters and Search Domain of the Finite-element-model Updating Process.

As first step of this updating process, a sensitivity analysis was performed to select the most relevant physical parameters of the model. For this purpose, an initial set of fifteen physical parameters, $\boldsymbol{\theta_{in}}$, have been considered for this purpose. The initial set of physical parameters consists of: (i) the Young's modulus of the steel of the longitudinal beams in different sections, $\theta_{in,1} - \theta_{in,6}$ [N/m^2]; (ii) the Young's modulus of the steel of the SPS panel, $\theta_{in,7}$ [N/m^2]; (iii) the Young's modulus of the polyurethane of the SPS panel, $\theta_{in,8}$ [N/m^2]; (iv) the Young's modulus of the steel of the bolts, $\theta_{in,9}$ [N/m^2]; (v) the Young's modulus of the steel of the lateral beams, $\theta_{in,10}$ [N/m^2]; (vi) the equivalent longitudinal stiffness of each support, $\theta_{in,11}$ [N/m]; (vii) the equivalent lateral stiffness of each support, $\theta_{in,12}$ [N/m]; (viii) the equivalent vertical stiffness of each support, $\theta_{in,13}$ [N/m]; (ix) the equivalent rotational stiffness (x-axis) of each support, $\theta_{in,14}$ [N/rad]; and (x) the equivalent rotational stiffness (y-axis) of each support, $\theta_{in,15}$ [N/rad]. The selection of this initial set of parameters assumed a symmetric behaviour of the structure.

Subsequently, as the modal strain energy associated with each physical parameter is an indicator of its influence on the variation of the natural frequencies (Fox and Kapoor, 1968), this energy has been considered as basis to establish a selection criterion. For this purpose, the ratio between the modal strain energy associated with each parameter and the overall modal strain energy of the structure has been computed. A sensitivity matrix, which represents the value of the modal strain energy ratio in terms of the considered physical parameter and vibration mode, was determined. Figure 7 shows a bar graph of this sensitivity matrix. The analysis of this sensitivity matrix allows determining the most relevant physical parameters of the model (those parameters that present a significant model strain energy ratio).
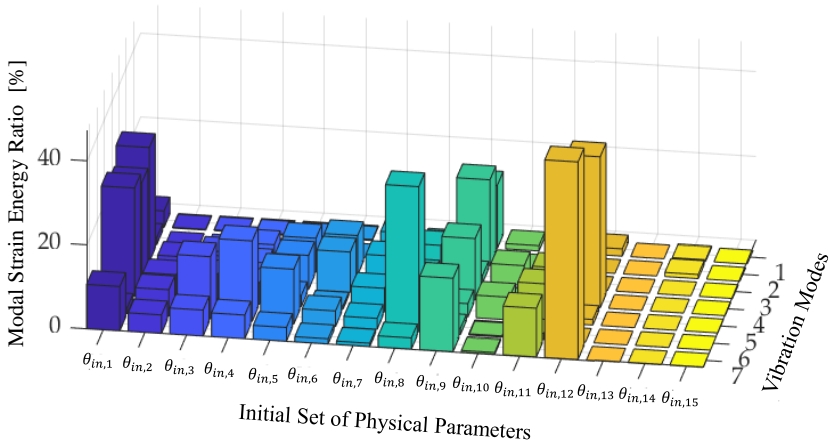
Figure 7. Sensitivity analysis in order to select the most relevant physical parameters of the model (being $\boldsymbol{\theta_{in}} = [\theta_{in,1}, \dots, \theta_{in,15}]$ the initial set of physical parameters).

As result of this analysis, the most relevant physical parameters of this model were (Figure 5) $\boldsymbol{\theta} = [\theta_1, \theta_2, \theta_3, \theta_4, \theta_5, \theta_6, \theta_7, \theta_8, \theta_9, \theta_{10}]$: (i) the Young's modulus of the steel of the longitudinal beams in different sections (Figure 5), $\theta_1 - \theta_6$ [N/m^2]; (ii) the Young's modulus of the polyurethane, θ_7 [N/m^2]; (iii) the Young's modulus of the steel of the bolts, θ_8 [N/m^2]; (iv) the equivalent longitudinal stiffness of each support, θ_9

[N/m]; and (v) the equivalent lateral stiffness of each support, θ_{10} [N/m]. Additionally a search domain was established to guarantee an adequate physical meaning of the updated value of the physical parameters. The lower, $\boldsymbol{\theta}_l$, and upper, $\boldsymbol{\theta}_u$, bounds of this search domain were defined as follows; $\boldsymbol{\theta}_l = [1.9 \cdot 10^{11}, 1.9 \cdot 10^{11}, 1.9 \cdot 10^{11}, 1.9 \cdot 10^{11}, 1.9 \cdot 10^{11}, 1.9 \cdot 10^{11}, 7.5 \cdot 10^8, 2.1 \cdot 10^{11}, 1.4 \cdot 10^7, 4.8 \cdot 10^6]$ and $\boldsymbol{\theta}_u = [2.3 \cdot 10^{11}, 2.3 \cdot 10^{11}, 2.3 \cdot 10^{11}, 2.3 \cdot 10^{11}, 2.3 \cdot 10^{11}, 2.3 \cdot 10^{11}, 1.5 \cdot 10^9, 2.1 \cdot 10^{12}, 1.1 \cdot 10^8, 3.8 \cdot 10^7]$.

Once both the physical parameters and their corresponding search domain have been established, the finite-element-model updating can be performed. Herein, this process has been carried out considering two approaches and the three mentioned computational intelligence algorithms.

4.4. Finite-element-model Updating under the Single-Objective Approach.

First, the finite-element-model updating of the footbridge was performed under the single-objective approach and the three mentioned computational algorithms (GA, HS and hybrid UKF-HS). The three considered algorithms were implemented in Matlab (Matlab, 2019). The main design variables considered for each computational algorithm were: (i) for the GA, a crossover ratio of 0.8 and a mutation ratio of 0.4; (ii) for the HS, a $HMCR$ ratio of 0.9, a PAR ratio of 0.3 and a bw equals to the 1% of the search domain of each parameter; and (iii) for the UKF-HS, the same value for the $HMCR$ ratio, the PAR ratio and the bw variable than the HS algorithm. These design parameters balance the ability of these computational algorithms to sweep the search domain and to reach accurately the global minimum of this search domain (Marwala, 2010; Jiménez-Alonso *et al.*, 2017). Additionally for the UKF-HS algorithm, the following parameters were assumed: (i) the $\mathbf{d}_{obs}$ vector is built from the experimental natural frequencies and a 7x1 vector filled with ones (since the residue of the vibration modes is defined from the $MAC_{exp,j}^{upd.j}$ ratio and the aim is to make the value of the $MAC_{exp,j}^{upd.j}$ as close as possible to the unit), (ii) a factor, $\lambda = 0.0001$, was considered to compute the sigma points (Astroza *et al.*, 2016); and (iii) a scalar factor, $\gamma = 0.99$, was considered to update the estimation error covariance matrix (Van Der Merwe and Wan, 2001).

For the definition of the single-objective function, the weights associated with the residuals must be defined. For this purpose, a sensitivity study, where the values of the weights were varied between 0 and 1 considering a step of 0.1 (eleven cases), was performed. In each case, a value was assigned to each weight and the value of the objective function at the end of the optimization process, f_f, was obtained. The combination of weights that achieves the lower value of the objective function, f_f, was selected. The HS algorithm was considered for this analysis. As result, the following weights were considered: (i) for the residuals associated with the natural frequencies, $\sum_j^7 w_{f,j} = 0.7$; and (ii) for the residuals associated with the vibration modes, $\sum_j^7 w_{m,j} = 0.3$.

Next, a sensitivity study was performed to analyse the influence of three hyper-parameters on the performance of the hybrid UKF-HS algorithm. For this purpose the following hyper-parameters were considered: (i) the number of iterations of the UKF algorithm, N_{UKF}; (ii) the initial estimation error covariance, $\boldsymbol{P}_0^{\theta}$; and (iii) the measurement noise covariance matrix, $\mathbf{R}_{ii}$.

Seven simulations were run for this purpose. For these simulations, the number of iterations, $Iter = 2$, and the population size, $Pop = 5$, have been maintained

constant; and the three considered hyper-parameters have been modified according to the following values: (i) three different values for the parameter, N_{UKF}, (1, 3 and 5); (ii) three different values for the parameter, $\boldsymbol{P}_0^{\theta}$, ($diag\left(\left(\frac{(\boldsymbol{\theta}_u-\boldsymbol{\theta}_l)}{500}\right)^2\right)$, $diag\left(\left(\frac{(\boldsymbol{\theta}_u-\boldsymbol{\theta}_l)}{2000}\right)^2\right)$ and $diag\left(\left(\frac{(\boldsymbol{\theta}_u-\boldsymbol{\theta}_l)}{4000}\right)^2\right)$); and (iii) three different values for the parameter, $\mathbf{R}_{ii}$ (0.1, 0.001 and 0.0001).

As comparison criteria, the convergence speed and the accuracy of the adjustment (the value of the objective function, f_f) have been taken into account. It must be remarked that the converge speed has been considered through the analysis of two parameters: (i) the simulation time, $Time$; and (ii) the number of evaluations, $Eval$. This second parameter allows considering jointly the effect on the converge speed of three characteristic parameters: (i) the number of iterations of the global algorithm, $Iter$; (ii) the population size, Pop; and (iii) the number of iterations of the UKF algorithm, N_{UKF}.

Table 2 shows the results of this sensitivity study. For the first hyper-parameter, N_{UKF}, an optimum value of $N_{UKF} = 3$ is considered since, a reduced value, $N_{UKF} = 1$, reduces the accuracy of the adjustment ($f_f = 0.0037$); and an excessive value, $N_{UKF} = 5$, increases the simulation time ($Time = 9.44 \cdot 10^3$ s). For the second hyper-parameter, $\boldsymbol{P}_0^{\theta}$, an optimum value of $\boldsymbol{P}_0^{\theta} = diag\left(\left(\frac{(\boldsymbol{\theta}_u-\boldsymbol{\theta}_l)}{2000}\right)^2\right)$ is established, since this value improves the accuracy of the adjustment ($f_f = 0.0033$) without compromising the simulation time ($Time = 5.71 \cdot 10^3$ s). Finally, for the third hyper-parameter, $\mathbf{R}_{ii}$, an optimum value of $\mathbf{R}_{ii} = 0.001$ is considered, since this value improves the accuracy of the adjustment ($f_f = 0.0033$) without compromising the simulation time ($Time = 5.71 \cdot 10^3$ s).

Table 2. Performance of the three considered algorithms to solve the updating problem under the single-objective approach (where $Iter$ is the number of iterations of the main algorithm; Pop is the population size; N_{UKF} is the number of iterations of the UKF algorithm; $\boldsymbol{P}_0^{\theta}$ is the initial estimation error covariance; $\mathbf{R}_{ii}$ is the measurement noise covariance matrix; $Eval$ is the number of evaluations of the objective function; $Time$ is the time [s] required until a convergence criterion is met; and f_f is the value of the objective function when the updating process has finished).

	$Iter$	Pop	N_{UKF}	$\boldsymbol{P}_0^{\theta}$	$\mathbf{R}_{ii}$	$Eval$	$Time$ [s]	f_f [-]
GA	50	20	---	---	---	1020	$9.79 \cdot 10^3$	0.0036
HS	500	20	---	---	---	520	$6.64 \cdot 10^3$	0.0033
UKF-HS	2	5	1	$diag\left(\left(\frac{(\boldsymbol{\theta}_u-\boldsymbol{\theta}_l)}{2000}\right)^2\right)$	0.001	147	$2.1 \cdot 10^3$	0.0037
	2	5	3	$diag\left(\left(\frac{(\boldsymbol{\theta}_u-\boldsymbol{\theta}_l)}{500}\right)^2\right)$	0.001	441	$5.68 \cdot 10^3$	0.0034
	2	5	3	$diag\left(\left(\frac{(\boldsymbol{\theta}_u-\boldsymbol{\theta}_l)}{2000}\right)^2\right)$	0.001	441	$5.71 \cdot 10^3$	0.0033
	2	5	3	$diag\left(\left(\frac{(\boldsymbol{\theta}_u-\boldsymbol{\theta}_l)}{4000}\right)^2\right)$	0.001	441	$5.69 \cdot 10^3$	0.0036

2	5	3	$diag\left(\left(\frac{(\boldsymbol{\theta}_u - \boldsymbol{\theta}_l)}{2000}\right)^2\right)$	0.1	441	$5.68 \cdot 10^3$	0.0060
2	5	3	$diag\left(\left(\frac{(\boldsymbol{\theta}_u - \boldsymbol{\theta}_l)}{2000}\right)^2\right)$	0.0001	441	$5.64 \cdot 10^3$	0.0040
2	5	5	$diag\left(\left(\frac{(\boldsymbol{\theta}_u - \boldsymbol{\theta}_l)}{2000}\right)^2\right)$	0.001	735	$9.44 \cdot 10^3$	0.0033

Subsequently, the performance of the updating process under the single-objective approach for the three considered computational algorithms was analysed. As hyper-parameters of the UKF-HS algorithm, the results of the above sensitivity analysis were taken into account. Table 2 also shows the results of this performance study. As Table 2 shows the hybrid UKF-HS algorithm is clearly the most efficient algorithm, since it presents the same accuracy than the HS algorithm ($f_f = 0.0033$) but a lower simulation time ($Time = 6.64 \cdot 10^3$s for the HS against $Time = 5.71 \cdot 10^3$ s for the hybrid UKF-HS) and number of iterations ($Eval = 520$ for the HS against $Eval = 441$ for the hybrid UKF-HS). Additionally, it is necessary to remark that the HS algorithm is more efficient (both convergence speed and accuracy) than the conventional GA for this optimization problem.

Additionally, Table 3 shows the updated value of the physical parameters of the model after the updating process considering the single-objective approach and the three considered computational algorithm. As Table 3 shows the correlation among the physical parameters obtained by the different algorithms is good.

Table 3. Updated value of the physical parameters of model, $\boldsymbol{\theta}$, after the updating process considering the single-objective approach and the three mentioned computational algorithms.

$\boldsymbol{\theta}$	GA	HS	UKF-HS
θ_1	$2.29 \cdot 10^{11}$	$2.28 \cdot 10^{11}$	$2.29 \cdot 10^{11}$
θ_2	$1.96 \cdot 10^{11}$	$1.96 \cdot 10^{11}$	$2.00 \cdot 10^{11}$
θ_3	$2.20 \cdot 10^{11}$	$2.15 \cdot 10^{11}$	$2.27 \cdot 10^{11}$
θ_4	$2.04 \cdot 10^{11}$	$1.91 \cdot 10^{11}$	$1.97 \cdot 10^{11}$
θ_5	$2.08 \cdot 10^{11}$	$2.00 \cdot 10^{11}$	$2.11 \cdot 10^{11}$
θ_6	$2.28 \cdot 10^{11}$	$2.19 \cdot 10^{11}$	$2.29 \cdot 10^{11}$
θ_7	$1.04 \cdot 10^9$	$1.28 \cdot 10^9$	$1.29 \cdot 10^9$
θ_8	$1.16 \cdot 10^{12}$	$1.53 \cdot 10^{12}$	$1.50 \cdot 10^{12}$
θ_9	$7.67 \cdot 10^7$	$7.50 \cdot 10^7$	$7.50 \cdot 10^7$
θ_{10}	$7.66 \cdot 10^6$	$7.72 \cdot 10^6$	$7.73 \cdot 10^6$

Finally, Table 4 shows the updated natural frequencies, $f_{upd,j}$, the relative differences, $\Delta f_{exp,j}^{upd,j}$, and the $MAC_{exp,j}^{upd.j}$ ratio for each considered vibration mode j after the updating process considering the single-objective approach and the three mentioned computational algorithms. As Table 4 shows the correlation between the experimental and numerical modal properties after the updating process is adequate for the three mentioned computational algorithms (all the relative differences, $\Delta f_{exp,j}^{upd,j}$, are lower than 5%, and all the $MAC_{exp,j}^{upd.j}$ ratios are greater than 0.9).

Table 4. Updated, $f_{upd,j}$, and experimental, $f_{exp,j}$, natural frequency, relative difference, $\Delta f_{exp,j}^{upd,j}$, and the $MAC_{exp,j}^{upd.j}$ ratio for each considered vibration mode j after

the updating process considering the single-objective approach and the three mentioned computational algorithms.

Mode (j)	$f_{exp,j}$ [Hz]	GA			HS			UKF-HS		
		$f_{upd,j}$ [Hz]	$\Delta f_{exp,j}^{upd.j}$ [%]	$MAC_{exp,j}^{upd.j}$ [-]	$f_{upd,j}$ [Hz]	$\Delta f_{exp,j}^{upd.j}$ [%]	$MAC_{exp,j}^{upd.j}$ [-]	$f_{upd,j}$ [Hz]	$\Delta f_{exp,j}^{upd.j}$ [%]	$MAC_{exp,j}^{upd.j}$ [-]
1	3.810	3.880	1.837	0.998	3.880	1.837	0.998	3.890	2.1	0.998
2	5.144	5.380	4.588	0.993	5.372	4.432	0.993	5.375	4.491	0.993
3	8.485	8.370	-1.355	0.988	8.400	-1.002	0.988	8.410	-0.884	0.988
4	12.366	11.930	-3.526	0.907	11.950	-3.364	0.905	12.002	-2.944	0.903
5	18.605	18.460	-0.779	0.986	18.630	0.134	0.987	18.670	0.349	0.987
6	20.459	20,160	-1.461	0.993	20.150	-1.51	0.992	20.250	-1.022	0.992
7	22.980	22,150	-3.612	0.947	22.420	-2.437	0.950	22.450	-2.306	0.950

In this manner, it has been validated that the hybrid UKF-HS algorithm is the most efficient algorithm among the three considered computational ones to perform the finite-element-model updating of civil engineering structure under the single-objective approach. Additionally, it has been checked that the performance of this hybrid algorithm depends on the adequate value of the three considered hyper-parameters (N_{UKF}, $\boldsymbol{P}_0^{\theta}$ and $\mathbf{R}_{ii}$).

4.5. Finite-element-model Updating under the Multi-Objective Approach.

Subsequently, the finite-element-model updating of the footbridge was performed under the multi-objective approach and the three mentioned computational algorithms (MGA, MHS and hybrid UKF-MHS). The main design variables considered for each computational algorithm were (Marwala, 2010; Jiménez-Alonso *et al.*, 2017): (i) for the MGA, a crossover ratio of 0.7, and a mutation ration of 0.4; (ii) for the MHS, a $HMCR$ ratio of 0.9, a PAR ratio of 0.7 and a bw equals to the 1% of the search domain of each parameters; and (iii) for the UKF-MHS, the same design variables than the HS algorithm (described above). The decision making problem, the selection of the best solution among the different element of the Pareto front, has been solved using the NBI method (Deb and Gupta, 2011).

As in the single-objective approach, first a sensitivity study was performed to analyse the influence of three hyper-parameters on the performance of the hybrid UKF-HS algorithm. For this purpose the following hyper-parameters were considered: (i) the number of iterations of the UKF algorithm, N_{UKF}; (ii) the initial estimation error covariance, $\boldsymbol{P}_0^{\theta}$; and (iii) the measurement noise covariance matrix, $\mathbf{R}_{ii}$. For the possible values of these hyper-parameters, the same values considered in the sensitivity analysis of the single-objective approach, were taken into account.

As comparison criteria, the convergence speed and the accuracy of the adjustment have been taken into account again. On the one hand, the converge speed has been assessed again via: (i) the simulation time, $Time$; and (ii) the number of evaluations, $Eval$. On the other hand, the accuracy of the adjustment has been assessed in this case via: (i) the distance between the selected point (best solution of the Pareto front) and the

origin, $Dist$; and (ii) the sum of the two terms of the objective function, Sum.

Eight simulations were run for this purpose. On the one hand, for the analysis of the N_{UKF} hyper-parameter, the number of iterations, $Iter = 3$, the population size, $Pop = 8$, and the new population size, $New\ Pop = 3$, have been fixed. On the other hand, for the analysis of both $\boldsymbol{P}_0^\theta$ and $\mathbf{R}_{ii}$ hyper-parameters, the number of iterations, $Iter = 3$, the population size, $Pop = 10$, and the new population size, $New\ Pop = 3$, have also been fixed. The results of this sensitivity study are also shown in Table 3.

In relation to the N_{UKF} hyper-parameter two relationships can be obtained: (i) a direct relationship between this hyper-parameter and the accuracy of the adjustment; and (ii) an indirect relationship between this hyper-parameter and the convergence speed. In relation to the $\boldsymbol{P}_0^\theta$ hyper-parameter, a direct relationship has been obtained. Thus, a reduction of the initial estimation error covariance involves an increase of the accuracy of the adjustment without compromising the simulation time. Nevertheless, the influence of this hyper-parameter is low (as Table 5 illustrates) and an intermediate value can be considered without affecting both the goodness of the adjustment and the simulation time. In relation to the $\mathbf{R}_{ii}$ hyper-parameter, it has been checked that the intermediate value, $\mathbf{R}_{ii} = 0.001$, improves the accuracy of the adjustment without compromising the simulation time.

Finally, the following values of the hyper-parameters were recommended: (i) $N_{UKF} = 3$; (ii) $\boldsymbol{P}_0^\theta = diag\left(\left(\frac{(\theta_u - \theta_l)}{2000}\right)^2\right)$; and (iii) $\mathbf{R}_{ii} = 0.001$. These values were considered for the subsequent performance analysis.

Table 5. Performance of the three considered algorithms to solve the updating problem under the multi-objective approach (where $Iter$ is the number of iterations of the main algorithm; Pop is the population size; $New\ Pop$ is the new population size; N_{UKF} is the number of iterations of the UKF algorithm; $\boldsymbol{P}_0^\theta$ is the initial estimation error covariance; $\mathbf{R}_{ii}$ is the measurement noise covariance matrix; $Eval$ is the number of evaluations of the objective function; $Time$ is the time [s] required until a convergence criterion is met; $Dist$ is the distance between the selected point and the origin; and Sum is the sum of the two terms of the objective function).

	Iter.	Pop.	New Pop.	N_{UKF}	$\boldsymbol{P}_0^\theta$	$\mathbf{R}_{ii}$	Eval	Time [s] $x10^5$	Dist $x10^4$	Sum $x10^4$
	25	50	---	---	---	---	1450	0.18	50.7	68.6
MGA	45	50	---	---	---	---	2570	0.33	50.2	66.9
	150	100	---	---	---	---	16600	2.12	52.0	68.0
	50	50	25	---	---	---	1300	0.17	45.4	62.1
MHS	100	100	25	---	--	---	2600	0.33	45.1	61.8
	300	200	50	---	---	---	15200	1.98	43.7	60.6
	3	10	3	3	$diag\left(\left(\frac{(\theta_u - \theta_l)}{2000}\right)^2\right)$	0.001	1197	0.16	45.2	62.1
	3	10	3	3	$diag\left(\left(\frac{(\theta_u - \theta_l)}{500}\right)^2\right)$	0.001	1197	0.15	46.0	63.5
UKF-MHS	3	10	3	3	$diag\left(\left(\frac{(\theta_u - \theta_l)}{4000}\right)^2\right)$	0.001	1197	0.15	44.6	61.4
	3	10	3	3	$diag\left(\left(\frac{(\theta_u - \theta_l)}{2000}\right)^2\right)$	0.1	1197	0.15	52.6	71.3
	3	10	3	3	$diag\left(\left(\frac{(\theta_u - \theta_l)}{2000}\right)^2\right)$	0.0001	1197	0.15	145.0	177.6

8	15	3	3	$diag\left(\left(\frac{(\boldsymbol{\theta}_u - \boldsymbol{\theta}_l)}{2000}\right)^2\right)$	0.001	2457	0.32	44.3	61.1
20	40	10	3	$diag\left(\left(\frac{(\boldsymbol{\theta}_u - \boldsymbol{\theta}_l)}{2000}\right)^2\right)$	0.001	15120	1.96	43.7	60.4
3	8	3	1	$diag\left(\left(\frac{(\boldsymbol{\theta}_u - \boldsymbol{\theta}_l)}{2000}\right)^2\right)$	0.001	357	0.05	50.6	68.2
3	8	3	3	$diag\left(\left(\frac{(\boldsymbol{\theta}_u - \boldsymbol{\theta}_l)}{2000}\right)^2\right)$	0.001	1071	0.14	49.1	66.5
3	8	3	5	$diag\left(\left(\frac{(\boldsymbol{\theta}_u - \boldsymbol{\theta}_l)}{2000}\right)^2\right)$	0.001	1785	0.23	45.2	62.0

Subsequently, the performance of the updating process under the multi-objective approach for the three considered computational algorithms was analysed. Three simulations have been performed for each computational algorithm in which several design parameters of the algorithms have been modified. The modified design variables are: (i) the number of iterations of the main algorithm, $Iter$; (ii) the population size, Pop; and (iii) the new population size, $New\ Pop$.

Table 5 shows the results of this performance analysis. According to these results, the hybrid UKF-MHS algorithm is again the most efficient algorithm, since it presents the same accuracy than the MHS algorithm ($Dist = 43.7 \cdot 10^4$ and $Sum < 60.6 \cdot 10^{-4}$) but a lower simulation time ($Time = 1.96 \cdot 10^5$ s) and number of iterations ($Eval = 151200$). Additionally, it must be noted that the MHS algorithm is again more efficient (both convergence speed and accuracy) than the conventional MGA for this optimization problem.

Additionally, Table 6 shows the updated value of the physical parameters of the model after the updating process considering the multi-objective approach and the three considered computational algorithm. The cases with a higher number of evaluations have been shown and compared (MGA, $Eval = 16600$; MHS, $Eval = 15200$; and UKF-MHS, $Eval = 15120$). Table 6 shows the correlation among the physical parameters obtained by the different algorithms is good.

Table 6. Updated value of the physical parameters of model, $\boldsymbol{\theta}$, after the updating process considering the multi-objective approach and the three mentioned computational algorithms.

$\boldsymbol{\theta}$	MGA	MHS	UKF-MHS
θ_1	$2.29 \cdot 10^{11}$	$2.27 \cdot 10^{11}$	$2.28 \cdot 10^{11}$
θ_2	$2.15 \cdot 10^{11}$	$2.29 \cdot 10^{11}$	$2.26 \cdot 10^{11}$
θ_3	$2.06 \cdot 10^{11}$	$2.22 \cdot 10^{11}$	$2.26 \cdot 10^{11}$
θ_4	$2.14 \cdot 10^{11}$	$2.22 \cdot 10^{11}$	$2.28 \cdot 10^{11}$
θ_5	$2.10 \cdot 10^{11}$	$1.92 \cdot 10^{11}$	$2.15 \cdot 10^{11}$
θ_6	$2.02 \cdot 10^{11}$	$2.26 \cdot 10^{11}$	$2.17 \cdot 10^{11}$
θ_7	$8.60 \cdot 10^{8}$	$1.30 \cdot 10^{9}$	$1.17 \cdot 10^{9}$
θ_8	$7.48 \cdot 10^{11}$	$1.57 \cdot 10^{12}$	$1.31 \cdot 10^{12}$
θ_9	$6.43 \cdot 10^{7}$	$7.50 \cdot 10^{7}$	$7.50 \cdot 10^{7}$
θ_{10}	$7.70 \cdot 10^{6}$	$7.61 \cdot 10^{6}$	$7.65 \cdot 10^{6}$

Finally, Table 7 shows the updated natural frequencies, $f_{upd,j}$, the relative differences, $\Delta f_{exp,j}^{upd,j}$, and the $MAC_{exp,j}^{upd,j}$ ratio for each considered vibration mode j after the updating process considering the multi-objective approach and the three mentioned computational algorithms. As Table 7 shows the correlation between the experimental
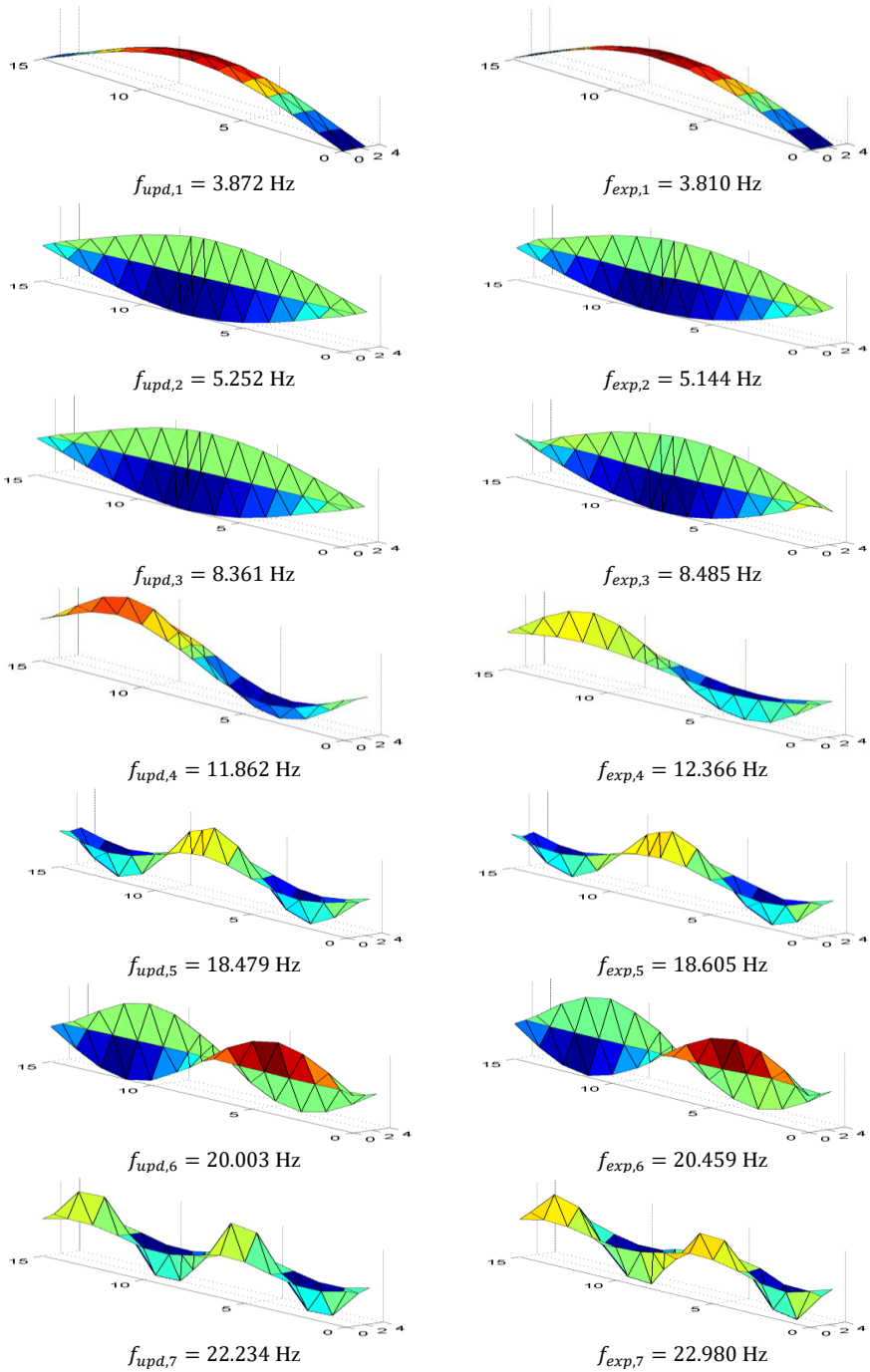
and numerical modal properties after the updating process is adequate for the three mentioned computational algorithms (all the relative differences, $\Delta f_{exp,j}^{upd,j}$, are lower than 5%, and all the $MAC_{exp,j}^{upd.j}$ ratios are greater than 0.9).

Table 7. Updated, $f_{upd,j}$, and experimental, $f_{exp,j}$, natural frequency, relative difference, $\Delta f_{exp,j}^{upd,j}$, and the $MAC_{exp,j}^{upd.j}$ ratio for each considered vibration mode j after the updating process considering the multi-objective approach and the three mentioned computational algorithms.

Mode (j)	$f_{exp,j}$ [Hz]	MGA			MHS			UKF-MHS		
		$f_{upd,j}$ [Hz]	$\Delta f_{exp,j}^{upd,j}$ [%]	$MAC_{exp,j}^{upd.j}$ [-]	$f_{upd,j}$ [Hz]	$\Delta f_{exp,j}^{upd,j}$ [%]	$MAC_{exp,j}^{upd.j}$ [-]	$f_{upd,j}$ [Hz]	$\Delta f_{exp,j}^{upd,j}$ [%]	$MAC_{exp,j}^{upd.j}$ [-]
1	3.810	3.900	2.362	0.998	3.871	1.601	0.998	3.872	1.627	0.999
2	5.144	5.283	2.702	0.994	5.270	2.449	0.994	5.252	2.100	0.994
3	8.485	8.373	-1.320	0.988	8.360	-1.473	0.988	8.361	-1.461	0.989
4	12.366	12.040	-2.636	0.902	11.933	-3.502	0.902	11.862	-4.076	0.901
5	18.605	18.360	-1.317	0.985	18.630	0.134	0.987	18.479	-0.677	0.987
6	20.459	20.471	0.059	0.993	20.100	-1.755	0.993	20.003	-2.229	0.993
7	22.980	21.880	-4.787	0.951	22.420	-2.437	0.951	22.234	-3.246	0.948

Finally, for the sake of completeness, Figure 8 illustrates the first seven numerical vibration modes, $\phi_{upd,j}$, obtained after the model updating of the footbridge performed considering the multi-objective approach and the UKF-MHS algorithm. The first seven experimental vibration modes, $\phi_{exp,j}$, have also been shown in Figure 8 (being the j considered vibration mode).

Thus, it has been validated that the hybrid UKF-MHS algorithm is the most efficient algorithm among the three considered computational ones to perform the finite-element-model updating of civil engineering structure under the multi-objective approach. Additionally it has been checked that the performance of the proposed algorithm depends clearly on the considered value of the three mentioned hyper-parameters (N_{UKF}, $\boldsymbol{P}_0^{\theta}$ and $\mathbf{R}_{ii}$).

.

$f_{upd,1} = 3.872$ Hz $f_{exp,1} = 3.810$ Hz

$f_{upd,2} = 5.252$ Hz $f_{exp,2} = 5.144$ Hz

$f_{upd,3} = 8.361$ Hz $f_{exp,3} = 8.485$ Hz

$f_{upd,4} = 11.862$ Hz $f_{exp,4} = 12.366$ Hz

$f_{upd,5} = 18.479$ Hz $f_{exp,5} = 18.605$ Hz

$f_{upd,6} = 20.003$ Hz $f_{exp,6} = 20.459$ Hz

$f_{upd,7} = 22.234$ Hz $f_{exp,7} = 22.980$ Hz

Figure 8. First seven updated, $\phi_{upd,j}$, and experimental, $\phi_{exp,j}$, vibration modes of the laboratory footbridge (being j the considered vibration mode).

5. Conclusions

FE model updating of civil engineering structures is usually performed under the maximum likelihood method. According to this method, the FE model updating problem is transformed into an optimization problem. Due to the complexity and the non-linear behaviour of the resulting objective function, computational intelligence algorithms are usually employed to solve this optimization problem. Among these computational algorithms, nature-inspired computational algorithms are especially effective to tackle this problem. Nevertheless, the use of these algorithms has a clear drawback, the high simulation time required to perform the updating process. In order to overcome this limitation, a hybrid UFK-HS optimization algorithm has been proposed, implemented and validated herein.

The proposed algorithm consists in combining two individual algorithms: (i) a local optimization algorithm, the square root unscented Kalman filter; and (ii) a global optimization algorithm, the harmony search algorithm.

The FE model updating of a real structure, a laboratory footbridge located at the University of Exeter (U.K.), has been considered herein to validate the performance of the new hybrid algorithm. The experimental modal properties of the structure were obtained by the signal processing (experimental modal analysis) of the records obtained during a forced vibration test. For comparison purposes, the FE model updating has been performed under two approaches (single-objective and multi-objective approaches) and considering three different computational intelligence algorithms: (i) genetic algorithms; (ii) harmony search; and (iii) the proposed hybrid UKF-HS algorithm.

Two comparison criteria have been considered herein: (i) the convergence speed; and (ii) the accuracy of the adjustment. The proposed hybrid UKF-HS algorithm has been shown as the most efficient algorithms to perform the finite-element-model updating of the laboratory footbridge under the two approaches (single-objective and multi-objective). Additionally, a sensitivity study has been performed to analysis the performance of the hybrid algorithm under the variation of three hyper-parameters: (i) the number of iterations of the UKF algorithm, N_{UFK}; (ii) the initial estimation error covariance, P_0^θ; and (iii) the measurement noise covariance matrix, $\mathbf{R}_{ii}$. As result of this study, an adequate value of these hyper-parameters must be considered to optimize the performance of the proposed hybrid algorithm.

Therefore, the proposed hybrid UKF-HS algorithm is an available tool to perform the finite-element-model updating of civil engineering structures for practical engineering applications. Nevertheless, further studies are needed to validate the performance of the proposed hybrid algorithm for the finite-element-model updating of different types of civil engineering structures.

Acknowledgements

References

Allemang RJ, Brown DL (1982). A correlation coefficient for modal vector analysis. Proc. 1st Int. Modal Anal. Conf., vol. 1, Orlando: Union College Press, p. 110–116.

Ansys Mechanical 19.0. Ansys Inc 2019 n.d. http://www.ansys.com (accessed May 2019).

Astroza R, Barrientos N, Li Y, Saavedra Flores E (2019). Calibration of a large nonlinear finite element model of a highway bridge with many uncertain parameters. Proc. IMAC XXXVII, Orlando (USA).

Astroza R, Nguyen LT, Nestorović T (2016). Finite element model updating using simulated annealing hybridized with unscented Kalman filter. *Computer and Structures*, 177: 176–191. doi: https://doi.org/10.1016/j.compstruc.2016.09.001.

Bartilson DT, Jang J, Smyth AW (2019). Finite element model updating using objective-consistent sensitivity-based parameter clustering and Bayesian regularization. *Mechanical Systems and Signal Processing*, 114: 328–345. doi: https://doi.org/10.1016/j.ymssp.2018.05.024.

Beck JL, Au S-K (2002). Bayesian updating of structural models and reliability using Markov chain Monte Carlo simulation. *Journal of Engineering Mechanics*, 128: 380–391. doi: https://doi.org/10.1061/(ASCE)0733-9399(2002)128:4(380).

Beck JL, Au S-K, Vanik MW (2001). Monitoring structural health using a probabilistic measure. *Computer-Aided Civil and Infrastructure Engineering*, 16: 1–11. doi: http://dx.doi.org/10.1111/0885-9507.00209.

Beck JL, Katafygiotis LS (1998). Updating models and their uncertainties. I: Bayesian statistical framework. *Journal of Engineering Mechanics*, 124: 455–461. doi: http://dx.doi.org/10.1061/(ASCE)0733-9399(1998)124:4(455).

Cheung SH, Beck JL (2009). Bayesian model updating using hybrid Monte Carlo simulation with application to structural dynamic models with many uncertain parameters. *Journal of Engineering Mechanics*, 135: 243–255. doi: https://doi.org/10.1061/(ASCE)0733-9399(2009)135:4(243).

Ching J, Chen Y-C (2007). Transitional Markov chain Monte Carlo method for Bayesian model updating, model class selection, and model averaging. *Journal of Engineering Mechanics*, 133: 816–832. doi: https://doi.org/10.1061/(ASCE)0733-9399(2007)133:7(816).

Ching J, Muto M, Beck JL (2006). Structural model updating and health monitoring with incomplete modal data using Gibbs sampler. *Computer-Aided Civil Infrastructure Engineering*, 21: 242–257. doi: https://doi.org/10.1111/j.1467-8667.2006.00432.x.

Clarke, JL (1996). Structural Design of Polymer Composites – EUROCOMP Design Code and Handbook. E&FN Spon.

Deb K, Gupta S (2011). Understanding knee points in bicriteria problems and their implications as preferred solution principles. *Engineering Optimization* 43: 1175–1204. doi: https://doi.org/10.1080/0305215X.2010.548863.

Deb K, Pratap A, Agarwal S, Meyarivan T (2002). A fast and elitist multi-objective genetic algorithm: NSGA-II. *IEEE Transactions on Evolutionary Computation*, 6: 182–197. doi: https://doi.org/10.1109/4235.996017.

Eurocode 3 (2005): Design of steel structures. CEN.

Fadel L, Fadel L, Kaminski Jr J, Riera JD (2012). Damage detection under ambient vibration by harmony search algorithm. *Expert Systems with Applications*, 39(10): 9704-9714. doi: https://doi.org/10.1016/j.eswa.2012.02.147.

Fan W, Qiao P (2011). Vibration-based damage identification methods: a review and comparative study. *Structural Health Monitoring,* 10(1):83–111. doi: http://dx.doi.org/10.1177/1475921710365419.

Fox R, Kapoor M (1968). Rates of change of eigenvalues and eigenvectors. *AIAA Journal*, 6: 2426–2429. doi: https://doi.org/10.2514/3.5008.

Friswell M, Mottershead JE (1995). Finite element model updating in structural dynamics. vol. 38. Springer Science & Business Media.

Fritzen C-P, Jennewein D, Kiefer T (1998). Damage detection based on model updating methods. *Mechanical System and Signal Processing*, 12: 163–186. doi: http://dx.doi.org/10.1006/mssp.1997.0139.

Geem ZW, Kim JH, Loganathan GV (2001). A new heuristic optimization algorithm: harmony search. *Simulation*, 76:60–68. doi: https://doi.org/10.1177/003754970107600201.

Guo J, Zhao X, Guo J, Yuan X, Dong S, Xiong Z (2017). Model updating of suspended-dome using artificial neural networks. *Advances in Structural Engineering,* 20: 1727–1743. doi: https://doi.org/10.1177/1369433217693629.

Hao H, Xia Y (2002). Vibration-based damage detection of structures by genetic algorithm. *Journal of Computing in Civil Engineering*, 16: 222–229. doi: https://doi.org/10.1061/(ASCE)0887-3801(2002)16:3(222).

Hasançebi O, Dumlupınar T (2013). Linear and nonlinear model updating of reinforced concrete T-beam bridges using artificial neural networks. *Computer and Structures*, 119: 1–11. doi: https://doi.org/10.1016/j.compstruc.2012.12.017.

Hudson EJ, Reynolds P (2017). Design and Construction of a Reconfigurable Pedestrian Structure. *Experimental Techniques*. doi: http://dx.doi.org/10.1007/s40799-016-0144-3.

Infantes M, Naranjo-Pérez J, Jiménez-Alonso JF, Sáez A (2019). Determining the Best Pareto-solution in a Multi-Objective Approach for Model Updating, IABSE Symposium, Guimaraes 2019: Towards a Resilient Built Environment Risk and Asset Management – Report pp. 523-530

Jazwinski, AH (1970). Stochastic processes and filtering theory, Academic Press.

Jiménez-Alonso JF, Hudson EJ, Pavic A, Sáez A (2017) Maximum Likelihood Methods for Finite Element Model Updating of Civil Engineering Structures: A Comparative Study. In Proceedings of the 4th International Conference on Mechanical Models in Structural Engineering CMMoST 2017, Madrid (Spain)

Jiménez-Alonso JF, Hudson EJ, Pavic A, Sáez A (2019). Probabilistic Finite Element Model Updating of Civil Engineering Structures: A Comparative Study, IABSE Symposium, Guimaraes 2019: Towards a Resilient Built Environment Risk and Asset Management – Report pp. 1269-1276

Jiménez-Alonso JF, Sáez A (2016). Model Updating for the Selection of an Ancient Bridge Retrofitting Method in Almeria, Spain. *Structural Engineering International*, 26: 17–26. doi: https://doi.org/10.2749/101686615X14355644771333.

Jin S, Cho S, Jung H, Lee J and Yun C (2014) A new multi-objective approach to finite element model updating. *Journal of Sound and Vibration*. 333(11): 2323–2338. doi: https://doi.org/10.1016/j.jsv.2014.01.015.

Julier SJ, Uhlmann JK (1997). New extension of the Kalman filter to nonlinear systems. Proceedings of the SPIE 3068, Signal Processing, Sensor Fusion, and Target Recognition VI 182–194. doi: https://doi.org/10.1117/12.280797.

Julier SJ, Uhlmann JK (2004). Corrections to "Unscented filtering and nonlinear estimation". Proceedings of the IEEE 2004, 92: 1958. doi: https://doi.org/10.1109/JPROC.2004.837637.

Kalman RE (1960). A new approach to linear filtering and prediction problems. *Journal of Basic Engineering*, 82: 35–45. doi: https://doi.org/10.1115/1.3662552.

Kaveh A, Javadi SM, Maniat M (2014). Damage assessment via modal data with a mixed particle swarm strategy, ray optimizer, and harmony search. *Asian Journal of Civil Engineering*, 15(1): 95–106.

Koh CG, Perry MJ (2009). Structural Identification and Damage Detection using Genetic Algorithms: Structures and Infrastructures Book Series, Vol. 6. Crc Press.

Levin RI, Lieven NAJ (1998a). Dynamic finite element model updating using neural networks. *Journal of Sound and Vibration*, 210: 593–607. doi: https://doi.org/10.1006/jsvi.1997.1364.

Levin RI, Lieven NAJ (1998b). Dynamic finite element model updating using simulated annealing and genetic algorithms. *Mechanical System and Signal Processing*, 12: 91–120. doi: https://doi.org/10.1006/mssp.1996.0136.

Lu Y, Tu Z (2004). A two-level neural network approach for dynamic FE model updating including damping. *Journal of Sound and Vibration*, 275: 931–952. doi: https://doi.org/10.1016/S0022-460X(03)00796-X.

Maia NMM, e Silva JMM. Theoretical and experimental modal analysis. Research Studies Press; 1997.

Manjarres D, Landa-Torres I, Gil-Lopez S, Del Ser J, Bilbao MN, Salcedo-Sanz S, et al (2013). A survey on applications of the harmony search algorithm. *Engineering Applications of Artificial Intelligence*, 26: 1818–1831. doi; https://doi.org/10.1016/j.engappai.2013.05.008.

Marwala T. (2010). Finite-Element-Model Updating Using Computational Intelligence Techniques. Applications to Structural Dynamics, p. 231. Springer, London.

Marwala T, Boulkaibet I, Adhikari S (2016). Probabilistic finite element model updating using bayesian statistics: applications to aeronautical and mechanical engineering. John Wiley & Sons.

Matlab Inc. MATLAB R2019a n.d. http://www.mathworks.com (accessed May 2019)

Mottershead JE, Link M, Friswell MI (2011). The sensitivity method in finite element model updating: a tutorial. *Mechanical Systems and Signal Processing*, 25: 2275-2296. doi: https://doi.org/10.1016/j.ymssp.2010.10.012.

Nguyen LT, Nestorović T (2015). Nonlinear Kalman filters for model calibration of soil parameters for geomechanical modeling in mechanized tunneling. *Journal of Computing in Civil Engineering*, 30: 04015025. doi: https://doi.org/10.1061/(ASCE)CP.1943-5487.0000495.

Nocedal J, Wright SJ (1999) Numerical optimization. Springer Series in Operations Research.

Papadimitriou C, Argyris C, Panetsos, P (2018). Information-driven modeling of structures using Bayesian framework. In: Conte J, Astroza R, Benzoni G, Feltrin G, Loh K, Moaveni B. (eds) Experimental Vibration Analysis for Civil Structures. EVACES 2017. Lecture Notes in Civil Engineering, vol 5. Springer, Cham.

Perera R, Fang S-E, Ruiz A (2010). Application of particle swarm optimization and genetic algorithms to multi-objective damage identification inverse problems with modelling errors. *Meccanica*, 45: 723–734. doi: https://doi.org/10.1007/s11012-009-9264-5.

Robert CP, Casella G (1999). The Metropolis—Hastings Algorithm. In: Monte Carlo Statistical Methods. Texts in Statistics. Springer, New York, NY pp. 231–283. doi: https://doi.org/10.1007/978-1-4757-3071-5_6.

Shabbir F, Omenzetter P (2015). Particle swarm optimization with sequential niche technique for dynamic finite element model updating. *Computer-Aided Civil and Infrastructure Engineering*, 30: 359–375. doi: https://doi.org/10.1111/mice.12100.

SPS (2019). Sandwich Plate System heavy engineering composite from Intelligent Engineering n.d. http:/www.ie-sps.com/ (accessed May 2019).

Tarantola A (2005). Inverse problem theory and methods for model parameter estimation. vol. 89. SIAM; doi: https://doi.org/10.1137/1.9780898717921.

Terejanu GA (2011). Unscented Kalman filter tutorial. Univ Buffalo Buffalo.

Teughels A, Maeck J, De Roeck G (2002). Damage assessment by FE model updating using damage functions. *Computer and Structures*, 80: 1869–1879. doi: http://dx.doi.org/10.1016/50045-7949(02)00217-1.

Vakilzadeh MK, Yaghoubi V, Johansson AT, Abrahamsson T. (2014). Manifold Metropolis adjusted Langevin algorithm for high-dimensional Bayesian FE model updating in structural dynamics. Proceedings of the 9th International Conference on Structural Dynamics, EURODYN 2014, Porto (Portugal).

Van Der Merwe R (2004). Sigma-point Kalman filters for probabilistic inference in dynamic state-space models. PhD Thesis. Oregon Health & Science University.

Van Der Merwe R, Wan EA (2001). The square-root unscented Kalman filter for state and parameter-estimation. Proceedings of the International Conference on Acoustics, Speech, and Signal Processing. Proceedings, 6, 3461–3464. doi: http://dx.doi.org/10.1109/ICASSP.2001.940586.

Wan EA, Van Der Merwe R (2000). The unscented Kalman filter for nonlinear estimation. Proceedings of the IEEE 2000 Adaptive Systems for Signal Processing, Communications, and Control Symposium; 153–158. doi: http://dx.doi.org/10.1109/ASSPCC.2000.882463.

Wan EA, Van Der Merwe R, Nelson AT (2000). NIPS'99 Proceedings of the 12th International Conference on Neural Information Processing Systems, 666–672.

Wang Y, Li ZX, Wang CM (2011). Concurrent multifactor optimisation techniques for model updating of long-span bridges. *Structure and Infrastructure Engineering*, 9(6): 578-593. doi: https://doi.org/10.1080/15732479.2011.595801.

Wang Y-O, Zong L, Shi Y-J, Yao N (2014). Damage detection and rehabilitation on a curvilinear steel box girder bridge by multistage model updating. *Structure and Infrastructure Engineering*, 11(11): 1420-1431. doi: https://doi.org/10.1080/15732479.2014.970202.

Yang X-S, Koziel S (2011). Computational optimization and applications in engineering and industry. vol. 359. Springer Science & Business Media.

Živanović S, Pavic A, Reynolds, P (2007). Finite element modelling and updating of a lively footbridge: The complete process. *Journal of Sound and Vibration*, 301 (1-2): 126-145 doi: https://doi.org/10.1016/j.jsv.2006.09.024.

Apéndice D
Articulo D

Naranjo-Pérez, J., Jiménez-Alonso, J. F., Sáez, A. Parameter identification of the dynamic Winkler soil-structure interaction model using a hybrid UKF-MHS algorithm. *Advances in Structural Engineering*. 2020.

- Civil Engineering: Q3 (87/132)

- Construction and Building Technology: Q3 (39/63)

Parameter identification of the dynamic Winkler soil-structure interaction model using a hybrid UKF-MHS algorithm

Javier Naranjo-Pérez[a], Javier Fernando Jiménez-Alonso[b*] and Andrés Sáez[c]

[a]PhD Candidate. Department of Continuum Mechanics and Structural Analysis Universidad de Sevilla, Camino de los Descubrimientos s/n, Seville, 41092, Spain.
[b*]Assistant Professor. Department of Continuum Mechanics and Structures, E.T.S. Ingenieros de Caminos, Canales y Puertos. Universidad Politécnica de Madrid, Calle del Profesor Aranguren, 3, Madrid, 28040, Spain.
[c]Full Professor. Department of Continuum Mechanics and Structural Analysis Universidad de Sevilla, Camino de los Descubrimientos s/n, Seville, 41092, Spain.

Abstract

Soil-structure interaction is a key aspect to take into account when simulating the response of civil engineering structures subjected to dynamic actions. To this end, and due to its simplicity and ease of implementation, the dynamic Winkler model has been widely used in practical engineering applications. In this model, soil-structure interaction is simulated by means of spring-damper elements. A crucial point to guarantee the adequate performance of the approach is to accurately estimate the constitutive parameters of these elements. To this aim, this paper proposes the application of a recently developed parameter identification method to address such problem. In essence, the parameter identification problem is transformed into an optimization problem, so that the parameters of the dynamic Winkler model are estimated by minimising the relative differences between the numerical and experimental modal properties of the overall soil-structure system. A recent and efficient hybrid algorithm, based on the combination of the Unscented Kalman Filter (UKF) and Multi-objective Harmony Search (MHS) algorithms, is satisfactorily implemented to solve the optimization problem. The performance of this proposal is then validated via its implementation in a real case-study involving an integral footbridge.

Keywords

[*]Corresponding author: Javier Fernando Jiménez-Alonso. Department of Continuum Mechanics and Structures. E.T.S. Ingenieros de Caminos, Canales y Puertos. Universidad Politécnica de Madrid, Calle del Profesor Aranguren, 3, 28040 Madrid (Spain) Ph:+34 91 0674154. e-mail: jf.jimenez@upm.es.

Introduction

Soil-structure interaction (SSI) is an important aspect to consider in civil engineering structures in order to mimic accurately their behaviour via numerical models (Tabatabaiefar *et al.*, 2016). One of the most widely used SSI models is the static Winkler model (Hirai, 2011), where the SSI phenomenon is simulated via the implementation of spring elements, whose behaviour is characterized by a stiffness coefficient. When dynamic actions come into play, it is necessary to implement a dynamic Winkler model (Allotey and El Naggar, 2008), where the SSI is simulated via spring-dampers elements, whose behaviour is characterized by both stiffness and damping coefficients. However, both the static and dynamic Winkler models present a clear limitation for their practical engineering application: the need to accurately estimate the value of the above constitutive parameters (stiffness/damping coefficients) that resemble the actual SSI. In fact, this parameter identification is not a straightforward issue since it involves testing jointly both systems: the soil and the structure.

In order to address such parameter identification problem, two sets of methods have been traditionally employed. In the first type of methods, the SSI phenomenon is characterized via the use of numerical models whose constitutive laws are previously determined via either laboratory (Drnevich *et al.*, 1978) or field tests (Badsar *et al.*, 2010; Campanella and Stewart, 1992; Cheng and Leong, 2018; Karl *et al.* 2006; Lai and Rix, 1998; Lee et al., 2016). Among the different methods, the so-called mixed FE-BE method has been widely implemented (Alamo et al., 2016; Yazdchi *et al*., 1999). In this approach, the finite element (FE) method, used to simulate the structure, and the boundary element (BE) method, employed to model the soil, are coupled by imposing compatibility and equilibrium equations at the soil-structure interphase. Although these methods constitute a valid attempt to simulate numerically the SSI phenomenon, they present three main limitations that discourage their use for practical engineering applications, namely: (i) the constitutive laws of the soil are estimated without taking into account the SSI phenomenon; (ii) the results rely strongly on such constitutive laws; and (iii) they are somehow complex to be implemented by practitioner engineers.

In order to overcome these limitations, a second type of methods emerged that also combined numerical and experimental techniques, although with a different perspective: the parameters that characterize the SSI phenomenon are estimated via the implementation of some kind of parameter identification algorithm. Among these identification algorithms, the so-called estimators have been extensively employed. Within these estimators, the maximum likelihood method has been widely adopted, due to its ease of implementation and good balance between computational cost and accuracy. This method transforms the parameter identification problem into an optimization problem, in which the parameters to be estimated are determined via the minimization of an objective function, defined in terms of the relative differences between some numerical and experimental data that reflect the behaviour of the soil-structure system. According to the best of the authors' knowledge, the first examples of this approach were reported by Maier and Gioda (1982) and Arai *et al.* (1984). In both studies, a gradient-based algorithm was considered as optimization method. Subsequently, Gens *et al.* (1996) used the Levenberg-Marquardt algorithm to solve the parameter identification problem during a tunnel excavation work. The main limitation of these methods is the local character of the optimization algorithm: local optimizers present a high risk of convergence to a local minimum and are highly dependent on the initial value of the design parameters.

Subsequently, in order to overcome these limitations, global optimization algorithms were considered to solve the parameter identification problem in geotechnical applications (Ledesma *et al.*, 1996a; Ledesma *et al.*, 1996b). Due to their good convergence and effectiveness to solve nonlinear problems, genetic algorithms have been widely used to this end (Srinivas and Deb, 1994). However, the use of genetic algorithms presents an important drawback: the high simulation time required to perform the optimization process for complex structures. For this reason, during the last twenty-five years, great efforts have been devoted to propose and implement alternative global optimizers that reduce the simulation time without comprising the accuracy of the solution.

On the other hand, when it becomes mandatory to take into account the stochastic character of either the soil or the structural system, another kind of identification methods are required, which involve estimators that filter the uncertainty associated with the stochastic nature of the constitutive parameters. Estimators based on the so-called Kalman filter (KF) have clearly imposed to this end (Kalman, 1960). The KF estimates the parameters of a linear system by considering statistical white noise of the experimental data. Thus, the mean and covariance of the parameters of the soil-structure interaction model are estimated iteratively in two steps (prediction and correction) in order to minimise the estimation error, and, therefore, achieve an unbiased true estimation of the parameters of the model. As the use of the KF was limited to linear systems, a new algorithm, the extended Kalman filter (EKF) was later developed to address the parameter identification problem for nonlinear systems (Jazwinski, 1970). The EKF algorithm is based on the local linearization of the nonlinear system and the subsequent application of the KF algorithm on the resulting linearized system. However, the performance of this algorithm is reduced as the nonlinear character of the system increases. In such case, a new enhanced version of the KF was proposed: the unscented Kalman filter (UKF). In this method, no linearization of the system is required, so that, instead, Gaussian behaviour of the system is assumed (Julier and Uhlmann, 1997). Thus, the covariance of the estimation process is determined from the propagation of a set of sample points through the nonlinear system. Thus, the UKF algorithm allows computing more accurately the mean and covariance of the estimated parameters than the EKF algorithm (up to the second order of the Taylor series expansion of the nonlinear function and up to the third order for Gaussian inputs) (Nguyen and Nestorović, 2015). However, these algorithms, based on KF, are local optimizers, and therefore may fail when finding the global optimum of functions with several extreme values.

For this reasons, the current trend to overcome all the above-mentioned limitations and reduce computational cost, is to solve the parameter identification problem by using hybrid algorithms that take advantage of the virtues of both local and global optimizers. For instance, a hybrid UKF-simulated annealing algorithm was proposed by Astroza *et al.* (2016) that allowed reducing the simulation time when compared to the sole implementation of the simulated annealing algorithm. More recently, Naranjo-Perez *et al.* (2020) proposed a hybrid UKF-harmony search (HS) algorithm for the FE model updating of complex civil engineering structures. This hybrid algorithm combined the virtues of two individual algorithms: (i) the (local) UKF algorithm, which reduces the uncertainty associated with the parameter identification based on experimental data; and (ii) the (global) HS algorithm (Geem *et al.*, 2001), which reduces significantly simulation times when compared to other classical metaheuristics algorithms (Jiménez-Alonso *et al.*, 2017).

In this paper, the UKF-HS algorithm is extended to consider a more general multi-objective approach (UKF-MHS), and it is further implemented to solve the parameter identification problem associated to the experimental identification of the dynamic Winkler model parameters. The parameter identification problem is herein formulated based on the FE model updating method under the maximum likelihood approach (Mottershead *et al.*, 2011). In this manner, the parameter identification problem is transformed into a multi-objective optimization problem (Marwala, 2010), with the objective functions defined in terms of the relative differences (residuals) between the numerical and experimental modal properties of the soil-structure interaction system. In particular, three types of residuals are next considered: (i) residuals based on the natural frequencies; (ii) residuals based on the damping ratios; and (iii) residuals based on the vibration modes. Therefore, the aim of the resulting optimization problem focuses on minimising the value of the objective functions via the modification of some pre-selected physical parameters of the structure. The solution of this optimization problem provides a point estimation of the value of such physical parameters. In this process, the numerical modal properties of the soil-structure system are obtained via the FE method, while its experimental modal properties are identified via the signal processing of its response recorded during either a forced vibration (Maia *et al.*, 1997) or an ambient vibration test (Magalhães and Cunha, 2011).

Thus, three are the main aspects that characterize the proposed parameter identification method:

(i)   it is a model-based identification method, so that the solution of the parameter identification problem involves the solution of a FE model updating problem;

(ii) the identification of the parameters defining the dynamic Winkler model is performed indirectly, by inferring them from the analysis of the overall experimental behaviour of the soil-structure system; and

(iii) a hybrid UKF-MHS algorithm is implemented to efficiently perform the parameter identification process.

Finally, the performance of this parameter identification method has been validated via its implementation in a real case-study. Concretely, a real steel-concrete composite integral footbridge has been considered to conduct the parameter identification of the dynamic Winkler model. The election of this structural type is based on the high influence of the SSI phenomenon on the dynamic behaviour of integral bridges (Rodriguez *et al.* 2011).

The paper is organized as follows. First, some basics about the use of dynamic Winkler models to numerically simulate the SSI phenomenon in civil engineering structures are presented. Subsequently, the parameter identification problem of the dynamic Winkler model is formulated in terms of a multi-objective optimization problem. Next, the performance of the proposed method is validated via its implementation for a real steel-concrete composite integral footbridge. Finally, some concluding remarks are drawn to close the paper.

Soil-structure interaction under the Dynamic Winkler Model

An adequate simulation of the SSI is a basic aspect for the accurate estimation of the response of the civil engineering structure under dynamic actions (Tabatabaiefar *et*

al., 2106). The SSI phenomenon depends clearly on the type of foundation. Two extreme cases are normally considered to simulate the behaviour of these foundations, the so-called: (i) direct; and (ii) deep foundations.

Direct foundations are usually rigid massive structures. Direct foundations may be modelled as an equivalent spring-damper element (Gazetas, 1991). The dynamic stiffness and damping coefficient of this element may be determined in terms of the amplitude of the vibration level of the structure. For low vibration levels, which are assumed herein, the SSI phenomenon on direct foundation may be simulate adequately considering only the stiffness component.

Thus, the value of the equivalent stiffness of an embedded direct foundation, either k_i for translational degrees of freedom [N/m] or k_{ri} for rotational degrees of freedom [N/rad] (being i the direction of the considered degree of freedom), may be determined (Gazetas, 1991) in terms of the equivalent stiffness of a surface direct foundation, either $k_{i,surf}$ for translational degrees of freedom [N/m] or $k_{ri,surf}$ for rotational degrees of freedom [N/rad], as follows (being x the longitudinal direction, y the lateral direction and z the vertical direction):

$$k_z = k_{z,surf}\left[1 + \frac{1}{21}\frac{D}{B}(1 + 1.3\chi)\right]\left[1 + 0.2\left(\frac{A_w}{A_b}\right)^{\frac{2}{3}}\right] \tag{1}$$

$$k_x = k_{x,surf}\left[1 + 0.15\sqrt{\frac{D}{B}}\right]\left[1 + 0.52\left(\frac{dA_w}{BL^2}\right)^{0.4}\right] \tag{2}$$

$$k_y = k_{y,surf}\left[\left[1 + 0.15\sqrt{\frac{D}{B}}\right]\left[1 + 0.52\left(\frac{dA_w}{BL^2}\right)^{0.4}\right]\right] \tag{3}$$

$$k_{rx} = k_{rx,surf}\left[1 + 1.26\frac{d}{B}\left[1 + \frac{d}{B}\left(\frac{d}{D}\right)^{-0.2}\sqrt{\frac{B}{L}}\right]\right] \tag{4}$$

$$k_{ry} = k_{ry,surf}\left[1 + 0.92\left(\frac{d}{L}\right)^{0.6}\left[1.5 + \left(\frac{d}{L}\right)^{1.9}\left(\frac{d}{D}\right)^{-0.6}\right]\right] \tag{5}$$

$$k_{rz} = k_{rz,surf}\left[1 + 1.4\left(1 + \frac{B}{L}\right)\left(\frac{d}{B}\right)^{0.9}\right] \tag{6}$$

$$k_{z,surf} = \frac{2G_sL}{1-v_s}\{0.73 + 1.54\chi^{0.75}\} \tag{7}$$

$$k_{y,surf} = \frac{2G_sL}{2-v_s}\{2 + 2.5\chi^{0.85}\} \tag{8}$$

$$k_{x,surf} = k_{y,surf} - \frac{0.2}{0.75-v_s}G_sL\left(1 - \frac{B}{L}\right) \tag{9}$$

$$k_{rx,surf} = \frac{G_s}{1-v_s}I_{bx}{}^{0.75}\left(\frac{L}{B}\right)^{0.25}\left(2.4 + 0.5\frac{B}{L}\right) \tag{10}$$

$$k_{ry,surf} = \frac{G_s}{1-v_s}I_{by}{}^{0.75}\left[3\left(\frac{L}{B}\right)^{0.15}\right] \tag{11}$$

$$k_{rz,surf} = GJ_b{}^{0.75}\left[4 + 11\left(1 - \frac{B}{L}\right)^{10.}\right] \tag{12}$$

where $G_s = \frac{E_s}{2(1+v_s)}$ is the shear modulus of the soil [N/m²]; E_s, is the longitudinal modulus of the soil [N/m²]; v_s is the Poisson's ratio of the soil [-], D is the total depth of the direct

foundation [m], d is the depth of the direct foundation in contact with the soil [m]; B is the half of the width of the direct foundation [m]; L is the half of the length of the direct foundation [m]; $A_b = 2B \cdot 2L$ is the lower surface of the direct foundation in contact with the soil [m²]; $A_w = 2L \cdot d$ is the lateral surface of the direct foundation in contact with the soil [m²]; I_{bx} is the moment of inertia of the lower surface of the direct foundation with respect to the x axis [m⁴]; I_{by} is the moment of inertia of the lower surface of the direct foundation with respect to the y axis [m⁴]; $J_b = I_{bx} + I_{by}$ is the torsional moment of inertia of the lower surface of the direct foundation [m⁴]; and χ is a shape parameter defined as $\chi = \frac{A_b}{4L^2}$ [-].

Deep foundations are slender flexible structures whose structural behaviour depends mainly on their length. Two types of models have been usually used to analyse the SSI phenomenon in the case of deep foundations: (i) spring models and (ii) spring-dampers models.

On the one hand, the spring models present as main assumption a fully coupling between the soil and the deep foundation. According to this model, the effect of the soil adjacent to the deep foundation is simulated by several spring elements located along the deep foundation. The response of these spring models have been usually obtained via either approximate solutions (Novak, 1974; Tajimi H, 1966) or numerical methods, such as the FE or the BE method (Alamo *et al.*, 2016).

On the other hand, the spring-damper models, in which the effect of the soil adjacent to the deep foundation is simulated by several spring-damper elements located along its length. These second models have been widely used to simulate the SSI phenomenon of civil engineering structure for practical engineering applications due to the well-balanced equilibrium between their complexity and the accurate of the results provided. Among the different spring-damper models, the dynamic Winkler model has been considered herein.

According to this model, the stiffness of each spring-damper element, $k = k(z)$, may be determined as follows:

$$k(z) = k_b(z) \cdot L_k \cdot D_p \qquad (13)$$

where $k(z)$ is the stiffness of the spring element [N/m] at depth z [m], $k_b(z)$ is the ballast coefficient [N/m³] at depth z [m], L_k is the length between springs [m] and D_p is the diameter of the deep foundation [m].

Additionally, the damping coefficient of each spring-damper element, c [sN/m], may be determined via the sum of two energy dissipation mechanisms (Gazetas and Dobry, 1984): (i) hysteretic damping and (ii) radiation damping.

$$c = c_h + c_r \qquad (14)$$

The hysteretic damping, c_h [sN/m], also called material damping, may be expressed as (Thavaraj, 2000):

$$c_h = \frac{2\beta k_b}{\omega} \qquad (15)$$

where β is the damping ratio of the soil [-]; k_b is the ballast coefficient of the soil [N/m³] and ω is the angular frequency of the applied force [rad/s].

Similarly, the radiation damping coefficient, c_r [sN/m], may be determined through an experimental relationship (Thavaraj, 2000). Among the different proposals,

the relationship proposed by Berger *et al.* (1977) has been considered herein because it is an angular frequency independent expression:

$$c_r = 4\frac{D_p}{2}\rho_s v_s \left(1 + \frac{v_c}{v_s}\right) \tag{16}$$

where ρ_s is the density of the soil [kg/m³]; $v_s = \sqrt{\frac{G_s}{\rho_s}}$ is the shear wave velocity [m/s] and v_c is a velocity defined as $v_c = \sqrt{\frac{2}{1-\nu_s}} v_s$ [m/s] where ν_s is the Poisson's ratio of the soil [-].

Finally, it is necessary to remark that herein the contribution of the hysteretic damping coefficient, c_h, has been neglected as assumption because it is two orders of magnitude lower than the radiation damping coefficient, c_r, within the frequency range of interest, $0 - 20$ Hz.

Parameter Identification Method of Dynamic Systems using a Hybrid UKF-MHS Algorithm

Parameter identification problem consists in estimating the constitutive parameters of a system by considering both the actual measurements of its real response and the predictions provided by a dynamic numerical model which simulates its behaviour. Thus, the objective of the parameter identification problem is to infer the value of these constitutive parameters which minimises the difference between the numerical and experimental behaviour of the system. For this reason, the parameter identification problem may be also referred as an inverse problem.

There are several methods to simulate numerically the response of the system during the parameter identification process. Among these methods, FE analysis has been widely used to model numerically the response of civil engineering structures. If the parameter identification method is based on a FE model, the solution of this parameters identification problem implies the updating of the corresponding FE model. Thus, this parameter identification problem may be transformed into a FE model updating problem (Marwala, 2010).

FE model updating of civil engineering structures for practical engineering applications is usually solved using some type of estimators. Estimators can be classified into two general groups (Chen, 2003, Rao *et al*., 2007): (i) point estimators and (ii) interval estimators. The first type returns a single value of each considered parameter and the second type returns an interval of possible values of each considered parameter. The maximum likelihood method, a point estimator, has been considered herein to perform this problem due to its efficiency and accuracy in the solution of the updating problem (Jiménez-Alonso *et al.*, 2017).

According to this method, the FE model updating problem may be formulated as a multi-objective optimization problem (Mottershead *et al.*, 2011). Thus, the objective of this problem is to minimise the value of the different terms of the objective function via the modification of some pre-selected physical parameters of the model (considered as design variables). This objective function is defined in terms of the relative differences between the numerical and experimental modal properties of the structure. Computational intelligence algorithms are normally considered to solve this optimization problem

(Marwala, 2010). However, these computational algorithms present two clear limitations: (i) they elapse a high simulation time when the complexity of the FE model increases; and (ii) they are not able to deal with the uncertainty associated with the experimental modal properties of the system.

In order to overcome these limitations, hybrid algorithms are normally employed. Among these algorithms, a recent proposal, the UKF-MHS algorithm (Naranjo-Perez *et al.*, 2020), has been considered herein due to its great efficiency and accuracy to solve the FE model updating problem of complex civil engineering structures.

As result of the optimization process, the so-called Pareto front is obtained. The Pareto front shows the set of possible solutions of the optimization problem. Subsequently, a decision making problem must be solved to select the best solution among all the elements of the Pareto front. The criterion provided by Jin *et al.* (2014) has been considered herein to cope with this decision making problem.

In next subsections, the proposed parameter identification method is described in detail. First, the formulation of the parameter identification problem as a multi-objective optimization problem has been presented. Subsequently, a theoretical background of the MHS and the UKF algorithms has been included. Finally, the proposed hybrid UKF-MHS algorithm has been described briefly.

Formulation of the parameter identification problem

As it has been mentioned above, the parameter identification problem may be formulated as a multi-objective optimization problem. The formulation of this problem may be expressed as follows:

$$\min(f_1(\boldsymbol{\theta}) \quad f_2(\boldsymbol{\theta}) \quad f_3(\boldsymbol{\theta})) = min\left(\frac{1}{2}\left[\sum_{j=1}^{n_f} r_{f,j}(\boldsymbol{\theta})^2\right]^{\frac{1}{2}} \quad \frac{1}{2}\left[\sum_{j=1}^{n_f} r_{m,j}(\boldsymbol{\theta})^2\right]^{\frac{1}{2}} \quad \frac{1}{2}\left[\sum_{j=1}^{n_f} r_{d,j}(\boldsymbol{\theta})^2\right]^{\frac{1}{2}}\right)$$
$$\text{s.t.} \quad \boldsymbol{\theta}_l \leq \boldsymbol{\theta} \leq \boldsymbol{\theta}_u$$
(17)

where $r_{f,j}(\boldsymbol{\theta})$, $r_{m,j}(\boldsymbol{\theta})$ and $r_{d,j}(\boldsymbol{\theta})$ are the residuals of the natural frequency, vibration mode and damping ratio respectively of the j considered vibration mode; n_f is the number of vibration modes considered in the analysis; $\boldsymbol{\theta}$ is the vector containing the pre-selected physical parameters of the FE model; and $\boldsymbol{\theta}_l$ and $\boldsymbol{\theta}_u$ are the lower and upper bound of the search domain of these physical parameters.

The three residuals may be determined in terms of the relative differences between the numerical and experimental modal properties of the structure as follows:

$$r_{f,j}(\boldsymbol{\theta}) = \frac{f_{\text{num},j}(\boldsymbol{\theta}) - f_{\text{exp},j}}{f_{\text{exp},j}}$$
(18)

$$r_{m,j}(\boldsymbol{\theta}) = \sqrt{\frac{\left(1 - \sqrt{\text{MAC}_{exp,j}^{num,j}(\boldsymbol{\theta})}\right)^2}{\text{MAC}_{exp,j}^{num,j}(\boldsymbol{\theta})}}$$
(19)

$$r_{d,j}(\boldsymbol{\theta}) = \frac{\xi_{\text{num},j}(\boldsymbol{\theta}) - \xi_{\text{exp},j}}{\xi_{\text{exp},j}}$$
(20)

where $f_{\text{num},j}(\boldsymbol{\theta})$ and $f_{\text{exp},j}$ are the numerical and experimental natural frequencies respectively; $\xi_{\text{num},j}(\boldsymbol{\theta})$ and $\xi_{\text{exp},j}$ are the numerical and experimental damping ratios respectively and $\text{MAC}_{exp,j}^{num,j}(\boldsymbol{\theta})$ is the Modal Assurance Criterion ratio defined as

(Allemang and Brown, 1982):

$$MAC_{exp,j}^{num,j}(\boldsymbol{\theta}) = \frac{\left(\phi_{\text{num},j}(\boldsymbol{\theta}) \cdot \phi_{\text{exp},j}\right)^2}{\left(\phi_{\text{num},j}^T(\boldsymbol{\theta}) \cdot \phi_{\text{num},j}(\boldsymbol{\theta})\right) \cdot \left(\phi_{\text{exp},j}^T \cdot \phi_{\text{exp},j}\right)} \tag{21}$$

being $\phi_{\text{num},j}(\boldsymbol{\theta})$ and $\phi_{\text{exp},j}$ the numerical and experimental vibration modes respectively and ^{T} denotes transpose.

Multi-objective Harmony Search Algorithm

The HS algorithm is a global metaheuristic algorithm inspired by the mental process for the creation of musical harmony (Geem *et al.*, 2001). The aim of the algorithm is to find the global minimum of a previously defined objective function by modifying a set of design variables (physical parameters) of a numerical model. The HS algorithm has been implemented successfully for several practical engineering applications (Yang and Koziel, 2011). This algorithm has shown a great effectiveness (a reduced simulation time without compromising the accuracy) in comparison with other conventional metaheuristic algorithms when it is implemented to solve nonlinear optimization problems (Wang *et al.*, 2015). The operating rules of this algorithm are similar to the ones which govern the performance of other conventional metaheuristic algorithms, such as genetic algorithms. However, in this case, the complexity of the numerical operations employed to control the evolution of the algorithm has been reduced to improve its performance. Despite the great effectiveness of this algorithm, it has been rarely applied, to the best of the authors' knowledge, for the parameters identification of systems based on the FE model updating method. The MHS algorithm is an extension of the previous algorithm which allows minimizing more than one objective function.

The MHS algorithm consists of the following steps:

(i) The harmony matrix, **H**, is initialised. This matrix contains the initial HMS generated solutions. Each solution represents a vector with the physical parameters to be updated. Subsequently, the different terms of the objective functions are evaluated for the different solutions in the harmony matrix, **H**.

(ii) New harmonies are improvised. This step consists in generating a new set of harmonies (parameter vectors) based on: (i) memory considerations; (ii) randomization; and (iii) pitch adjustments. According to this, each parameter can adopt a value from a previous value in the harmony matrix, **H**, or be assigned randomly. The probability that a parameter is selected from the harmony matrix, **H**, is controlled by the variable $HMCR$. Thus, for each parameter, a random number, between 0 and 1, is generated and if this number is lower than or equal to $HMCR$, the parameter is chosen randomly from the matrix **H**. Otherwise, a random value among the possible values of the search domain is assigned to the parameter. When the parameter is defined from **H**, it can be modified additionally. The probability, that this parameter can be modified, is determined by the variable PAR. A random number is generated again between 0 and 1 and if it is lower than or equal to PAR, the parameter value is adjusted by subtracting or adding a previously defined value, the so-called bandwidth, bw. Otherwise, the parameter value remains unchanged.

(iii) The new solutions and the previous solutions in the harmony matrix **H** are then classified using both the non-dominating sorting technique (Deb *et al.*, 2002) and the crowding distance. Hence, the so-called Pareto front is defined in terms of the non-

dominated solutions. Finally, in order to restore the initial size of the harmony matrix, **H**, the worst solutions, according to a crowding distance criterion, are removed.

(iv) These steps are repeated iteratively until a stop criterion is reached.

Thus, Figure 1 shows the flowchart of the MHS algorithm.
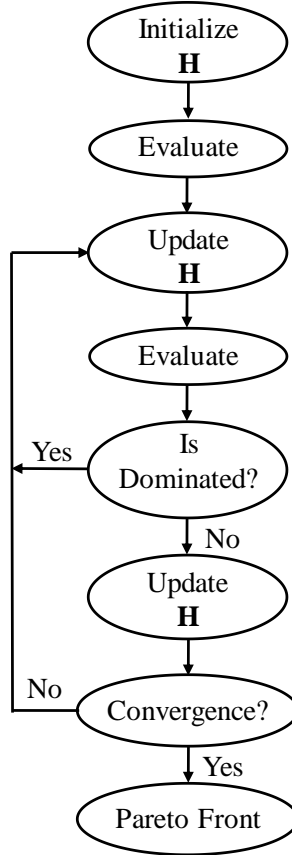
Figure 1. Flowchart of the MHS algorithm.

Unscented Kalman Filter

The UKF algorithm is a derivative free estimator for nonlinear systems. This algorithm belongs to the class of filters named sigma-points Kalman filters (Julier and Uhlmann, 1997). Its implementation as parameter estimator was proposed by Wan and Van Der Merwe (2000) and Wan *et al.* (2000).

The parameter identification can be addressed as,

$$\boldsymbol{\theta}_k = \boldsymbol{\theta}_{k-1} + \mathbf{w}_{k-1} \tag{22}$$

$$\mathbf{z}_k = \boldsymbol{h}(\boldsymbol{\theta}_k) + \mathbf{v}_k \tag{23}$$

where **θ** is a vector with the physical parameters to be estimated; **z** is a vector with the

outputs of the modelling function h; $\mathbf{w}$ is a vector which takes into account the process noise; and $\mathbf{v}$ is a vector which takes into account the observation noise.

Both type of noise are assumed to be white Gaussian with zero-mean and uncorrelated covariance matrices $\mathbf{Q}$ and $\mathbf{R}$, respectively. The matrix $\mathbf{R}$ can be divided into two components (Tarantola, 2005): (i) the modelling noise covariance; and (ii) the measurement noise covariance. If the same FE model is considered for each step, the first component of the matrix $\mathbf{R}$ can be neglected.

The UKF algorithm addresses the nonlinear estimation by considering $2n_d + 1$ (being n_d the number of parameters) deterministic sampling points (so-called sigma points) to derive the posterior mean and covariance matrix, $\mathbf{P}$, via their propagation (the so-called unscented transformation) through the nonlinear function, h (Julier and Uhlmann, 2004). Thus, the main computational effort of this algorithm is the computation of the new sigma points. Additionally, it is necessary to remark as limitation that the posterior covariance matrix, $\mathbf{P}$, must be positive semidefinite, as these sigma points are obtained by the square-root decomposition of this matrix. Even though the square-root decomposition can be efficiently derived using the Cholesky factorization ($\mathbf{A} = \sqrt{\mathbf{P}} = chol(\mathbf{P})$) being $\mathbf{P} = \mathbf{A}\mathbf{A}^{\mathbf{T}}$ and ^{T} the transpose function), the matrix $\mathbf{P}$ is still updated at each iteration and numerical errors can give a non-positive-semidefinite matrix $\mathbf{P}$. The square-root UKF algorithm, proposed by (Van Der Merwe and Wan, 2001), overcomes this problem as it avoids factorising at each step. This algorithm propagates directly the matrix $\mathbf{A}$ and guarantees that the covariance matrix, $\mathbf{P}$, is positive semidefinite.

The $2n_d + 1$ sigma points are defined as,

$$(\boldsymbol{\chi}_{k-1})_0 = \widehat{\boldsymbol{\theta}}_{k-1|k-1} \tag{24}$$

$$(\boldsymbol{\chi}_{k-1})_i = \widehat{\boldsymbol{\theta}}_{k-1|k-1} + \eta(\mathbf{A}_{k-1|k-1})_i \quad i = 1, 2, \dots, n_d \tag{25}$$

$$(\boldsymbol{\chi}_{k-1})_{i+n_d} = \widehat{\boldsymbol{\theta}}_{k-1|k-1} - \eta(\mathbf{A}_{k-1|k-1})_i \quad i = 1, 2, \dots, n_d \tag{26}$$

where $\widehat{\boldsymbol{\theta}}$ are the posterior parameters estimated at the previous step and $\eta = \sqrt{(n_d + \lambda)}$ being λ a scaling parameter. The sigma points have their associated weights,

$$W_0 = \frac{\lambda}{n_d + \lambda} \tag{27}$$

$$W_i = W_{i+n_d} = \frac{1}{2(n_d + \lambda)} \quad i = 1, 2, \dots, n_d \tag{28}$$

As a particular case of the KF, the square-root UKF consists of two steps: (i) the prediction step; and (ii) the correction (update) step.

First, the prediction step is conducted based on the prior model to assess the sigma points and predict the estimates of the estimation error covariance, $\mathbf{A}^\theta$, the model outputs error covariance, $\mathbf{S}^z$, and the cross covariance, $\mathbf{P}^{\theta z}$. The estimation error covariance is given by $\mathbf{A}_k = \gamma^{-1/2}\mathbf{A}_{k-1}$, being γ a scalar factor slightly less than 1. Since $W_i > 0$ for all $i \geq 1$, the model outputs error covariance, $\mathbf{S}^z$, can be expressed as,

$$\mathbf{S}_k^z = \sum_0^{2n_d} W_i \left[\left(\mathbf{z}_{k|k-1}^{\mathrm{i}} - \widehat{\mathbf{z}}_{k|k-1} \right) \cdot \left(\mathbf{z}_{k|k-1}^{\mathrm{i}} - \widehat{\mathbf{z}}_{k|k-1} \right)^T \right] + \mathbf{R} = \left[\sqrt{W_i} \left(\mathbf{z}_{k|k-1}^{\mathrm{i}} - \widehat{\mathbf{z}}_{k|k-1} \right), \sqrt{\mathbf{R}} \right] \cdot \left[\sqrt{W_i} \left(\mathbf{z}_{k|k-1}^{\mathrm{i}} - \widehat{\mathbf{z}}_{k|k-1} \right)^T, \sqrt{\mathbf{R}}^T \right]^T + W_0 \left[\left(\mathbf{z}_{k|k-1}^0 - \widehat{\mathbf{z}}_{k|k-1} \right) \cdot \left(\mathbf{z}_{k|k-1}^0 - \widehat{\mathbf{z}}_{k|k-1} \right)^T \right] \quad for \ i = 1:2n_d \tag{29}$$

where $\mathbf{z}_{k|k-1}^{\mathrm{i}}$ indicates that the variable $\mathbf{z}^{\mathrm{i}}$ was computed at the step k considering the

data from the step $k - 1$.

A QR factorization[1], qr, can be used to express the first term as the product of an orthogonal matrix $\mathbf{O}_k \in \mathbb{R}^{2n_d+r \times r}$ and an upper triangular matrix $\mathbf{S}_k^z \in \mathbb{R}^{r \times r}$, being r the number of measurements. The last term can be taken into account through a rank 1 update to Cholesky factorization[2], $cholupdate$ (Matlab, 2019). Therefore, the matrix $\mathbf{S}_k^z$ can be calculated as (Terejanu, 2011):

$$\mathbf{S}_k^z = qr\left(\left[\sqrt{W_{1:2n_d}} \cdot \left[\left(\mathbf{z}_{k|k-1} \right)_{1:2n_d} - \hat{\mathbf{z}}_{k|k-1} \right], \ \sqrt{\mathbf{R}} \right] \right) \qquad (30)$$

$$\mathbf{S}_k^z = cholupdate\left(\mathbf{S}_k^z, \ \left(\mathbf{z}_{k|k-1} \right)_0 - \hat{\mathbf{z}}_{k|k-1}, \ \mathrm{sgn}(W_0)W_0 \right) \qquad (31)$$

Subsequently, the correction step uses both the measurements, $\mathbf{z}^{obs}$, and the model outputs to determine the posterior mean and covariance of the parameter estimation by considering the Kalman's gain matrix, $\mathbf{K}$. The following algorithm is shown below.

Initial Step:

$$\hat{\boldsymbol{\theta}}_0 = \boldsymbol{\theta}_{prior} \qquad (32)$$

$$\mathbf{A}_0^\theta = chol(\mathbf{P}_0^\theta) \qquad (33)$$

Main loop: $for \ k = 1 : N_{UKF}$ (number of iterations of the UKF)

Prediction step:

Calculate the $2n_d + 1$ Sigma Points: $(\boldsymbol{\chi}_{k-1})_i$

$$\left(\boldsymbol{\chi}_{k|k-1} \right)_i = (\boldsymbol{\chi}_{k-1})_i$$

$$\boldsymbol{\theta}_{k|k-1} = \Sigma_0^{2n_d} W_i \cdot \left(\boldsymbol{\chi}_{k|k-1} \right)_i$$

$$\mathbf{A}_{k|k-1}^\theta = \gamma^{-\frac{1}{2}} \mathbf{A}_{k-1}^\theta$$

$$\left(\mathbf{z}_{k|k-1} \right)_i = \boldsymbol{h}\left(\left(\boldsymbol{\chi}_{k|k-1} \right)_i \right)$$

$$\hat{\mathbf{z}}_{k|k-1} = \Sigma_0^{2n_d} W_i \cdot \left(\mathbf{z}_{k|k-1} \right)_i$$

$$\mathbf{S}_{k|k-1}^z = qr\left(\left[\sqrt{W_{1:2n}} \cdot \left[\left(\mathbf{z}_{k|k-1} \right)_{1:2n} - \hat{\mathbf{z}}_{k|k-1} \right] \ \sqrt{\mathbf{R}} \right] \right)$$

$$\mathbf{S}_{k|k-1}^z = cholupdate\left(\mathbf{S}_{k|k-1}^z, \left(\mathbf{z}_{k|k-1} \right)_0 - \hat{\mathbf{z}}_{k|k-1}, \mathrm{sgn}(W_0) \right)$$

$$\mathbf{P}_{k|k-1}^{\theta z} = \Sigma_0^{2n_d} \left(W_i \left[\left(\boldsymbol{\chi}_{k|k-1} \right)_i - \hat{\boldsymbol{\theta}}_{k|k-1} \right] \cdot \left[\left(\mathbf{z}_{k|k-1} \right)_i - \hat{\mathbf{z}}_{k|k-1} \right]^T \right)$$

Correction (update) step:

$$\mathbf{K}_k = \left(\mathbf{P}_{k|k-1}^{\theta z} / \mathbf{S}_{k|k-1}^z{}^T \right) / \mathbf{S}_{k|k-1}^z$$

---

[1] The QR factorization, qr, of a matrix $\mathbf{M}$ allows expressing the matrix as $\mathbf{M} = \mathbf{QR}$. Here, $\mathbf{M}$ is an m-by-n matrix, $\mathbf{R}$ is an m-by-n upper triangular matrix and $\mathbf{Q}$ is an m-by-m unitary matrix.

[2] If $\mathbf{R} = chol(\mathbf{A})$, the Cholesky factor of the rank 1 update $\mathbf{A} + \mathbf{v}\mathbf{v}^T$ may be written as $\mathbf{S} = cholupdate(\mathbf{R}, \mathbf{v})$.

$$\widehat{\boldsymbol{\theta}}_{k|k} = \widehat{\boldsymbol{\theta}}_{k|k-1} + \mathbf{K}_k(\mathbf{z}^{obs} - \widehat{\mathbf{z}}_{k|k-1})$$

$$\mathbf{U} = \mathbf{K}_k \mathbf{S}_{k|k-1}^z$$

$$\mathbf{A}_{k|k}^{\theta} = cholupdate(\mathbf{A}_{k|k-1}^{\theta}, \mathbf{U}, -1)$$

$$end$$

The hybrid UKF- MHS algorithm

The hybrid UKF-MHS algorithm is a local-global optimization algorithm which takes advantage of the virtues of the two well-known optimization algorithms to reduce the simulation time of the optimization process without compromising the accuracy of the solutions provided (Naranjo-Pérez *et al.*, 2020).

The general layout of this algorithm is shown in Figure 2 and it may be summarized as follows: (i) the MHS algorithm proposes a set of candidate values for the parameters; (ii) for each candidate value, the UKF algorithm obtains the value of $\boldsymbol{\theta}_{k|k}$; (iii) the different terms of the objective function are evaluated for each value of $\boldsymbol{\theta}_{k|k}$; (iv) the solutions are classified according to the non-dominating sorting technique; (v) the process is repeated iteratively until some convergence criterion is met; and (vi) finally the Pareto front is obtained.
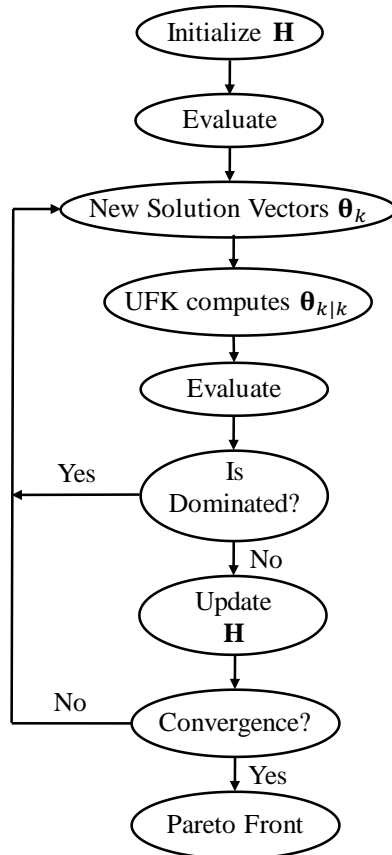
Application example: Parameter identification of the dynamic Winkler model of a real integral footbridge

Description of the structure and preliminary finite element model

As benchmark structure, a real integral footbridge located at Paradas (Seville, Spain) has been considered herein (Figure 3a). The footbridge is a steel-concrete composite integral structure with a single span of 12 m of length. The cross-section of the structure consists in a steel-concrete composite box-girder formed by a steel box-girder of 0.40 m of depth and a concrete slab of 0.2 x 2.5 m^2. The two abutments are supported on 4 micropiles with a diameter, D_p, of 0.2 m and a length, L_p, of 15 m (Figure 3b).
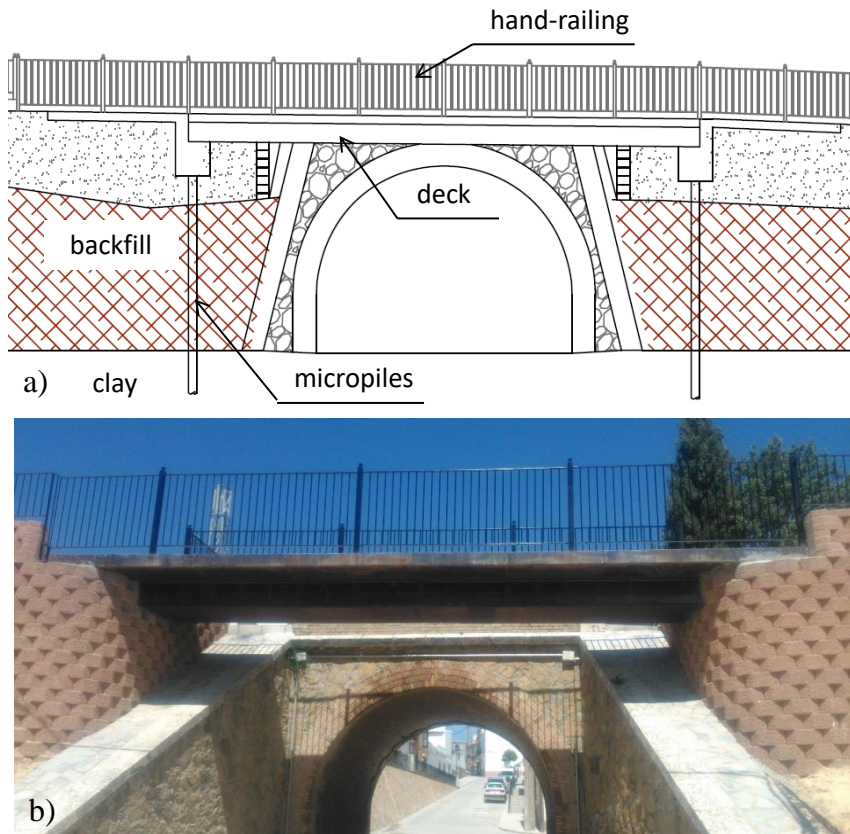
Figure 3. Lateral view of Paradas footbridge (Seville, Spain). a) Graphical representation and b) Footbridge in its current state.

A preliminary FE model of the footbridge was built using the FE analysis package Ansys (Ansys, 2019). The concrete slab, the steel box-girder, the hand-railing and the

micropiles were modelled by 3D beam elements (BEAM188). The mesh consists of 0.25 m long elements for the concrete slab and the steel box-girder and 0.50 m long for the hand-railing and the micropiles. The SSI has been simulated by 1D spring-damper elements (COMBIN14) according to the model proposed by Krizek (2011) for this type of structure. A spring-damper element was placed at each node of the different micropiles. The tip of each micropile was assumed to be simply supported. The FE model of the overall structure is shown in Figure 4c.

The mechanical properties of both the concrete and the steel were established according to the Eurocode 4 (Eurocode 4, 1994). For the steel; density, $\rho_{st} = 7850$ kg/m^3, Young's modulus, $E_{st} = 2.1 \cdot 10^{11}$ N/m^2 and Poisson's ratio, $\nu_{st} = 0.3$; and for the concrete, density, $\rho_c = 2500$ kg/m^{3,}, Young's modulus, $E_c = 3 \cdot 10^{10}$ N/m^2 and Poisson's ratio, $\nu_c = 0.2$. A global structural damping ratio was considered for all the vibration modes. The value of this damping ratio was taken from the Synpex guidelines (Butz *et al.*, 2007), which proposes $\xi_{num} = 0.6$ % for steel-concrete composite footbridges.

According to the geotechnical report of the design project, the vertical profile of the soil was characterised by: (i) a first backfill material layer about 5 m of thickness and (ii) a subsequent clay layer. The abutments were embedded around 0.9 m in the soil. The following mechanical properties were assumed for the simulation of the SSI phenomenon (according to the recommendations of the geotechnical report): (i) for the backfill material; density, $\rho_{s,1} = 1800$ kg/m^3, Young's modulus, $E_{s,1} = 7.2 \cdot 10^8$ N/m^2, Poisson's ratio, $\nu_{s,1} = 0.35$ and ballast coefficient, $k_{b1} = 4 \cdot 10^7$ N/m^3; and (ii) for the clay layer, density, $\rho_{s,2} = 1800$ kg/m^3, Young's modulus, $E_{s,2} = 4 \cdot 10^7$ N/m^2, Poisson's ratio, $\nu_{s,2} = 0.3$ and ballast coefficient, $k_{b2} = 1.2 \cdot 10^8$ N/m^3.

The SSI phenomenon was simulated considering two interaction sub-models: (i) the soil-abutment interaction (direct foundation) and (ii) the soil-pile interaction (deep foundation).

The soil-abutment interaction was simulated by six spring elements (3 translations and 3 rotations) in each abutment. The stiffness of these springs has been calculated using the Eqns. (1) to (12) according to the proposal of Gazetas (1991). Additionally, each abutment was modelled by a massive node which simulated its mechanical properties (Figure 4a and Figure 4d).

The soil-pile interaction was simulated via the dynamic Winkler model (Figure 4b). The equivalent spring-damper elements were placed along the length of the pile. Thus, the stiffness, k, of each spring-damper element was computing using the Eqn. (13) and the damping, c, of each spring-damper element was computing using the Eqn. (16) which relates this magnitude with the mechanical properties of the soil.
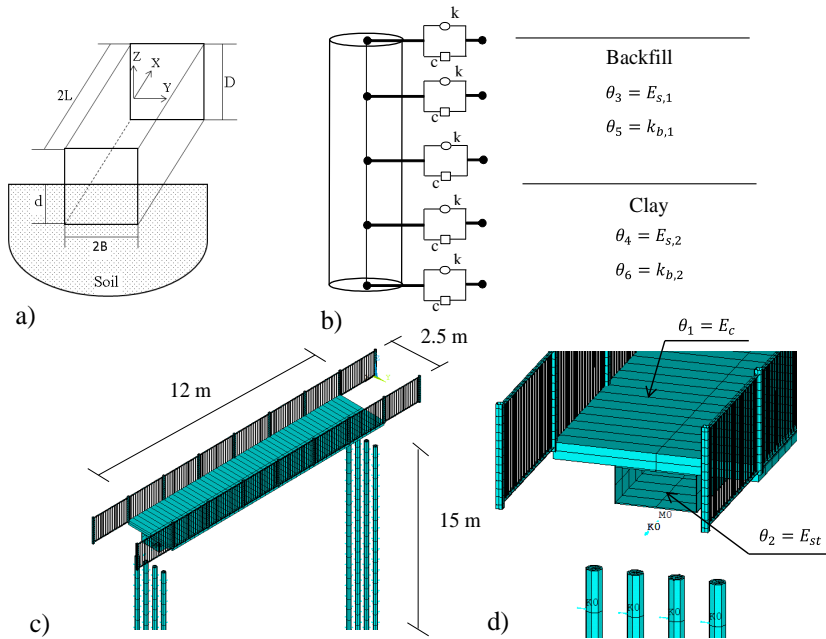
Figure 4. Numerical models considered in this study: a) geometric definition of the direct foundation of each abutment b) dynamic Winkler model for modelling the soil-pile interaction, c) overall view of the FE model of the Paradas footbridge and d) detail of the FE model showing the concrete-slab, steel box girder, abutment (as a massive node), hand-railing and micropiles.

Subsequently, a numerical FE damped modal analysis was performed in order to obtain the modal properties of the footbridge. As result of this analysis, Table 1 shows the first three numerical natural frequencies of the footbridge, $f_{num,j}(\boldsymbol{\theta})$ (being j the considered vibration mode). Additionally, Figure 5b illustrates the first three numerical vibration modes of the considered footbridge (labelled as *Num.*).

Ambient vibration test, operational modal analysis and parameters identification

Subsequently, the modal properties of the footbridge were identified experimentally via the signal processing of the measures recorded during an ambient vibration test. In this experimental test, the response of the structure under ambient vibration was recorded at different points. Concretely, a gridline with 2x7 points was instrumented. The points were separated longitudinally 2 m and transversally 2.5 m. Three high sensitive triaxial force-balanced accelerometers (Kinemetrics Episnesor ES-T) were used during this ambient test. Two of these devices were considered as references, at two fixed locations, and the other accelerometer was moving to the defined points (Figure 5a). Twelve set-ups, with a duration of 600 s and a sampling frequency of 100 Hz, were performed.
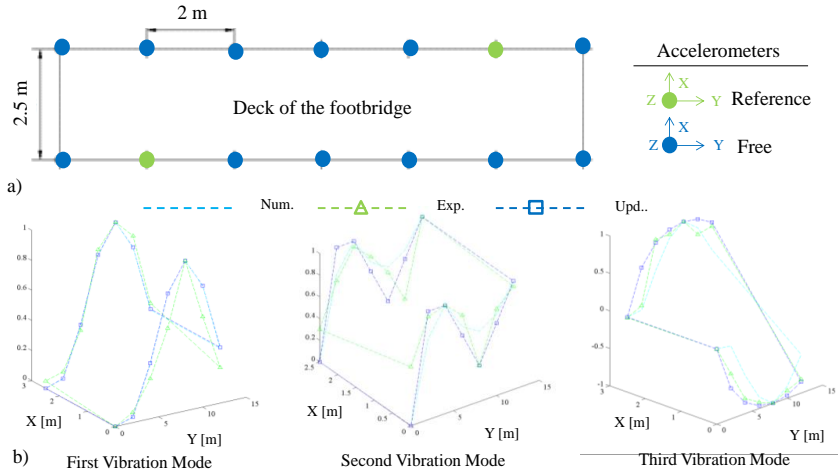
Figure 5. a) Layout of the ambient vibration test and b) Numerical ($Num.$), experimental ($Exp.$) and updated ($Upd.$) vibration modes.

The experimental identification of the modal properties was conducted in time domain using the UPC-Merge algorithm, as it is implemented in the software Artemis (Artemis, 2016). This identification method, framed within the Stochastic Subspace Identification method (Magalhães and Cunha, 2011), merges the records of the different setups which allows improving the estimates of the experimental modal properties of the footbridge (Döhler *et al.*, 2010). The three first identified natural frequencies, $f_{\text{exp,j}}$, and associated damping ratios, $\zeta_{\text{exp,j}}$ (Magalhães *et al.*, 2010) are shown in Table 1. Figure 5b also illustrates the first three experimental vibration modes of the considered footbridge (labelled as $Exp.$).

In order to determine the correlation between the numerical and experimental modal properties of this footbridge, the relative difference between natural frequencies, $\Delta f_{exp,j}^{numj}(\boldsymbol{\theta})$, damping ratios, $\Delta\zeta_{exp,j}^{num,j}(\boldsymbol{\theta})$, and the $MAC_{exp,j}^{num,j}(\boldsymbol{\theta})$ ratios are also shown in Table 1.

Table 1. Numerical, $f_{\text{num,j}}(\boldsymbol{\theta})$, and experimental, $f_{\text{exp,j}}$, natural frequencies, numerical, $\zeta_{\text{num,j}}(\boldsymbol{\theta})$, and experimental, $\zeta_{\text{exp,j}}$, damping ratios, relative differences between natural frequencies, $\Delta f_{exp,j}^{numj}(\boldsymbol{\theta})$, and damping ratios, $\Delta\zeta_{exp,j}^{num,j}(\boldsymbol{\theta})$, and the $MAC_{exp,j}^{num,j}(\boldsymbol{\theta})$ ratios.

Mode	$f_{\text{num,j}}(\boldsymbol{\theta})$ [Hz]	$f_{\text{exp,j}}$ [Hz]	$\zeta_{\text{num,j}}(\boldsymbol{\theta})$ [%]	$\zeta_{\text{exp,j}}$ [%]	$\Delta f_{exp,j}^{numj}(\boldsymbol{\theta})$ [%]	$\Delta\zeta_{exp,j}^{num,j}(\boldsymbol{\theta})$ [%]	$MAC_{exp,j}^{num,j}(\boldsymbol{\theta})$ [-]
1	15.322	15.602	3.103	4.650	1.795	33.268	0.975
2	32.179	35.971	1.121	1.049	10.542	6.863	0.692
3	38.614	40.017	0.700	4.846	3.506	85.555	0.907

Thus, Table 1 shows a bad correlation between the numerical and experimental modal properties of the footbridge: (i) the relative difference between the second

numerical and experimental natural frequency, $\Delta f_{exp,2}^{num2}(\boldsymbol{\theta})$, is greater than 5%; (ii) the $MAC_{exp,2}^{num,2}(\boldsymbol{\theta})$ ratio of the second vibration mode is clearly lower than 0.90 (Živanović *et al.*, 2007); and (iii) the relative differences of the damping ratios among the first and third vibrations modes are greater than 30 %.

Hence, the value of the physical parameters of the FE model originally considered to simulate numerically the dynamic behaviour of the footbridge are not adequate and a parameter identification method must be used to improve the performance of this numerical model.

In this manner, the above mentioned parameters identification method was implemented in the mathematical package Matlab (Matlab, 2019) to perform the identification process. As one of the main factors, which may have a greater influence on the dynamic behaviour of the structure, is the SSI phenomenon, the parameter identification method focused on the parameter identification of the dynamic Winkler model.

Thus, the main objective of this identification process is to estimate the value of the most relevant physical parameters of the numerical model which minimises the relative differences between the numerical and experimental modal properties of the footbridge. In order to select these parameters, two criteria were considered: (i) to consider those physical parameters which mobilize more modal strain energy (Fox and Kapoor 1968); and (ii) to take into account those parameters which characterize the SSI phenomenon. As result of this selection process, a vector of six parameters, $\boldsymbol{\theta}$, was considered (Figure 4): (i) the Young's modulus of the concrete, E_c; (ii) the Young's modulus of the steel, E_{st}; (iii) the Young's modulus of the backfill, $E_{s,1}$; (iv) the Young's modulus of the clay, $E_{s,2}$; (v) the ballast coefficient of the backfill, $k_{b,1}$; and (vi) the ballast coefficient of the clay, $k_{b,2}$. In relation to these parameters, it is necessary to remark that there is a clear relationship between the Young's modulus of the soil and the damping coefficient of the dynamic Winkler model (as it has been expressed by Eqn. (16)). Therefore, it may be assumed that the first two parameters characterize the behaviour of the structure and the remaining four parameters characterize the SSI phenomenon.

Additionally, a search domain has been established in order to avoid ill-conditioning problems and to ensure that the estimative of these parameters maintains an adequate physical meaning. In this sense, three facts must be remarked: (i) the upper bound of the Young's modulus of the steel is strangely high because the stiffeners and diaphragms have been modelled in a simplified way, only an equivalent added mass has been included for this purpose; (ii) the lower and upper bound of the search domain of the parameters which characterize the behaviour of the soil have been established according to the recommendations of the European standards (Eurocode 7, 2004); and (iii) the upper bound of Young's modulus of the backfill was increased in order to simulate the effect of the dynamic compaction on this layer.

The lower, $\boldsymbol{\theta_l}$, and upper, $\boldsymbol{\theta_u}$, bounds of the search domain of each considered physical parameter are shown in Table 2.

Table 2. Bounds (lower, $\boldsymbol{\theta_l}$, and upper, $\boldsymbol{\theta_u}$, bounds) of the search domain for each considered physical parameter and the corresponding updated value, $\boldsymbol{\theta_{upd}}$, after the identification process.

$\boldsymbol{\theta}$	Definition	$\boldsymbol{\theta_l}$	$\boldsymbol{\theta_{upd}}$	$\boldsymbol{\theta_u}$

θ_1	Concrete Young's Modulus E_c [N/m^2]	$2.7 \cdot 10^{10}$	$3.67 \cdot 10^{10}$	$4 \cdot 10^{10}$
θ_2	Steel Young's Modulus, E_{st} [N/m^2]	$1.9 \cdot 10^{11}$	$2.28 \cdot 10^{11}$	$2.4 \cdot 10^{11}$
θ_3	Backfill Young's Modulus, $E_{s,1}$ [N/m^2]	$3 \cdot 10^6$	$7.77 \cdot 10^8$	$4 \cdot 10^9$
θ_4	Clay Young's Modulus, $E_{s,2}$ [N/m^2]	$3 \cdot 10^6$	$3.5 \cdot 10^7$	$4.8 \cdot 10^7$
θ_5	Backfill Ballast Coefficient, $k_{b,1}$ [N/m^3]	$1.3 \cdot 10^7$	$4.16 \cdot 10^7$	$2.1 \cdot 10^8$
θ_6	Clay Ballast Coefficient, $k_{b,2}$ [N/m^3]	$1.3 \cdot 10^7$	$1.27 \cdot 10^8$	$2.1 \cdot 10^8$

An initial population of 40 harmonies (parameter vectors) were generated. For each harmony, $\boldsymbol{\theta}_k$, the UKF algorithm obtains the value of $\boldsymbol{\theta}_{k|k}$. For this purpose, the number of iterations of the UKF algorithm is set to 5. The measurement noise covariance matrix is derived from the standard deviations provided by the experimental identification of the modal properties. The vector of observed measurements, $\mathbf{d}_{obs}$, was defined as follows: (i) the first three terms and the last three terms corresponded to the three experimental natural frequencies and modal damping ratios respectively; (ii) the second three terms were associated with the mode shapes; and (iii) as the residual of the mode shapes is defined in terms of the *MAC* ratios and therefore the objective is to make these values closer to one, then these three second terms were equal to one. The parameter, λ, which defines the sigma points, was defined as $\lambda = 0.0001$ according to the recommendations provided by Astroza *et al.* (2016) and the scalar factor was set as, $\gamma = 0.99$, following the recommendations provided by Van Der Merwe and Wan, (2001). The non-dominated solutions are stored in the matrix $\mathbf{H}$. Then, an iterative process with a total number of iterations of 20 was run.

In each iteration, a new set of 20 individuals (harmonies) was created. For each harmony, the UKF algorithm calculates $\boldsymbol{\theta}_{k|k}$. Then, the above mentioned FE model was updated considering the parameters $\boldsymbol{\theta}_{k|k}$ as inputs. Subsequently, the numerical natural frequencies, mode shapes and damping ratios were obtained considered this updated FE model. Next, the three objective functions were computed and the dominated solutions were neglected. When the stop criterion (maximum number of iterations) was reached, the optimal Pareto front was obtained.

Finally, a decision making problem was solved to select the best solution among the different elements of the Pareto front. As it was mentioned above, the criterion provided by Jin *et al.* (2014) has been considered herein. Thus, the point estimation, $\boldsymbol{\theta}_{\mathbf{upd}}$, of the physical parameters of the model after the identification process is shown in Table 2. Additionally, Figure 5b illustrates the first three numerical vibration modes of the considered footbridge after the parameter identification process (labelled as $Upd.$),

Once the identification process was finished, it was possible to estimate the value of the parameters of the dynamic Winkler model. Thus, the parameter of the spring-damper elements for each layer may be estimated as: (i) for the backfill layer, $k_1 = 4.16 \cdot 10^6$ N/m and $c_1 = 7.93 \cdot 10^5$ sN/m; and (ii) for the clay layer, $k_2 = 1.27 \cdot 10^7$ N/m and $c_2 = 1.68 \cdot 10^5$ sN/m.

Table 3. Updated, $f_{\text{upd},j}(\boldsymbol{\theta})$, and experimental, $f_{\text{exp},j}$, natural frequencies, updated, $\zeta_{\text{upd},j}(\boldsymbol{\theta})$, and experimental, $\zeta_{\text{exp},j}$, damping ratios, relative differences between natural frequencies, $\Delta f_{exp,j}^{updj}(\boldsymbol{\theta})$, and damping ratios, $\Delta \zeta_{exp,j}^{upd,j}(\boldsymbol{\theta})$, and the $MAC_{exp,j}^{upd,j}(\boldsymbol{\theta})$ ratios.

Mode	$f_{\text{upd},j}(\boldsymbol{\theta})$ [Hz]	$f_{\text{exp},j}$ [Hz]	$\zeta_{\text{upd},j}(\boldsymbol{\theta})$ [%]	$\zeta_{\text{exp},j}$ [%]	$\Delta f_{exp,j}^{upd,j}(\boldsymbol{\theta})$ [%]	$\Delta \xi_{exp,j}^{upd,j}(\boldsymbol{\theta})$ [%]	$MAC_{exp,j}^{upd,j}(\boldsymbol{\theta})$ [-]
1	16.380	15.602	4.588	4.650	4.987	1.333	0.975
2	35.377	35.971	1.058	1.049	1.651	0.858	0.907
3	40.599	40.017	4.701	4.846	1.454	2.992	0.964

Thus, the adequate performance of the proposed identification method is supported by three facts:

(i) the good correlation between the numerically updated and experimental modal properties of the footbridge that follows the identification process: the relative differences, $\Delta f_{exp,j}^{upd,j}(\boldsymbol{\theta})$, between the numerical and experimental natural frequencies were lower than 5 %, the relative differences, $\Delta \xi_{exp,j}^{upd,j}(\boldsymbol{\theta})$, between the numerical and experimental damping ratios were lower than 3%, and the $MAC_{exp,j}^{upd,j}(\boldsymbol{\theta})$ ratios were greater than 0.90;

(ii) the good agreement observed between the parameters of the dynamic Winkler model provided by this proposal and the values recommended by European standards (Eurocode 7, 2004); and

(iii) the good correlation between the damping coefficient of the soil obtained by this identification method and the values reported by other studies in the literature (Hashash and Park, 2001).

Finally, one additional conclusion can be drawn from this study: the importance of considering the SSI phenomenon in the modelling of integral bridges. As Table 3 illustrates, the experimental damping ratios associated with the three identified vibration modes are greater than the values recommended by international guidelines (Butz *et al.*, 2007). Therefore, the adequate characterization of the dynamic Winkler model plays a key role when simulating the actual behaviour of this type of civil engineering structures.

Conclusions

In this paper, the experimental identification of the parameters of the dynamic Winkler soil-structure interaction model (stiffness and damping coefficients) has been addressed based on the extension of a recently developed hybrid UKF-MHS algorithm. Implementation details of the proposed approach have been discussed in detail and its performance has been illustrated via a real engineering case-study. According to this proposal, the parameter identification problem is transformed successively into two problems: (i) a FE model updating problem; and (ii) a multi-objective optimization problem.

In this manner, the parameter identification problem has been formulated in terms of a multi-objective optimization problem, where the objective function to be minimized is defined in terms of the relative differences (residuals) between the numerical and

experimental modal properties of the soil-structure system. To this end, three types of residuals have been considered: (i) residuals associated with the natural frequencies; (ii) residuals associated with the damping ratios; and (iii) residuals associated with the vibration modes. The numerical behaviour of the system has been simulated using the FE method, whilst its experimental modal properties have been identified via the signal processing of the dynamic response of the structure recorded during an experimental vibration test. As design variables, the most relevant physical parameters of the structure were adopted. The optimization has been conducted using a hybrid UKF-MHS algorithm.

The performance of the method has been validated via its application to a real steel-concrete composite integral footbridge, for which the parameters of the dynamic Winkler model have been identified experimentally. The obtained results illustrate: (i) the good agreement between the numerical and experimental modal properties of the structure after the identification process; and (ii) the good correlation between the values of the Winkler parameters obtained according to this proposal and the values recommended by European standards (Eurocode 7, 2004).

The proposed approach exhibits three main advantages when addressing the parameter identification of the dynamic Winkler SSI model: (i) the parameter identification can be performed indirectly based on the solution of an inverse problem defined in terms of the overall numerical and experimental behaviour of the structure; (ii) no complex geotechnical test are needed to perform the parameter identification; and (iii) the method is quite simple and may be straightforwardly implemented for practical engineering applications.

In conclusion, the proposed method becomes a valid tool to characterize the parameters of the dynamic SSI Winkler model for practical engineering applications. Nevertheless, additional studies are recommended in order to better characterize the parameters of the dynamic Winkler model for different types of civil engineering structures supported on different types of soils.

Declaration of Conflicting Interests

The authors declare no potential conflicts of interest with respect to the research, authorship, and publication of this paper.

Acknowledgements

Funding

References

Alamo GM, Martínez-Castro AE, Padrón LA, Aznárez JJ, Gallego R, Maeso O (2016). Efficient numerical model for the computation of impedance functions of inclined pile groups in layered soils. *Engineering Structures*; 126: 379–390. doi: https://doi.org/10.1016/j.engstruct.2016.07.047.

Allemang RJ, Brown DL (1982). A correlation coefficient for modal vector analysis. Proc. 1st Int. Modal Anal. Conf., Vol. 1, Orlando: Union College Press, p. 110–116.

Allotey, N., El Naggar, M.H. (2008). Generalized dynamic Winkler model for nonlinear soil–structure interaction analysis. *Canadian Geotechnical Journal,* 45(4): 560-573. doi: https://doi.org/10.1139/T07-106.

Ansys Mechanical 19.0. Ansys Inc 2019. https://www.ansys.com/.

Arai K, Ohta H, Kojima K (1984). Estimation of soil parameters based on monitored movement of subsoil under consolidation. *Soils and Foundations*; 24(4): 95–108. doi: https://doi.org/10.3208/sandf1972.24.4_95.

ARTeMIS Modal 2016. http://www.svibs.com/

Astroza R, Nguyen LT, Nestorović T (2016). Finite element model updating using simulated annealing hybridized with unscented Kalman filter. *Computers and Structures*; 177: 176–191. doi: https://doi.org/10.1016/j.compstruc.2016.09.001.

Badsar SA, Schevenels M, Haegeman W, Degrande G (2010). Determination of the material damping ratio in the soil from SASW tests using the half-power bandwidth method. *Geophysical Journal International*, 182: 1493–508. doi: http://dx.doi.org/10.1111/j.1365-246X.2010.04690.x.

Berger E, Mahi SA, Pyke R (1977). Simplified method for evaluating soil-pile-structure interaction effects. Offshore Technol. Conf., Offshore Technology Conference.

Butz CH., Heinemeyer CH.; Goldack A., Keil A., Lukic M., Caetano E., Cunha A. (2007). "Advanced Load Models for Synchronous Pedestrian Excitation and Optimised Design Guidelines for Steel Footbridges (SYNPEX)". RFCS-Research Project RFS-CR-03019.

Campanella RG, Stewart WP (1992). Seismic cone analysis using digital signal processing for dynamic site characterization. *Canadian Geotechnical Journal*, 29: 477-486. doi: https://doi.org/10.1139/t92-052.

Chen, Z (2003). Bayesian filtering: From Kalman filters to particle filters, and beyond. *Statistics*, 182: 1–69. doi: https://doi.org/10.1080/02331880309257.

Cheng Z, Leong E.C. (2018). Determination of damping ratios for soils using bender element tests. *Soil Dynamic and Earthquake Engineering,* 111: 8-13. doi: https://doi.org/10.1016/j.soildyn.2018.04.016.

Deb K, Pratap A, Agarwal S, Meyarivan T (2002). A fast and elitist multi-objective genetic algorithm: NSGA-II. *IEEE Transactions on Evolutionary Computation*, 6: 182–197. doi: https://doi.org/10.1109/4235.996017.

Drnevich VP, Hardin BO, Shippy DJ (1978). Modulus and Damping of Soils by the Resonant-Column Method. Dynamic Geotechnical Testing. doi: http://dx.doi.org/10.1520/STP35673S

Döhler M., Andersen P, Mevel L (2010). Data merging for Multi Setup Operational Modal Analysis with Data Driven SSI. 28th International Modal Analysis Conference.

Eurocode 4 (1994): Design of Composite Steel and Concrete Structures. CEN.

Eurocode 7 (2004): Geotechnical design - Part 1: General rules. CEN.

Fox R, Kapoor M (1968). Rates of change of eigenvalues and eigenvectors. *AIAA Journal*, 6: 2426–2429. doi: https://dx.doi.org/doi.org/10.2514/3.5008.

Gazetas G (1991). Formulas and charts for impedances of surface and embedded foundations. *Journal of Geotechnical Engineering*, 117: 1363–1381. doi: https://doi.org/10.1061/(ASCE)0733-9410(1991)117:9(1363).

Gazetas G, Dobry R (1984). Horizontal response of piles in layered soils. *Journal of Geotechnical Engineering*, 110:20–40. doi: https://doi.org/10.1061/(ASCE)0733-9410(1984)110:1(20).

Geem ZW, Kim JH, Loganathan GV (2001). A new heuristic optimization algorithm: harmony search. *Simulation*, 76: 60–68. doi: https://doi.org/10.1177/003754970107600201.

Gens A, Ledesma A, Alonso EE (1996). Estimation of Parameters in Geotechnical Backanalysis: II. Application to a Tunnel Excavation Problem. *Computers and Geotechnics*, 18(1): 29-46. doi: https://doi.org/10.1016/0266-352X(95)00022-3.

Hashash YMA, Park D (2001). Non-linear one-dimensional seismic ground motion propagation in the Mississippi embayment. *Engineering Geology,* 62: 185-206. doi: https://doi.org/10.1016/S0013-7952(01)00061-8.

Hirai, H (2011). A Winkler model approach for vertically and laterally loaded piles in nonhomogeneous soil. *International Journal for Numerical and Analytical Method in Geomechanics*, 36(17): 1869-1897. doi: https://doi.org/10.1002/nag.1078.

Jazwinski, AH (1970). Stochastic processes and filtering theory, Academic Press.

Jimenez-Alonso JF, Hudson E, Pavic A, Sáez A (2017). Maximum likelihood methods for finite element model updating of civil engineering structures: A comparative study. In: Proceedings of 4th International Conference on Mechanical Models in Structural Engineering, Madrid, Spain.

Jin S, Cho S, Jung H, Lee J and Yun C (2014) A new multi-objective approach to finite element model updating. *Journal of Sound and Vibration*, 333(11): 2323–2338. doi: https://doi.org/10.1016/j.jsv.2014.01.015.

Julier SJ, Uhlmann JK (1997). New extension of the Kalman filter to nonlinear systems. Signal Process. Sens. Fusion Target Recognit. VI, vol. 3068, International Society for Optics and Photonics, p. 182–194. doi: https://doi.org/10.1117/12.280797.

Julier SJ, Uhlmann JK (2004). Corrections to "Unscented filtering and nonlinear estimation". Proc IEEE; 92(12): 1958-1958. doi: https://doi.org/10.1109/JPROC.2004.837637.

Kalman RE (1960). A new approach to linear filtering and prediction problems. *Journal of Basic Engineering*, 82: 35–45. doi : https://doi.org/10.1115/1.3662552.

Karl L, Haegeman W, Degrande G (2006). Determination of the material damping ratio and the shear wave velocity with the Seismic Cone Penetration Test. *Soil Dynamic and Earthquake Engineering*, 26:1111–1126. doi: http://dx.doi.org/10.1016/j.soildyn.2006.03.001.

Krizek J (2011). Soil–structure interaction of integral bridges. *Structural Engineering International*, 21: 169–174. doi: https://doi.org/10.2749/101686611X12994961034372.

Lai CG, Rix GJ (1998). Simultaneous Inversion of Rayleigh Phase Velocity and Attenuation for Near-Surface Site Characterization. Georgia Institute of Technology. National Science Foundation and U.S. Geological Survey.

Ledesma A, Gens A, Alonso EE (1996a). Estimation of parameters in geotechnical backanalysis—I. Maximum likelihood approach. *Computers and Geotechnics*, 18: 1–27. doi: https://doi.org/10.1016/0266-352X(95)00021-2.

Ledesma A, Gens A, Alonso EE (1996b). Parameter and variance estimation in geotechnical backanalysis using prior information. *International Journal for Numerical and Analytical Methods in Geomechanics*, 20: 119–141. doi:

https://doi.org/10.1002/(SICI)1096-9853(199602)20:2<119::AID-NAG810>3.0.CO;2-L.

Lee J-H, Lee J-J, Choi J-S, Yun C-B (2016). A Semi-Analytical Approach to Predict Ground Vibration by Identification of Soil Properties and Train-Transit Loads. *Advances in Structural Engineering*, 15(6): 1013-1029. doi: https://doi.org/10.1260/1369-4332.15.6.1013.

Magalhães F, Cunha A (2011). Explaining operational modal analysis with data from an arch bridge. *Mechanical Systems and Signal Processing*, 25: 1431–1450. doi: https://doi.org/10.1016/j.ymssp.2010.08.001.

Magalhães F, Cunha A, Caetano E, Brincker R (2010). Damping estimation using free decays and ambient vibration tests. *Mechanical Systems and Signal Processing*, 24:1274–1290. doi: https://doi.org/10.1016/j.ymssp.2009.02.011.

Maia NMM, Silva JMM, He J and et al. (1997). Theoretical and Experimental Modal Analysis, Research studies Press Ltd., Somerset, England.

Maier G, Gioda G (1982). Optimization methods for parametric identification of geotechnical systems. Numerical Methods in Geomechanics, Springer; 1982, p. 273–304. doi: https://doi.org/10.1007/978-94-009-7895-9_12.

Marwala T. (2010). Finite-Element-Model Updating Using Computational Intelligence Techniques. Applications to Structural Dynamics, p. 231. Springer, London.

Matlab R2019a http://www.mathworks.com/

Mottershead JE, Link M, Friswell MI (2011). The sensitivity method in finite element model updating: a tutorial. *Mechanical Systems and Signal Processing*, 25: 2275-2296. doi: https://doi.org/10.1016/j.ymssp.2010.10.012.

Naranjo-Pérez J, Jiménez-Alonso JF, Pavic A, Sáez A. (2020). Finite-element-model updating of civil engineering structures using a hybrid UKF-HS algorithm. *Structure and Infrastructure Engineering* (accepted for publication).

Nguyen LT, Nestorović T (2015). Nonlinear Kalman filters for model calibration of soil parameters for geomechanical modeling in mechanized tunneling. *Journal of Computing in Civil Engineering*; 30(2): 04015025. doi: https://doi.org/10.1061/(ASCE)CP.1943-5487.0000495.

Novak M (1974). Dynamic stiffness and damping of piles. *Canadian Geotechnical Journal*, 11: 574–598. doi: https://doi.org/10.1139/t74-059.

Rao CR, Toutenburg H, Fieger A (2007). Linear Models and Generalizations: Least Squares and Alternatives. 2nd ed. Springer; 2007.

Rodriguez J, Martinez F, Marti J (2011). Integral bridge for high-speed railway. *Structural Engineering International*, 21: 297–303. doi: https://doi.org/10.2749/101686611X13049248219881.

Srinivas N, Deb K (1994). Multiobjective optimization using nondominated sorting in genetic algorithms. *Evolutionary Computation*; 2: 221–248. doi: https://doi.org/10.1162/evco.1994.2.3.221.

Tabatabaiefar SHR, Fatahi B, Samali B (2016). Numerical and Experimental Investigations on Seismic Response of Building Frames under Influence of Soil-Structure Interaction. *Advances in Structural Engineering*, 17(1): 109-130. doi: https://doi.org/10.1260/1369-4332.17.1.109.

Tajimi H (1966). Earthquake response of foundation structures. Rep. of Fac. Sci. Eng. Nihon University.

Tarantola A (2005). Inverse problem theory and methods for model parameter estimation. vol. 89. SIAM. doi: https://doi.org/10.1137/1.9780898717921.

Terejanu GA (2011). Unscented Kalman filter tutorial. Univ Buffalo Buffalo.

Thavaraj T (2000). Seismic analysis of pile foundations for bridges. PhD Thesis. University of British Columbia.

Van Der Merwe R, Wan EA (2001). The square-root unscented Kalman filter for state and parameter-estimation. 2001 IEEE International Conference on Acoustics, Speech, and Signal Processing. Proceedings, p. 3461–3464. doi: http://dx.doi.org/10.1109/ICASSP.2001.940586.

Wan EA, Van Der Merwe R (2000). The unscented Kalman filter for nonlinear estimation. Proceedings of the IEEE 2000 Adaptive Systems for Signal Processing, Communications, and Control Symposium; p. 153–158. doi: http://dx.doi.org/10.1109/ASSPCC.2000.882463.

Wan EA, Van Der Merwe R, Nelson AT (2000). Dual estimation and the unscented transformation. Proceedings of the 12th International Conference on Neural Information Processing Systems, p. 666–672.

Wang, X, Gao, X-Z, Zenger, K (2015). An Introduction to Harmony Search Optimization Method. Springer International Publishing.

Yang X-S, Koziel S (2011). Computational optimization and applications in engineering and industry. vol. 359. Springer Science & Business Media.

Yazdchi M, Khalili N, Valliappan S (1999). Dynamic soil–structure interaction analysis via coupled finite-element–boundary-element method. *Soil Dynamic and Earthquake Engineering*, 18: 499–517. doi: http://dx.doi.org/10.1016/S0267-7261(99)00019-6.

Živanović S, Pavic A, Reynolds, P (2007). Finite element modelling and updating of a lively footbridge: The complete process. *Journal of Sound and Vibration*, 301 (1-2): 126-145 doi: https://doi.org/10.1016/j.jsv.2006.09.024.

Apéndice E
Articulo E

Infantes M, Naranjo-Pérez J, Jiménez-Alonso JF, Sáez A (2019). Determining the Best Pareto-solution in a Multi-Objective Approach for Model Updating. IABSE Symposium, Guimaraes 2019: Towards a Resilient Built Environment Risk and Asset Management – Report pp. 523-530.

Determining the Best Pareto-solution in a Multi-Objective Approach for Model Updating

María Infantes

Department of Mechanics, Universidad de Córdoba, Cordoba, Spain

Javier Naranjo-Pérez, Andrés Sáez

Department of Continuum Mechanics, Universidad de Sevilla, Seville, Spain

Javier F Jiménez-Alonso

Department of Building Structures, Universidad de Sevilla, Seville, Spain

Contacting author: me2mainm@uco.es

Abstract

Using a multi-objective optimization algorithm avoid the use of weighting factors to balance the different residuals in a finite element model updating procedure under the maximum likelihood method. By using this approach, the fittest model is not unique and a set of solutions that form a curve, so-called Pareto optimal front, is obtained. Within this paper, first a review of the state of the art on the criteria used to determine the most adequate model among all the solutions of the Pareto front is presented. Subsequently, a case study of a real footbridge is considered. A finite element model of the footbridge is updated based on its experimental modal parameters. The Non-Dominated Sorting Genetic Algorithm is used to obtain the Pareto front. Since all the solutions in the Pareto front are non-dominated, the selection of the best candidate requires a reasonable criterion. Herein, different procedures to select the best updated model are discussed.

Keywords: model updating; footbridge; multi-objective optimization; decision making; bend angle.

1. Introduction

Model updating emerged in the 1990 as a tool of great importance for the construction, design and maintenance of mechanical systems and civil engineering structures. Essentially, this technique involves defining numerical models that capture reality as accurately as possible. The classical reference by Friswell and Motterhead [1] introduces the first group of techniques used for Finite Element (FE) model updating. The basic techniques use experimental vibration test results as reference for numerical solution. Once the experimental identification of the modal parameters of the considered structure is done, the main stages of a FE model updating procedure can be summarized as follows:

i. Experimental and FE model correlation. This correlation provides information about the discrepancies between both models. The most used correlations are: the natural frequency

relative differences, the comparison of mode shapes, the Modal Assurance Criterion (MAC).

ii. Updating parameters selection. In order to obtain a more accurate FE model, some parameters are changed in the updating process. Usually the selection is based on the most sensitive parameters which causes the discrepancy.

iii. Finite Element Model updating procedure. The correction process can be carried out by two basic approaches: 1) direct methods in which the mass and stiffness matrices are directly updated; 2) iterative methods, where parameters are gradually updated until the FE model reproduces the experimental results.

The iterative methods, which are the most extensively used, transform the updating process into an optimization problem. The objective function is defined in terms of the maximum likelihood method. According to this, the relative differences between the experimental and numerical modal parameters of the structure must be minimized. As optimization method, a nature-inspired algorithm is usually used.

2. Theoretical background

In conventional FE model updating, the objective is to minimize the relative differences between the numerical and experimental modal parameters of the considered structure. In most cases, two types of residues are established, one relating to natural frequencies ($r_{f,j}$) and the other to the shape of the vibration modes ($r_{s,jl}$). Although different expressions for these residues have been proposed in the literature, those used in the case study in section 4 are:

$$r_{f,j} = \frac{f_{NUM,j} - f_{EXP,j}}{f_{EXP,j}}, \; j = 1,...,m_f \qquad (1)$$

$$r_{s,jl} = \frac{\phi_{NUM,j}^l}{\phi_{NUM,j}^r} - \frac{\phi_{EXP,j}^l}{\phi_{EXP,j}^r} \quad \begin{cases} j = 1,...,m_f \\ l = 1,...,m_s \end{cases} \qquad (2)$$

where $f_{NUM,j}$ and $f_{EXP,j}$ are the numerical and experimental natural frequencies of mode j and $\phi_{NUM,j}^l$ and $\phi_{EXP,j}^l$ are the numerical and experimental coordinate l of vibration mode j. The number of modes considered is m_f and m_s is the number of coordinates of each mode. The

superscript r denotes one of those m_s coordinates taken as reference for each mode.

In order to achieve the minimization of the previous residues, generally a single objective optimization technique is used. One of the concerns while defining the objective function is how to balance the residuals of the different modal properties, i.e. natural frequencies and mode shapes. This is usually overcome by adding weighting factors whose values are computed by means of a trial-and-error strategy. In this approach, the objective function is defined as:

$$f = \frac{1}{2}$$
$$\left(\left[\sum_{j=1}^{m_f} w_{f,j} \cdot r_{f,j}^2 \right]^{1/2} + \left[\sum_{j=1}^{m_f} \sum_l' \right.\right. \quad (3)$$

where $w_{f,j}$ and $w_{s,jl}$ are the weighting functions relative to the different natural frequencies and the coordinates of the vibration modes considered, respectively.

An alternative is to perform a multi-objective optimization in which the residuals of the modal parameters are minimized independently. Two or more objective functions are defined:

$$f_1 = \frac{1}{2} \left[\sum_{j=1}^{m_f} r_{f,j}^2 \right]^{1/2} \qquad (4)$$

$$f_2 = \frac{1}{2} \left[\sum_{j=1}^{m_f} \sum_{l=1}^{m_s} r_{s,jl}^2 \right]^{1/2} \qquad (5)$$

By using this approach, the fittest model is not unique and a set of solutions that form a curve, called Pareto optimal front, is obtained. A solution is called non-dominated if none of the objectives can be improved without sacrificing at least one other objective. There are many different multi-objectives optimization algorithms available in the literature [2]. Herein, the NSGA-II [3] is used. This evolutionary algorithm proceeds creating an initial set of random solutions. Then, different operators of selection, crossover and mutation are used to generate new solutions and two additional operators called *Non-Dominated Sorting* and *crowded comparison operator* are used to identify the non-dominated solutions. This last step is repeated until some stop criteria is satisfied.

3. Decision-Making Strategies

Multi-objective optimization deals with problems that involve more than one objective function to be optimized simultaneously. Generally, these objectives are conflicting and no single solution exist that optimizes each objective at once (c.f. Figure 1). This involves a multi-criteria decision-making discipline in order to choose a preferred solution among all the solution identified as Pareto optimal. The multi-criteria analysis main goal is to aid in the task of choosing solutions that best fit the interest of the decision maker (DM). These helping tools can be classified based on the time when the DM is consulted:

- *A priori* methods. These methods require that enough preference information is expressed before the optimization process.
- Interactive methods. The DM is expected to express preferences at each iteration of the optimization algorithm. As an example, there exist a variant of the NSGA-II, so-called TKR-NSGA-II [4], that introduces preferences throughout the performance.
- *A posteriori* methods. The DM has to introduce preferences after the optimization process.

A posteriori approach divides the problem into an optimization procedure and a decision-making process. The DM can select the most preferred solution provided with all the trade-off information. This last consideration, together with the simplicity of the algorithms compared to the other two approaches, make it the usual choice.

Decision-making techniques usually include preferences based on global interest and experience. There exist several ways of modelling DM preferences, including:

i. Trade-off between objectives.
ii. Goal specification.
iii. Ranking objectives, including outranking method.
iv. Fuzzy logic.
v. Attributes in the solution.

Methods ii to v, are subject to explicit knowledge by the DM about the significance of the different objectives. The reader is referred to [5] for further information about this modelling preferences methods.
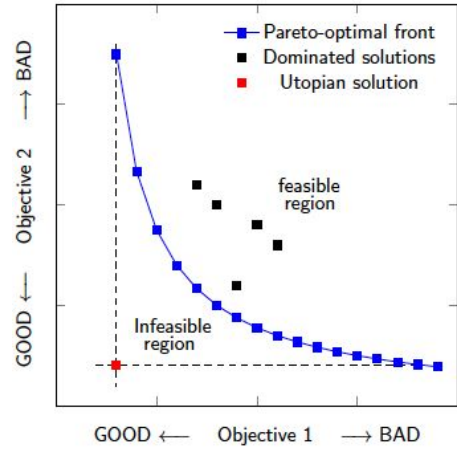
Figure 1. Bi-objective optimization trade-off representation

Trade-off methods are an intuitive formulation of preferences. The most interesting solutions of the Pareto front seem to be which for a small improvement in one objective would lead to a large deterioration in at least one other objective. This solution is named as knee point. There are several definitions of a knee point. Some of them are included below.

- Das [6]: normal boundary intersection method

DEFINITION*: Given a normalized Pareto front, two extreme points are used to construct a boundary line. The Pareto-optimal solution having the maximum distance to the boundary line along the normal direction is defined as the knee point.*

- Branke et al. [7]: reflex-angle method

Consider the reflex angle given by:

$$\theta(\boldsymbol{f}, \boldsymbol{f^L}, \boldsymbol{f^R}) = \theta^L + \pi - \theta^R \tag{6}$$

$$\theta^L = \tan^{-1} \frac{f_2^L - f_2}{f_1 - f_1^L} \tag{7}$$

$$\theta^R = \tan^{-1} \frac{f_2 - f_2^R}{f_1^R - f_1} \tag{8}$$

being $\boldsymbol{f} = (f_1, f_2)$ the Pareto-optimal point considered and $\boldsymbol{f^L} = (f_1^L, f_2^L)$, $\boldsymbol{f^R} = (f_1^R, f_2^R)$ its left and right neighbouring points.

DEFINITION: *A knee point is the Pareto-optimal solution having the maximum reflex angle.*

- Branke et al. [7]: utility-based focus

Consider the next linear marginal utility function:

$$U(\boldsymbol{f},\lambda) = \lambda f_1 + (1-\lambda)f_2 \tag{9}$$

with $\lambda \in [0,1]$.

DEFINITION: Let the minima-count c_j of the jth Pareto-optimal solution be zero initially. *For every $\lambda^{(i)}$ vector created by uniformly specifying its components in $[0,1]$, a Pareto-optimal solution j having the minimum $U(\boldsymbol{f},\lambda^i)$ is assessed and its minima-count is incremented by one. After a number of $\lambda^{(i)}$ vectors are considered, the Pareto-Optimal solution having the maximum value of c_j is the knee point.*

- Deb & Gupta [8]: bend-angle method

Consider the bend angle defined by:

$$\theta(\boldsymbol{f},\boldsymbol{f^L},\boldsymbol{f^R}) = \theta^L - \theta^R \tag{10}$$

with θ^L, θ^R defined by Equations (7) and (8). Normalized values of the objectives it is suggested for the calculation of the bend-angle.

DEFINITION: *A knee point is the Pareto-optimal solution having the maximum positive bend-angle.*

- Deb & Gupta [8]: trade-off approach

This method is related to the preference trade-off information supplied by the user. Parameters α and β are specified taking care of different scaling objectives. Therefore, objectives do not need to be normalized.

DEFINITION: *The Pareto-optimal point having the maximum range of (α,β)-inferior points (c.f. Figure 2) is a knee point.*
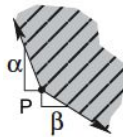
Figure 2. Inferior (α,β) region of point P. Adapted from [8].

In section 5, a comparison of this different knee points identification methods to find the updated model of next case study is developed.

4. Case Study: footbridge in Bormujos

To investigate the performance of the different Decision-Making approaches, a footbridge placed in Bormujos (Seville) is used as a case study. This test structure is a steel Warren truss footbridge, as depicted in Figure 3, with four continuous spans 3.5 m wide with a total length of 96 m. The footbridge has two neoprene supports on each abutment and each one of the three piers has an 11 m long pile foundation.

Figure 3. Interior view of the test footbridge

In this section, first the preliminary three-dimensional FE model of the footbridge, which serves as a basis for the following updating procedure, is explained in detail. Then, the ambient vibration test and the operational modal analysis (OMA) of the experimental results is presented in order to identify the actual modal parameters of the structure. Finally, the FE model is updated by performing a multi-objective optimization.

4.1 Preliminary Finite Element Model

The FE model of the footbridge was developed using the software ANSYS [9]. The members of the truss, the deck supports (stringers and floor beams), the piers and also the piles were modelled using beam elements (BEAM188). For the deck and the roof of the footbridge, a four nodes shell element (SHELL181) was employed. The handrail was also included using both elements mentioned above. In Figure 4 an extruded perspective of the FE model is presented.

The pile caps were modelled as a rigid link (CERIG), while in the abutments a not completely fixed support by means of springs (COMBIN14) was considered. The stiffness in the abutments was computed using the Gazetas's formulation [10]. The soil-structure interaction was taken into account by adding 1D spring elements (COMBIN14) along the length of the piles. The stiffness of these elements was calculated assuming the Winkler model. References of this two formulations can be also found in [11].
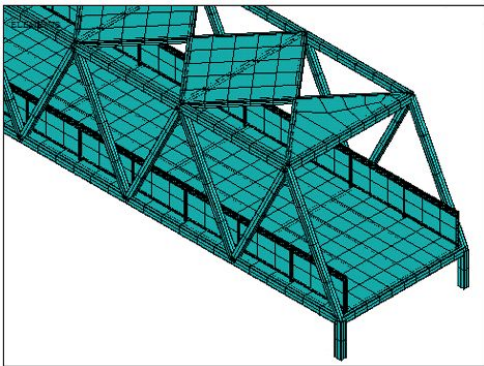

Figure 4. FE model of the footbridge

Proper selection of the updating parameters is a crucial decision since it can limit the adjustment of the FE model with the experimental results. A systematic option is to develop a sensitivity analysis of the FE model to determine which parameters have the greatest influence on the modal response. The formulation used herein is the Fox and Kapoor proposal [12] which evaluates the sensitivity of stiffness parameters using the modal strain energy. After the sensitivity analysis, twelve parameters were selected, namely:

- Stiffness of the springs that model the soil-structure interaction (three layers).
- Stiffness to longitudinal and transverse displacement in the abutments.
- Stiffness to rotation around the vertical and transversal axes in the abutments.
- Young modulus of the deck panel.
- Young modulus of the truss in the four spans.

4.2 Ambient vibration test and operational modal analysis

The aim of the ambient vibration test is to identify the modal parameters of the footbridge that will be used as reference properties for the FE model updating. In this kind of test, the excitation of the structure is always caused by environmental loads such as wind or traffic.

The data acquisition system was composed of a laptop computer, a central signal acquisition and processing unit equipped with analog-to-digital converter (Granite model of *Kinemetrics, Inc.*) and three tri-axial accelerometers (Episensor model of *Kinemetrics, Inc.*). The test layout is schematically represented in Figure 5. Thirty-two steps were defined with one mobile accelerometer placed at each set-up point, while two sensors were kept fixed as reference, placed at the red points in Figure 5. A recording time of 10 min and a sampling rate of 100 Hz were considered in the measurements. These assumptions ensure that frequencies from 1 to 50 Hz are properly recorded [13, 14].
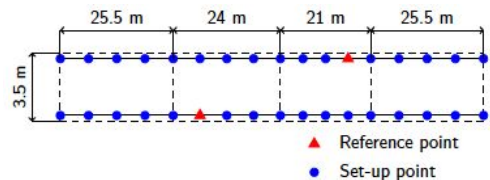

Figure 5. Plan view of the accelerometers layout in the ambient vibration test

The ARTeMIS Software [15] was used to analyse the experimental test data. Both frequency-domain and time-domain methods were used in order to identify the footbridge modal parameters. The Unweighted Principal Component Merged Test Setups (UPC-Merged) method manages to estimate the first eleven global modes also numerically identified. It is a Stochastic Subspaces Identification (SSI) method which consists of the generalization of the UPC algorithm to apply it when the test consists of several set-ups [16]. Table 1 shows the differences between the experimental values and the preliminary numerical solution of modal parameters. MAC parameter in Table 1 refers to Modal Assurance Criterion [17].

Table 1. Comparison between numerical and experimental modal parameters

Mode	f_{num} [Hz]	f_{exp} [Hz]	Δf [%]	MAC
1º lateral	1.704	1.872	8.97	0.997
2º lateral	3.560	3.506	1.54	0.969
3º lateral	6.424	5.851	9.79	0.922
longitudinal	6.610	6.914	4.40	0.966
4º lateral	8.868	8.217	7.92	0.958
5º lateral	9.486	8.515	11.40	0.929
1º vertical	9.483	9.189	3.20	0.947
2º vertical	9.720	9.483	2.50	0.914
3º vertical	11.788	11.240	4.88	0.876
6º lateral	13.854	11.828	17.13	0.765
4º vertical	14.068	12.812	9.80	0.816

The high MAC values, above 0.75 in all cases, suggest that the modes are correctly identified. However, relative differences in the value of the natural frequency exceeds 10% in some cases, which justifies updating the model.

4.3   Finite Element Model Updating

For the model updating procedure, a multi-objective optimization of the two objectives referred in Equations (4) and (5) was carried out by using the algorithm NSGA-II [3]. A population of 150 individuals and a total number of 300 generations were set to find the Pareto solution. The other details of NSGA-II are tabulated in Table 2. The optimizations performance was carried out in Matlab [18] using free codes implemented by Kalami Heris available in [19]. The pareto optimal solution obtained is shown in Figure 6.

Table 2. Details of NSGA-II for the multi-objective optimization

Parameters	Values and operators
Population size// Type	150//Double
Selection	Tournament (size=4)
No. of generations	300
Distance measure	Distance-crowding
Crossover	Two-points
Crossover probability	0.7
Mutation probability	0.05
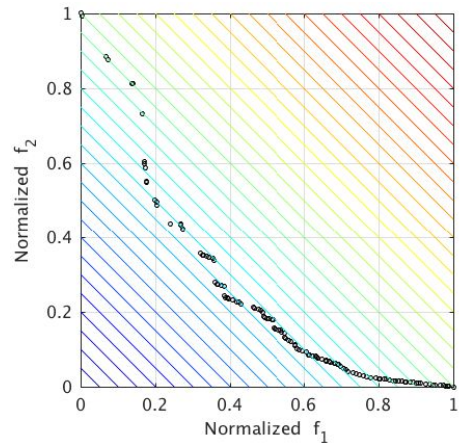
Figure 6. Normalized Pareto front 2D representation with isolines for 1-norm

5.   D-M strategies comparison

The choice of a single update FE model among all the solutions of the Pareto front is not an easy task. A multi-criteria decision-making strategy is therefore used to choose a single preferred solution in a systematic way. A knee point is almost always the most preferred solution. That is because it requires a large sacrifice in one objective to gain a small amount in the other. Several definitions of knee points are compared with the aim of finding the most suitable for model updating problems.
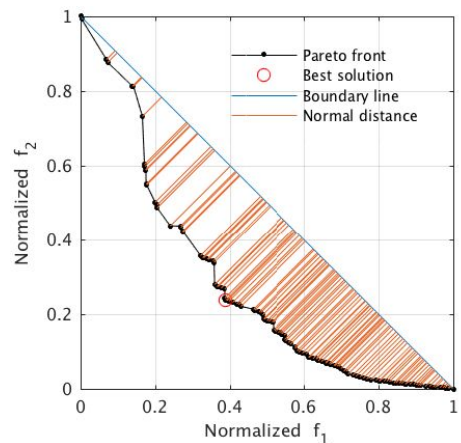

Figure 7. Knee point identification by the normal boundary intersection (NBI) method

The first considered definition is that proposed by Das [6] based on the normal boundary intersection (NBI) method. As it can be seen in Figure 7, the Pareto front is normalized and the solution with the maximum normal distance respect to the boundary line is chosen as the knee point. Other formulations, including utility-based focus [7] and angle-based approaches [8] are compared in Figure 8. Both reflex and bend angle methods selected almost the same solution. That is explained because their definition is very similar. Instead, the knee point identified by the NBI method is different. These differences lie in the definition of the knee points. Angle-based definitions are stated in a local sense, i.e. only use neighbouring points information. In contrast, the NBI method uses extreme points information. Utility function selected precisely an extreme point as the preferred solution. This may be because the utility function does not take into account the different scaling of the objectives.

In Table 3 the relative improvements of the two objectives are presented. The solution selected by the NBI method is the one that improves both objectives in a balanced way: 37% and 3% for the frequency residue and vibration mode residue, respectively.

Finally, Figure 9 shows the performance of the trade-off approach proposed by Deb & Gupta. This last method accounts for the user's preferences. Regarding a model updating problem the analyst usually has no preference over either of the two objectives, so that several different values of parameters α and β have been analysed. The options with the highest percentage points in the (α, β)-inferior region are those for which the parameter relating to the frequency residue (β) is higher (in absolute value) than that relating to the vibration mode residue (α).

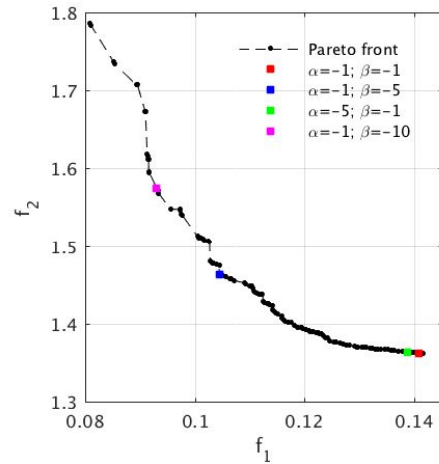Figure 8. Graphical comparison of the knee points

Figure 9. Knee point identification by trade-off approach for different values of α and β

Table 3. Comparison of the objective function improvements for the knee points obtained with the different definitions

	Initial value	NBI method		Reflex-angle method		Utility function focus		Bend angle method	
		Updating value	Δf_i (%)	Updating value	Δf_i (%)	Updating value	Δf_i (%)	Updating value	Δf_i (%)
f_1	0.1432	0.1043	37.2579	0.1007	42.2173	0.1416	1.1411	0.1004	42.6471
f_2	1.5125	1.4647	3. 2659	1.5106	0.1245	1.3614	11.1004	1.5131	0.0414

6. Conclusions

Multi-objective optimization is a useful tool to solve model updating problems. In contrast to single-objective optimization techniques, this approach avoids using weighting factors for the different residues. Nonetheless, the solution provided by multi-objective algorithms is not unique and a decision-making strategy must be followed. This study focuses on the review of different methods that help in the selection of the most suitable solution. To check the performance of these methods a FE model updating of a real footbridge is conducted. The results report that the normal boundary intersection method successes in finding the most balanced solution in terms of the relative improvement of both objectives simultaneously in this case study. In addition, this method does not require any prior information of the user's preferences as the trade-off approach by Deb & Gupta [8]. As concluding remark, multi-objective optimization, used in combination with the NBI method, has proved to be an effective proposal to finding the most adjusted FE model.

7. References

[1]   Friswell M, Mottershead JE. *Finite element model updating in structural dynamics*. Springer Science & Business Media, 1995.

[2]   Wright S, Nocedal J. Numerical optimization. *Springer Sci* 1999; 35: 7.

[3]   Deb K, Pratap A, Agarwal S, et al. A fast and elitist multiobjective genetic algorithm: NSGA-II. *IEEE Trans Evol Comput* 2002; 6: 182–197.

[4]   Bechikh S, Said LB, Ghédira K. Searching for knee regions of the Pareto front using mobile reference points. *Soft Comput* 2011; 15: 1807–1823.

[5]   Rachmawati L, Srinivasan D. Preference incorporation in multi-objective evolutionary algorithms: A survey. In: *Evolutionary Computation, 2006. CEC 2006. IEEE Congress on*. IEEE, 2006, pp. 962–968.

[6]   Das I. On characterizing the "knee" of the Pareto curve based on normal-boundary intersection. *Struct Optim* 1999; 18: 107–115.

[7]   Branke J, Deb K, Dierolf H, et al. Finding knees in multi-objective optimization. In: *International conference on parallel problem solving from nature*. Springer, 2004, pp. 722–731.

[8]   Deb K, Gupta S. Understanding knee points in bicriteria problems and their implications as preferred solution principles. *Eng Optim* 2011; 43: 1175–1204.

[9]   *ANSYS® Academic Research Mechanical, Release 18.0*. ANSYS, Inc.

[10]   Gazetas G. Formulas and charts for impedances of surface and embedded foundations. *J Geotech Eng* 1991; 117: 1363–1381.

[11]   Manterola J. *Puentes: apuntes para su diseño, cálculo y construcción*. Colegio de ingenieros de caminos, canales y puertos, 2006.

[12]   Fox R, Kapoor M. Rates of change of eigenvalues and eigenvectors. *AIAA J* 1968; 6: 2426–2429.

[13]   Maia NMM, e Silva JMM. *Theoretical and experimental modal analysis*. Research Studies Press, 1997.

[14]   Cantieni R. Experimental methods used in system identification of civil engineering structures. In: *Proceedings of the International Operational Modal Analysis Conference (IOMAC)*. 2005, pp. 249–260.

[15]   *ARTeMIS Modal 2016*. Structural Vibration Solutions A/S.

[16]   Döhler M, Andersen P, Mevel L. Data merging for multi-setup operational modal analysis with data-driven SSI. In: *Structural Dynamics, Volume 3*. Springer, 2011, pp. 443–452.

[17]   M-ograve PW, ller, Friberg O. Updating large finite element models in structural dynamics. *AIAA J* 1998; 36: 1861–1868.

[18]   *Matlab for Student R2018b*. Mathworks.

[19]   Mostapha Kalami Heris. *Portfolio Optimization using Classic Methods and Intelligent Methods (PSO, ICA, NSGA-II, and SPEA2) in MATLAB*, http://yarpiz.com/wp-content/uploads/2015/09/ypap112-port-folio-optimization.zip.

Apéndice F
Articulo F

Naranjo-Pérez, J., Infantes, M., Jiménez-Alonso, J.F., A. Sáez. A collaborative machine learning-optimization algorithm to improve the finite element model updating of civil engineering structures. Submitted for publication.

Naranjo-Pérez, J., Jiménez-Alonso, J.F., Díaz, I.M., Quaranta, G., A. Sáez. Motion-Based Design of Passive Damping Systems to Reduce Wind-Induced Vibrations of Stay Cables under Uncertainty Conditions. *Appl. Sci*. **2020**, 10, 1740.

Motion-Based Design of Passive Damping Systems to Reduce Wind-Induced Vibrations of Stay Cables under Uncertainty Conditions

Javier Naranjo-Pérez [1] , Javier F. Jiménez-Alonso [2],[*] , Iván M. Díaz [2] , Giuseppe Quaranta [3] and Andrés Sáez [1]

[1] Department of Continuum Mechanics and Structural Analysis, Universidad de Sevilla, 41092 Seville, Spain; jnaranjo3@us.es (J.N.-P.); andres@us.es (A.S.)

[2] Department of Continuum Mechanics and Theory of Structures, E.T.S. Ingenieros de Caminos, Canales y Puertos, Universidad Politécnica de Madrid, 28040 Madrid, Spain; ivan.munoz@upm.es

[3] Department of Structural and Geotechnical Engineering, Sapienza University of Rome, 00184 Rome, Italy; giuseppe.quaranta@uniroma1.it

[*] Correspondence: jf.jimenez@upm.es; Tel.: +34-910-674-152

Abstract: Stay cables exhibit both great slenderness and low damping, which make them sensitive to resonant phenomena induced by the dynamic character of external actions. Furthermore, for these same reasons, their modal properties may vary significantly while in service due to the modification of the operational and environmental conditions. In order to cope with these two limitations, passive damping devices are usually installed at these structural systems. Robust design methods are thus mandatory in order to ensure the adequate behavior of the stay cables without compromising the budget of the passive control systems. To this end, a motion-based design method under uncertainty conditions is proposed and further implemented in this paper. In particular, the proposal focuses on the robust design of different passive damping devices when they are employed to control the response of stay cables under wind-induced vibrations. The proposed method transforms the design problem into a constrained multi-objective optimization problem, where the objective function is defined in terms of the characteristic parameters of the passive damping device, together with an inequality constraint aimed at guaranteeing the serviceability limit state of the structure. The performance of the proposed method was validated via its application to a benchmark structure with vibratory problems: The longest stay cable of the Alamillo bridge (Seville, Spain) was adopted for this purpose. Three different passive damping devices are considered herein, namely: (i) viscous; (ii) elastomeric; and (iii) frictions dampers. The results obtained by the proposed approach are analyzed and further compared with those provided by a conventional method adopted in the Standards. This comparison illustrates how the newly proposed method allows reduction of the cost of the three types of passive damping devices considered in this study without compromising the performance of the structure.

Keywords: motion-based design; uncertainty conditions; constrained multi-objective optimization; reliability analysis; passive structural control; cable-stayed bridges

1. Introduction

One of the main elements that governs the dynamic behavior of cable-stayed bridges is their stay cables [1]. This structural system has both a high flexibility and a low damping, which makes it susceptible to suffer both from different vibratory problems [2] and exhibit significant changes in its modal properties induced by the modification of the operational and environmental conditions [3].

The vibratory problems observed in cables of cable-stayed bridges may be classified in terms of the structural elements excited during the vibration phenomenon into the following [2]: (i) local-global vibratory problems, in which the vibrations involve the excitation of both the cables and the deck of the structure [4]; and (ii) local vibratory problems, in which only the cables of the structure are excited laterally [5]. These vibratory problems may be caused by either of the following: (i) direct excitation sources, such as road traffic, wind [6] or earthquake action [7], or (ii) indirect excitation sources, such as linear internal resonances, parametric excitations or dynamic bifurcations.

In this paper, we focus on the case of wind-induced vibrations of stay cables, as this is the source problem of many vibratory issues reported in the literature [2]. As wind-induced vibrations can cause different structural problems on stay cables (like fatigue or comfort problems), two types of measures are normally adopted to mitigate the cable vibrations [8], consisting of either of the following: (i) modifying its natural frequency via the installation of a secondary net of cables [9]; or (ii) increasing its damping ratio via the installation of external control systems [2]. Such control systems for stay cables may be classified into three different groups [8]: (i) active [10]; (ii) semi-active [11]; and (iii) passive [12].

Active control systems for stay cables focus on controlling the dynamic response of the cable via the modification of its tensional state [13]. For this purpose, some kind of actuator, following the orders of a controller, acts on the cable in order to minimize the difference between the actual response of the cable (recorded by a sensor) and the allowable response value [14]. Although the theoretical research on the use of these devices has experienced a significant growth in recent years, their practical implementation in real cable-stayed bridges has been limited due to their high cost and the robustness problems associated with the power supply needed to guarantee their operation [2].

On the other hand, semi-active control systems focus on modifying the constitutive parameters of external damping devices deployed to control the response of the stay cable under external actions [15]. Among the different semi-active devices, magnetorheological dampers have been widely studied and implemented in real cable-stayed bridges [16]. Although semi-active damping devices outperform their passive damping counterparts [17] with a lower cost than active control systems, their efficiency is limited when they are employed under uncertainty conditions, since their performance highly depends on the control algorithm considered for the design [18].

Finally, passive control systems for stay cables focus on increasing the damping ratio of the cables via the installation of external devices, whose characteristic parameters are originally designed to mitigate the dynamic response of the structural system [19]. Due to the robustness of such passive damping devices [20], they have been installed successfully on numerous real cable-stayed bridges to reduce wind-induced vibrations [21]. Nevertheless, these devices present as main limitation, a lower flexibility to adapt the system response to the variability of both the external actions and the modification of the stay cable parameters induced by loading, when compared to the active and semi-active devices. In order to overcome this limitation, two strategies may be adopted as outlined: either (i) to install a hybrid control system [22]; or (ii) to design the passive damping device taking into account these uncertainty conditions via a robust design method [23].

Different design methods have been developed for this purpose. Among the different proposals, Kovacs was the first researcher to study the optimum design of viscous dampers for stay cables [24]. Subsequently, Pacheco et al. provided a universal curve which allows the representation of the modal damping of the first vibration mode of a taut cable in terms of the damping coefficient of the viscous damper [25]. The maximum of this curve corresponds to the optimum damping ratio of the taut cable when a viscous damper is installed on it. Later, Krenk et al. obtained an analytical expression for this curve [26]. Alternatively, other authors, such as Yoneda and Maeda, proposed an analytical model of the damped cable to determine the optimum parameters of the passive damper [27]. Although the design parameters obtained following any of these approaches are similar, so that they are currently employed for the practical design of passive damping devices, they fail to take into account a key aspect: the uncertainty associated with the variation of both the external actions and the modification of the modal properties of the stay cables [28].

In order to overcome this limitation, a motion-based design method [29] under uncertainty conditions is formulated, implemented and further validated in this paper. In fact, this proposal generalizes the formulation of a well-known design method, the so-called motion-based design method under deterministic conditions [30], to the abovementioned uncertainty conditions. The proposed motion-based design method under uncertainty conditions transforms the design problem into a constraint multi-objective optimization problem. Hence, the main objective of this problem is to find the optimum values of the characteristic parameters of the passive damping device which meet the design requirements for the structure. For this purpose, a multi-objective function is defined in terms of these parameters, together with an inequality constraint aimed at guaranteeing the compliance of the design requirements. Such design requirements are defined in terms of the vibration serviceability limit state of the structure. Since this serviceability limit state is defined under stochastic conditions, the failure probability of its compliance must be limited [31] and a reliability analysis must be performed [32,33]. For practical engineering applications [34], an equivalent reliability index is usually considered instead of the probability of failure. Thus, the formulation of the inequality constraint is realized in terms of the reliability index, which cannot exceed an allowable value [35]. For the computation of the reliability index, a sampling technique, the Monte Carlo method has been considered herein [36].

Finally, in order to validate the performance of the proposed method, it was applied to the robust design of three different passive damping devices (viscous, elastomeric, and friction dampers) where they are installed on the longest stay cable of the Alamillo bridge (Seville, Spain). To this end, only the effect of the rain–wind interaction phenomenon and the turbulent component of the wind action were considered. The results were compared with those obtained applying a conventional approach. This comparative study reveals that the proposed method allows the reduction of the cost of the passive damping devices while ensuring the structural reliability of the stay cable.

The manuscript is organized as follows: First, the motion-based design method under uncertainty conditions is described in detail. Next, a damper-cable interaction model under wind action, based on the finite element (FE) method, is presented. Subsequently, the performance of the proposed method is illustrated and further validated with a case-study (Alamillo bridge, Seville, Spain). In the final section, some concluding remarks are drawn to complete the paper.

2. Motion-Based Design of Structures under Uncertainty Conditions

2.1. Motion-Based Design of Structures under Deterministic Conditions

Structural optimization is a computational tool which can be used to assist engineering practitioners in the design of current structural systems [37]. Thus, this computational tool allows the optimum size, shape or topology of the structure to be found which meet the design requirements established by the designer/manufacturer/owner. Among the different structural optimization methods, the performance-based design method has been widely employed to design passive damping devices for civil engineering structures [23,30]. When the design requirements are defined in terms of the vibration serviceability limit state of the structure, the performance-based design method is denominated the motion-based design method [29]. This general design method was adapted herein for the design of passive damping devices when they are used to control the dynamic response of civil engineering structures. As assumption, all the variables, involved in this problem, are deterministic.

Thus, the motion-based design method under deterministic conditions transforms the design problem into a constrained multi-objective optimization problem. Therefore, the main objective of this problem is to find the optimum value of the characteristic parameters of the passive damping devices which guarantee an adequate serviceability structural behavior. For this purpose, a multi-objective function is minimized. The multi-objective function, $f(\theta)$, is defined in terms of the characteristic parameters, θ, of the considered passive damping devices. Additionally, the space domain is constrained including two restrictions in the optimization problem: (i) an inequality constraint, $g_{det}(\theta)$; and (ii) a search domain. $[\theta_{min}, \theta_{max}]$. As the relation between the objective function and the design

variables is nonlinear, global optimization algorithms are normally considered to solve this constrained multi-objective optimization problem. [38]. Accordingly, the motion-based design problem under deterministic conditions can be formulated as follows:

$$\text{Find } \theta \text{ to Minimize } f(\theta)$$
$$\text{Subjected to } \begin{cases} g_{det}(\theta) \leq 0 \\ \theta_{min} < \theta < \theta_{max} \end{cases} \tag{1}$$

where θ is the vector of the design variables; $f(\theta)$ is the multi-objective function to be minimized; θ_{min} and θ_{max} are the lower and upper bounds of the search domain; and $g_{det}(\theta)$ is a function which defines the inequality constraint.

Therefore, the key aspect of this optimization problem is the definition of the inequality constraint. In the case of slender civil engineering structures, whose design is conditioned by their dynamic response [29], the compliance of the vibration serviceability limit state can be considered for this purpose. According to the most advanced design guidelines [6,34], the vibration serviceability limit state of a structure is met if the movement of the structure, $d_s(\theta)$, which can be characterized by its displacement, velocity or acceleration, is lower than an allowable value, d_{lim}, defined in terms of the considered comfort requirements. Thus, the inequality constraint of the abovementioned optimization problem may be expressed as follows:

$$g_{det}(\theta) = \frac{d_s(\theta)}{d_{lim}} - 1 \leq 0 \tag{2}$$

Finally, as the result of this multi-objective optimization process, a set of possible solutions is obtained. This set of possible solutions is denominated the Pareto front. Accordingly, a subsequent decision-making problem must be solved, the selection of the best solution among the different elements of this Pareto front. Two possible alternatives are normally considered for this purpose [23]: (i) the selection of the best-balanced solution among all the elements of the Pareto front; and (ii) the consideration of additional requirements to solve this decision-making problem. The selection between both alternatives depends on the designer's own criterion and the particular conditions of the problem.

### 2.2. Motion-Based Design of Structures under Stochastic Conditions

In order to generalize the implementation of the motion-based design method to scenarios with stochastic conditions, it is necessary to consider during the design process the uncertainty associated with the variability of both the external actions and the modal properties of the structure. For this purpose, two types of methods are normally employed [33]: (i) probabilistic methods; and (ii) fuzzy logic methods. Between these two methods, a probabilistic approach was considered herein because engineering practitioners are more used to dealing with probability concepts than with fuzzy logic problems. Concretely, a structural reliability method [39] was adapted herein to deal with the aforementioned uncertainty. According to this method, the vibration serviceability limit state can be expressed as a probabilistic density function, $g_{unc}(\theta)$, which is defined in terms of the capacity of the structure, C_s, and the demand of the external actions, $D_a(\theta)$ (where both terms are random variables characterized by their probability density function). Thus, the vibration serviceability limit state can be defined as follows:

$$g_{unc}(\theta) = \begin{cases} C_s - D_a(\theta) & \text{if } g_{unc}(\theta) \text{ is assumed normally distributed} \\ \frac{C_s}{D_a(\theta)} & \text{if } g_{unc}(\theta) \text{ is assumed log-normally distributed} \end{cases} \tag{3}$$

The above relation (Equation (3)) allows the computation of the probability of failure of the structural system, $p_f(\theta)$, to the vibration serviceability limit state. This probability of failure, $p_f(\theta)$, may be determined as follows:

$$p_f(\theta) = \begin{cases} \text{Prob}[g_{unc}(\theta) < 0] & \text{if } g_{unc}(\theta) \text{ is assumed normally distributed} \\ \text{Prob}[g_{unc}(\theta) < 1] & \text{f } g_{unc}(\theta) \text{is assumed log} - \text{normally distributed} \end{cases} \quad (4)$$

On the other hand, as it is shown in Figure 1, it is possible to characterize the probability of failure, $p_f(\theta)$, via an equivalent index, the so-called reliability index, $\beta_s(\theta)$.
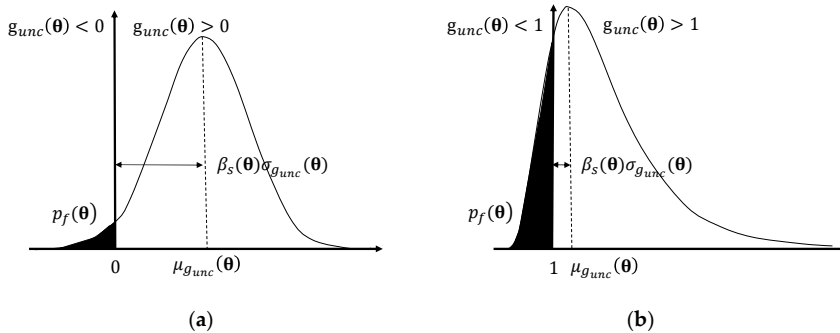
Figure 1. Probability density function of the vibration serviceability limit state, $g_{unc}(\theta)$: (**a**) $g_{unc}(\theta)$ follows a normal distribution; and (**b**) $g_{unc}(\theta)$ follows a log-normal distribution.

The relation between the probability of failure, $p_f(\theta)$, and the reliability index, $\beta_s(\theta)$, may be expressed as follows:

$$p_f(\theta) = \begin{cases} F_{g_{unc}}(0) = \Phi\left(-\dfrac{\mu_{g_{unc}}(\theta)}{\sigma_{g_{unc}}(\theta)}\right) = \Phi(-\beta_s(\theta)) & \text{normally distributed} \\ F_{g_{unc}}(1) = \Phi\left(\dfrac{\ln \mu_{C_s}/\mu_{D_a}(\theta)}{\sqrt{\sigma_{lnC_s}^2 + \sigma_{lnD_a(\theta)}^2}}\right) = \Phi(-\beta_s(\theta)) & \text{log} - \text{normally distributed} \end{cases} \quad (5)$$

where $F_{g_{unc}}$ is the cumulative probability distribution function of $g_{unc}(\theta)$; $\mu_{g_{unc}}(\theta)$ and $\sigma_{g_{unc}}(\theta)$ are respectively the mean and standard deviation of $g_{unc}(\theta)$; Φ is the standard normal cumulative distribution function; μ_{C_s} and $\mu_{D_a}(\theta)$ are respectively the mean of the probabilistic distribution function of C_s and $D_a(\theta)$; and σ_{lnC_s} and $\sigma_{lnD_a(\theta)}$ are respectively the standard deviation of the log-normal distribution of C_s and $D_a(\theta)$.

In this manner, the use of the reliability index, $\beta_s(\theta)$, allows the computation of the vibration serviceability limit state under uncertainty conditions to be simplified. Hence, this design requirement is met if the reliability index, $\beta_s(\theta)$, is greater than the allowable reliability index, β_t, established by the designer/manufacturer/owner of the structure. In order to evaluate this inequality constraints, the reliability index, $\beta_s(\theta)$, is usually computed via sampling techniques and the recommended values of the allowable reliability index, β_t, can be found in literature [39]. In this study, Monte Carlo simulations [36] were considered in order to evaluate numerically the reliability index, $\beta_s(\theta)$, and the value proposed by the European guidelines [34] was considered for the allowable reliability index, β_t.

Finally, the motion-based design method under uncertainty conditions may be formulated as follows:

$$\begin{array}{c} \text{Find } \theta \text{Minimize } f(\theta) \\ \text{Subjected to} \begin{cases} g_{unc}(\theta) = \dfrac{\beta_t}{\beta_s(\theta)} - 1 \leq 0 \\ \theta_{\min} < \theta < \theta_{\max} \end{cases} \end{array} \quad (6)$$

According to this, one of the main virtues of the motion-based design method is highlighted. The method allows the deterministic and stochastic design problems to be dealt with using a similar formulation. Only the inequality constraint must be modified to adapt the formulation to the particular conditions of each problem. This virtue facilitates the implementation of this method for the robust design of passive damping devices when they are used to control the dynamic response of slender civil engineering structures.

3. Damper-Cable Interaction Model under Wind Action

The damper-cable interaction model, considered herein to evaluate the dynamic response of a stay cable damped by different passive control systems under wind action, is described in detail in this section. First, the interaction model based on the FE method is introduced. Later, the method employed to simulate the wind action is presented.
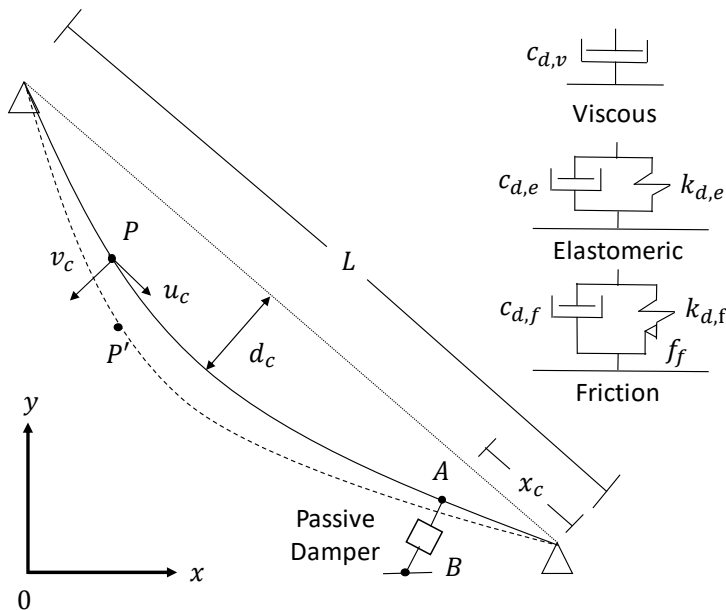
3.1. Modelling the Damper-Cable Interaction

The analysis of the dynamic behavior of stay cables has been studied extensively over the last four decades. Thus, analytical [40], numerical [30], and experimental studies [41] have been performed for this purpose. Among the different proposals, a numerical method, the FE method was considered herein to develop a damper-cable interaction model. This method presents three main advantages when it is implemented for this particular problem [30]: (i) its easy implementation for practical civil engineering applications; (ii) it allows a direct interaction of element with different constitutive laws (cable and dampers); and (iii) it simplifies the simulation of some effects such us the nonlinear behavior of the cable [40], the sag effect [42], and the influence of the external dampers on the modal properties of the cables (locking effect) [43].

The implementation of the FE method for this particular problem is based on the numerical integration of the weak formulation of the differential equilibrium equation of a vibrating stay cable in the lateral direction. Figure 2 shows an inclined cable of length, L [m], suspended between two supports at different level which presents a sag, d_c [m], with respect to the axis aligned with the two supports. The application of a small displacement causes the motion of a generic point from the self-weight configuration, P, to, P', where u_c and v_c represent the component of the movement of the cable respectively in the parallel and perpendicular direction to the axis traced between the two supports. The equation, which governs the vibration of a taut cable in the lateral direction under the assumptions of linear and flexible behavior, may be expressed as follows:

$$H\frac{\partial^2 v_c}{\partial x^2} - \frac{\partial^2}{\partial x^2}\left(EI\frac{\partial^2 v_c}{\partial x^2}\right) = m\frac{\partial^2 v_c}{\partial t^2} \tag{7}$$

where v_c is the lateral displacement of the cable [m]; H is the axial force of the cable [N]; EI is the bending stiffness of the cable [Nm²] (where E is the Young's modulus [N/m²] and I is the moment of inertia of the cross-section of the cable [m⁴]); and m is the mass per unit length of the cable [kg/m]. According to the Equation (7), the vibration of the cable is governed by both its tensional state and its bending stiffness [44,45]. Additional phenomena can be simulated via the selection of the adequate finite-element. A nonlinear two-node element with six degrees of freedom per node has been considered herein to simulate the cable behavior. This element allows both the nonlinear geometrical and stress-stiffness behavior of the cable to be simulated adequately [46].

In order to take into account, the initial tensional and deformational state of a stay cable during either a modal or a transient analysis, a preliminary static nonlinear analysis must be performed. In this preliminary static analysis, the equilibrium form of the cable under its self-weight and a preliminary axial force is achieved. As a result of this analysis, both the stress and the shape of the cable are updated, which is a key aspect to simulate numerically its real behavior.

Figure 2. Damper-cable interaction model considered and mechanical model of each passive damper (viscous, elastomeric, and friction).

Subsequently, the modelling problem must focus on the simulation on the passive damping devices behavior. Three passive damping devices were considered herein (Figure 2). For these three passive damping devices, a linear constitutive law was assumed. The effect of these three passive damping devices on the cable may be simulated by an equivalent damping force. Each equivalent damping force is related to the energy that each damping device is able to dissipate, and it is opposed to the movement of the cable. Thus, each passive damping device has been modelled by a finite element whose behavior is equivalent to the corresponding damping force (Figure 2). This assumption has two advantages: (i) the relative movements between the damper and the cable, which govern the behavior of the damper, were obtained straight; and (ii) the effect of the dampers on the modal properties of the structure was taken into account directly.

First, the effect of a viscous damper is equivalent to a damping force which is proportional to a damping coefficient, $c_{d,v}$ [sN/m], and the relative velocity, $\dot{v}_r(t)$ [m/s], between the two extremes of the damper $(\dot{v}_r(t) = \dot{v}_{d,A}(t) - \dot{v}_{d,B}(t)$, where $\dot{v}_{d,A}(t)$ is the velocity of the extreme of the damper in contact with the cable and $\dot{v}_{d,B}(t)$ is the velocity of the extreme of the damper in contact with the deck, as it is illustrated in Figure 2. The viscous damping force of this damper, $F_{d,v}(t)$, may be expressed as [47]:

$$F_{d,v}(t) = c_{d,v}\dot{v}_r(t) \tag{8}$$

Second, the effect of the elastomeric damper may be simulated via the Kelvin–Voigt model. The equivalent viscoelastic damping force is characterized by two components: (i) a viscous damping component which is expressed in terms of a damping coefficient, $c_{d,e}$ [sN/m], and the relative velocity, $\dot{v}_r(t)$ [m/s]; and (ii) an elastic component which is expressed in terms of a stiffness coefficient, $k_{d,e}$ [N/m], and the relative displacement between the two extremes, $v_r(t)$ [m] $(v_r(t) = v_{d,A}(t) - v_{d,B}(t)$, where $v_{d,A}(t)$ is the displacement of the extreme of the damper in contact with the cable and $v_{d,B}(t)$ is the

displacement of the extreme of the damper in contact with the deck, as it is illustrated in Figure 2. The viscoelastic damping force of this damper may be defined as [48,49]:

$$F_{d,e}(t) = c_{d,e}\dot{v}_r(t) + k_{d,e}v_r(t) \tag{9}$$

Finally, the effect of the friction damper may be mimicked via the extended Kelvin–Voigt model. The definition of the equivalent damping force involves three components: (i) a viscous damping component which is expressed in terms of a damping coefficient, $c_{d,f}$ [sN/m], and the relative velocity, $\dot{v}_r(t)$ [m/s]; (ii) an elastic component which is expressed in terms of a stiffness coefficient, $k_{d,f}$ [N/m], and the relative displacement, $v_r(t)$ [m], and (iii) a friction component defined in terms of a static friction force, f_f [N] (where, $f_f = \mu \cdot N$, being μ the friction coefficient [−] and N the normal force [N]) and a symbolic function, $\text{sgn}\big(\dot{v}_r(t)\big)$ (which returns −1, 0, and 1 in case $\dot{v}_r(t) < 0$, $\dot{v}_r(t) = 0$ and $\dot{v}_r(t) > 0$, respectively). The equivalent damping force of this damper may be expressed as [50]:

$$F_{d,f}(t) = c_{d,f}\dot{v}_r(t) + k_{d,f}v_r(t) + f_f \cdot \text{sgn}\big(\dot{v}_r(t)\big) \tag{10}$$

These damping devices are usually located at a certain distance, x_c [m], of the lower anchorage of the stay cable (Figure 2) due to constructive limitations. Nevertheless, due to their mechanical characteristics, they can have influence on both the damping and the natural frequencies (locking effect) of the stay cable.

3.2. Modelling the Wind Action

Subsequently, the effect of the wind-induced forces was simulated numerically. The wind simulation was carried out under the assumption that the cable is a cylinder immersed in a turbulent flow [2]. Hence, the wind flow is composed of three components: (i) a mean wind velocity, $\mathcal{U}$ [m/s]; (ii) a fluctuating longitudinal velocity, $u(t)$ [m/s]; and (iii) a fluctuating transversal velocity, $v(t)$ [m/s].

The wind forces can be decomposed into a mean and a fluctuating component assuming the following hypothesis: (i) a quasi-steady behavior of the wind-induced forces; and (ii) small components of the turbulence with respect to the mean wind velocity, $\mathcal{U}$ [51]. The expression of these two components can be expressed as follows (assuming a linearized approximation [52]):

$$F_D(t) = F_D + f_{Du}(t) + f_{Dv}(t) \tag{11}$$

$$F_L(t) = F_L + f_{Lu}(t) + f_{Lv}(t) \tag{12}$$

where $F_D(t)$ is the drag force [N]; $F_L(t)$ is the lift force [N]; F_D is the mean wind drag force; F_L is the mean wind lift force; $f_{Du}(t)$ is the drag force induced by the longitudinal component of the wind; $f_{Lu}(t)$ is the lift force induced by the longitudinal component of wind; $f_{Dv}(t)$ is the drag force induced by the transversal component of wind; and $f_{Lv}(t)$ is the lift force induced by the transversal component of the wind. These magnitudes can be determined using the following relationships [2]:

$$F_D = 0.5\rho\mathcal{U}^2 D C_D \tag{13}$$

$$f_{Du}(t) = \rho\mathcal{U}u(t)D C_D \tag{14}$$

$$f_{Dv}(t) = 0.5\rho\mathcal{U}v(t)D\big(C'_D - C_L\big) \tag{15}$$

$$F_L = 0.5\rho\mathcal{U}^2 D C_L \tag{16}$$

$$f_{Lu}(t) = \rho\mathcal{U}u(t)D C_L \tag{17}$$

$$f_{Lv}(t) = 0.5\rho\mathcal{U}v(t)D\big(C_L - C'_D\big) \tag{18}$$

where ρ is the density of the air [kg/m^3]; D is the outer diameter of the cable [m]; C_D is the drag coefficient [−]; and C_L the lift coefficient [−]. The coefficients C'_D and C'_L are the derivative of C_D and C_L, respectively, with respect to the angle α neighboring β (Figure 3). As the section of the cable is assumed to be circular in this study, these derivatives are therefore null because of the symmetry, and hence these two coefficients can be neglected.
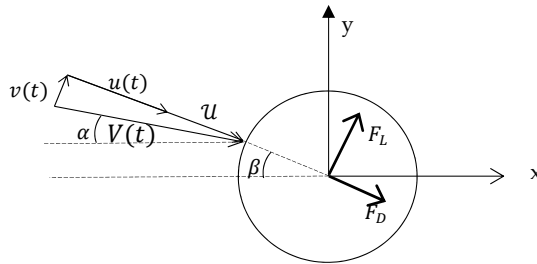

Figure 3. Reference coordinate system, drag force component, lift force component, and wind velocity components.

Finally, in order to determine the wind forces it is necessary to generate simulations of wind velocities. For this purpose, the wave superposition spectral-based method was considered [8]. This method allows the numerical determination of a series of wind velocities via the superposition of trigonometric functions. On the one hand, the amplitude of these functions is obtained in terms of a coherence function, which considers the spatial variability of the wind velocity, and the power spectral density function of the turbulent wind velocity. On the other hand, the phase of the trigonometric functions is generated randomly. The coherence function is defined using the relationship proposes by Davenport [53]. The power spectral density function proposed by the European guidelines [54] was considered herein.

4. Application Example

The proposed motion-based design method under uncertainty conditions was validated herein via the design of three passive damping devices when they are used to control the wind-induced vibrations of the longest cable of a real bridge. For this purpose, the Alamillo bridge (Seville, Spain) was considered (Figure 4). The length of the deck of this bridge is 200 m. Unlike most cable-stayed bridges, the Alamillo bridge has not back-stays. An inclination of its pylon of 32° with respect to the vertical axis compensates the lack of the back-stays [55]. A total of 26 stays (13 parallel pairs) with a longitudinal separation of 12 m guarantees an adequate connection between the deck and the pylon.
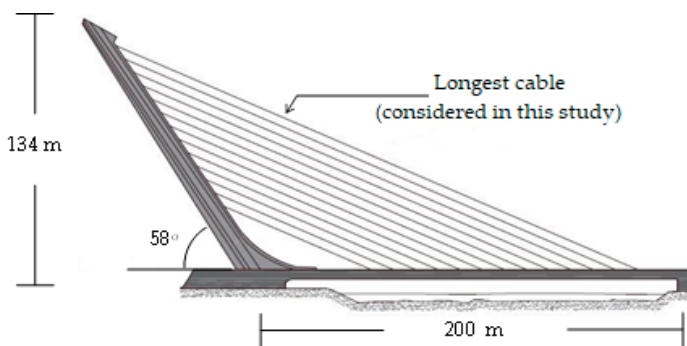
Figure 4. Illustrative scheme of the Alamillo bridge.

Previous research reported that the longest stay cable of this bridge, which has both a low damping and mass ratio, was prone to vibrate due to the wind action. Concretely, it was detected that the main sources of vibration of this cable were the rain–wind interaction phenomenon and the turbulent component of the wind action [56]. Therefore, this stay cable was considered as a benchmark to validate the performance of the proposed design method. For this purpose, three different passive damping devices (viscous, elastomeric and friction dampers) were designed according to the proposed method, and the results obtained were compared with the ones provided by a conventional method adopted by the Standards [6]. Additionally, the uncertainty associated with the variation of the modal properties of the cable due to the modifications of the operational and environmental conditions was taken into account in this design process. The development of this case-study was organized in the following steps: (i) a FE model of the cable was built and its numerical modal properties were obtained via a numerical modal analysis; (ii) a transient analysis was performed to evaluate the vibration serviceability limit state of the structure; (iii) as this limit state was not met, the three passive damping devices were designed according to both methods (the new proposal and the conventional one); and (iv) finally, the results obtained were compared and some conclusions were drawn to close the section.

4.1. FE Model and Numerical Modal Analysis

The FE model of the cable was built using the software Ansys [57]. The geometrical and mechanical properties of the cable under study were as follows: (i) its length, $L = 2.92 \times 10^2$ m; (ii) its outer diameter, $D = 0.20$ m; (iii) the effective area of its cross section, $A = 8.38 \times 10^{-3}$ m^2; (iv) the effective moment of inertia, $I = 5.58 \times 10^{-4}$ m^4; (v) its mass per unit length, $m = 60$ kg/m; (vi) an axial force, $H = 4.13 \times 10^6$ N; (vii) a Young's modulus, $E = 1.6 \times 10^{11}$ N/m^2; and (viii) the angle between the cable and the deck, $\gamma = 26°$. The cable was modelled by a mesh of 100 equal-length beam elements (BEAM188). In order to simulate numerically the sag effect, a nonlinear static analysis was previously performed. The objective of this preliminary analysis was to find both the initial tensional state and pre-deformed shape of the cable. The self-weight of the cable and its initial axial force were considered as loads for this preliminary nonlinear static analysis. Subsequently, the results of this analysis were used to update the geometry and tensional state of the cable. Later, the linear perturbation method was considered to perform the modal analysis [57]. Additionally, the stress stiffening effect was taken into account to perform this modal analysis.

As result of this numerical modal analysis, the first six natural frequencies were obtained. Table 1 shows the value of these first six natural frequencies (f_i being the natural frequencies of the ith vibration mode).

Table 1. Numerical natural frequencies of the cable.

Natural Frequency	f_1	f_2	f_3	f_4	f_5	f_6
Value [Hz]	0.452	0.905	1.351	1.802	2.254	2.706

4.2. Assessment of the Vibration Serviceability Limit State of the Cable under Uncertainty Conditions

As it was expected, according to the numerical natural frequencies obtained (Table 1), this cable was prone to vibrate under wind action due to both the turbulent component of the wind (the first two natural frequencies are lower than 1 Hz [58]) and the rain–wind interaction phenomenon (the six natural frequencies are lower than 3 Hz [6]). For this reason, the assessment of the vibration serviceability limit state of this stay cable was performed herein following the recommendations of the Federal Highway Administration (FHWA) guidelines [6].

On the one hand, in order to avoid the wind-induced vibrations associated with the rain–wind interaction phenomenon, it must be checked that the damping ratio of all the vibration modes, whose natural frequencies are lower than 3 Hz, are greater than a recommended value [6,59]. In order to determine this recommended value, the FHWA guidelines [6] establishes that the rain–wind interaction

phenomenon can be neglected if the Scruton number, S_c, is greater than 10 for all the considered vibration modes. This condition may be expressed as follows:

$$S_{c,i} = \frac{m\xi_i}{\rho D^2} > 10 \tag{19}$$

where ξ_i is the damping ratio of the ith vibration mode.

Thus, this requirement is equivalent to guaranteeing a minimum damping ratio for each considered vibration mode. The minimum required damping ratio may be determined as follows:

$$\xi_i > \frac{10\rho D^2}{m} \tag{20}$$

As expected, due to the results of previous experimental tests, the damping ratio associated with the first six vibration modes of this cable did not meet this condition [56]. Hence, it was necessary to increase the value of these damping ratios. A passive damping device can be designed and installed on the cable for this purpose.

On the other hand, in order to analyze the effect of the turbulent component of wind action on the dynamic behavior of the cable, a transient analysis was performed. As a result of this transient analysis, the dynamic response of the cable under wind action can be obtained and the vibration serviceability limit state of the cable can be assessed. According to the FHWA guidelines [6], this limit state is met if the maximum displacement of the cable is lower than an allowable displacement which is defined in terms of the user tolerance. Table 2 shows the allowable displacement of the cable in terms of the design level required [6]. In this study, a recommended design level was established for the vibration serviceability limit state.

Table 2. User tolerance limits for the different design levels [6].

Design Level	Allowable Displacement [m] [1]
preferred	0.5D
recommended	1.0D
not to exceed	2.0D

[1] *D* is the outer diameter of the cable.

Additionally, as the dynamic response of the stay cable was sensitive to the variation of its modal properties associated with the change of the operational and environmental conditions during its overall life cycle, a reliability analysis about the compliance of the vibration serviceability limit state was performed. For this purpose, it was assumed that the axial force of the cable is a random variable normally distributed. According to the results provided by Stromquist-LeVoir et al., it could be also assumed that this random variable has a range of variation of ± 10% [60]. A sample of stay cables with different values of the axial force was generated. The vibration serviceability limit state was assessed on this sample. For this purpose, the vibration serviceability limit state must be reformulated in order to take into account the uncertainty conditions. According to this, this limit state is met if a reliability index, $\beta_s(\theta)$, is greater than an allowable reliability index, β_t.

In order to compute the reliability index, $\beta_s(\theta)$, the maximum displacement of the stay cable (obtained from the different transient analyses performed on the sample of stay cables), which constitutes the demand of the wind action, $D_a(\theta)$, and the allowable displacement of the stay cable (established by the FHWA guidelines [6]), which constitutes the capacity of the structure, C_s, were determined. Additionally, as the wind action is defined according to a return period of 50 years, the corresponding value of the allowable reliability index is $\beta_t = 1.35$, according to the European guidelines [34].

As a numerical method in order to both determine the sample and compute the reliability index, $\beta_s(\theta)$, the Monte Carlo method was considered herein. A convergence analysis was performed to

determine the size of the sample [61]. As a result of this convergence analysis, the size of the sample was established at 100.

Finally, in order to evaluate the demand of the wind action, $D_a(\theta)$, the wind forces must be determined. For this purpose, simulations of the wind velocities were generated. The simulation of these wind velocities was addressed employing the wave superposition spectral-based method [8]. Both the von Karma spectra and a coherence function, as they are defined by the European guidelines [54], were employed herein. The following design parameters were considered for the wind simulation [54]: (i) basic wind velocity, $v_{b,0} = 26$ m/s; (ii) a directional factor, $c_{dir} = 1$; (iii) a season factor, $c_{sea} = 1$; (iv) a orography factor, $c_{oro} = 1$; (v) an terrain type III category (which involves a terrain factor, $k_r = 0.216$; a roughness length, $z_o = 0.3$ m; and a minimum height, $z_{min} = 5$ m); (vi) a duration of each simulation of 300 s; and (vii) a time step of 5×10^{-3} s [62]. In this study, the wind velocities were generated at ten different heights of the cable (resulting from dividing the cable into ten equal-length segments), as Figure 5 depicts. This mesh density was considered for all the simulations conducted in the paper, in order to ensure that all the obtained results were consistent. Although preliminary analyses performed by the authors concluded that the meshing in Figure 5 was adequate for our aims (illustrating the performance of the proposed motion-based approach), the reader should be aware of the fact that the numerical simulation of the structural response under wind excitation depends on such mesh density, so that further analyses are recommended. A graphical user interface [63] was developed in the commercial software Matlab [64] to evaluate the wind action following the above guidelines.
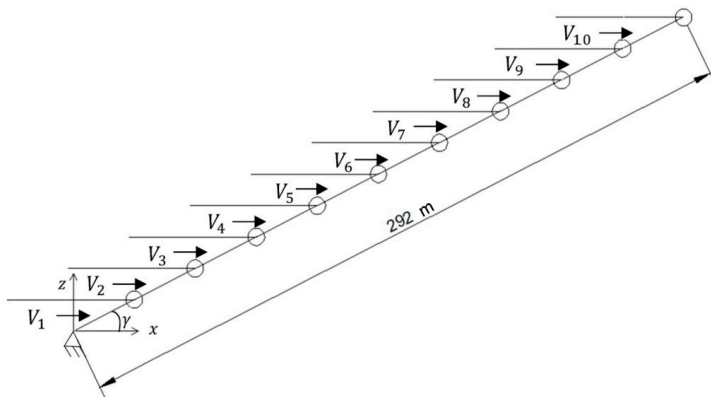
Figure 5. Representation of the ten different heights where the wind action is applied.

The application of Equations (11) and (12) allows the wind-induced forces in terms of the wind velocities to be computed. For this purpose, the following values for the characteristic parameters were adopted: (i) a density of the air, $\rho = 1.23$ kg/m^3; (ii) a drag coefficient, $C_D = 1.2$ [2]; and (iii) a lift coefficient, $C_L = 0.3$ [6].

Finally, a transient analysis (time history simulation) was performed for each element of the sample. The nonlinear geometrical behavior of the stay cables was considered for this analysis. A Newmark-beta method (an unconditionally stable method with parameters $\beta_m = 1/4$ and $\gamma_m = 1/2$) was considered to solve the transient analysis. Hence, the reliability index, $\beta_s(\theta)$, was computed from the results of this set of transient analysis. Subsequently, the vibration serviceability limit state of the stay cable under uncertainty conditions was assessed. Thus, the reliability index, $\beta_s(\theta)$, was lower than the allowable reliability index, β_t, so this limit state was not met.

In order to improve the dynamic behavior of this stay cables, different passive damping devices were installed at this stay cable. These passive damping devices were designed according to the proposed method. This design problem is described in next section.

4.3. Motion-Based Design of Passive Damping Devices under Uncertainty Conditions

Three different passive damping devices were considered for this study: (i) viscous damper; (ii) elastomeric damper; and (iii) friction damper. The FE method was employed to simulate the behavior of these damping devices. The software Ansys [57] was employed for this purpose. Figure 2 depicts the mechanical models, which simulate the behavior of each damper. For each passive damper, the following model was considered: (i) the viscous damper was modelled by a 1D element (COMBIN14) whose characteristic parameter was the damping coefficient, $c_{d,v}$ [sN/m]; the elastomeric damper was also modelled by a 1D element (COMBIN14) whose characteristic parameters were the damping coefficient, $c_{d,e}$ [sN/m], and the stiffness coefficient, $k_{d,e}$. [N/m]; and (iii) the frictioin damper was modelled by a 1D element (COMBIN40) whose characteristic parameters were the damping coefficient, $c_{d,f}$ [sN/m], the stiffness coefficient, $k_{d,f}$ [N/m], and the friction force, f_f [N].

Consequently, the different dampers were implemented in the numerical model and designed according to the motion-based design method under uncertainty conditions. The three dampers were installed at a length of $x_c = 0.03L$ according to the recommendations of Ref. [2]. The damper-cable interaction model is shown in Figure 2.

A search domain, $[\theta_{\min}, \theta_{\max}]$, for the characteristic parameters of the dampers was included in the optimization problem to ensure the physical meaning of the solutions obtained. The search domain was defined as follows: (i) the lower bound of the search domain, $\theta_{\min}$, was defined as $\theta_{\min} = \left[c_{min}, k_{min}, f_{f_{min}}\right]$ (where c_{min} is the minimum value of the damping coefficient; k_{min} is the minimum value of the stiffness coefficient, and $f_{f_{min}}$ is the minimum value of the friction force); and (ii) the upper bound of the search domain, $\theta_{\max}$, was defined as $\theta_{\max} = \left[c_{max}, k_{max}, f_{f_{max}}\right]$ (where c_{max} is the maximum value of the damping coefficient; k_{max} is the maximum value of the stiffness coefficient, and $f_{f_{max}}$ is the maximum value of the friction force).

The lower, c_{min}, and upper, c_{max}, bounds of the damping coefficient were determined considering both the requirement of the Scruton number [6] and the optimum damping coefficient of the Pacheco's universal curve [25]. According to this, the following bounds were established: (i) $c_{min} = 4.8 \times 10^4$ sN/m; and (ii) $c_{max} = 1.64 \times 10^5$ sN/m. This search range guarantees that any solution of this design problem avoids the occurrence of the rain–wind interaction phenomenon.

The search domain of the stiffness coefficient and the friction force were based on the results of previous research [2]. According to these results, the following bounds were established: (i) for the stiffness coefficient, $k_{min} = 5 \times 10^4$ N/m and $k_{max} = 5 \times 10^5$ N/m; and (ii) for the friction force, $f_{f_{min}} = 1 \times 10^4$ N and $f_{f_{max}} = 4 \times 10^4$ N.

In order to avoid falling into a local minimum, a global computational algorithm was considered for this optimization problem. Among the different computational algorithms, genetic algorithms were considered herein [65] for its simplicity and great efficiency to solve structural optimization problems.

Genetic algorithms are nature-inspired computational algorithms based on Darwin's natural selection theory. According to this, each possible value of the characteristic parameters of the damper is identified as a chromosome. Subsequently, each set of characteristic parameters is grouped into an individual (parameter vector). Later, the value of this parameter vector is improved via an iterative process where the value of the objective function is optimized. The optimization process can be summarized in the following steps: (i) an initial random population of parameter vectors is generated; (ii) the objective function is evaluated for all the individuals; (iii) a new population is created using three mechanisms (selection, crossover, and mutation); (iv) the objective function is evaluated for the individuals of the new population; (v) the steps (iii) and (iv) are repeated until some convergence criterion is met. The following parameters were considered for the considered genetic algorithms: (i) an initial population of 5 individuals; (ii) a crossover fraction of 0.4; (iii) a mutation fraction of 0.9; and (iv) a total number of iterations equal to 6.

As result of the optimization process, a Pareto front was obtained. Subsequently, a decision-making problem should be solved, the selection of the best solution among the different elements of the Pareto front. In order to address this problem, an additional condition was included. Among the
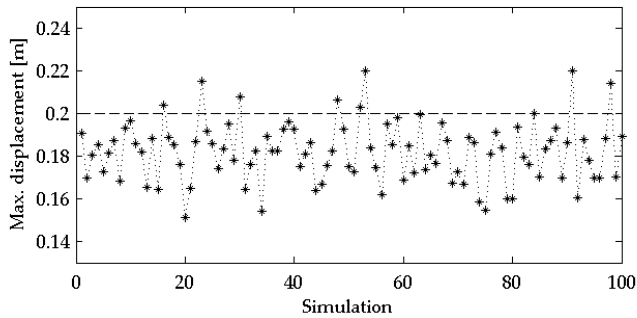
different elements of the Pareto front, the element of the Pareto front with a lower value of the damping coefficient was selected as best solution. The commercial software Ansys [57] and Matlab [64] were used to solve this design problem. The results of the optimization problem are summarized in the next sub-sections.

4.3.1. Viscous Damper

First, the motion-based design of the viscous damper under uncertainty conditions was performed. The design problem of this viscous damper may be formulated as follows:

$$\text{find } \theta = c_{d,v} \text{ to minimize } f(\theta) = c_{d,v}$$
$$\text{subject to} \begin{cases} c_{\min} < c_{d,v} < c_{\max} \\ \beta_s(\theta) \geq \beta_t = 1.35. \end{cases} \quad (21)$$

As result of the optimization process, the damping coefficient, $c_{d,v}$, was obtained. The optimum value obtained was $c_{d,v} = 1.06 \times 10^5$ sN/m. The reliability index for this solution was, $\beta_s(\theta) = 1.37$, which met the design requirements. Figure 6 shows the maximum displacement at the mid-span of the cable damped by the viscous damper for the different elements of the sample.
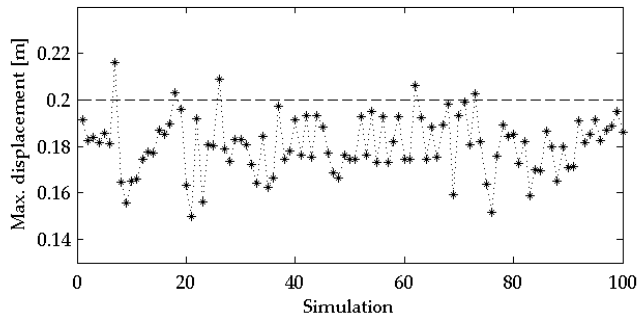

Figure 6. Maximum displacement at the mid-span of the stay cable damped by the viscous damper for the different elements of the sample.

4.3.2. Elastomeric Damper

Subsequently, the motion-based design of the elastomeric damper under uncertainty conditions may be addressed. The design problem of this elastomeric damper may be defined as follows:

$$\text{find } \theta = \begin{bmatrix} c_{d,e}, & k_{d,e} \end{bmatrix} \text{ to minimize } f(\theta) = [f_1, \ f_2] = \begin{bmatrix} c_{d,e}, & k_{d,e} \end{bmatrix}$$
$$\text{subject to} \begin{cases} c_{\min} < c_{d,e} < c_{\max} \\ k_{\min} < k_{d,e} < k_{\max} \\ \beta_s(\theta) \geq \beta_t = 1.35 . \end{cases} \quad (22)$$

As result of the design process, the parameters of the elastomeric damper ($c_{d,e}$ and $k_{d,e}$) were obtained. The best solution among all the elements of the Pareto front was $c_{d,e} = 1.22 \times 10^5$ sN/m and $k_{d,e} = 1.30 \times 10^5$ N/m. The reliability index associated with this solution is, $\beta_s(\theta) = 1.49$, which met the design requirements. Figure 7 shows the maximum displacement at the mid-span of the cable damped by the elastomeric damper for the different elements of the sample.
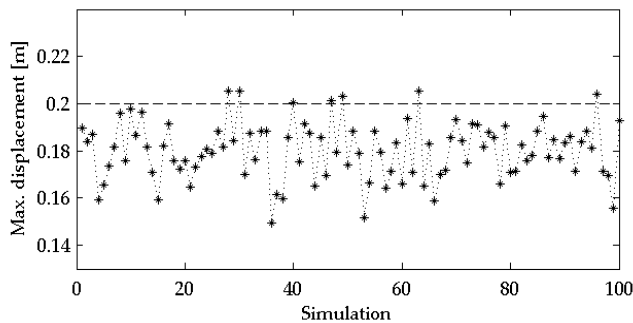
Figure 7. Maximum displacement at the mid-span of the stay cable with the elastomeric damper for the different elements of the sample.

4.3.3. Friction Damper

Finally, the motion-based design of the friction damper under uncertainty conditions was performed. The design problem of this friction damper may be formulated as follows:

$$\text{find } \theta = \left[c_{d,e}, \ k_{d,e}, \ f_f \right] \text{ to minimize } \mathbf{f}(\theta) = [f_1, \ f_2, \ f_3] = \left[c_{d,e}, \ k_{d,e}, \ f_f \right]$$

$$\text{subject to} \begin{cases} c_{\min} < c_{d,f} < c_{\max} \\ k_{\min} < k_{d,f} < k_{\max} \\ f_{f_{\min}} < k_f < f_{f_{\max}} \\ \beta_s(\theta) \geq \beta_t = 1.35 \ . \end{cases} \tag{23}$$

After the design process, the optimum value of the damping coefficient, stiffness coefficient, and friction force which characterize the friction damper were obtained. The optimum solution was $c_{d,f} = 1.24 \times 10^5$ sN/m, $k_{d,f} = 6.74 \times 10^4$ N/m and $f_f = 2.95 \times 10^4$ N. The reliability index associated with this solution was $\beta_s(\theta) = 1.55$, which met the design requirements. Figure 8 shows the maximum displacement at the mid-span of the cable damped by the friction damper for the different elements of the sample.

Figure 8. Maximum displacement at the mid-span of the stay cable damped by the friction damper for the different elements of the sample.

4.4. Discussion of Results

Finally, the performance of the proposed method was validated comparing the abovementioned results with the ones provided by a conventional one, the optimum damping coefficient of the Pacheco's

universal curve [25]. This optimum value for a viscous damper can be determined using the following relationship:

$$c_{opt} = 0.10 \frac{mL\omega_1}{\frac{x_c}{L}},$$ (24)

where $\omega_1 = 2\pi f_1$ is the fundamental angular natural frequency of the stay cable [rad/s] and x_c is the distance between the anchorage of the cable and the point where the damper is implemented (Figure 2). As in the remaining cases, the viscous damper is located at the point, $x_c = 0.03L$, with respect to the lower anchorage. The optimum damping coefficient, according to this conventional method for the viscous damper was $c_{opt} = 1.64 \times 10^3$ sN/m.

Thus, two main conclusions may be obtained via the comparison of the abovementioned results: (i) the motion-based design method under uncertainty conditions allows reduction of the characteristic parameter of the viscous damper by about 35% with respect to the conventional method; and (ii) for this case-study, the viscous damper appears to be the best choice to control the dynamic response of the longest cable of the Alamillo bridge, as a minimum value of the damping coefficient was obtained for this passive damper. The proposed method allows a better adjustment to the design requirements of the problem, reducing, as consequence, the size and the cost of the passive damping devices. Hence, the performance of the motion-based design method, for this particular problem, has been validated.

5. Conclusions

Stay cables are prone to vibrate under wind-induced vibrations, so that passive damping devices are usually employed to control their response. Nevertheless, the performance of these damping devices is directly affected by the sensitivity of the stay cables to both the variability of the external actions and the modification of the constitutive modal properties of the cables induced by the changes of the operational and environmental conditions. Accordingly, it is necessary to establish design methods which overcome these limitations and can be easily implemented for practical engineering applications.

For this purpose, a motion-based design method under uncertainty conditions was proposed and implemented herein. In this approach, the design problem is transformed into a constrained multi-objective optimization problem. Thus, the different components of the multi-objective function are defined in terms of the characteristic parameters of the considered passive damping device; and an inequality constraint is additionally included to guarantee an acceptable probability of failure of the structural system. As design criterion to evaluate the probability of failure, the compliance of the vibration serviceability limit state (according to the FHWA guidelines) was considered. Therefore, the computation of the probability of failure was performed via a reliability index. In this manner, the compliance of the vibration serviceability limit state is met if the reliability index is greater than an allowable value (according to the European guidelines). A sampling technique, the Monte Carlo method, was considered to determine numerically this index.

The performance of the method was validated numerically via its implementation for the design of three different passive damping devices (viscous, elastomeric, and friction dampers) when they are used to control the wind-induced vibrations of the longest stay cable of the Alamillo bridge (Seville). To this end, the effects of the rain-wind interaction phenomenon and the turbulent component of the wind action were considered as excitation sources. Additionally, and for comparison purposes, the passive damping devices were also designed according to a conventional method. As result of this study, a clear reduction of the values of the characteristic parameters of the dampers was obtained when the motion-based design method was applied, when compared to the results of the conventional method. Thus, the proposed method allows improvement of the design of passive damping devices for stay cables under wind-induced vibrations considering uncertainty conditions. This improvement is reflected in a reduction of both the size and the budget of the devices, which facilitates its installation. Nevertheless, despite the good performance of the proposed approach, further studies are recommended to validate experimentally the long-term behavior of passive damping devices designed according to this proposal.

References

1. Abdel-Ghaffar, A.M.; Khalifa, M.A. Importance of Cable Vibration in Dynamics of Cable-Stayed Bridges. *J. Eng. Mech.* **1991**, *117*, 2571–2589. [CrossRef]
2. Caetano, E. *Cable Vibrations in Cable-Stayed Bridges*; IABSE: Zürich, Switzerland, 2007; Volume 9.
3. Lepidi, M.; Gattulli, V. Static and dynamic response of elastic suspended cables with thermal effects. *Int. J. Solids Struct.* **2012**, *49*, 1103–1116. [CrossRef]
4. Caetano, E.; Cunha, A.; Gattulli, V.; Lepidi, M. Cable–deck dynamic interactions at the International Guadiana Bridge: On-site measurements and finite element modelling. *Struct. Control Health Monit.* **2008**, *15*, 237–264. [CrossRef]
5. Domaneschi, M.; Martinelli, L. Extending the benchmark cable-stayed bridge for transverse response under seismic loading. *J. Bridge Eng.* **2013**, *19*, 04013003. [CrossRef]
6. *Wind-Induced Vibration of Stay Cables*; FHWA-HRT-05-083; Federal Highway Administration: New York, NY, USA, 2007.
7. Dyke, S.J.; Caicedo, J.M.; Turan, G.; Bergman, L.A.; Hague, S. Phase I benchmark control problem for seismic response of cable-stayed bridges. *J. Struct. Eng.* **2003**, *129*, 857–872. [CrossRef]
8. Cremona, C. *Comportement Au Vent Des Ponts*; Presses De L'ecole Natinale Des Ponts Et Chaussées; Association Francaise De Génie Civil: Paris, France, 2002.
9. Caracoglia, L.; Zuo, D. Effectiveness of cable networks of various configurations in suppressing stay-cable vibration. *Eng. Struct.* **2009**, *31*, 2851–2864. [CrossRef]
10. Bossens, F.; Preumont, A. Active tendon control of cable-stayed bridges: A large-scale demonstration. *Earthq. Eng. Struct. Dyn.* **2001**, *30*, 961–979. [CrossRef]
11. Johnson, E.A.; Baker, G.A.; Spencer, B.F., Jr.; Fujino, Y. Semiactive Damping of Stay Cables. *J. Eng. Mech.* **2007**, *133*, 1–11. [CrossRef]
12. Ali, H.-E.M.; Abdel-Ghaffar, A.M. Seismic Passive Control of Cable-Stayed Bridges. *Shock Vib.* **1995**, *2*, 918721. [CrossRef]
13. Rodellar, J.; Mañosa, V.; Monroy, C. An active tendon control scheme for cable-stayed bridges with model uncertainties and seismic excitation. *J. Struct. Control* **2002**, *9*, 75–94. [CrossRef]
14. Huang, P.; Wang, X.; Wen, Q.; Wang, W.; Sun, H. Active Control of Stay Cable Vibration Using a Giant Magnetostrictive Actuator. *J. Aerosp. Eng.* **2018**, *31*, 04018074. [CrossRef]
15. Zhou, H.J.; Sun, L.M. Damping of stay cable with passive-on magnetorheological dampers: A full-scale test. *Int. J. Civ. Eng.* **2013**, *11*, 154–159.
16. Chen, Z.H.; Lam, K.H.; Ni, Y.Q. Enhanced damping for bridge cables using a self-sensing MR damper. *Smart Mater. Struct.* **2016**, *25*, 085019. [CrossRef]
17. YeganehFallah, A.; Attari, N.K.A. Robust control of seismically excited cable stayed bridges with MR dampers. *Smart Mater. Struct.* **2017**, *26*, 035056. [CrossRef]
18. Zhao, Y.-L.; Xu, Z.-D.; Wang, C. Wind vibration control of stay cables using magnetorheological dampers under optimal equivalent control algorithm. *J. Sound Vib.* **2019**, *443*, 732–747. [CrossRef]
19. Xu, Y.L.; Zhou, H.J. Damping cable vibration for a cable-stayed bridge using adjustable fluid dampers. *J. Sound Vib.* **2007**, *306*, 349–360. [CrossRef]
20. Shi, X.; Zhu, S. Magnetic negative stiffness dampers. *Smart Mater. Struct.* **2015**, *24*, 072002. [CrossRef]
21. Zhou, P.; Fang, Q. Match of Negative Stiffness and Viscous Damping in A Passive Damper for Cable Vibration Control. Available online: https://www.hindawi.com/journals/sv/2019/3208321/ (accessed on 30 September 2019).

22.   Caracoglia, L.; Jones Nicholas, P. Passive hybrid technique for the vibration mitigation of systems of interconnected stays. *J. Sound Vib.* **2007**, *307*, 849–864. [CrossRef]

23.   Jiménez-Alonso, J.F.; Sáez, A. Robust optimum design of tuned mass dampers to mitigate pedestrian-induced vibrations using multi-objective genetic algorithms. *Struct. Eng. Int.* **2017**, *27*, 492–501. [CrossRef]

24.   Kovacs, I. Zur frage der seilschwingungen und der seildämpfung. *Bautechnik* **1982**, *59*, 325–332.

25.   Pacheco, B.M.; Fujino, Y.; Sulekh, A. Estimation curve for modal damping in stay cables with viscous damper. *J. Struct. Eng.* **1993**, *119*, 1961–1979. [CrossRef]

26.   Krenk, S. Vibrations of a taut cable with an external damper. *J. Appl. Mech.* **2000**, *67*, 772–776. [CrossRef]

27.   Yoneda, M.; Maeda, K. A study on practical estimation method for structural damping of stay cables with dampers. *Doboku Gakkai Ronbunshu* **1989**, *1989*, 455–458. [CrossRef]

28.   Ontiveros-Pérez, S.P.; Miguel, L.F.F.; Miguel, L.F.F. Robust Simultaneous Optimization of Friction Damper for the Passive Vibration Control in a Colombian Building. *Procedia Eng.* **2017**, *199*, 1743–1748. [CrossRef]

29.   Connor, J.J. *Introduction to Structural Motion Control, MIT-Prentice Hall Series on Civil, Environmental and Systems Engineering*; Prentice Hall: Bergen, NJ, USA, 2003.

30.   Naranjo-Pérez, J.; Jiménez-Manfredi, J.; Jiménez-Alonso, J.; Sáez, A. Motion-based design of passive damping devices to mitigate wind-induced vibrations in stay cables. *Vibration* **2018**, *1*, 269–289. [CrossRef]

31.   Hao, P.; Wang, B.; Li, G.; Meng, Z.; Wang, L. Hybrid Framework for Reliability-Based Design Optimization of Imperfect Stiffened Shells. *AIAA J.* **2015**, *53*, 2878–2889. [CrossRef]

32.   Wang, L.; Wang, X.; Li, Y.; Lin, G.; Qiu, Z. Structural time-dependent reliability assessment of the vibration active control system with unknown-but-bounded uncertainties. *Struct. Control Health Monit.* **2017**, *24*, e1965. [CrossRef]

33.   Rathi, A.K.; Chakraborty, A. Reliability-based performance optimization of TMD for vibration control of structures with uncertainty in parameters and excitation. *Struct. Control Health Monit.* **2017**, *24*, e1857. [CrossRef]

34.   *EN 1990 Eurocode 0: Basis of Structural Design*; European Committee for Standardization: Brussels, Belgium, 2005.

35.   Wang, L.; Liu, J.; Yang, Y. A nonprobabilistic time-variant reliability-based optimization approach to the reliable active controller design of structural vibration considering convex uncertainties. *Struct. Control Health Monit.* **2018**, *25*, e2269. [CrossRef]

36.   Binder, K.; Heermann, D. *Monte Carlo Simulation in Statistical Physics: An Introduction; Graduate Texts in Physics*, 5th ed.; Springer-Verlag: Berlin/Heidelberg, Germany, 2010; ISBN 978-3-642-03162-5.

37.   Arora, J.S. *Optimization of Structural and Mechanical Systems*; World Scientific Publishing Co. Pte. Ltd.: 5 Toh Tuck Link, Singapore, 2007.

38.   Nocedal, J.; Wright, S.J. *Numerical Optimization*; Springer Verlag: New York, NY, USA, 1999.

39.   Holický, M. *Reliability Analysis for Structural Design*; African Sun Media: Stellenbosch, South Africa, 2009.

40.   Warnitchai, P.; Fujino, Y.; Susumpow, T. A non-linear dynamic model for cables and its application to a cable structure system. *J. Sound Vib.* **1995**, *187*, 695–712. [CrossRef]

41.   Caetano, E.; Cunha, A.; Taylor, C.A. Investigation of dynamic cable–deck interaction in a physical model of a cable-stayed bridge. Part I: Modal analysis. *Earthq. Eng. Struct. Dyn.* **2000**, *28*, 481–498. [CrossRef]

42.   Johnson, E.A.; Christenson, R.E.; Spencer, B.F., Jr. Semiactive damping of cables with sag. *Comput. Aided Civ. Infrastruct. Eng.* **2003**, *18*, 132–146. [CrossRef]

43.   Zhou, Q.; Nielsen, S.R.; Qu, W.L. Semiactive control of three-dimensional vibrations of an inclined sag cable with magnetorheological dampers. *J. Sound Vib.* **2006**, *296*, 1–22. [CrossRef]

44.   Mehrabi, A.B.; Tabatabai, H. Unified finite difference formulation for free vibration of cables. *J. Struct. Eng.* **1998**, *124*, 1313–1322. [CrossRef]

45.   Hoang, N.; Fujino, Y. Analytical study on bending effects in a stay cable with a damper. *J. Eng. Mech.* **2007**, *133*, 1241–1246. [CrossRef]

46.   Yu, Z.; Xu, Y.L. Mitigation of three-dimensional vibration of inclined sag cable using discrete oil dampers—I. Formulation. *J. Sound Vib.* **1998**, *214*, 659–673. [CrossRef]

47.   Connor, J.; Laflamme, S. Optimal Passive Damping Distribution. In *Structural Motion Engineering*; Springer: Berlin/Heidelberg, Germany, 2014; pp. 141–197.

48.   Xu, Z.-D.; Shen, Y.-P.; Zhao, H.-T. A synthetic optimization analysis method on structures with viscoelastic dampers. *Soil Dyn. Earthq. Eng.* **2003**, *23*, 683–689. [CrossRef]

49. Zhou, H.; Sun, L.; Xing, F. Free vibration of taut cable with a damper and a spring. *Struct. Control Health Monit.* **2014**, *21*, 996–1014. [CrossRef]

50. Seong, J.-Y.; Min, K.-W. An analytical approach for design of a structure equipped with friction dampers. *Procedia Eng.* **2011**, *14*, 1245–1251. [CrossRef]

51. Hong, S. Time Domain Buffeting Analysis of Large-Span Cable-Stayed Bridge. Master's Thesis, FEUP. University of Porto, Porto, Portugal, 2009.

52. Solari, G. Gust-excited vibrations. In *Wind-Excited Vibrations of Structures*; Springer: Berlin/Heidelberg, Germany, 1994; pp. 195–291.

53. Davenport, A.G. The Dependence of Wind Loads on Meteorological Parameter. *Wind Eff. Build. Struct.* **1968**, *1*, 19–82.

54. *EN 1991-1-4 Eurocode 1. Actions on Structures—Part 1–4: General Actions—Wind Actions*; European Committee for Standardization: Brussels, Belgium, 2005.

55. Casas, J.R.; Aparicio, A.C. Monitoring of the Alamillo cable-stayed bridge during construction. *Exp. Mech.* **1998**, *38*, 24–28. [CrossRef]

56. Casas, J.R.; Aparicio, A.C. Rain–wind-induced cable vibrations in the Alamillo cable-stayed bridge (Sevilla, Spain). Assessment and remedial action. *Struct. Infrastruct. Eng.* **2010**, *6*, 549–556. [CrossRef]

57. Ansys Mechanical 19.0. Ansys Inc. 2019. Available online: http://www.ansys.com/ (accessed on 1 October 2019).

58. Simiu, E.; Scanlan, R.H. *Wind Effects on Structures: Fundamentals and Applications to Design*, 3rd ed.; John Willey & Sons, Inc.: New York, NY, USA, 1996.

59. *EN 1993-1-11 Eurocode 3: Design of Steel Structures-Part 1–11: Design of Structures with Tension Components*; European Committee for Standardization: Brussels, Belgium, 2006.

60. Stromquist-LeVoir, G.; McMullen, K.F.; Zaghi, A.E.; Christenson, R. Determining Time Variation of Cable Tension Forces in Suspended Bridges Using Time-Frequency Analysis. *Adv. Civ. Eng.* **2018**, *2018*. [CrossRef]

61. Naranjo-Pérez, J.; Jiménez-Alonso, J.F.; Díaz, I.M.; Sáez, A. Motion-based design of viscous dampers for cable-stayed bridges under uncertainty conditions. In Proceedings of the 5th International Conference on Mechanical Models in Structural Engineering, CMMoST 2019, Alicante, Spain, 23–25 Ocober 2019.

62. Park, S.; Bosch, H.R. *Mitigation of Wind-Induced Vibration of Stay Cables: Numerical Simulations and Evaluations*; Federal Highway Administration: Hampton, VA, USA, 2014.

63. Jurado, D. Simulación Estocástica De Cargas Para Análisis Dinámico De Estructuras En Ingeniería Civil. Master's Thesis, Universidad de Sevilla, Seville, Spain, 2017.

64. Matlab Inc. Matlab R2019b. Available online: http://www.mathworks.com/ (accessed on 15 October 2019).

65. Koh, C.G.; Perry, M.J. *Structural Identification and Damage Detection Using Genetic Algorithms: Structures and Infrastructures Book Series*; CRC Press: Boca Raton, FL, USA, 2017; Volume 6.